Spatial regulation

of dual flagellar systems

Dissertation

zur Erlangung des akademischen Grades

Doktor der Naturwissenschaft (Dr. rer. nat.)

dem Fachbereich Biologie der

Philipps-Universität Marburg (HKZ: 1180)

am 31.10.2016

vorgelegt von

Florian Roßmann, MSc

geboren in Mutlangen

Erstgutachter: Prof. Dr. Kai Thormann

Zweitgutachter: Prof. Dr. Martin Thanbichler

Tag der Disputation:

Marburg an der Lahn, 2016

Die Untersuchungen zur vorliegenden Arbeit wurden von August 2012 bis Oktober 2016 unter der Leitung von Prof. Dr. Kai Thormann am Max-Planck-Institut für terrestrische Mikrobiologie in Marburg und am Institut für Mikrobiologie und Molekularbiologie an der Justus-Liebig-Universität Gießen durchgeführt.

Vom Fachbereich Biologie der Philipps-Universität Marburg
(HKZ: 1180) als Dissertation angenommen am:

Erstgutachter: Prof. Dr. Kai M. Thormann

Zweitgutachter: Prof. Dr. Martin Thanbichler

Tag der mündlichen Prüfung:

Die während der Promotion erzielten Ergebnisse sind zum Teil in folgenden Originalpublikationen veröffentlicht:

Chapter 2:

Bubendorfer S, **Koltai M**, **Rossmann F**, **Sourjik V**, **Thormann KM**. 2014. Secondary bacterial flagellar system improves bacterial spreading by increasing the directional persistence of swimming. Proc. Natl. Acad. Sci. USA. 111(31): 11485-90.

Chapter 3:

Schuhmacher JS*, **Rossmann F***, **Dempwolff F**, **Knauer C**, **Altegoer F**, **Steinchen W**, **Dörrich AK**, **Klingl A**, **Stephan M**, **Linne U**, **Thormann KM**, **Bange G**. 2015. MinD-like ATPase FlhG effects location and number of bacterial flagella during C-ring assembly. Proc. Natl. Acad. Sci. USA. 112(10):3092-7

Chapter 4:

Rossmann F*, **Brenzinger S***, **Knauer C**, **Dörrich AK**, **Bubendorfer S**, **Ruppert U**, **Bange G**, **Thormann KM**. 2015. The role of FlhF and HubP as polar landmark proteins in *Shewanella putrefaciens* CN-32. Mol Microbiol. 98(4):727-42

* diese Autoren wirkten gleichberechtigt an der Publikation mit

Erklärung

Ich versichere, dass ich meine Dissertation:

“Spatial regulation of dual flagellar systems”

selbstständig, ohne unerlaubte Hilfe angefertigt und mich dabei keiner anderen als der von mir ausdrücklich bezeichneten Quellen und Hilfen bedient habe. Die Dissertation wurde in der jetzigen oder einer ähnlichen Form noch bei keiner anderen Hochschule eingereicht und hat noch keinen sonstigen Prüfungszwecken gedient.

Marburg (Lahn), den 31. Oktober 2016

_____

Florian Roßmann

When we get to the very, very small world […]
we have a lot of new things that would happen that
represent completely new opportunities for design […]
At the atomic level we have new kinds of forces and
new kinds of possibilities, new kinds of effects.
The problem of manufacture and reproduction of
materials will be quite different […]
inspired by biological phenomena in which chemical forces
are used in a repetitious fashion to produce all kinds of weird effects
(one of which is the author) […]

Richard P. Feynman (1959)

Table of contents

Summary

Many cellular processes are highly spatially ordered, with spatial separation regulated by cellular factors called landmark proteins. Examples of compartmentalized processes are those involved in bacterial motility. In bacteria, swimming and swarming require the formation of flagella - long, rotating, helical filaments driven by a membrane-embedded motor. Landmark proteins likely regulate the numerous flagellation patterns found in a variety of bacterial species. In polarly flagellated bacteria, primarily encountered in marine habitats, the SRP-like GTPase FlhF and the MinD-like ATPase FlhG are known to control flagellar positioning and number. HubP, another polar factor identified in *Vibrio cholerae*, was shown to be involved in the localization of proteins which are a part of other cellular processes such as chemotaxis, enabling the cell to navigate efficiently towards more favorable conditions.

The polarly flagellated gammaproteobacterium *Shewanella putrefaciens* CN-32 possesses two flagellar systems encoded in two gene clusters, enabling the cell to form a single polar and multiple lateral flagella. However, genes for only a single chemotaxis system are located on the chromosome. The primary polar system is required for the main propulsion of the cell. Since only the motor switch protein of the polar system, $FliM_1$, harbors the binding domain of the chemotaxis response regulator CheY, the chemotaxis system also acts exclusively on this flagellar motor. Secondary, lateral flagella enable the cell to turn more efficiently by biasing the directional changes of the swimming cell towards smaller turn angles. This leads to a higher directional persistence in the swimming path of the cell.

Since the positions of both the polar and lateral flagella play key roles in this special movement pattern, the mode of action of the regulators FlhF and FlhG on the dual flagellation was examined. While FlhF determinates the position of the nascent flagellum by recruiting flagellar components to the cell pole, direct interaction, likely at the cell pole, of FlhF and FlhG restricts polar accumulation of FlhF by stimulating its GTPase activity. The placement of the lateral flagellar system seems to be FlhF-independent. In addition to interaction with FlhF, FlhG was shown to be involved in the assembly of the cytoplasmic portion of the flagellar motor. For this purpose, FlhG binds $FliM_1$ at the binding motif also recognized by CheY. As the motor switch protein of the lateral system, $FliM_2$, lacks this binding domain, lateral flagella assemble independently of FlhG. Since FlhG was also shown to act on flagellar transcription, polar localization of FlhG might form a part of a feedback loop regulating flagellar transcription and assembly.

In *V. cholerae*, the polar landmark HubP was shown to interact with both FlhF and FlhG. The ortholog of *V. cholerae* HubP was identified in *S. putrefaciens* and affected its flagella-mediated motility. In addition to

its interaction with FlhFG and the chemotaxis system, *Sp*HubP and *Vc*HubP appears to be involved in chromosome segregation and polar recruitment of other yet unidentified factors.

These results indicate that the polar flagellar system requires the presence of several factors to assemble a functional flagellum and to function in concert with the chemotaxis system. These factors do not affect assembly and function of the lateral flagellum, which seems to assemble stochastically and independently.

Zusammenfassung

Viele zelluläre Prozesse sind räumlich genau angeordnet, wobei die räumliche Trennung durch bestimmte zelluläre Faktoren, sogenannte Marker-Proteine, reguliert wird. Solche Prozesse, welche räumlich getrennt ablaufen, sind zum Beispiel auch an der bakteriellen Bewegung beteiligt. Bakterien bilden zum Schwimmen und Schwärmen Flagellen aus. Dies sind lange, spiralförmige Filamente die von einem, in der Zellmembran eingebettenen, Motor betrieben werden. Marker-Proteine sind wahrscheinlich für die Ausbildung der vielen verschiedenen Flagellierungsarten zuständig. Diese sind in verschiedenen Bakterienarten anzutreffen. Polar flagellierte Bakterien kommen vor allem in marinen Lebensräumen vor. Die Position und die Anzahl der Flagellen regulieren die GTPase FlhF, welche Ähnlichkeiten zum Signalerkennungspartikel aufweist, und die ATPase FlhG (die homolog zu MinD ist). Es wurde gezeigt, dass ein weiterer Faktor, welcher in *Vibrio cholerae* entdeckt wurde, HubP, an der Lokalisierung von anderen in zellulären Prozessen beteiligten Proteinen eingebunden ist. Ein solcher Prozess ermöglicht zum Beispiel Chemotaxis, was die Zelle dazu befähigt sich effizient in Richtung vorteilhafterer Bedingungen zu bewegen.

Das polar flagellierte Gammaproteobakterium *Shewanella putrefaciens* CN-32 besitzt zwei Flagellensysteme, welche durch zwei Gencluster codiert werden. Diese ermöglichen die Bildung einer einzigen polaren und mehreren lateralen, seitlich angeordneten Flagellen. Allerdings sind auf dem Chromosom nur die Gene für ein einziges Chemotaxissystem vorhanden. Das primäre, polare System fungiert als Hauptantrieb für die Zelle. Da nur das Motor-Umschaltprotein des polaren Systems, $FliM_1$, eine Bindedomäne für den Chemotaxis-Antwortregulator CheY besitzt, wirkt das Chemotaxissystem ausschließlich auf diesen Flagellenmotor. Die sekundären, lateralen Flagellen befähigen die schwimmende Zelle durch Beeinflussung der Bewegungsrichtung hin zu kleineren Drehwinkeln, sich effizienter zu drehen. Dies führt zu einer verbesserten Beibehaltung der Bewegungsrichtung.

Da die Position der polaren und der lateralen Flagelle eine Schlüsselrolle in diesem besonderen Bewegungsmuster spielt, wurde die Wirkungsweise der Regulatoren FlhF und FlhG auf die duale Flagellierung untersucht. Während FlhF durch die Rekrutierung flagellarer Bestandteile zum Zellpol die Position der sich bildenden Flagelle bestimmt, beschränkt die direkte, wahrscheinlich polare Interaktion zwischen FlhF und FlhG durch Verstärkung der GTPase-Aktivität von FlhF dessen Ansammlung am Pol. Die Platzierung der lateralen Flagelle hingegen geschieht vermutlich unabhängig von FlhF. Zusätzlich zur Interaktion mit FlhF ist FlhG auch am Zusammenbau des cytoplasmatischen Teils des Flagellenmotors beteiligt. FlhG bindet dazu an das Bindemotiv von $FliM_1$, welches auch von CheY erkannt wird. Da dem Motor-Umschaltprotein des lateralen Systems, $FliM_2$, diese Bindedomäne fehlt, müssen laterale Flagellen unabhängig von FlhG zusammengebaut werden. Da gezeigt wurde, dass FlhG auch auf die

Flagellentranskription wirkt, könnte FlhG ein Teil eines Rückkopplungsmechanismus sein, welcher die Expression der Flagellenkomponenten und deren Zusammenbau reguliert.

In *V. cholerae* zeigte sich, dass das Marker-Protein HubP sowohl mit FlhF als auch mit FlhG interagiert. Ein Ortholog von HubP wurde auch in *S. putrefaciens* identifiziert wo es auch die flagellen-vermittelte Bewegung beeinflusst. Zusätzlich zur Interaktion mit FlhFG und dem Chemotaxissystem, scheint *Sp*HubP und *Vc*HubP auch an der Chromosomenverteilung und der polaren Rekrutierung anderer, noch nicht identifizierter Faktoren beteiligt zu sein.

Diese Ergebnisse weisen darauf hin, dass für den Zusammenbau einer funktionsfähigen, polaren Flagelle und deren Zusammenspiel mit dem Chemotaxissystem viele verschiedene Faktoren vorhanden sein müssen. Diese Faktoren beeinflussen nicht den Zusammenbau und die Funktion der lateralen Flagelle. Dieser erfolgt anscheinend zufällig und unabhängig.

Chapter 1:

Introduction

1.1. Cell Polarity

As a ubiquitous feature of living matter, many individual biological features have highly organized shapes, structures, and functions. Cell polarity is the phenomenon of asymmetric cellular distribution of various biomolecules causing an asymmetric cell shape or spatial separation of cellular processes. Eukaryotic cells, for example, are highly compartmentalized, leading to the formation of organelles separated by membranes or protein structures (1). An example of cell polarity in single-cell organisms is the budding yeast *Saccharomyces cerevisiae*, which is highly polarized during mating and budding (2, 3). Also bacteria are not only reaction vessels, where biomolecules diffuse freely and randomly. Discoveries in the last 20 years revealed that certain processes require the localization of key proteins or protein complexes (4, 5). An important example is the formation of the mid-cell division plane (6).

In bacteria, localization of proteins and other biomolecules along the cytoplasmic membrane can occur by sensing the membrane curvature or special lipid compositions. Apart from that, asymmetric protein localization often requires the presence of matrix-dependent, self-organizing, non-polymer-forming landmark proteins, such as ParA/MinD-like ATPases, GTPases, or polymer forming landmark proteins as reviewed in (7). ParA/MinD-like ATPases and many GTPases, such as SRP (signal recognition particle)-like GTPases belong to the SRP, MinD, and BioD (SIMIBI)-type nucleoside triphosphate-binding proteins. SIMIBI proteins can be activated by ATP or GTP binding, resulting in the formation of homo- or heterodimers (8, 9).

Together with ParB, the ATPase ParA controls chromosome segregation in a variety of bacterial organisms (10). ParB can bind to centromere-like *parS* sites on the chromosome, located in close proximity to the origin of replication (*ori*). ATP-bound ParA forms polymers and binds nonspecifically to chromosomal DNA. Interactions between ParA(ADP) and ParB/*parS* causes stimulation of ParA ATPase activity and depolymerization and dissociation of ParA(ADP) from the DNA. The ParB/*parS* complex then interacts with the next nucleoid-bound ParA(ATP) by migrating along the chromosome and pulling the *ori* to the cell pole while leaving a path of unbound DNA and dissociated ParA molecules (Fig. 1) (11).

MinD is another representative of the group of matrix-dependent, self-organizing ParA/MinD-like ATPases. In the well-studied model organism *E. coli*, the Min system, composed of the proteins MinD and MinC, has its longest dwell time close to the poles of the cell. This prevents assembly of FtsZ monomers into a ring-like structure that determinates the division plane, called the Z-ring, in this region. This, in turn, leads to septum formation at mid-cell (12). Binding of ATP to MinD results in the formation of a membrane-associated homodimer and enables interaction with the effector MinC at the dimer interface (13). This

interaction activates MinC, decreasing rigidity of the bonds within FtsZ polymers and results in Z-ring fragmentation (14). MinE also forms a ring-like structure which stimulates MinD ATPase activity by interacting with membrane-bound MinD, triggering ATP hydrolysis to ADP and ultimately its dissociation from MinC and its monomerization (15). This cycle causes oscillations of MinCDE between the cell pole, permitting Z-ring formation exclusively at mid-cell (Fig. 1) (16, 17).

Similar to ParA/MinD-like ATPases, SRP-like GTPases exist in a GTP-bound active form and a biologically inactive GDP-bound state (8). Well-known representatives include the GTPases Ffh and FtsY, involved in co-translational protein targeting to the cytoplasmic membrane in prokaryotes such as *E. coli*. Together with the 4.5S SRP RNA, the SRP Ffh can bind to the ribosome-nascent chain complex carrying a translated nascent polypeptide with a signal sequence at its N-terminus. Upon GTP binding, Ffh forms a heterodimer with the SRP receptor FtsY. Interaction with the cytoplasmic membrane supports dimerization and activates the complex. Transfer of the cargo, comprising the nascent chain complex, to the translocon SecYEG allows subsequent secretion or integration of the nascent polypeptide into the membrane. Analogous to MinD/ParA-like ATPases, GTP hydrolysis leads to complex dissociation and initiation of the next cycle (Fig. 1) (18).

In contrast to non-polymer forming landmark proteins, polymer-forming proteins may sense geometrical cues, like the curvature of cytoplasmic membranes, due to their high surface coverage (7). DivIVA of *Bacillus subtilis* can form polymers and localizes at the negatively curved cell poles, where it fulfills a similar role as MinE in *E.coli* by recruiting MinCD via the adapter protein MinJ. Depolymerization of the Z-ring prevents septum formation at the new cell poles and restricts Z-ring localization to mid-cell (19, 20).

Though many landmark proteins are involved in chromosome segregation, cell division or co-translational protein translocation, other subcellularly localized factors are involved in bacterial motility and chemotaxis. Examples for spatially regulated cellular processes in bacteria are depicted in Figure 1.

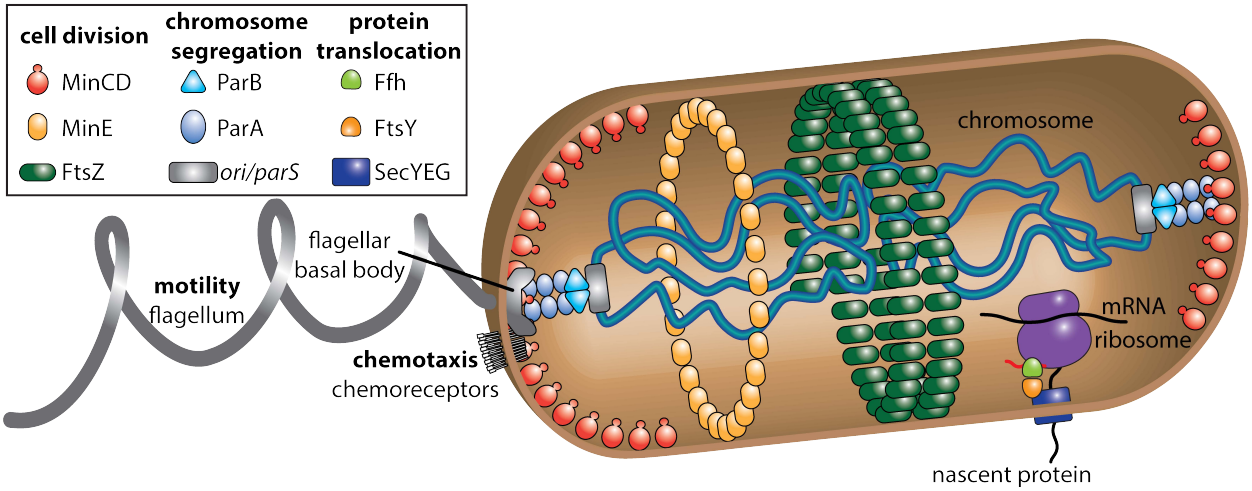

Fig: 1: Cell polarity in polarly flagellated gammaproteobacteria. Examples of spatially ordered cellular processes include cell division (Min system), chromosome segregation (ParAB*parS* system), protein translocation (SRP-Sec system), flagella-mediated motility and chemotaxis. The illustration includes their arrangement with the bacterial chromosome (blue) the flagellum (grey) and the cytoplasmic membrane (brown). Adapted from (7).

1.2. Bacterial Motility

Motility is an intrinsic feature of various species, enabling movement towards more favorable conditions and playing an important role in individual and population survival. While some organisms passively rely on moving water, wind, or other mobile creatures to spread and colonize new environments, many species utilize active, directed motility. Microorganisms naturally move by physical phenomena like convection or Brownian motion. In addition, numerous species have evolved intricate strategies for active motility, adapting these mechanisms to their respective habitats as an important aspect of their lifestyle (21).

Some bacterial species possess the ability to move across surfaces using swarming, twitching or gliding motility. Swarming across surfaces was already known in the early years of bacteriology, as researchers routinely cultivated bacteria on solid substrates and studied colony spreading (22). Gliding motility has also been observed for many years. *Myxococcus xanthus* uses this slow form of movement to spread on dry, solid surfaces. In 1961, another form of motility was described as “slow, hesitating and intermittent” (23) and later termed twitching motility. Twitching is mediated by repeated polymerization and retraction of filamentous protein extensions called type IV pili, as for example observed in the human pathogen *Pseudomonas aeruginosa* (24). While gliding motility enables movement on dry surfaces, flagella-mediated swarming can be facilitated on a thin layer of liquid. In addition to this form of operation, flagella are also used by many bacteria to propel themselves in liquid or viscous environments.

1.3. Flagella

1.3.1. Flagellation Pattern

Flagella are helical, proteinaceous filaments extending from the bacterial cell body and act as propellers. These organelles of locomotion can vary in number and arrangement in different bacterial species. Some bacteria, like representatives of the genera *Escherichia* or *Salmonella*, are peritrichously flagellated, with multiple flagella distributed on the cell surface away from the cell pole. Other species only possess a single flagellum at a lateral position, like the medial flagellated *Rhodobacter sphaeroides* (25). Bacteria with flagella positioned at the cell pole are lophotrichous, with multiple flagella at one pole, as found in *Helicobacter*, *Agrobacterium* and some representatives of *Pseudomonas sp.*; amphitrichous with flagella at both poles, as in *Campylobacter*; or monotrichous with single polar flagella restricted to one single cell pole, as represented by *Vibrio, Pseudomonas* or *Caulobacter*. Figure 2A illustrates these different flagellation patterns and lists the representative genera (26). These different flagellation patterns allow bacteria to improve spreading under different environmental conditions (27).

Though the different flagellation patterns have been known for many years and are used to characterize different bacterial groups, most of the molecular mechanisms establishing these flagellation patterns remain elusive.

1.3.2. Structure of the flagella

Despite these obvious differences in flagella number and arrangement, the structure of the flagellar motor itself is remarkably conserved. The flagellar motor is a multi-protein complex consisting of more than 20 different proteins. Its rotating segment can be divided into three parts: the filament, composed of the flagellin proteins; the hook; and the basal body. The latter is an axial rod with ring-like structures crossing the layers of the bacterial cell wall. In gram-negative bacteria, the basal body consists of the periplasmic P- and L-rings, the cytoplasmic membrane-embedded MS-ring, and the C-ring extending into the cytoplasm (Figure 2B) (28, 29).

The C-ring, composed of the proteins FliG, FliM and FliN, is the central gearbox participating in torque generation. Torque is then transferred via the rod and the hook to the filament. The motor is powered by membrane-embedded ion channels called stators. These protein complexes are anchored in the peptidoglycan layer, forming a dynamic ring structure around the MS-ring. Ion fluxes through the stator complexes is thought to result in a conformational change of the stator subunit MotA which is transmitted to FliG. This interaction generates the torque necessary for flagella rotation (30, 31).

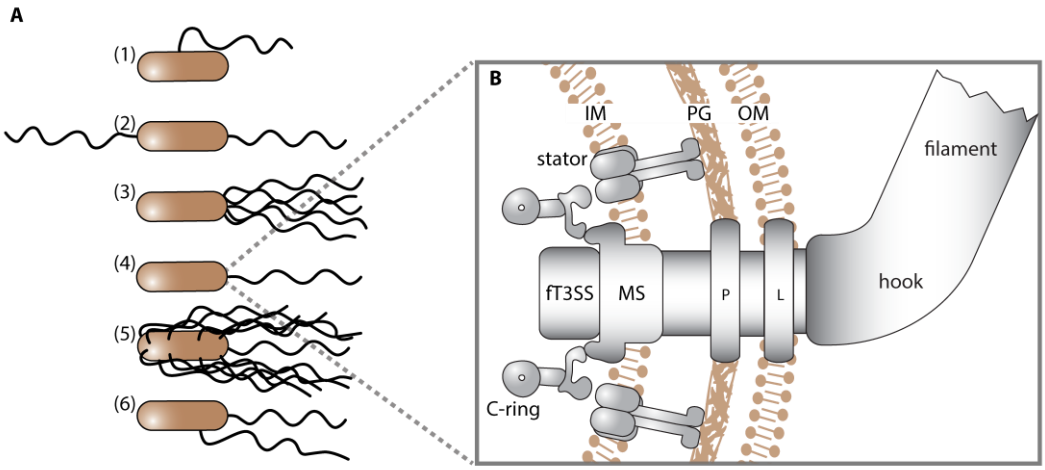

Fig: 2: Characteristics of bacterial flagella. (A) Flagellation patterns: (1) medial (2) amphitrichous (3) lophotrichous (4) polar/monotrichous (5) peritrichous (6) dual, polar/lateral. (B) Close-up cross section of the flagellar motor from a Gram-negative bacterium. (OM = outer membrane; IM = inner membrane; PG = peptidoglycan layer; fT3SS = flagellar type III secretion system; MS = MS-ring; P = P-ring; L = L-ring). Adapted from (120)

To secrete large amounts of distal, flagellar components across the barrier of the cytoplasmic membrane and the cell wall, the flagellar system harbors its own secretion machinery. This flagellar type III secretion system (fT3SS) shows high similarities to the central part of the injectisome found in some gram-negative bacteria, responsible for effector secretion into eukaryotic host cells (32). The fT3SS is located inside the cup-like structure of the C-ring and the central pore of the MS-ring (33).

Apart from the variations in number and placement of flagella, many species have adapted the bacterial motor corresponding to their environmental niches. The best studied flagellar motor is that of *Salmonella enterica* serovar typhimurium. Averaging multiple electron microscopy pictures revealed a three-dimensional model of the basal body (34). Recent developments in visualization techniques have allowed the comparison of a wide range of flagellar motors *in vivo* (35). Major differences were found in the width of the motor, ranging from 34 nm in *Caulocacter crescentus* to 57 nm in *Treponema primitia* (36). The absence of P- and L-ring structures in gram-positive bacteria is characteristic of species such as *Bacillus subtilis* (37). In spirochetes, the flagella reside within the periplasmic space (38).

Unlike the structural part of the flagellum, precisely, the mechanistic core containing the flagellar MS and C-ring, regulation of transcription and assembly of the flagellar differs significantly between different species.

1.3.3. Regulation of flagellar gene expression

In *E coli*, production of flagellar components consumes approximately 2% of the cellular energy provided for biosynthesis. Rotation demands additional 0.1% of the total energy (Macnab 1996). Due to this high metabolic cost and to coordinate assembly of the flagellar proteins, both transcription and assembly must be tightly regulated. In *E.coli* and *S. enterica*, flagellar genes are expressed in a three-tiered hierarchy. In class I genes, the master regulators FlhD and FlhC are expressed, likely dependent on the "housekeeping" sigma factor RpoD (σ^{70}) in response to a variety of environmental stimuli (39). Together, FlhDC activate the expression of class II genes (40), which encode for structural proteins of the basal body, including the MS-ring and the export apparatus. Along with the anti-sigma factor FlgM, the alternative sigma factor (σ^{28}) FliA (RpoF) is also expressed in this class, activating expression of class III genes (41). FlgM inhibits FliA-dependent transcription by directly binding to the sigma factor if present in the cytoplasm, once formation of the hook-basal body complex is complete, FlgM is secreted by the fT3SS, allowing the transcription of genes expressed in class III only after completion of the flagellar core structure (42). Proteins of this transcriptional tier are responsible for hook formation and the stator complexes. The flagellin protein - named FliC in *E. coli* and *S. enterica* - is also expressed in this final step of the transcriptional hierarchy (43, 44).

While the regulation cascade of *E.coli* serves as a paradigm for the regulation of flagellar gene expression, mechanisms of transcriptional control vary strongly outside of the group of enteric bacteria (45).

Due to their relevance as human pathogens, representatives of *Vibrio* or *Pseudomonas* species serve as model organisms for polar flagellar systems. In these bacteria, expression of a single polar flagellum is most likely organized in four transcriptional tiers (classes I to IV). The activator for each subsequent transcriptional level is expressed in the previous level. The role of flagellar master regulator is carried out by FleQ in *P. aeruginosa* (46) or its ortholog FlrA in *V. cholerae* (47). FlrA is expressed in class I and acts as a sigma factor 54 (σ^{54}/RpoN)-dependent enhancer binding protein. These group of proteins can form hexameric rings and usually bind up to 150 bp upstream of σ^{54}-dependent promotors where they initiate transcription in an ATP-dependent manner (48). FlrA activates expression of the regulators FlrB and FlrC, which function as a two-component system and are formed in class II. FlrB and FlrC control expression of basal body proteins in a σ^{54}-factor-dependent manner in class III. Expression of the flagellin proteins FlaA and FlaB are also under control of the σ^{28}-factor FliA in class IV. The sodium ion-dependent stator PomAB of *Vibrio* and the proton-dependent stator MotAB of *Pseudomonas* are also expressed in this class (45, 49). This hierarchical expression cascade should ensure that flagellar components are not expressed simultaneously but are sequentially assembled.

1.3.4. Flagellar Positioning and Assembly

The described secretory mechanism of the anti-sigma factor FlgM is only one example of the crosstalk between flagellar gene expression and assembly. While this mechanism is also present in polarly flagellated bacteria (47, 50), gene expression of earlier flagellar proteins is regulated by similar gene expression circuits linking flagellar positioning, transcription, and assembly.

The first step of flagellar assembly is the determination of the assembly site of the nascent flagellum. This can either be randomly achieved by "diffusion and capture" mechanisms or via landmark proteins similar to those previously discussed (26). In peritrichously flagellated *E. coli* and *S. enterica*, no exact determinants of flagellar placement and number have been identified so far. While flagellar number can vary drastically due to environmental stimuli acting on the expression of the FlhDC operon and other flagellar regulators (44), a sufficient amount of flagella distributed on the cell surface might not require the regulation of flagellar placement (26). However, in the gram-positive, peritrichously flagellated bacterium *B. subtilis*, basal bodies were found to be positioned symmetrically around mid-cell and missing at the cell pole. The SRP-like GTPase FlhF and MinD-like ATPase FlhG are involved in regulating this grid-like flagellation pattern (51).

Polar flagella may require more thorough regulation of flagellar placement than lateral flagella to ensure that both mother and daughter cells are flagellated (26). Due to its unique lifestyle comprising the development of a stalked cell and a flagellated swarmer cell, the cell cycle of *C. crescentus* has been extensively studied and multiple polar landmark proteins involved in flagella formation were identified. In swarmer cells, TipF was shown to be recruited to the cell pole by another polar landmark protein, the transmembrane protein TipN. This occurs in response to increasing levels of the second messenger cyclic diguanosine monophosphate (cdG), which is known to activate motility and inversely repress biofilm formation (52). TipF then recruits other factors as well as flagellar components to the cell pole (53).

In many other polarly flagellated bacteria, the proteins FlhF and FlhG are involved in the spatiotemporal regulation of flagella formation. Both flagellar landmark proteins also belong to the SIMIBI class (9). FlhF shares some homology with Ffh and FtsY, described above, though GTP-binding induces homodimerization, not heterodimerization, of FlhF (54). Since deletion of FlhF causes absent or delocalized flagella in various genera like *Vibrio* (55) and *Pseudomonas* (56), FlhF was thought to be responsible for regulating flagellar positioning. FlhF has an N-terminal B domain with putative regulatory function, a

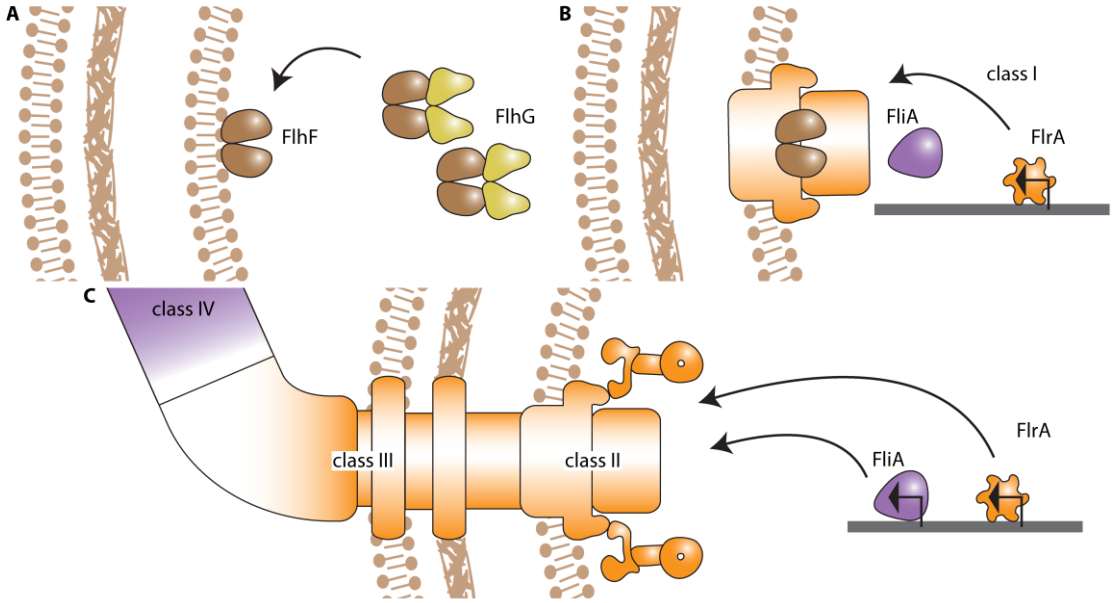

Fig. 3: Assembly of polar flagella in gamma-proteobacteria. (A) FlhF determinates the nascent flagellar assembly site. FlhG restricts FlhF polar localization. (B) FlrA, expressed in class I, activates transcription of the class II genes (orange). FlhF recruits early flagellar components to the cell pole. (C) The class III proteins (orange) are produced and incorporated in the flagellar basal body. FliA, expressed in class II activates the expression of the flagellin in class IV which are then secreted and assembled (violet).

central N domain required for polar localization of FlhF, and a C-terminal G domain responsible for GTPase activity and dimer formation (54, 57, 58).

When overexpressed, FlhF was shown to localize to the cell pole, independent of the master regulator FlrA and any FlrA-regulated flagellar proteins. Polar localization of FlhF is sufficient to target the integral constituent of the MS-ring, the membrane protein FliF, to the cell pole (58). However, it is unknown if FliF is inserted into the cytoplasmic membrane first or if it is preceded by proteins of the fT3SS (33, 59). Direct interactions between FlhF and any possible first flagellar components have not been identified so far.

In *Campylobacter jejuni*, *B. subtilis*, and *V. cholerae* FlhF interacts directly with FlhG (57, 60–62). If FlhG is missing, FlhF accumulates at the cell pole, promoting the formation of more flagella. This leads to a hyperflagellation phenotype observed in various organisms. Consequently, Kusumoto and colleagues concluded that FlhG prevents polar localization of FlhF and thereby restricting the polar flagellar number to one (57, 62). In addition, FlhF and FlhG were shown to influence transcription of flagellar proteins. Deletion of FlhG in *V. cholerae* or *P. aeruginosa* (termed FleN in the latter species) results in an upregulation of flagellar genes. In *P. aeruginosa*, this is facilitated by direct interaction of FleN with the activator FleQ (55, 63). In contrast, FlhF shows moderate negative regulation of the expression of certain

flagellar genes (55, 64). In summary, FlhF and FlhG together regulate flagellar gene transcription, positioning, and number.

Although the architecture of the C-ring is known, it remains unclear if the C-ring proteins FliM and FliN are assembled during or after MS-ring formation and whether assembly is sequential or occurs through the attachment of preassembled building blocks (33, 65). *B. subtilis* possesses a FliN-paralog, FliY. In addition to a FliN-like domain, FliY harbors a CheC-like domain. In *Helicobacter hepaticus*, *C. jejuni* and *Leptospira interrogans*, both FliN and FliY are present. The exact function of these additional C-ring components is unknown (Chen et al. 2011).

In *E.coli*, successful C-ring assembly is a crucial prerequisite for the secretion and assembly of the external components of the flagellum. It was shown that upregulation of the transcriptional master regulators FlhCD in *S. enterica* can bypass the requirement for subsequent flagellar type III secretion important for rod, hook and filament formation (66). After formation of the C-ring, cytoplasmic and inner membrane components of the fT3SS are assembled. Rod and PL-ring proteins are also secreted using the Sec II pathway and assembled. This leads to the formation of a pore in the outer membrane, enabling fT3SS-mediated secretion of hook-associated proteins, including the major hook protein FlgE. A ruler protein FliK is involved in measuring the length of the hook by a not entirely understood mechanism, causing a substrate specificity switch of the fT3SS. This enables secretion and assembly of the flagellin subunits and the cap protein FliD (32, 67). This sequential assembly process ensures correct arrangement of multiple components in different locations of the flagellar multi-protein complex.

1.3.5. Secondary Flagella Systems

Flagellar motility is responsible for moving bacteria between different habitats. These changing conditions requires mechanisms to adapt flagellar motility on multiple layers. The expression of an additional flagella set is one possible adaptation mechanism employed by many bacteria with a single polar flagellum. Functional secondary flagella are found in many *Vibrio* species like *V. alginolyticus* (68) and *V. parahaemolyticus* (69), in *Aeromonas* species (70, 71) or in *Rhodospirillum centenum* (72). Most of these additional flagellar systems are encoded in distinct gene clusters (73). Some strains of *E. coli*, *Yersinia pestis*, *Y. pseudotuberculosis*, and *Chromobacterium violaceum* also harbor such gene clusters, although they may be partly non-functional, indicating that these additional flagellar systems might be more common than previously suspected (74).

Most lateral flagella were shown to be induced upon surface contact and in medium with an increased viscosity (73). Peritrichous (or lateral) flagellation seems to support flagella-mediated swarming and swimming under these conditions (27). In *E.coli* and *S. enterica,* peritrichous flagella form bundles (75) and are important for the formation of rafts, made of "side-by-side groups" of swarming cells (27). Recent studies suggest that the rotation of flagella and secreted surfactin lead to increased hydration and reduced surface tension, which can promote swarming (76, 77). Although flagellar bundles do not seem to have increased torque compared to single flagella (78), peritrichous flagellation seems to be beneficial in viscous media (79), likely by decreasing the viscosity of the medium (80). Thus, polar flagella are sufficient for swimming in marine habitats (81) while lateral flagella are more beneficial for spreading and adhesion on host surfaces or on mucosal layers, as seen with certain fish and human pathogens (82, 83).

Induction of lateral flagella formation upon surface contact and changes in medium viscosity requires a sensory system which can react to mechanical changes. Among other mechanisms, the polar flagellum of *V. parahaemolyticus* was shown to act as a mechanosensor. Inhibition of motor function, such as by increasing flagellar rotation load in high-viscous medium or specific blockage of sodium ions fluxes in the polar stators, leads to induction of lateral flagellar gene expression (84). Polar motors are mostly propelled by a sodium ion-dependent stator complex, while the proton motive force is used by the stators of lateral flagellar systems. Inhibition of rotation by surface contact or high viscosity might cause changes in sodium ion fluxes, which are sensed by a yet unknown mechanism, and subsequently activate lateral flagellar gene expression (85, 86). Since transcription of lateral flagella is regulated in a hierarchical manner similar to other flagellar systems, the lateral flagellar master regulator LafK or $FlrA_2$ are likely to be involved (87).

As only few studies have been performed on lateral flagella action and transcriptional regulation of flagella induction, even less is known about the targeting of components of secondary flagellar system components to their respective assembly sites, assembly, or function in chemotaxis.

1.4. Chemotaxis

In addition to the long-term adaptation mechanisms involving transcriptional regulation of flagellar motility, the flagellar apparatus must respond quickly to changes in the environment to successfully direct the cell to more favorable destinations. The cytoplasmic C-ring of the flagellar motor is easily accessible to cytoplasmic effector proteins involved in chemotaxis, like the chemotaxis response regulator CheY. This allows the cell to bias its random movement in response to chemical gradients. Attractants like nutrients, and repellents, like toxins in the extracellular environment, are sensed by transmembrane chemoreceptor

proteins. These receptors, also called methyl-accepting chemotaxis proteins (MCPs), are organized to form large chemotaxis arrays. A core unit consist of different MCPs responding to various environmental stimuli and the histidine kinase CheA, which are connected by an associated adaptor protein CheW (88). The MCPs are constitutively methylated by the methyltransferase CheR, resulting in reduced sensitivity of the MCPs. Decreased binding of an attractant to the MCP due to low attractant concentrations leads to an increased autophosphorylation activity of CheA and subsequently increased phosphorylation of two other proteins, CheB and the chemotaxis response regulator CheY, by CheA. Dephosphorylation of CheY is enhanced by the phosphatase CheZ. The esterase CheB acts as an antagonist to CheR by hydrolyzing the methyl esters of the chemoreceptors, resulting in reduced CheA activity. This forms a feedback loop that allows the cell to efficiently respond to changes in the cellular environment (89–91). Phosphorylated CheY can bind to a conserved motif present at the N-terminus of the C-ring protein FliM, which belongs to the "motor switch complex" of the flagellar motor. Some models suggest that this interaction induces pivoting of FliM and results in a corresponding rotation of the C-terminus of FliG. These conformational changes at the interface between FliG and the stator subunit MotA lead to an inverted sense of rotation from a counter-clockwise (CCW) to a clockwise (CW) direction (65, 92).

In peritrichously flagellated bacteria, a CCW rotating bundle drives forward movement of the cell. Reversal of rotation of one or more flagella causes the cell to tumble and change its direction of swimming. Depending on the gradient of an attractant or repellent, the cell adapts the frequencies of tumbling and swimming. If environmental conditions become more favorable, swimming and tumbling frequencies decrease. The cell is, therefore, able to swim towards an attractant or away from a repellent (28, 93).

Monotrichously flagellated bacteria can use different mechanisms to reorient the cell. Brownian motion acts on the cell by randomly changing displacement and direction, especially close to surfaces (94). The single medial flagellum of *R. sphaeroides*, which only rotates unidirectionally in a CW direction, enables chemotaxis by short stops in rotation. During these stops, which are mediated by binding of multiple homologs of CheY to FliM, Brownian motion and relaxation of the helical filament is responsible for random reorientation of the cell (25, 95). Additionally, a three-step swimming pattern was discovered in polar flagellated *V. alginolyticus*, which is different from the run-tumble pattern of *E. coli*. In this model, the reversal of flagellar rotation causes a buckling instability of the hook after backward movement when the rotation switches from CW to CCW, causing the cell to change its swimming direction by a mean angle of about 90° (96, 97).

The formation of large aggregates with thousands of chemoreceptors and associated proteins was observed in *E. coli* (98, 99), *R. sphaeroides* (100) and polar flagellated cells like *C. crescentus* (101) and

other bacterial species (102). Interestingly, polar localization of the chemotaxis system occurs in many of these organisms independently of the flagellation pattern. In *E. coli*, the cell poles are non-flagellated but the rest of the old-pole half of the cell is equipped with more flagella than the other half. Therefore, the old cell pole of *E. coli* acts mostly as the lagging pole during swimming and was shown to exhibit a larger cluster of chemoreceptors than the leading pole (103). The formation of an average of 3.7 polar and lateral chemotaxis clusters per cell may occur by stochastic nucleation of new clusters and expansion of existing clusters. Anchoring at lateral positions before cell division occurs presumably via unknown intracellular structures. Likely, the curvature of the membrane or a special lipid composition leads to the accumulation of dynamic clusters at the rounded cell pole after cell division (104, 105).

In many polarly flagellated bacteria, landmark proteins are responsible for polar recruitment of chemosensory complexes, which are partly identified (105). In some species, the same mechanisms responsible for flagellar placement seem to be involved in localization of the chemotaxis machinery, like TipN and TipF in *C. crescentus* (106) and FlhF in *P. aeruginosa* (107). However, the relationship of flagellar positioning and localization of the chemotaxis system have not been studied in detail.

1.5. The dual flagellar system of *Shewanella putrefaciens* CN-32

As previously explained, some bacteria harbor multiple flagellar systems (73). Other bacteria possess multiple homologs of various chemotaxis proteins, like *R. centenum* (108), *V. cholerae* (109) and *R. sphaeroides* (110), some of which localize at the cell pole or in the cytoplasm (95, 111). In *R. sphaeroides* three of six CheY-homologs act on the single subpolar flagellum (fla1). The other three are responsible for chemotaxis mediated by the multiple polar flagella (fla2) (112). In *R. centenum*, the additional chemotaxis proteins seem to be involved only in transcriptional regulation of the polar and lateral flagella (108). In most other dual flagellated organisms, like *V. alginolyticus* (113) and *V. parahaemolyticus* (114), a single chemotaxis system acts on both flagellar systems.

While dual flagellation might be beneficial for pathogen motility, less is known about the function of such dual flagellar systems in marine or freshwater environments. Members of the genus *Shewanella*, a member of the gamma-proteobacteria, are present in a wide range of aquatic habitats (115). *Shewanella oneidensis* MR-1 was shown to carry two different sets of stators, one sodium ion-dependent and one proton-dependent, which can both be incorporated into the single polar flagellar motor (116, 117). Other representatives possess two complete flagellar systems, such as like *S. piezotolerans* WP3 (118) and *S. putrefaciens*. *S. putrefaciens* CN-32 harbors two flagellar systems encoded by two distinct gene clusters

located apart from each other on the bacterial chromosome. Cluster 1 encodes genes responsible for expression of a single polar flagellum; genes encoding the expression of multiple lateral flagella are found in cluster 2 (119). Interestingly, both systems were expressed also under planktonic conditions and not only, as previously reported for other secondary flagellar systems, in highly viscous medium or in swarming cells. Expression of the lateral MS-ring protein $FliF_2$ was significantly increased in complex medium compared to minimal medium, indicating nutrient-dependent regulation of lateral flagellar gene expression. Similar to *V. parahaemolyticus*, the sodium ion-dependent stator PomAB is used by the polar flagellar motor, whereas the lateral MotAB stator is proton-dependent. Other structural components were also shown to act specifically on their respective flagellar system. Both systems contributed to wt-like spreading in soft agar swim plates. However, cells lacking the lateral filament did not swim slower; in fact, they swan even slightly faster than the wt (119). These observations indicate that secondary flagella might have functions under planktonic conditions beyond the mechanisms previously observed in other dually flagellated organisms. Due to the variety of available genetic tools, *S. putrefaciens* can be used as a model organism to study the specificity of regulatory and structural components of the flagellar apparatus and the chemotaxis system. Since dual flagellation is an example of a highly compartmentalized process, analysis of the two flagellar systems will also improve our understanding of basic mechanisms of the spatial and numerical regulation of polar and lateral flagella in a single organism.

In this Ph.D. thesis, I aimed to address the following questions:

1.) What is the contribution of the polar and the additional lateral filament of *Shewanella putrefaciens* to motility under planktonic conditions?
2.) How are the position and number of the polar and lateral flagella determined?
3.) How is the position of the chemotaxis system in dual flagellated systems determined?

References

1. **Drubin DG**, **Nelson WJ**. 1996. Origins of Cell Polarity. Cell **84**:335–344.
2. **Chant J**. 1999. Cell polarity in yeast. Annu Rev Cell Dev Biol **15**:365–91.
3. **Nelson WJ**. 2003. Adaptation of core mechanisms to generate cell polarity. Nature **422**:766–74.
4. **Shapiro L**, **McAdams HH**, **Losick R**. 2009. Why and how bacteria localize proteins. Sci **326**:1225–1228.
5. **Laloux G**, **Jacobs-Wagner C**. 2014. How do bacteria localize proteins to the cell pole? J Cell Sci **127**:11–9.

6. **Bi EF**, **Lutkenhaus J**. 1991. FtsZ ring structure associated with division in *Escherichia coli*. Nature **354**:161–4.

7. **Treuner-Lange A**, **Søgaard-Andersen L**. 2014. Regulation of cell polarity in bacteria. J Cell Biol **206**:7–17.

8. **Bange G**, **Sinning I**. 2013. SIMIBI twins in protein targeting and localization. Nat Struct Mol Biol **20**:776–80.

9. **Leipe DD**, **Wolf YI**, **Koonin E V**, **Aravind L**. 2002. Classification and evolution of P-loop GTPases and related ATPases. J Mol Biol **317**:41–72.

10. **Harms A**, **Treuner-Lange A**, **Schumacher D**, **Søgaard-Andersen L**. 2013. Tracking of Chromosome and Replisome Dynamics in *Myxococcus xanthus* Reveals a Novel Chromosome Arrangement. PLoS Genet **9**:e1003802.

11. **Wang X**, **Rudner DZ**. 2014. Spatial organization of bacterial chromosomes. Curr Opin Microbiol **22**:66–72.

12. **Lutkenhaus J**, **Pichoff S**, **Du S**. 2012. Bacterial cytokinesis: From Z ring to divisome. Cytoskeleton. **69**:778-90

13. **Wu W**, **Park KT**, **Holyoak T**, **Lutkenhaus J**. 2011. Determination of the structure of the MinD-ATP complex reveals the orientation of MinD on the membrane and the relative location of the binding sites for MinE and MinC. Mol Microbiol **79**:1515–1528.

14. **Dajkovic A**, **Lan G**, **Sun SX**, **Wirtz D**, **Lutkenhaus J**. 2008. MinC Spatially Controls Bacterial Cytokinesis by Antagonizing the Scaffolding Function of FtsZ. Curr Biol **18**:235–244.

15. **Hu Z**, **Lutkenhaus J**. 2001. Topological Regulation of Cell Division in *E. coli*. Mol Cell **7**:1337–1343.

16. **Fu X**, **Shih Y-L**, **Zhang Y**, **Rothfield LI**. 2001. The MinE ring required for proper placement of the division site is a mobile structure that changes its cellular location during the *Escherichia coli* division cycle. Proc Natl Acad Sci **98**:980–985.

17. **Hale CA**, **Meinhardt H**, **De Boer PAJ**. 2001. Dynamic localization cycle of the cell division regulator MinE in *Escherichia coli*. EMBO J **20**:1563–1572.

18. **Akopian D**, **Shen K**, **Zhang X**, **Shan S**. 2013. Signal recognition particle: an essential protein-targeting machine. Annu Rev Biochem **82**:693–721.

19. **Eswaramoorthy P**, **Erb ML**, **Gregory JA**, **Silverman J**, **Pogliano K**, **Pogliano J**, **Ramamurthi KS**. 2011. Cellular architecture mediates DivIVA ultrastructure and regulates min activity in *Bacillus subtilis*. MBio **2**:00257-11-.

20. **Marston AL**, **Thomaides HB**, **Edwards DH**, **Sharpe ME**, **Errington J**. 1998. Polar localization of the MinD protein of *Bacillus subtilis* and its role in selection of the mid-cell division site. Genes Dev **12**:3419–3430.

21. **Jarrell KF**, **McBride MJ**. 2008. The surprisingly diverse ways that prokaryotes move. Nat Rev Microbiol **6**:466–476.

22. **Henrichsen J**. 1972. Bacterial surface translocation: a survey and a classification. Bacteriol Rev **36**:478–503.

23. **Lautrop H**. 1961. *Bacterium anitratum* transferred to the genus Cytophaga. Int Bull Bacteriol

Nomencl Taxon **11**:107–108.

24. **Burrows LL**. 2012. Twitching Motility: Type IV Pili in Action. Annu Rev Microbiol **66**:493–520.

25. **Armitage JP**, **Macnab RM**. 1987. Unidirectional, intermittent rotation of the flagellum of *Rhodobacter sphaeroides*. J Bacteriol **169**:514–518.

26. **Schuhmacher JS**, **Thormann KM**, **Bange G**. 2015. How bacteria maintain location and number of flagella? FEMS Microbiol Rev 39:812-22

27. **Kearns DB**. 2010. A field guide to bacterial swarming motility. Nat Rev Microbiol **8**:634–44.

28. **Berg HC**. 2003. The rotary motor of bacterial flagella. Annu Rev Biochem **72**:19–54.

29. **Sowa Y**, **Berry RM**. 2008. Bacterial flagellar motor. Q Rev Biophys **41**:103–132.

30. **Lloyd SA**, **Tang H**, **Wang X**, **Billings S**, **Blair DF**. 1996. Torque generation in the flagellar motor of *Escherichia coli*: Evidence of a direct role for FliG but not for FliM or FliN. J Bacteriol **178**:223–231.

31. **Zhou J**, **Lloyd SA**, **Blair DF**. 1998. Electrostatic interactions between rotor and stator in the bacterial flagellar motor. Proc Natl Acad Sci U S A **95**:6436–41.

32. **Diepold A**, **Armitage JP**. 2015. Type III secretion systems: the bacterial flagellum and the injectisome. Philos Trans R Soc B Biol Sci **370**:20150020.

33. **Altegoer F**, **Bange G**. 2015. Undiscovered regions on the molecular landscape of flagellar assembly. Curr Opin Microbiol **28**:98–105.

34. **Francis NR**, **Sosinsky GE**, **Thomas D**, **DeRosier DJ**. 1994. Isolation, characterization and structure of bacterial flagellar motors containing the switch complex. J Mol Biol **235**:1261-70

35. **Zhao X**, **Norris SJ**, **Liu J**. 2014. Molecular Architecture of Bacterial Flagellar Motor in Cells. Biochemistry **53**:4323-33

36. **Chen S**, **Beeby M**, **Murphy GE**, **Leadbetter JR**, **Hendrixson DR**, **Briegel A**, **Li Z**, **Shi J**, **Tocheva EI**, **Müller A**, **Dobro MJ**, **Jensen GJ**. 2011. Structural diversity of bacterial flagellar motors. EMBO J **30**:2972–2981.

37. **Kubori T**, **Okumura M**, **Kobayashi N**, **Nakamura D**, **Iwakura M**, **Aizawa S-I**. 1997. Purification and characterization of the flagellar hook-basal body complex of *Bacillus subtilis*. Mol Microbiol **24**:399–410.

38. **Li C**, **Motaleb A**, **Sal M**, **Goldstein SF**, **Charon NW**. 2000. Spirochete periplasmic flagella and motility. J Mol Microbiol Biotechnol **2**:345–54.

39. **Yanagihara S**, **Iyoda S**, **Ohnishi K**, **Iino T**, **Kutsukake K**. 1999. Structure and transcriptional control of the flagellar master operon of *Salmonella typhimurium*. Genes Genet Syst **74**:105–111.

40. **Kutsukake K**, **Ohya Y**, **Iino T**. 1990. Transcriptional analysis of the flagellar regulon of *Salmonella typhimurium*. J Bacteriol **172**:741–747.

41. **Ohnishi K**, **Kutsukake K**, **Suzuki H**, **Iino T**. 1990. Gene fliA encodes an alternative sigma factor specific for flagellar operons in *Salmonella typhimurium*. MGG Mol Gen Genet **221**:139–147.

42. **Hughes KT**, **Gillen KL**, **Semon MJ**, **Karlinsey JE**. 1993. Sensing structural intermediates in bacterial flagellar assembly by export of a negative regulator. Sci **262**:1277–1280.

43. **Soutourina OA**, **Bertin PN**. 2003. Regulation cascade of flagellar expression in Gram-negative bacteria. FEMS Microbiol Rev **27**: 505-23

44. **Fitzgerald DM**, **Bonocora RP**, **Wade JT**. 2014. Comprehensive mapping of the *Escherichia coli* flagellar regulatory network. PLoS Genet **10**:e1004649.

45. **McCarter LL**. 2006. Regulation of flagella. Curr Opin Microbiol **9**:180–186.

46. **Hickman JW**, **Harwood CS**. 2008. Identification of FleQ from *Pseudomonas aeruginosa* as a c-di-GMP-responsive transcription factor. Mol Microbiol **69**:376–389.

47. **Prouty MG**, **Correa NE**, **Klose KE**. 2001. The novel sigma54- and sigma28-dependent flagellar gene transcription hierarchy of Vibrio cholerae. Mol Microbiol **39**:1595–1609.

48. **Bush M**, **Dixon R**. 2012. The Role of Bacterial Enhancer Binding Proteins as Specialized Activators of 54-Dependent Transcription. Microbiol Mol Biol Rev **76**:497–529.

49. **Wilhelms M**, **Molero R**, **Shaw JG**, **Tomas JM**, **Merino S**. 2011. Transcriptional hierarchy of *Aeromonas hydrophila* polar-flagellum genes. J Bacteriol **193**:5179–5190.

50. **Starnbach MN**, **Lory S**. 1992. The fliA (rpoF) gene of *Pseudomonas aeruginosa* encodes an alternative sigma factor required for flagellin synthesis. Mol Microbiol **6**:459–469.

51. **Guttenplan SB**, **Shaw S**, **Kearns DB**. 2013. The cell biology of peritrichous flagella in *Bacillus subtilis*. Mol Microbiol **87**:211–229.

52. **Romling U**, **Galperin MY**, **Gomelsky M**. 2013. Cyclic di-GMP: the First 25 Years of a Universal Bacterial Second Messenger. Microbiol Mol Biol Rev **77**:1–52.

53. **Davis NJ**, **Cohen Y**, **Sanselicio S**, **Fumeaux C**, **Ozaki S**, **Luciano J**, **Guerrero-Ferreira RC**, **Wright ER**, **Jenal U**, **Viollier PH**. 2013. De- and repolarization mechanism of flagellar morphogenesis during a bacterial cell cycle. Genes Dev **27**:2049–62.

54. **Bange G**, **Petzold G**, **Wild K**, **Parlitz RO**, **Sinning I**. 2007. The crystal structure of the third signal-recognition particle GTPase FlhF reveals a homodimer with bound GTP. Proc Natl Acad Sci U S A **104**:13621–13625.

55. **Correa NE**, **Peng F**, **Klose KE**. 2005. Roles of the regulatory proteins FlhF and FlhG in the *Vibrio cholerae* flagellar transcription hierarchy. J Bacteriol **187**:6324–6332.

56. **Murray TS**, **Kazmierczak BI**. 2006. FlhF is required for swimming and swarming in *Pseudomonas aeruginosa*. J Bacteriol **188**:6995–7004.

57. **Kazmierczak BI**, **Hendrixson DR**. 2013. Spatial and numerical regulation of flagellar biosynthesis in polarly flagellated bacteria. Mol Microbiol **88**:655–663.

58. **Green JC**, **Kahramanoglou C**, **Rahman A**, **Pender AM**, **Charbonnel N**, **Fraser GM**. 2009. Recruitment of the earliest component of the bacterial flagellum to the old cell division pole by a membrane-associated signal recognition particle family GTP-binding protein. J Mol Biol **391**:679–690.

59. **Li H**, **Sourjik V**. 2011. Assembly and stability of flagellar motor in *Escherichia coli*. Mol Microbiol **80**:886–899.

60. **Parrish JR**, **Yu J**, **Liu G**, **Hines JA**, **Chan JE**, **Mangiola BA**, **Zhang H**, **Pacifico S**, **Fotouhi F**, **DiRita VJ**, **Ideker T**, **Andrews P**, **Finley RL**. 2007. A proteome-wide protein interaction map for *Campylobacter jejuni*. Genome Biol **8**:R130.

61. **Bange G**, **Kummerer N**, **Grudnik P**, **Lindner R**, **Petzold G**, **Kressler D**, **Hurt E**, **Wild K**, **Sinning I**. 2011. Structural basis for the molecular evolution of SRP-GTPase activation by protein. Nat Struct Mol Biol **18**:1376–1380.

62. **Kusumoto A**, **Shinohara A**, **Terashima H**, **Kojima S**, **Yakushi T**, **Homma M**. 2008. Collaboration of FlhF and FlhG to regulate polar-flagella number and localization in *Vibrio alginolyticus*. Microbiology **154**:1390–1399.

63. **Dasgupta N**, **Arora SK**, **Ramphal R**. 2000. fleN, a gene that regulates flagellar number in *Pseudomonas aeruginosa*. J Bacteriol **182**:357–364.

64. **Balaban M**, **Joslin SN**, **Hendrixson DR**. 2009. FlhF and its GTPase activity are required for distinct processes in flagellar gene regulation and biosynthesis in *Campylobacter jejuni*. J Bacteriol **191**:6602–6611.

65. **Stock D**, **Namba K**, **Lee LK**. 2012. Nanorotors and self-assembling macromolecular machines: The torque ring of the bacterial flagellar motor. Curr Opin Biotechnol **23**:545–554.

66. **Erhardt M**, **Hughes KT**. 2010. C-ring requirement in flagellar type III secretion is bypassed by FlhDC upregulation. Mol Microbiol **75**:376–393.

67. **Cohen EJ**, **Hughes KT**. 2014. Rod-to-Hook transition for extracellular flagellum assembly is catalyzed by the L-ring-dependent rod scaffold removal. J Bacteriol **196**:2387–2395.

68. **Ulitzer S**. 1975. The mechanism of swarming of *Vibrio alginolyticu*s. Arch Microbiol **104**:67–71.

69. **Shinoda S**, **Okamoto K**. 1977. Formation and function of *Vibrio parahaemolyticus* lateral flagella. J Bacteriol **129**:1266–1271.

70. **Kirov SM**, **Tassell BC**, **Semmler AB**, **O'Donovan LA**, **Rabaan AA**, **Shaw JG**. 2002. Lateral flagella and swarming motility in *Aeromonas* species. J Bacteriol **184**:547–555.

71. **Shimada T**, **Sakazaki R**, **Suzuki K**. 1985. Peritrichous flagella in mesophilic strains of *Aeromonas*. Jpn J Med Sci Biol **38**:141–5.

72. **Ragatz L**, **Jiang ZY**, **Bauer CE**, **Gest H**. 1995. Macroscopic phototactic behavior of the purple photosynthetic bacterium *Rhodospirillum centenum*. Arch Microbiol **163**:1–6.

73. **Merino S**, **Shaw JG**, **Tomás JM**. 2006. Bacterial lateral flagella: An inducible flagella system. FEMS Microbiol Lett **263**:127–135.

74. **Ren C-P**, **Beatson SA**, **Parkhill J**, **Pallen MJ**. 2005. The Flag-2 locus, an ancestral gene cluster, is potentially associated with a novel flagellar system from *Escherichia coli*. J Bacteriol **187**:1430–40.

75. **Berg HC**. 2003. The rotary motor of bacterial flagella. Annu Rev Biochem **72**:19–54.

76. **Ke W-J**, **Hsueh Y-H**, **Cheng Y-C**, **Wu C-C**, **Liu S-T**. 2015. Water surface tension modulates the swarming mechanics of *Bacillus subtilis*. Front Microbiol **6**:1017.

77. **Partridge JD**, **Harshey RM**. 2013. More than motility: *Salmonella* flagella contribute to overriding friction and facilitating colony hydration during swarming. J Bacteriol **195**:919–929.

78. **Darnton NC**, **Turner L**, **Rojevsky S**, **Berg HC**. 2007. On torque and tumbling in swimming *Escherichia coli*. J Bacteriol **189**:1756–1764.

79. **Atsumi T**, **Maekawa Y**, **Yamada T**, **Kawagishi I**, **Imae Y**, **Homma M**. 1996. Effect of viscosity on

swimming by the lateral and polar flagella of *Vibrio alginolyticus*. J Bacteriol **178**:5024–5026.

80. **López HM**, **Gachelin J**, **Douarche C**, **Auradou H**, **Cl??ment E**. 2015. Turning Bacteria Suspensions into Superfluids. Phys Rev Lett **115**.

81. **Minamino T**, **Imada K**. 2015. The bacterial flagellar motor and its structural diversity. Trends Microbiol.

82. **Kirov SM**, **Castrisios M**, **Shaw JG**. 2004. *Aeromonas* flagella (polar and lateral) are enterocyte adhesins that contribute to biofilm formation on surfaces. Infect Immun **72**:1939–1945.

83. **Zhu S**, **Kojima S**, **Homma M**. 2013. Structure, gene regulation and environmental response of flagella in *Vibrio*. Front Microbiol **4**:410.

84. **Kawagishi I**, **Imagawa M**, **Imae Y**, **McCarter L**, **Homma M**. 1996. The sodium-driven polar flagellar motor of marine *Vibrio* as the mechanosensor that regulates lateral flagellar expression. Mol Microbiol **20**:693–699.

85. **Belas R**. 2014. Biofilms, flagella, and mechanosensing of surfaces by bacteria. Trends Microbiol **22**:517–27.

86. **McCarter LL**. 2004. Dual flagellar systems enable motility under different circumstances. J Mol Microbiol Biotechnol **7**:18–29.

87. **Wilhelms M**, **Gonzalez V**, **Tomas JM**, **Merino S**. 2013. *Aeromonas hydrophila* Lateral Flagellar Gene Transcriptional Hierarchy. J Bacteriol **195**:1436–1445.

88. **Li M**, **Hazelbauer GL**. 2011. Core unit of chemotaxis signaling complexes. Proc Natl Acad Sci **108**:9390–9395.

89. **Porter SL**, **Wadhams GH**, **Armitage JP**. 2011. Signal processing in complex chemotaxis pathways. Nat Rev Microbiol **9**:153–165.

90. **Wadhams GH**, **Armitage JP**. 2004. Making sense of it all: Bacterial chemotaxis. Nat Rev Mol Cell Biol **5**:1024–1037.

91. **Baker MD**, **Wolanin PM**, **Stock JB**. 2006. Signal transduction in bacterial chemotaxis. Bioessays **28**:9–22.

92. **Bren a**, **Eisenbach M**. 1998. The N terminus of the flagellar switch protein, FliM, is the binding domain for the chemotactic response regulator, CheY. J Mol Biol **278**:507–14.

93. **Berg HC**. 2004. E. Coli in Motion. Book, Springer.

94. **Li G**, **Tam LK**, **Tang JX**. 2008. Amplified effect of Brownian motion in bacterial near-surface swimming. Proc Natl Acad Sci U S A2008/11/19. **105**:18355–18359.

95. **Porter SL**, **Wadhams GH**, **Armitage JP**. 2008. Rhodobacter sphaeroides: complexity in chemotactic signalling. Trends Microbiol.

96. **Son K**, **Guasto JS**, **Stocker R**. 2013. Bacteria can exploit a flagellar buckling instability to change direction. Nat Phys **9**:494–498.

97. **Xie L**, **Altindal T**, **Chattopadhyay S**, **Wu XL**. 2011. Bacterial flagellum as a propeller and as a rudder for efficient chemotaxis. Proc Natl Acad Sci U S A **108**:2246–2251.

98. **Maddock JR**, **Shapiro L**. 1993. Polar location of the chemoreceptor complex in the Escherichia coli

cell. Science **259**:1717–1723.

99. **Sourjik V**, **Berg HC**. 2000. Localization of components of the chemotaxis machinery of Escherichia coli using fluorescent protein fusions. Mol Microbiol **37**:740–751.

100. **Wadhams GH**, **Martin AC**, **Warren A V**, **Armitage JP**. 2005. Requirements for chemotaxis protein localization in Rhodobacter sphaeroides. Mol Microbiol **58**:895–902.

101. **Briegel A**, **Li Z**, **Werner J**, **Gitai Z**, **Jensen RB**, **Jensen GJ**. 2008. Location and architecture of the Caulobacter crescentus chemoreceptor array. Mol Microbiol **69**:30–41.

102. **Briegel A**, **Ortega DR**, **Tocheva EI**, **Wuichet K**, **Li Z**, **Chen S**, **Müller A**, **Iancu C V**, **Murphy GE**, **Dobro MJ**, **Zhulin IB**, **Jensen GJ**. 2009. Universal architecture of bacterial chemoreceptor arrays. Proc Natl Acad Sci U S A **106**:17181–6.

103. **Ping L**. 2010. The asymmetric flagellar distribution and motility of Escherichia coli. J Mol Biol **397**:906–916.

104. **Thiem S**, **Sourjik V**. 2008. Stochastic assembly of chemoreceptor clusters in Escherichia coli. Mol Microbiol **68**:1228–36.

105. **Jones CW**, **Armitage JP**. 2015. Positioning of bacterial chemoreceptors. Trends Microbiol **23**:247–256.

106. **Huitema E**, **Pritchard S**, **Matteson D**, **Radhakrishnan SK**, **Viollier PH**. 2006. Bacterial birth scar proteins mark future flagellum assembly site. Cell **124**:1025–37.

107. **Kulasekara BR**, **Kamischke C**, **Kulasekara HD**, **Christen M**, **Wiggins PA**, **Miller SI**. 2013. c-di-GMP heterogeneity is generated by the chemotaxis machinery to regulate flagellar motility. Elife **2**.

108. **Berleman JE**, **Bauer CE**. 2005. A che-like signal transduction cascade involved in controlling flagella biosynthesis in *Rhodospirillum centenum*. Mol Microbiol **55**:1390–1402.

109. **Boin MA**, **Austin MJ**, **Häse CC**. 2004. Chemotaxis in *Vibrio cholerae*. FEMS Microbiol Lett **239**:1–8.

110. **Hamblin P a**, **Maguire B a**, **Grishanin RN**, **Armitage JP**. 1997. Evidence for two chemosensory pathways in *Rhodobacter sphaeroides*. Mol Microbiol **26**:1083–1096.

111. **Ringgaard S**, **Hubbard T**, **Mandlik A**, **Davis BM**, **Waldor MK**. 2015. RpoS and quorum sensing control expression and polar localization of *Vibrio cholerae* chemotaxis cluster III proteins in vitro and in vivo. Mol Microbiol **97**:660–75.

112. **Del Campo AM**, **Ballado T**, **De La Mora J**, **Poggio S**, **Camarena L**, **Dreyfus G**. 2007. Chemotactic control of the two flagellar systems of *Rhodobacter sphaeroides* is mediated by different sets of CheY and FliM proteins. J Bacteriol **189**:8397–8401.

113. **Kojima M**, **Kubo R**, **Yakushi T**, **Homma M**, **Kawagishi I**. 2007. The bidirectional polar and unidirectional lateral flagellar motors of *Vibrio alginolyticus* are controlled by a single CheY species. Mol Microbiol **64**:57–67.

114. **Sar N**, **McCarter L**, **Simon M**, **Silverman M**. 1990. Chemotactic control of the two flagellar systems of *Vibrio parahaemolyticus*. J Bacteriol **172**:334–341.

115. **Hau HH**, **Gralnick JA**. 2007. Ecology and biotechnology of the genus *Shewanella*. Annu Rev Microbiol **61**:237–258.

116. **Paulick A**, **Delalez NJ**, **Brenzinger S**, **Steel BC**, **Berry RM**, **Armitage JP**, **Thormann KM**. 2015. Dual stator dynamics in the *Shewanella oneidensis* MR-1 flagellar motor. Mol Microbiol **96**:993–1001.

117. **Paulick A**, **Koerdt A**, **Lassak J**, **Huntley S**, **Wilms I**, **Narberhaus F**, **Thormann KM**. 2009. Two different stator systems drive a single polar flagellum in *Shewanella oneidensis* MR-1. Mol Microbiol **71**:836–850.

118. **Wang F**, **Wang J**, **Jian H**, **Zhang B**, **Li S**, **Wang F**, **Zeng X**, **Gao L**, **Bartlett DH**, **Yu J**, **Hu S**, **Xiao X**. 2008. Environmental adaptation: genomic analysis of the piezotolerant and psychrotolerant deep-sea iron reducing bacterium *Shewanella piezotolerans* WP3. PLoS One **3**:e1937.

119. **Bubendorfer S**, **Held S**, **Windel N**, **Paulick A**, **Klingl A**, **Thormann KM**. 2012. Specificity of motor components in the dual flagellar system of *Shewanella putrefaciens* CN-32. Mol Microbiol **83**:335–350.

120. **Schuhmacher JS**, **Rossmann F**, **Dempwolff F**, **Knauer C**, **Altegoer F**, **Steinchen W**, **Dörrich AK**, **Klingl A**, **Stephan M**, **Linne U**, **Thormann KM**, **Bange G**. 2015. MinD-like ATPase FlhG effects location and number of bacterial flagella during C-ring assembly. Proc Natl Acad Sci U S A **112**:3092–3097.

Contributions to publications

Chapter 2:

Secondary bacterial flagellar system improves bacterial spreading by increasing the directional persistence of swimming.

Sebastian Bubendorfer was responsible for the generation of the mutant strains lacking the polar and lateral filament, the CheY mutants and various fluorescence-marked strains. He also performed the racing experiments and motility assays and acquired the fluorescence microscopy pictures. Mihaly Koltai performed the numerical simulations of the swimming cells and generated a chemotaxis model. Florian Roßmann was responsible for overexpression and purification of CheY and the subsequent generation of an anti-CheY antibody. Furthermore, he acquired the trajectories of the swimming cells and calculated the turning angle distribution. Sebastian Bubendorfer, Mihaly Koltai, Victor Sourjik and Kai Thormann designed the research. Sebastian Bubendorfer, Mihaly Koltai, Florian Roßmann, Victor Sourjik and Kai Thormann analyzed the data. Sebastian Bubendorfer, Mihaly Koltai, Victor Sourjik and Kai Thormann wrote the manuscript.

Chapter 3:

MinD-like ATPase FlhG effects location and number of bacterial flagella during C-ring assembly

Jan Schuhmacher, Uwe Linne, Carina Knauer, Florian Altegoer and Wieland Steinchen generated mutant strains of *B subtilis*, performed protein purification, biochemical characterization and crystallization of FlhG. Florian Roßmann generated the FlhG mutant strains of *S. putrefaciens*, performed fluorescence microscopy, generated the FlhG antibody and prepared the samples for transmission electron microscopy. Felix Dempwolff performed fluorescence microscopy of *B subtilis*. Anja Dörrich generated the *S. putrefaciens* FliM ΔEIDAL mutant and performed fluorescence microscopy. Andreas Klingl performed transmission electron microscopy. Jan Schuhmacher, Florian Roßmann, Milena Stephan, Gert Bange and Kai Thormann designed the research. Jan Schuhmacher, Florian Roßmann, Felix Dempwolff, Andreas Klingl, Uwe Linne, Gert Bange and Kai Thormann analyzed the data. Jan Schuhmacher, Gert Bange and Kai Thormann wrote the manuscript.

Chapter 4:

The role of FlhF and HubP as polar landmark proteins in *Shewanella putrefaciens* CN-32

Florian Roßmann generated the FlhF and HubP mutant strains. He established the flagella fluorescence maleimide staining technique. He performed fluorescence microscopy-based localization studies of HubP, FlhF, various chemotaxis components and the polar filaments. He also generated the FlhF antibody. Susanne Brenzinger localized the chemotaxis components and the chromosome partitioning system, analyzed the swimming and twitching motility and performed FRAP (fluorescence recovery after photobleaching). Anja Dörrich generated the ZapA fluorescent fusion. Sebastian Bubendorfer was involved in generation of the flagellin substitution mutants and the fluorescent fusion of the MCPs (methyl accepting proteins). Ulrike Ruppert was involved in strain generation under supervision of Florian Roßmann. Florian Roßmann, Susanne Brenzinger, Gert Bange and Kai Thormann designed the research. Florian Roßmann, Susanne Brenzinger, Carina Knauer, Gert Bange and Kai Thormann analyzed the data. Florian Roßmann, Susanne Brenzinger, Carina Knauer, Gert Bange and Kai Thormann wrote the manuscript.

Chapter 2:

Secondary bacterial flagellar system improves bacterial spreading by increasing the directional persistence of swimming.

published in Proceedings of the National Academy of Sciences of the United States of America

Secondary bacterial flagellar system improves bacterial spreading by increasing the directional persistence of swimming

Sebastian Bubendorfer[a,b,c,1], Mihaly Koltai[a,d,1], Florian Rossmann[a,b], Victor Sourjik[a,d], and Kai M. Thormann[a,b,2]

[a]Max Planck Institute for Terrestrial Microbiology and LOEWE Research Center for Synthetic Microbiology (SYNMICRO), 35043 Marburg, Germany; [b]Institute for Microbiology and Molecular Biology, IFZ Interdisciplinary Research Centre, Justus Liebig University Giessen, 35392 Giessen, Germany; [c]Institute for Medical Microbiology and Hospital Epidemiology, Hannover Medical School, 30625 Hannover, Germany; and [d]Zentrum für Molekulare Biologie der Universität Heidelberg, DKFZ-ZMBH Alliance, 69120 Heidelberg, Germany

Edited by Caroline S. Harwood, University of Washington, Seattle, WA, and approved June 29, 2014 (received for review March 28, 2014)

As numerous bacterial species, *Shewanella putrefaciens* CN-32 possesses a complete secondary flagellar system. A significant subpopulation of CN-32 cells induces expression of the secondary system under planktonic conditions, resulting in formation of one, sometimes two, filaments at lateral positions in addition to the primary polar flagellum. Mutant analysis revealed that the single chemotaxis system primarily or even exclusively addresses the main polar flagellar system. Cells with secondary filaments outperformed their monopolarly flagellated counterparts in spreading on soft-agar plates and through medium-filled channels despite having lower swimming speed. While mutant cells with only polar flagella navigate by a "run-reverse-flick" mechanism resulting in effective cell realignments of about 90°, wild-type cells with secondary filaments exhibited a range of realignment angles with an average value of smaller than 90°. Mathematical modeling and computer simulations demonstrated that the smaller realignment angle of wild-type cells results in the higher directional persistence, increasing spreading efficiency both with and without a chemical gradient. Taken together, we propose that in *S. putrefaciens* CN-32, cell propulsion and directional switches are mainly mediated by the polar flagellar system, while the secondary filament increases the directional persistence of swimming and thus of spreading in the environment.

bacterial motility | cell reorientation | CheY | lateral flagella

The ability to actively explore and exploit the environment provides a major advantage for all kinds of organisms, including bacteria (1, 2). Among bacteria, flagella are common and efficient organelles of locomotion that consist of long, helical, proteinaceous filaments extending from the cell's surface and are rotated by a membrane-embedded motor to which they are attached by the flexible hook structure. The majority of flagellar motors function in a bidirectional fashion and can rotate either counterclockwise (CCW) or clockwise (CW) (3, 4). Most bacterial species navigate using a random walk that originates from an alternation of straight runs and cell reorientations. In the absence of gradients, such random walk results in a uniform spreading in the environment. In gradients of environmental stimuli, bacterial random walk becomes biased, whereby cells use temporal comparisons of the stimulus strength to suppress reorientations while swimming in a favorable direction. This behavior is controlled by one or more chemotaxis systems, which transduce environmental stimuli to control flagellar motors (5). Signals perceived by an array of sensor proteins are converted into the phosphorylation state of a soluble signal-transmitting protein, CheY. Phosphorylated CheY can directly interact with the flagellar motor and induce a switch in rotation or a motor break. In peritrichously flagellated bacteria with several filaments, such as the paradigm system of *Escherichia coli*, CCW rotation leads to formation of a flagellar bundle that drives the cell run. A switch to CW rotation of one or several motors is followed by disassembly of the bundle, leading to reorientation of the cell ("tumble") and a change in the swimming direction upon resuming CCW rotation of flagella (6, 7). However, numerous bacterial species are polarly flagellated, which results in a pattern of swimming that is different from that of *E. coli*. Recent studies on *Vibrio alginolyticus* that swims using single polar flagellar filament demonstrated that the filament drives the cell forward when rotating CCW but pulls the cells backward when switching to CW rotation. Cell reorientation occurs through rapid cell realignment ("flick"), which is mediated through a buckling instability of the flagellar hook upon resuming CCW rotation. The "run-reverse-flick" realignment occurs in an angle of about 90° and allows efficient spreading and chemotaxis of *Vibrio* and likely also *Pseudomonas* species (8–10).

In addition to a primary polar flagellar system, a number of bacterial species, including *Aeromonas*, *Azospirillum*, *Rhodobacter*, *Shewanella*, or *Vibrio* spp., possess a distinct secondary flagellar system (11, 12). Several previous studies have provided evidence that this secondary system is induced under conditions of increased viscosity or on surfaces, leading to the formation of numerous lateral flagella. For *Vibrio* species, a single polar filament is advantageous for rapid swimming under planktonic conditions, while the lateral set of flagella provides superior performance for swarming or for swimming under viscous conditions (13, 14). We

Significance

Flagella-mediated motility is an important or even crucial propagation factor for many bacteria. A number of polarly flagellated species possess a distinct secondary flagellar system, which, as current models suggest, allows more effective swimming under conditions of elevated viscosity or across surfaces. In this study, we demonstrate that such a secondary flagellar system may also exert beneficial effects in bacterial spreading by increasing the directional persistence through lowering the cellular turning angles. The strategy of increasing directional persistence to improve animal spreading efficiency has been proposed previously by theoretical modeling, and here we provide a specific example of how this strategy is used by bacteria.

Author contributions: S.B., M.K., V.S., and K.M.T. designed research; S.B., M.K., and F.R. performed research; S.B., M.K., F.R., V.S., and K.M.T. analyzed data; and S.B., M.K., V.S., and K.M.T. wrote the paper.

The authors declare no conflict of interest.

This article is a PNAS Direct Submission.

Freely available online through the PNAS open access option.

[1]S.B. and M.K. contributed equally to this work.

[2]To whom correspondence should be addressed. Email: Kai.Thormann@mikro.bio.uni-giessen.de.

This article contains supporting information online at www.pnas.org/lookup/suppl/doi:10.1073/pnas.1405820111/-/DCSupplemental.

have recently demonstrated that cells of the species *Shewanella putrefaciens* CN-32 possess a functional secondary system that is highly homologous to those identified in *Aeromonas hydrophila* and *Vibrio* sp. (15). Notably, we observed that, in a significant fraction of the cells, the secondary flagellar system is already induced under planktonic conditions in complex media, leading to the formation of a single or sometimes two additional filament (s) at a lateral position at the cell's surface. Here, we show that these additional filaments function in enhancing efficient spreading and chemotaxis of the cells by increasing the directional persistence.

Results

Swimming Cells with Secondary Filaments Spread Faster than Cells with Polar Flagella only. Our previous experiments strongly indicated that CN-32 cells possessing a secondary flagellar system cover significantly larger distances in soft agar plates than cells with polar flagella only (15). To further elucidate a potential beneficial role of additional flagellar filaments in efficient spreading, we analyzed expression and production of the secondary flagellar systems within the population. To this end, we used a strain in which the flagellar motor protein $FliM_2$, a component only occurring in flagellar basal bodies of the lateral secondary system, was functionally fused to sfGFP. Cells producing the $FliM_2$-sfGFP fusion protein were placed on soft-agar plates, and after formation of a visible halo caused by radial expansion of the bacterial population, samples were taken from the lateral extension zone with increasing distance to the center (Fig. 1). Expression and localization of $FliM_2$-sfGFP was determined by fluorescence microscopy. Close to the center of the lateral extension zone, about 50% of sampled cells displayed green fluorescent foci at various lateral positions within the cell. This portion of $FliM_2$-sfGFP-producing cells was similar to that observed in planktonic cultures. In contrast, all cells isolated from the fringes of the swimming halos were found to produce $FliM_2$-sfGFP with three fluorescent foci on average at various lateral positions. Flagellar staining revealed that these cells possessed one or sometimes two additional filaments (Fig. S1), and the additional $FliM_2$-sfGFP foci likely represented incomplete secondary flagellar complexes.

In a complementary approach using soft-agar plates, we directly compared the spreading performance of CN-32 cells with or without functional secondary flagella. To this end, we constructed a strain in which we deleted the genes encoding the flagellin subunits of the secondary flagellar system, $flaA_2$ and $flaB_2$. Flagellar staining and subsequent microscopy revealed that $\Delta flaAB_2$ cells exclusively formed single polar flagellar filaments. Growth and the percentage of swimming cells of both strains were almost identical. To enable discrimination between wild-type and $\Delta flaAB_2$ cells by fluorescence microscopy, both strains were fluorescently tagged by chromosomal integration of constitutively expressed *gfp* or *mCherry*. Then 1:1 mixtures of exponentially growing GFP/mCherry-producing mutant and wild-type cells were allowed to spread in soft agar for 16 h. Samples were taken at different distances from the center of the radial extension zone, and the ratio of the wild-type and mutant cells was quantified by fluorescence microscopy (Fig. 1). We observed that the larger the distance relative to the center of the lateral extension zone which was covered by the cells, the further the ratio of both strains was shifted toward the wild type. At the fringes of the swimming zones, more than 90% of the population consisted of wild-type cells. Filament staining and microscopy revealed that the vast majority of the cells in the sample from the outer rim possessed a single lateral filament in addition to the primary polar one (Fig. S1).

To further determine whether the observed advantage of cells with a secondary flagellar system is not restricted to conditions occurring in soft-agar plates, we conducted a similar spreading competition experiment using chambers that consist of two reservoirs connected by a channel. One reservoir was inoculated with a 1:1 mixture of GFP/mCherry-producing wild-type and $\Delta flaAB_2$ cells. After 12 h of incubation, samples were taken from

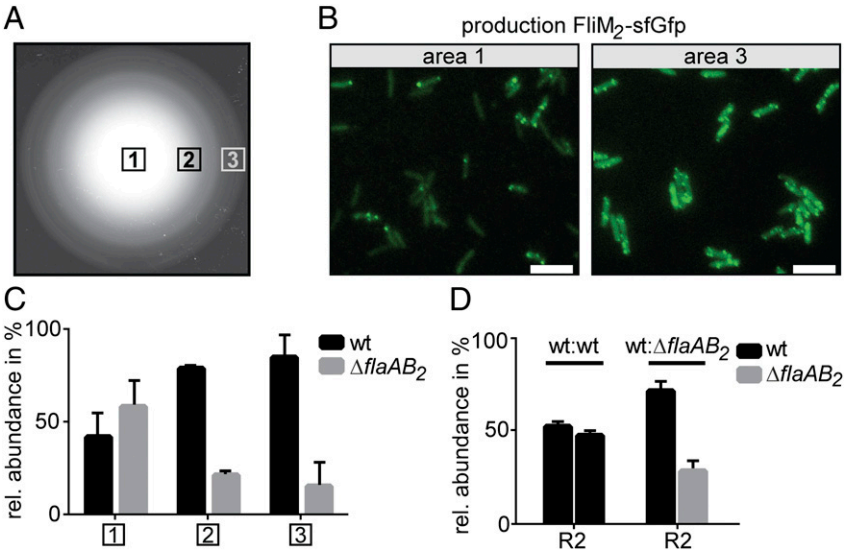

Fig. 1. Cells with synchronously functional polar and lateral flagellar systems outperform mutants with polar flagella only in both soft-agar and liquid medium. (*A*) Representation of CN-32 cells' radial extension in soft agar (0.25%); 3 μL of exponentially growing cultures of the corresponding strains were allowed to spread for 16 h. Numbers in boxes mark the corresponding sampling areas (1, center; 2, intermediate; 3, rim). (*B*) Micrographs of CN-32 *fliM2-sfgfp* cells isolated from sampling area 1 (*Left*) and sampling area 3 (*Right*). Scale bars represent 5 μm. (*C*) Percentage of fluorescently labeled wild-type and $\Delta flaAB_2$-mutant cells in samples isolated from the corresponding sampling areas; 1:1 mixtures of mCherry-labeled wild type and Gfp-labeled mutant (and vice versa) were used to inoculate the plate. (*D*) Percentage of fluorescently labeled wild-type and $\Delta flaAB_2$-mutant cells after traveling from reservoir 1 (R1) to reservoir 2 (R2) through a medium-filled channel. R1 was seeded with 1:1 mixtures of the wild type, and wild type and mutant, respectively, and incubated for 16 h. The error bars represent SDs from at least three samples out of two independent experiments each.

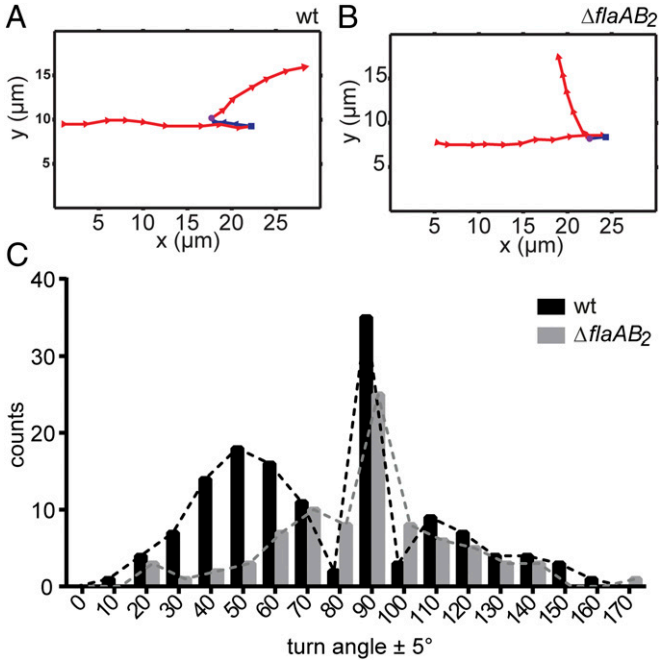

Fig. 2. The presence of a lateral filament affects the trajectories of swimming cells. A representative trajectory is displayed for the wild-type (*A*) and the Δ*flaAB*$_2$ mutant (*B*), demonstrating a typical forward run (red triangles), reversal (blue square), short backward run (blue triangles), flick (purple circle), and forward run movement. The time between each trajectory point equals 0.07 s. (*C*) Turning angle distribution of wild-type (black) and Δ*flaAB*$_2$-mutant (gray) cells.

the second reservoir, and fluorescence microscopy and flagellar staining were applied to dissect the population of cells that had traveled through the channels. Similar to the observations in soft-agar plates, the resulting population was significantly enriched in wild-type cells with a single additional lateral filament (Fig. 1).

The Presence of Lateral Flagella Affects the Directional Changes. The results of the competition experiments demonstrated that the presence of one or two additional secondary flagellar filaments enhances spreading of CN-32 cells. Preliminary experiments have demonstrated that the presence of the secondary system does not provide an increase in swimming speed (15). To determine whether this is also the case for cells that have covered the greatest distance in soft agar, we determined the swimming speeds of Δ*flaAB*$_2$ and wild-type cells that were isolated from the fringes of the swimming halos formed on soft-agar plates (Fig. S2). The population of wild-type cells with additional lateral filaments had a velocity of 46.95 ± 14.52 μm·s^{-1} and were significantly slower than Δ*flaAB*$_2$ cells which exhibited swimming speeds of 57.30 ± 17.18 μm·s^{-1}. Thus, an increase in velocity could be excluded as the reason for the beneficial role of the secondary flagellar system in swimming motility. However, while recording cell trajectories for measuring swimming speeds, we noticed that cells with lateral flagellar filaments exhibited marked differences in their movement patterns compared with cells with polar filaments only. Cells with single polar flagella periodically (about 10 s) switched from forward to backward swimming. Under the conditions tested, the time interval for backtracking was short (0.3 s), in which time the cells covered less than 5 μm distance. Upon resuming forward movement, quick cellular realignments occurred at a range of angles that centered at 90° (Fig. 2). Thus, swimming of monopolarly flagellated *S. putrefaciens* CN-32 cells apparently follows the "forward-reverse-flick" pattern that has recently been described for *Vibrio* species (8, 9). A similar forward-backward movement with respect to time and distance intervals was observed for cells with secondary lateral filaments. However, the directional changes upon resuming forward movement occurred at a much wider array of angles, with an average turning angle below 90° (Fig. 2). In addition, the average period between directional switching events increased to about 20 s. We proposed that these two factors, smaller average turning angle and longer runs, may benefit spreading of wild-type cells by increasing directional persistence of swimming, i.e., correlation in the swimming direction over time.

Main Propulsion and Directional Switches Are Mediated by the Primary Flagellar System of *S. putrefaciens* CN-32. We further conducted a complementary set of experiments in which we determined the potential interaction of the chemotaxis system with the two different flagellar motors. According to the genome data, *S. putrefaciens* CN-32 has a single chemotaxis system with a broad sensory repertoire represented by 37 putative methyl-accepting chemotaxis sensor proteins. To dissect the chemotaxis pathway in CN-32, we determined the effect of defined mutants in CheY on the two potential receiving motor systems. To this end, we constructed a constitutively active version of CheY (*cheY*$^{D12K;Y105W}$; CheY-GOF "gain of function") and a non-active version (*cheY*^{D56N}; CheY-LOF; loss of function) (16, 17). The mutated *cheY* versions were introduced into CN-32 wild type and the mutant backgrounds Δ*flaAB*$_1$ and Δ*flaAB*$_2$. In addition, a *cheY* deletion (Δ*cheY*) was constructed in all three strains. Δ*cheY* and CheY-LOF mutations in the wild-type background resulted in straight forward-swimming cells, and almost no directional changes were observed in planktonic cultures. In contrast, in cells bearing a CheY-GOF mutation, the average period between forward and backward movements was drastically shortened (<4 s compared with ~20 s for wild-type cells). All strains were characterized for their ability to navigate in soft-agar plates (Fig. 3).

Wild-type cells bearing Δ*cheY*, CheY-LOF, or CheY-GOF mutations exhibited a drastically reduced radial expansion. Notably, the level of lateral extension in all three mutants was almost identical to that of a Δ*flaAB*$_1$ mutant. Furthermore, cells lacking the ability to form the primary polar filament (Δ*flaAB*$_1$)

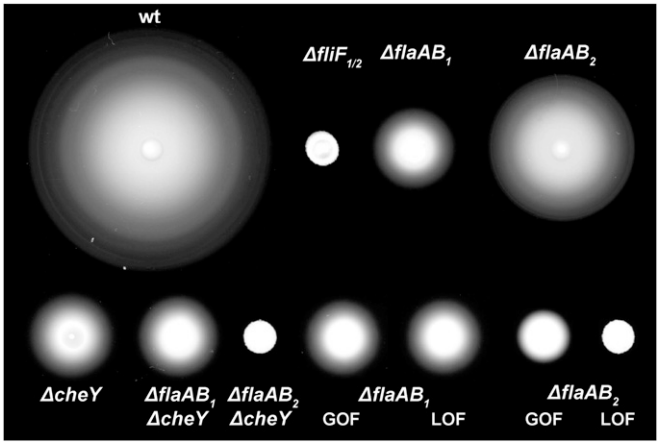

Fig. 3. CheY interacts with the polar flagellar system. Displayed is the radial extension of CN-32 wild-type and flagellar/chemotaxis mutants in 0.25% soft agar. The strains are labeled accordingly. The nonmotile Δ*fliF*$_{1/2}$ mutant served as a negative control. Strains indicated with "*cheY* GOF" harbor the gain-of-function variant of CheY; those indicated with "*cheY* LOF" harbor the corresponding loss-of-function variant. Note that the arrangement of the strains on the plate has been shifted for clarity. An image of the original plate can be found in Fig. S3.

were not further affected in swimming motility by additional mutations in or loss of CheY. In contrast, the same CheY mutations introduced into strain background *ΔflaAB*$_2$, which lacks the secondary system, resulted in cells that were no longer (*ΔflaAB*$_2$ *ΔcheY*; *ΔflaAB*$_2$ CheY-LOF) or just barely (*ΔflaAB*$_2$ CheY-GOF) capable of navigating through soft agar. Thus, the observed radial expansion of the *cheY* mutants on soft agar plates was mainly or exclusively conferred by the secondary lateral system.

In addition, we used light microscopy on *ΔflaAB*$_1$ mutants to identify potential differences in swimming behavior due to loss or mutation of CheY. All actively swimming cells were observed to move in irregular patterns, likely due to the lateral position of the flagellar filament, and never switched from forward to backward movement. Cells that were tethered to the glass surface by the lateral flagellar filament displayed constant CCW rotation, and we did not observe directional switches in any of the strains tested (Movie S1). Based on these results, we concluded that CheY predominantly or even exclusively interacts with the primary polar motor. Thus, main propulsion and chemotaxis-induced forward-backward movements are mediated by the primary polar flagellar system. On the other hand, the lateral system has a role in confining the cellular reorientation to smaller angles.

Computational Model of Spreading of *Shewanella* Wild-Type and Mutant Cells. To determine whether the observed differences in swimming behavior are sufficient to explain the observed advantage in spreading, we performed a mathematical analysis and computer simulations of motility and chemotaxis of wild-type vs. mutant cells. The movement of cells in a uniform environment without gradients can be described analytically as a 2D correlated random walk (18, 19). In this approximation, the mean square displacement (MSD) of the population after time t, $R(t)$, can be obtained from the autocorrelation function of the velocity:

$$\begin{aligned} <v(t)v(0)> &= \exp\left(-(\lambda+2D_r)t\right)\, v^2 \exp(\lambda\gamma t) \\ &= v^2\exp\left(-\left[\lambda(1-\gamma)+2D_r\right]t\right), \end{aligned} \qquad [1]$$

where λ is the turning rate, i.e., reciprocal of the mean run duration, D_r is the coefficient of rotational diffusion, v is the speed of swimming, and γ is the persistence factor of the movement, i.e., the mean of the cosine of the turning angles, $\gamma = <\cos(\Theta)>$. Here we assumed an exponential distribution of run durations and neglected the short backtracking movement of *S. putrefaciens* CN-32 following runs. Double integration in time on Eq. **1** then gives the value of the MSD:

$$R(t) = \frac{2\,v^2\left\{\exp\left[-t\left(2D_r+\lambda(1-\gamma)\right)\right]+2D_r t-1\right\}+2\lambda\, v^2(1-\gamma)t}{\left(2D_r+\lambda(1-\gamma)\right)^2}. \qquad [2]$$

Since the exponential term in the numerator goes to zero on the relevant timescale of the experiments (hours), Eq. **2** simplifies to:

$$R(t) = \frac{2\,v^2 t}{2D_r+\lambda(1-\gamma)} - \frac{2\,v^2}{\left(2D_r+\lambda(1-\gamma)\right)^2}. \qquad [3]$$

Eq. **3** shows that the value of $R(t)$ increases at higher values of the persistence factor γ, as proposed already in a previous theoretical study describing insect movement (18). The lower average turning angle observed for the wild-type cell movement can thus yield higher persistence and lead to faster spreading. This conclusion was confirmed by calculating the root mean square distance (RMSD) for the mutant and wild-type strains using the full expression of Eq. **2** and the experimentally determined parameter values (Fig. 4*A* and Fig. S4).

In addition to this analytical calculation, we performed numerical simulations taking into account backward runs. The values of turning angles were generated by assigning discrete probability values to the experimentally measured angles and binning randomly generated numbers by the probability intervals. Durations of individual backward and forward runs were generated using Monte Carlo simulations as in Gillespie's algorithm (20), assuming exponential probability distributions with the experimentally determined means. Numerical simulations confirmed that the higher persistence factor of the wild-type cells' movement yields more efficient spreading, if the other parameters have identical values (Fig. 4*B* and Fig. S4). Although the experimental values of the run duration and swimming speed are different for the wild-type compared with mutant cells, the effects of their longer run periods and lower speed are mutually compensatory, as can be calculated from Eq. **2** (Fig. 4*A* and Fig. S4) and confirmed by numerical simulations (Fig. 4*B* and Fig. S4). Therefore, ∼90% of the difference in the RMSD results from the higher persistence of the wild-type movement. While the calculated difference in the RMSD is rather small, it yields a consistent increase in the ratio of wild-type to mutant cells at the edge of the simulated spreading population (Fig. 4*C*), similar to that observed experimentally (Fig. 1*C*).

Such enhancement of cell spreading in uniform environments might thus alone explain the benefit conferred by the lateral flagella. Nevertheless, higher persistence of movement has also been proposed to have a positive effect on the chemotactic movement of bacteria in gradients (21–23). We thus simulated the effect of the difference in the measured turning angle distribution on the chemotactic movement using the phenomenological model of chemotaxis described in Locsei (22). This model does not require knowledge of detailed biochemical parameters and assumes that the pathway response to weak stimuli (in shallow gradients) can be described as a convolution integral of the stimulus history with the impulse response (24, 25). Although the impulse response function was measured for *E. coli* (see details in *SI Materials and Methods*), it is believed to be generally required for bacterial chemotaxis (26) and should thus be applicable for *S. putrefaciens* CN-32. We further varied the time window for sensing and the gradients' steepness, to investigate the effect of persistence under different conditions.

Wild-type cells indeed showed faster chemotactic movement in shallow attractant gradients (Fig. 4*D*), suggesting that under these conditions, the observed higher persistence of movement is sufficient to enhance chemotaxis. This difference became negligible in steeper gradients (Fig. 4*D* and Fig. S4), presumably because already short directional runs in steep gradient enable cells to experience strong chemotactic stimulation. Moreover, the model used here is likely to become imprecise in steep gradients. The positive effect of persistence on the chemotactic efficiency is also diminished by the increase in the run time (Fig. S4), because during longer runs rotational diffusion results in the loss of directional correlation. The exact relation between the run time and the benefit of persistence depends on the value of the coefficient of rotational diffusion, which is not known exactly for *S. putrefaciens* CN-32.

Discussion

For numerous bacterial species, flagella-mediated motility is an important if not crucial factor for successful propagation. Different types of flagellation provide advantages under different environmental conditions, and it has been speculated that some species have maintained two complete flagellar systems to allow more effective motility under a wider range of conditions than could be provided by a single system only (11). In this study, we have provided evidence that a secondary lateral flagellar system

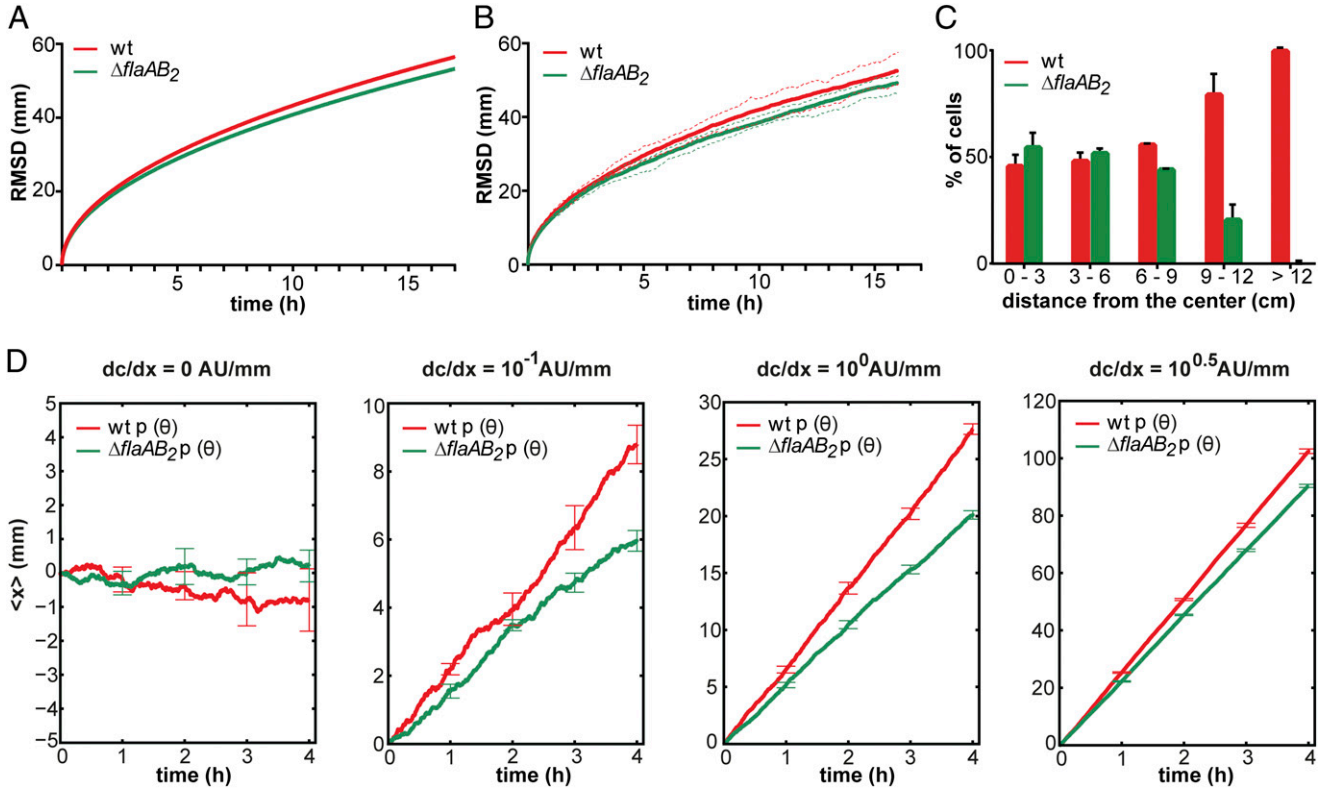

Fig. 4. Modeling and simulations of spreading and chemotaxis for wild-type and Δ*flaAB*$_2$ cells. (*A*) Analytical solution for nondirectional spreading of bacterial cells (RMSD) in absence of chemotactic gradient, using Eq. **2** with experimentally measured parameter values (v_{mutant} = 57 μm/s, λ_{mutant} = 0.1 s^{-1}, γ_{mutant} = 0.058 and v_{WT} = 47 μm/s, λ_{WT} = 0.05s^{-1}, γ_{WT} = 0.214). The coefficient of rotational diffusion was set to D_r = 0.023 $rad^2 \cdot s^{-1}$. (*B*) Numerical simulations of the population spreading with same parameters as in *A* and using the experimentally measured turning angle distribution, also including backtracking. The lines show the mean of 10 independent simulations, with RMSD of 200 cells determined in each simulation. Dashed lines show minimal and maximal values. (*C*) Percentage of wild-type and Δ*flaAB*$_2$ cells from *B* after 16 h, at different (radial) distances from the center. The ratio of wild-type to mutant cells rises with increasing distance from the center. The error bars are based on 10 independent simulations. (*D*) Simulations of chemotaxis in gradients, using the experimentally measured turning angle distributions for wild-type and Δ*flaAB*$_2$ cells. The scaling factor ε (see *SI Materials and Methods*) was set to ε = 0.1. Results are from five independent simulations, each including 1,000 cells. Gradients of indicated steepness (d*c*/d*x*) are linearly increasing along the *x* axis, with $c = 0$ at $x = -100$. At the onset of simulation, cells are placed in random orientations at $x = 0$. The mean position, $\langle x \rangle$, of the cell population along the *x* axis indicates chemotactic drift along the gradient. The units of distance are millimeters, whereas the unit for concentration *c* is arbitrary. The basal turning rate was set to λ_0 = 0.2 s^{-1}. For simulations with other values of λ_0 and ε, see Fig. S4.

may not only add propulsion forces for viscous environments or for swarming across surfaces but also enables more efficient spreading under conditions where polar flagella would be sufficient for swimming.

It was shown previously that cells of *S. putrefaciens* are capable of highly efficient chemotactic swimming that, for example, allows cells to successfully track motile marine algae (27). Here, we have demonstrated that *S. putrefaciens* CN-32 and presumably other *Shewanella* sp. most likely navigate by a run-reverse-flick mechanism as has recently been proposed to mediate efficient chemotaxis in *Vibrio* species (8, 9, 28). *S. putrefaciens* CN-32 with a single polar filament exhibit cellular reversals and quick cellular rearrangements by an angle of ∼90° upon resuming forward swimming. Under the conditions tested, e.g., with little or no gradient of attractants or repellents, the full run-reverse-flick three-step cycle occurred in less than 0.1 s. In contrast, the secondary lateral flagella function in a unidirectional fashion and were only observed to exhibit CCW rotation, as has similarly been described in an earlier study on the lateral system of *V. alginolyticus* (29). However, while, in this species, CheY is able to interact with both flagellar motor systems and slows down rotation of the lateral filaments, we have found no indication that CheY affects lateral flagellar rotation in CN-32. Functional modulation of the flagellar motors requires specific interactions between CheY and the motor protein FliM (5). Notably, $FliM_2$ of the lateral system has little homology to $FliM_1$ of the polar motor and lacks the predicted CheY binding domain that is well conserved in $FliM_1$ (Fig. S5). Also the homology between FliM of the lateral systems in CN-32 and *V. parahaemolyticus* is surprisingly low, indicating that $FliM_2$ of the secondary flagellar system *of S. putrefaciens* CN-32 has lost the ability to functionally interact with CheY. In contrast, we demonstrate that the secondary system of CN-32 exhibits its function by decreasing the cellular turning angle. In addition, directional switches of the cells were observed at lower frequency, which might indicate that the secondary filament is even able to fully suppress a visible directional change. Using mathematical modeling and computer simulations, we propose that the resulting lowering of the turning angle distribution of a bacteria's movement leads to more efficient spreading and chemotaxis due to higher directional persistence. Our results are consistent with previous theoretical studies (18) but provide a specific example of how this strategy is used by bacteria. We expect that this function of lateral flagella will be similarly applicable to many of the other numerous bacterial species that are equipped with secondary flagellar systems. Some findings in previous studies indicate that this might be the case: The expression of a secondary flagellar system of *Bradyrhizobium japonicum* planktonic cultures in planktonic cultures has been

demonstrated (30), and *V. alginolyticus* strains lacking the lateral flagellar system exhibit a reduced radial extension in soft-agar assays similarly as observed for *S. putrefaciens* CN-32 (31). Given the heterogeneity in steepness of nutrient gradients in many habitats such as marine environments (32), spreading of numerous bacterial species would benefit from an increase in directional persistence conferred by secondary lateral flagella.

Materials and Methods

Bacterial Strains. The bacterial strains and plasmids that were used in this study are summarized in Table S1 and Table S2. Construction of plasmids and strains was essentially carried out as previously described (15, 33) using oligonucleotides listed in Table S3. Detailed information is provided in *SI Materials and Methods*.

Motility Assays. Motility of *S. putrefaciens* CN-32 wild-type or mutant single cells or the spreading of cell cultures were monitored using liquid cultures or soft-agar plates, respectively, essentially using protocols that were established earlier (15). Liquid-culture motility assays were performed using early exponential phase cultures of *S. putrefaciens* CN-32. To this end, 1×10^8 cells of an overnight culture were added to fresh medium and were grown to an OD_{600} of 0.3–0.4 at 30 °C. From this culture, 400 μL were used for immediate microscopical analyses using a Leica TCS SP5 (Leica Microsystems) confocal laser scanning microscope equipped with a resonance scanner at 27 frames per second. Single cells were tracked and velocities calculated by measuring track lengths per time. The angle of reorientation events was determined for cells that remained in the focal plane prior and after the directional change occurred.

Soft-agar plates had an agar concentration of 0.25% (wt/vol), and 3 μL of *S. putrefaciens* CN-32 culture were spotted for a motility assay. The plates were incubated for an adequate amount of time at 30 °C, and the radial extension of the cultures was documented. To be able to compare the radial extension of different mutant strains with that of wild-type *S. putrefaciens* CN-32, the appropriate cultures were always spotted onto the same soft-agar plate. Comparative motility performance assays were also performed in μ-Slide VI 0,1 ibiTreat chambers (Ibidi GmbH). Cells from the late exponential growth phase were washed and dissolved in fresh medium containing 15 $\mu g \cdot mL^{-1}$ chloramphenicol to inhibit bacterial growth. 50 μL 1:1 mixtures of appropriately labeled wild-type and $\Delta flaAB_2$-mutant cells were loaded in one of the wells and the chambers were incubated for 16 h at room temperature. Then samples were taken from the second reservoir and characterized accordingly.

Flagellar Staining. Staining and microscopy of flagellar filaments was essentially performed as described earlier (see *SI Materials and Methods*).

Fluorescence Microscopy. Before fluorescence microscopy, the strains of interest were cultured to midexponential phase or were isolated from soft-agar plates by pipetting. Between 1 and 2 μL of diluted cultures were added on top of an agarose-pad to immobilize cells. An Axio Imager.M1 fluorescence microscope (Zeiss) equipped with a Zeiss Plan Apochromate 100×/1.4 DIC objective was used to visualize single cells. Image acquisition and processing was carried out using the Metamorph 7.5.4.0 software (Molecular Devices). At least 300 cells per data point were evaluated.

Numerical Simulations. Numerical simulations of bacterial swimming were performed used custom-written MATLAB scripts as described in *SI Materials and Methods*.

ACKNOWLEDGMENTS. This work was supported by Grants TH 831/5-1 and SO 421/12-1 from the Deutsche Forschungsgemeinschaft (DFG) within the framework of the DFG Priority Programme SPP1617, the Max Planck Society, and the European Research Council (Advanced Grant 294761-MicRobE).

1. Kelly FX, Dapsis KJ, Lauffenburger DA (1988) Effect of bacterial chemotaxis on dynamics of microbial competition. *Microb Ecol* 16(2):115–131.
2. Lauffenburger DA (1991) Quantitative studies of bacterial chemotaxis and microbial population dynamics. *Microb Ecol* 22(1):175–185.
3. Sowa Y, Berry RM (2008) Bacterial flagellar motor. *Q Rev Biophys* 41(2):103–132.
4. Minamino T, Imada K, Namba K (2008) Molecular motors of the bacterial flagella. *Curr Opin Struct Biol* 18(6):693–701.
5. Sourjik V, Wingreen NS (2012) Responding to chemical gradients: Bacterial chemotaxis. *Curr Opin Cell Biol* 24(2):262–268.
6. Berg HC, Brown DA (1972) Chemotaxis in *Escherichia coli* analysed by three-dimensional tracking. *Nature* 239(5374):500–504.
7. Berg HC (2004) *E. coli in Motion* (Springer, New York).
8. Son K, Guasto JS, Stocker R (2013) Bacteria can exploit a flagellar buckling instability to change direction. *Nat Phys* 9(8):494–498.
9. Xie L, Altindal T, Chattopadhyay S, Wu XL (2011) From the cover: Bacterial flagellum as a propeller and as a rudder for efficient chemotaxis. *Proc Natl Acad Sci USA* 108(6): 2246–2251.
10. Qian C, Wong CC, Swarup S, Chiam KH (2013) Bacterial tethering analysis reveals a "run-reverse-turn" mechanism for *Pseudomonas* species motility. *Appl Environ Microbiol* 79(15):4734–4743.
11. McCarter LL (2004) Dual flagellar systems enable motility under different circumstances. *J Mol Microbiol Biotechnol* 7(1-2):18–29.
12. Merino S, Shaw JG, Tomás JM (2006) Bacterial lateral flagella: An inducible flagella system. *FEMS Microbiol Lett* 263(2):127–135.
13. Atsumi T, et al. (1996) Effect of viscosity on swimming by the lateral and polar flagella of *Vibrio alginolyticus*. *J Bacteriol* 178(16):5024–5026.
14. Sar N, McCarter L, Simon M, Silverman M (1990) Chemotactic control of the two flagellar systems of *Vibrio parahaemolyticus*. *J Bacteriol* 172(1):334–341.
15. Bubendorfer S, et al. (2012) Specificity of motor components in the dual flagellar system of *Shewanella putrefaciens* CN-32. *Mol Microbiol* 83(2):335–350.
16. Scharf BE, Fahrner KA, Berg HC (1998) CheZ has no effect on flagellar motors activated by CheY13DK106YW. *J Bacteriol* 180(19):5123–5128.
17. Sanders DA, Gillece-Castro BL, Stock AM, Burlingame AL, Koshland DE, Jr (1989) Identification of the site of phosphorylation of the chemotaxis response regulator protein, CheY. *J Biol Chem* 264(36):21770–21778.
18. Kareiva PM, Shigesada N (1983) Analyzing insect movement as a correlated random walk. *Oecologia* 56(2-3):234–238.
19. Theves M, Taktikos J, Zaburdaev V, Stark H, Beta C (2013) A bacterial swimmer with two alternating speeds of propagation. *Biophys J* 105(8):1915–1924.
20. Gillespie DT (1977) Exact stochastic simulation of coupled chemical reactions. *J Phys Chem* 81(25):2340–2361.
21. Nicolau DV, Jr, Armitage JP, Maini PK (2009) Directional persistence and the optimality of run-and-tumble chemotaxis. *Comput Biol Chem* 33(4):269–274.
22. Locsei JT (2007) Persistence of direction increases the drift velocity of run and tumble chemotaxis. *J Math Biol* 55(1):41–60.
23. Taktikos J, Stark H, Zaburdaev V (2013) How the motility pattern of bacteria affects their dispersal and chemotaxis. *PLoS ONE* 8(12):e81936.
24. Block SM, Segall JE, Berg HC (1982) Impulse responses in bacterial chemotaxis. *Cell* 31(1):215–226.
25. Segall JE, Block SM, Berg HC (1986) Temporal comparisons in bacterial chemotaxis. *Proc Natl Acad Sci USA* 83(23):8987–8991.
26. Clark DA, Grant LC (2005) The bacterial chemotactic response reflects a compromise between transient and steady-state behavior. *Proc Natl Acad Sci USA* 102(26): 9150–9155.
27. Barbara GM, Mitchell JG (2003) Bacterial tracking of motile algae. *FEMS Microbiol Ecol* 44(1):79–87.
28. Altindal T, Xie L, Wu XL (2011) Implications of three-step swimming patterns in bacterial chemotaxis. *Biophys J* 100(1):32–41.
29. Kojima M, Kubo R, Yakushi T, Homma M, Kawagishi I (2007) The bidirectional polar and unidirectional lateral flagellar motors of *Vibrio alginolyticus* are controlled by a single CheY species. *Mol Microbiol* 64(1):57–67.
30. Kanbe M, Yagasaki J, Zehner S, Göttfert M, Aizawa S (2007) Characterization of two sets of subpolar flagella in *Bradyrhizobium japonicum*. *J Bacteriol* 189(3):1083–1089.
31. Kawagishi I, Maekawa Y, Atsumi T, Homma M, Imae Y (1995) Isolation of the polar and lateral flagellum-defective mutants in *Vibrio alginolyticus* and identification of their flagellar driving energy sources. *J Bacteriol* 177(17):5158–5160.
32. Stocker R, Seymour JR (2012) Ecology and physics of bacterial chemotaxis in the ocean. *Microbiol Mol Biol Rev* 76(4):792–812.
33. Lassak J, Henche AL, Binnenkade L, Thormann KM (2010) ArcS, the cognate sensor kinase in an atypical Arc system of *Shewanella oneidensis* MR-1. *Appl Environ Microbiol* 76(10):3263–3274.

Supporting Information

Bubendorfer et al. 10.1073/pnas.1405820111

SI Materials and Methods

Bacterial Strains, Growth Conditions, and Media. The comprehensive list of strains used in this study is found in Table S1. *Escherichia coli* strains DH5a λpir, BL-21 and WM3064 and *Shewanella putrefaciens* CN-32) were routinely grown in LB medium at 37 °C and 30 °C, respectively. To enable growth of the 2,6-diaminopimelic acid (DAP)-auxotroph *E. coli* WM3064, medium was supplemented with DAP at a final concentration of 300 μM. To solidify media, LB agar was prepared using 1.5% (wt/vol) agar. Whenever needed, media were supplemented with 100 $mg{\cdot}mL^{-1}$ ampicillin, 50 $mg{\cdot}mL^{-1}$ kanamycin and/or 10% (wt/vol) sucrose. To prepare agarose pads for fluorescence microscopy, LM100 medium (10 mM Hepes, pH 7.3; 100 mM NaCl; 100 mM KCl; 0.02% yeast extract; 0.01% peptone; 15 mM lactate) was solidified by adding 1% (wt/vol) agarose.

Strains and Vector Constructions. The complete list of plasmids used in this study can be found in Table S2. DNA manipulations were conducted following standard protocols or the manufacturer's instructions (1). Genomic DNA of *S. putrefaciens* CN-32 was isolated basically as described earlier (2). Kits used for the isolation and purification of PCR products or plasmids were purchased either from HISS Diagnostics GmbH or Omega bio-tek GmbH. Enzymes that were used in this study were purchased from New England Biolabs, Biozym Scientific GmbH and Fermentas. Construction of markerless in-frame deletion mutants in *S. putrefaciens* CN-32 was performed as described earlier, using the primers (listed in Table S3) and the suicide vector pNPTS138-R6KT (3).

For single-cell visualization of different *S. putrefaciens* CN-32 strains, a plasmid-encoded system for *in cis* continuous transcription of *sfgfp* or *mcherry* was constructed that was inserted via single homologous recombination into the genome of *S. putrefaciens* CN-32, leaving the vector backbone within the genome. For this, three fragments comprising the *glmS* site fragment for target recombination, the *motAB* promoter site of *S. oneidensis* MR-1, and either *sfgfp* or *mcherry* were fused using overlap PCR and integrated in pNPTS138-R6KT resulting in the fragments *glmS*::P*motAB-sfgfp* or *glmS*::P*motAB-mcherry*.

Flagellar Staining. Staining of flagellar filaments was performed similar to earlier studies (4). Ten microliters of an exponentially growing culture were spotted onto a microscopy slide and subsequently stained before visualization. Microscopy and image acquisition was pursued with the help of an Axio Imager.M1 microscope (Zeiss) equipped with a Zeiss Plan Apochromate 100×/1.4 DIC objective.

Immunodetection of Proteins. To determine production levels and stability of CheY or CheY variants (Fig. S6), we obtained lysates from exponentially growing LB cultures. Cells of the appropriate strain corresponding to an OD_{600} of 10 were harvested by centrifugation and resuspended in sample buffer (5) and heated at 99 °C for 5 min. Ten microliters of sample were resolved by SDS/PAGE using 11% (wt/vol) polyacrylamide gels. Subsequently, proteins were transferred to nitrocellulose Immobilon-P membrane (Millipore) by semidry transfer. To detect wild-type CheY and CheY variants via Western blotting, antibodies were raised against CheY in rabbits. To this end, strep-tagged CheY was heterologously produced in *E.coli* BL21 and purified using an appropriate affinity purification protocol (IBA GmbH). Antibody generation was carried out by Eurogentec Germany GmbH. A dilution of 1:500 of final-bleed serum was used to detect CheY subsequent to blotting protein to nitrocellulose membrane. Goat anti-rabbit horseradish peroxidase coupled Ig (Thermo Fischer Scientific) was used as secondary antibody in a dilution of 1:20,000 to detect primary antibodies.

Numerical Simulations of Swimming in a Uniform Environment. In numerical simulations, the movement of an individual cell in the x and y coordinates during the mth run was described as

$$\begin{aligned} x(t+l) &= x(t) + v * l(m) * \cos\big(\alpha(m)\big) \\ y(t+l) &= y(t) + v * l(m) * \sin\big(\alpha(m)\big) \end{aligned} \qquad \textbf{[S1]}$$

where t is time, $l(m)$ is the duration of the mth run, v is the speed of movement, and $\alpha(m)$ is the orientation of the cell during the mth run. Here we assumed that $\alpha(m)$ changes from the m-1th to the mth run as

$$\alpha(m) = \alpha(m-1) + \Theta(m) \qquad \textbf{[S2]}$$

where $\Theta(m)$ is the turning angle preceding the mth run. Because there are no observable tumbling periods for *Shewanella* cells, we assumed in our simulations that cells turn instantaneously at the end of runs (and after the short backtracking period). Taking into account rotational diffusion, cell orientation in our simulations changes at every time step Δt as

$$\alpha(t+\Delta t) = \alpha(t) + \eta \qquad \textbf{[S3]}$$

where η is the term due to rotational diffusion. We assumed the random variable η to be normally distributed as

$$N(m,\sigma) = N\left(0, [2D_r \Delta t]^{1/2}\right) \qquad \textbf{[S4]}$$

where D_r is the coefficient of rotational diffusion. A value of $D_r = 0.023\ rad^2{\cdot}s^{-1}$ was used, which is the value determined for *Pseudomonas putida* (6), a bacteria of similar size and polar flagellation.

Run durations l and turning angles Θ have experimentally measured probability distributions p(l) and p(Θ), respectively. We assume that p(l) is exponentially distributed.

Monte Carlo simulations were performed by drawing random numbers from the probability distributions of forward run durations, backward run durations and turning angles. The probability distribution for turning angles was obtained by binning our experimental data using 10° bins. For run durations, the means were experimentally measured, and values were generated from the exponential distribution with the respective mean. The results are displayed in Fig. 4 and Fig. S4.

All scripts were written in MATLAB, using MATLAB's *randn* algorithm to generate random numbers.

Chemotaxis Model. Since the biochemical parameters of the chemotaxis pathway in *Shewanella* are not known, we used a model of chemotaxis that captures the basic response properties of the pathway without detailed pathway description. Following Locsei (7), we assume that, in shallow gradients, the probability of discontinuing a run and turning, the "turning rate," depends linearly on the recent concentration history of the cell and is given by:

$$\lambda(t) = \lambda_0\big(1 - \Delta(t)\big), \qquad \textbf{[S5]}$$

where λ_0 is the basal turning rate (equal to the reciprocal of mean run duration if there is no gradient present) and $\Delta(t)$ is the fractional change of the turning rate.

The turning rate is biased by a response function mapping the attractant concentration history of the cell into the fractional change of the turning rate:

$$\Delta(t) = \int_{-\infty}^{t} c(\tau)R(t-\tau)d\tau, \qquad \textbf{[S6]}$$

where $c(\tau)$ is the concentration of attractant experienced by the cell at time τ, and $R(t\text{-}\tau)$ is the response function of the cell, specifying the impulse response to the chemoattractant. The turning rate is then given as the convolution integral of the impulse response and the attractant concentration history, treating the chemotaxis system as linear. This model is motivated by the experiments of Berg and Segall and coworkers (8, 9) and has been shown by previous publications to capture the adaptive properties of the chemotaxis pathway (7, 10, 11).

As *Shewanella* is also capable of chemotaxis, its response function should have a similar shape to that of *E. coli*, so that the cell is capable of performing temporal comparisons. $R(t)$ as a function of time should then be double-lobed, with the important property (1, 3) that:

$$\int_{0}^{\infty} R(t)dt = 0, \qquad \textbf{[S7]}$$

and that $R(t)$ should decay to zero for $t >> 1/\lambda_0$ (for $t > 4/\lambda_0$ in the case of *E. coli*).

The response function is usually described (1–3) as having the form:

$$R(t) = W\exp(-\lambda_0 t)\left\{1 - A\left[\lambda_0 t + \frac{(\lambda_0 t)^2}{2}\right]\right\}, \qquad \textbf{[S8]}$$

where W and A are parameters to scale the response.

Following Locsei (3), we use a simpler, sinusoidal response function, for the sake of computational simplicity:

$$R(t) = \left\{\begin{array}{l} \varepsilon\dfrac{\lambda_0^2}{v_{swim}}\dfrac{\pi}{8}\sin\left(\dfrac{\pi\lambda_0 t}{2}\right), \text{ if } 0 \le t \le 4/\lambda_0, \\ 0, \text{ otherwise} \end{array}\right\}, \qquad \textbf{[S9]}$$

so that only the last $4/\lambda_0$ seconds of the cell's concentration history has to be stored and used for the calculation.

We discretize time into time steps of 0.1 s, and the turning rate is calculated by a discrete approximation of the convolution integral of Eq. **S6**, using MATLAB's *trapz* function. A random number p is then generated at each time step (*randn* function of MATLAB), and if $P < 0.1\lambda_0$ (the unit of λ_0 is s^{-1}, but time steps are in 0.1 s), the cell turns, with a turning angle generated from the discrete probability distribution of turning angles we have from our experiments. Otherwise the run is continued. Rotational diffusion is also taken into account at each time step, as described above.

Results of the simulations at different values of the model parameters are shown in Fig. S4. The values for the steepness of gradients displayed in the plots show the derivative d[c]/dx, the unit of distance being millimeters, whereas the unit for concentration [c] is arbitrary.

1. Sambrook K, Fritsch EF, Maniatis T (1989) *Molecular Cloning: A Laboratory Manual* (Cold Spring Harbor Lab Press, Cold Spring Harbor, NY).
2. Pospiech A, Neumann B (1995) A versatile quick-prep of genomic DNA from gram-positive bacteria. *Trends Genet* 11(6):217–218.
3. Lassak J, Henche AL, Binnenkade L, Thormann KM (2010) ArcS, the cognate sensor kinase in an atypical Arc system of *Shewanella oneidensis* MR-1. *Appl Environ Microbiol* 76(10):3263–3274.
4. Heimbrook ME, Wang WL, Campbell G (1989) Staining bacterial flagella easily. *J Clin Microbiol* 27(11):2612–2615.
5. Laemmli UK (1970) Cleavage of structural proteins during the assembly of the head of bacteriophage T4. *Nature* 227(5259):680–685.
6. Theves M, Taktikos J, Zaburdaev V, Stark H, Beta C (2013) A bacterial swimmer with two alternating speeds of propagation. *Biophys J* 105(8):1915–1924.
7. Locsei JT (2007) Persistence of direction increases the drift velocity of run and tumble chemotaxis. *J Math Biol* 55(1):41–60.
8. Segall JE, Block SM, Berg HC (1986) Temporal comparisons in bacterial chemotaxis. *Proc Natl Acad Sci USA* 83(23):8987–8991.
9. Block SM, Segall JE, Berg HC (1982) Impulse responses in bacterial chemotaxis. *Cell* 31(1):215–226.
10. Clark DA, Grant LC (2005) The bacterial chemotactic response reflects a compromise between transient and steady-state behavior. *Proc Natl Acad Sci USA* 102(26): 9150–9155.
11. Schnitzer MJ (1993) Theory of continuum random walks and application to chemotaxis. *Phys Rev E Stat Phys Plasmas Fluids Relat Interdiscip Topics* 48(4):2553–2568.

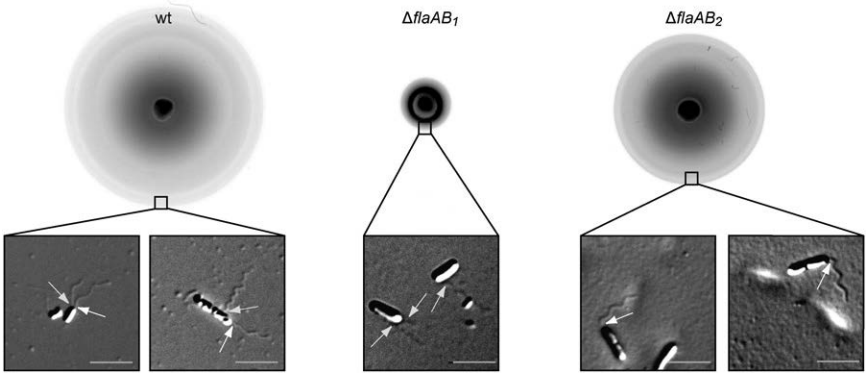

Fig. S1. Motility and flagellar staining of wild type, *ΔflaAB*$_1$ and *ΔflaAB*$_2$. Three-microliter droplets of the appropriate exponentially growing cell culture were spotted on motility plates (0.25% soft agar) and incubated for 16 h before documentation of radial extension. Cells were isolated from the outer rim of the lateral extension zones and subjected to flagella staining. White arrows indicate localization of polar flagella and yellow arrows indicate localization of lateral flagella. (Scale bar, 5 μm.)

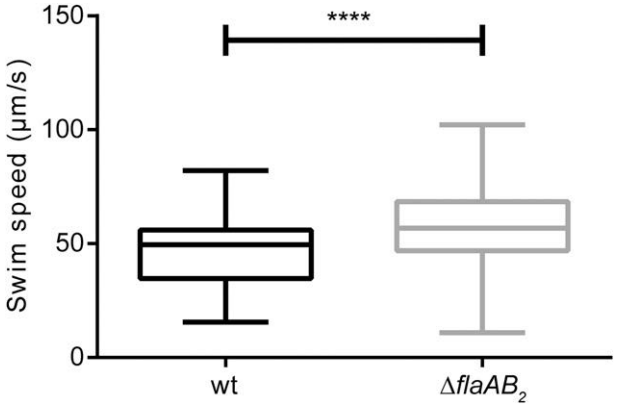

Fig. S2. Swimming speeds of wild-type and Δ*flaAB*$_2$-mutant cells isolated from the outer rim of lateral extension zones on soft-agar plates. Mean swimming speeds of wild-type and Δ*flaAB*$_2$-mutant cells are 46.9 ± 14.5 μm/s and 57.3 ± 17.2 μm/s, respectively. According to the Student *t* test, the swimming speeds of wild-type and Δ*flaAB*$_2$-mutants cells are significantly different. ****, $P \leq 0.0001$.

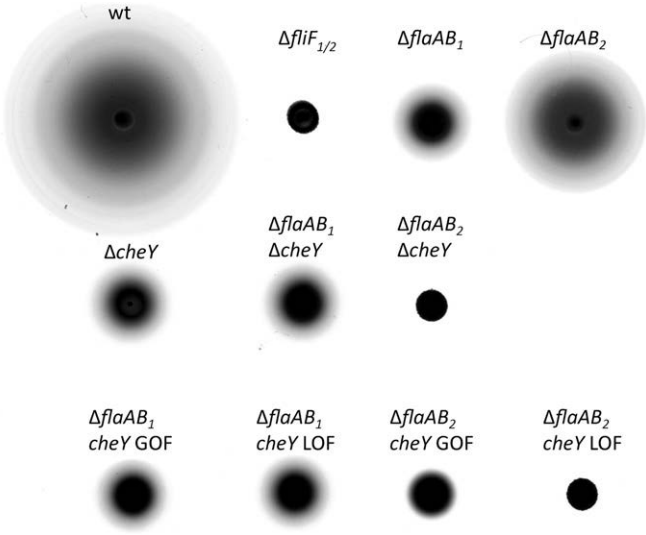

Fig. S3. CheY interacts with the polar flagellar system (original image of Fig. 3). Displayed is the radial extension of CN-32 wild-type and flagellar/chemotaxis mutants in 0.25% soft agar. The strains are labeled accordingly. The nonmotile ΔfliF$_{1/2}$ mutant served as a negative control. Strains indicated with "*cheY* GOF" harbor the gain-of-function variant of CheY, those indicated with "*cheY* LOF" harbor the corresponding loss-of-function variant.

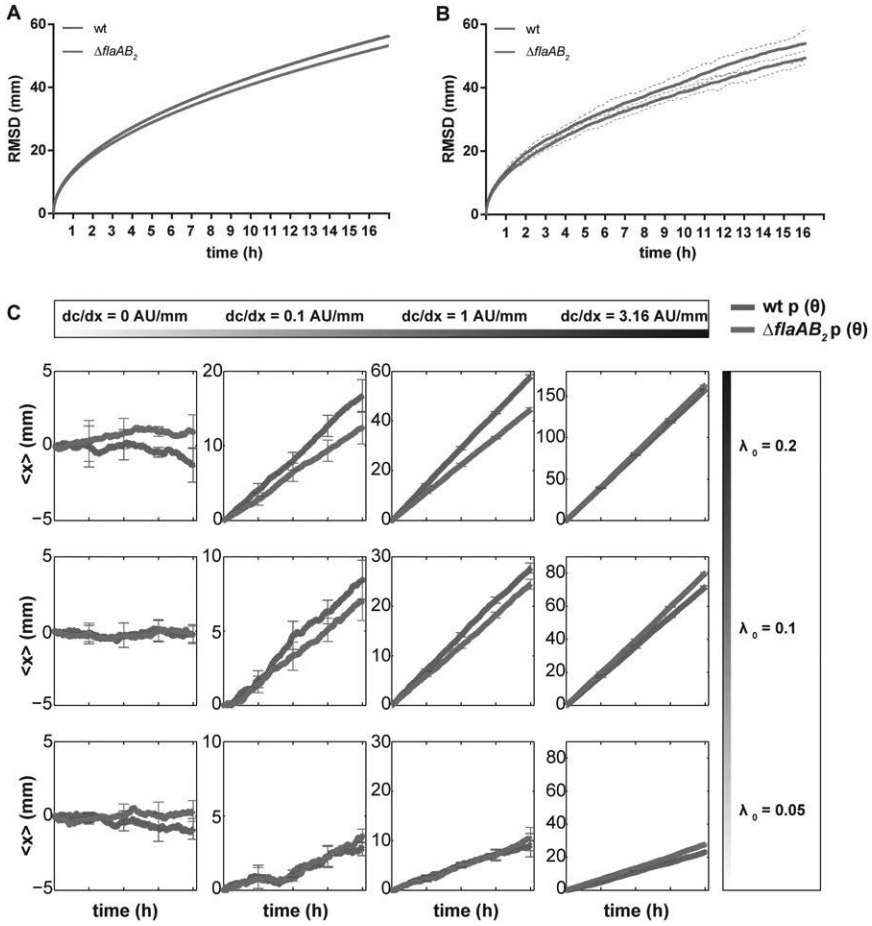

Fig. S4. Modeling and simulations of spreading and chemotaxis for wild-type and Δ*flaAB*$_2$ cells. (*A*) Analytical solution for the root mean square displacement (RMSD) of cells using identical parameter values ($v = 57\mu$m/s, λ=0.1 s^{-1}), except for the persistence factor ($\gamma_{WT} = 0.214$, $\gamma_{mutant} = 0.058$). (*B*) Numerical simulations with same parameters as in *A*, but including backtracking, with duration of backtracking 0.3 s on average. The lines show the mean of 10 independent simulations, with RMSD of 200 cells determined in each simulation. Error bars show minimal and maximal values. (*C*) Simulations of chemotaxis in gradients, using the experimentally measured turning angle distributions for wild-type and Δ*flaAB*$_2$ cells. The scaling factor ε was set to $\varepsilon = 0.2$. Results are from five independent simulations, each including 1,000 cells. Gradients of indicated steepness (d*c*/d*x*) are linearly increasing along the *x* axis, with $c = 0$ at $x = -100$. At the onset of simulation, cells are placed in random orientations at $x = 0$. The mean position, <*x*>, of the cell population along the *x* axis indicates chemotactic drift along the gradient. The units of distance are millimeters, whereas the unit for concentration *c* is arbitrary. The basal turning rate λ_0 is varied.

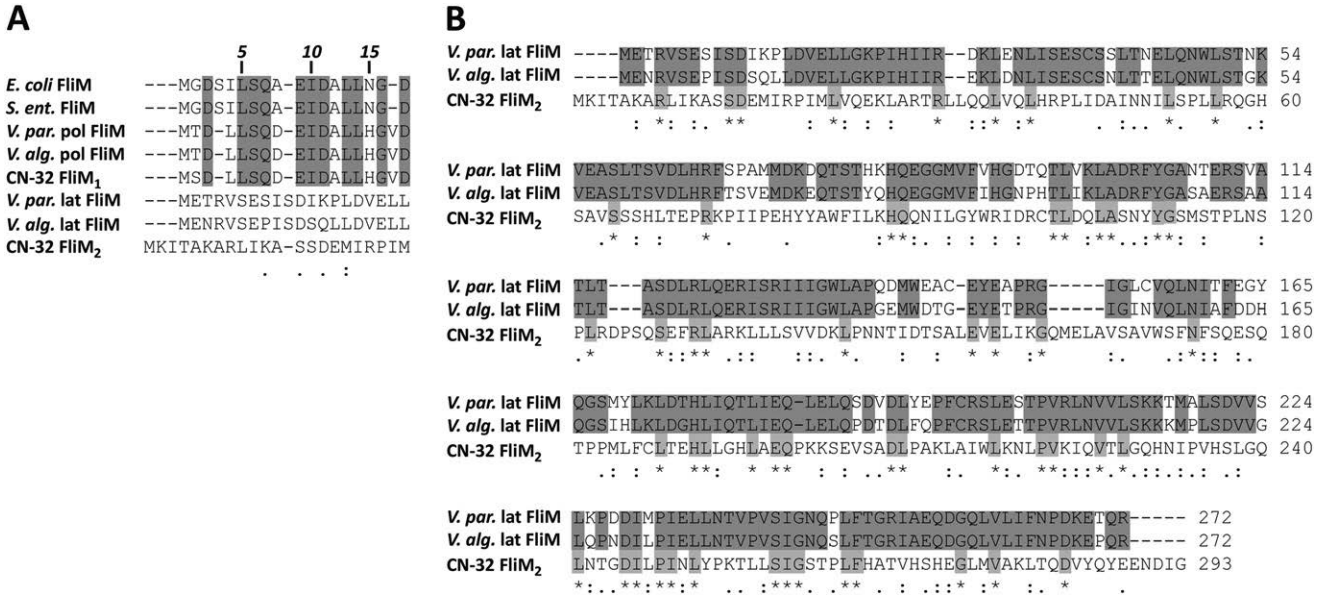

Fig. S5. Alignments of CN-32 $FliM_1$ and $FliM_2$. (*A*) Sequence alignment of the N-terminal part of FliM required for functional interaction with CheY. Amino acid residues marked in red depict identical residues in FliM of *E. coli*, *Salmonella enterica* sv. Typhimurium and FliM of the primary polar flagellar system of *V. parahaemolyticus*, *V. alginolyticus*, and *S. putrefaciens*. (*B*) Sequence alignment of full-length FliM of the secondary flagellar systems in *V. parahaemolyticus*, *V. alginolyticus*, and *S. putrefaciens* CN-32. Conserved amino acid residues are marked in red (for *Vibrio*) or green (for CN-32). All alignments were performed using Clustal Omega (www.ebi.ac.uk/Tools/msa/clustalo/).

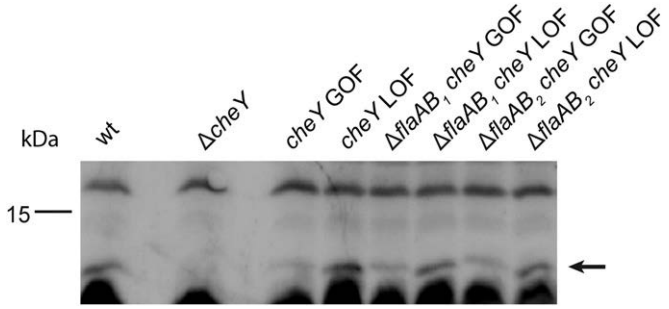

Fig. S6. Stability and protein levels of CheY bearing active site residue substitutions. Detection of wild-type, constitutively active (GOF), and inactive (LOF) versions of CheY by immunoblotting using antibodies raised against CheY. Arrows indicate the position corresponding to the appropriate protein versions.

Table S1. Bacterial strains that were used in this study

Strain	Genotype	Reference*
Escherichia coli		
DH5α λpir	ϕ80d*lacZ* ΔM15 Δ(*lacZYA-argF*)U169 *recA1 hsdR17 deoR thi-l supE44 gyrA96 relA1*/λpir	(1)
WM3064	*thrB1004 pro thi rpsL hsdS lacZ* ΔM15 RP4 - 1360 Δ(*araBAD*) 567Δ*dapA* 1341::[*erm pir*(wt)]	W. Metcalf, University of Illinois, Urbana - Champaign
BL-21 Star (DE3)	F– *ompT hsdS*$_B$(r_B– m_B–) *gal dcm rne131* (DE3)	Invitrogen
Shewanella putrefaciens		
S271	CN-32, wild type	(2)
S2241	*fliM*$_1$*-mcherry*, Sputcn32_2569-6xGly-*mcherry*-His6; markerless chromosomal fusion of *fliM*$_1$ to *mcherry* (C-terminal)	(3)
S2244	*fliM*$_2$*-sfgfp*, Sputcn32_3479-6xGly-*sfgfp*-His6; markerless chromosomal fusion of *fliM*$_2$ to *sfgfp* (C-terminal)	(4)
S2575	Δ*flaAB*$_1$, ΔSputcn32_2585–Sputcn32_2586; markerless deletion of polar flagellin genes	This study
S2576	Δ*flaAB*$_2$, ΔSputcn32_3455–Sputcn32_3456; markerless deletion of lateral flagellin genes	This study
S2356	Δ*cheY*, ΔSputcn32_2558; markerless deletion of chemotaxis response regulator *cheY* gene	This study
S2844	*cheY* GOF, *cheY*$^{D12K/Y106W}$, markerless insertion of *cheY* with substituted aspartic acid 12 to lysine and tyrosine 106 to tryptophan into Δ*cheY* replacing the *cheY*-deletion; constitutively active version of CheY (gain of function)	This study
S2845	*cheY* LOF, *cheY*^{D56N}, markerless insertion of *cheY* with substituted aspartic acid 56 to asparagine into Δ*cheY* replacing the *cheY*-deletion; constitutively inactive version of CheY (loss of function)	This study
S2589	Δ*flaAB*$_1$ Δ*cheY*; markerless deletion of *cheY* gene in Δ*flaAB*$_1$ background	This study
S2859	Δ*flaAB*$_1$ *cheY* GOF; markerless insertion of *cheY*-GOF in Δ*flaAB*$_1$ background	This study
S2860	Δ*flaAB*$_1$ *cheY* LOF; markerless insertion of *cheY*-LOF in Δ*flaAB*$_1$ background	This study
S2590	Δ*flaAB*$_2$ Δ*cheY*; markerless deletion of *cheY* gene in Δ*flaAB*$_2$ background	This study
S2868	Δ*flaAB*$_2$ *cheY* GOF; markerless insertion of *cheY*-GOF in Δ*flaAB*$_2$ background	This study
S2869	Δ*flaAB*$_2$ *cheY* LOF; markerless insertion of *cheY*-LOF in Δ*flaAB*$_2$ background	This study
S2908	*glmS*::*motABp-sfgfp*, insertion of pNPTS138-R6KT-*glmS-motABp-sfgfp* into the wild-type chromosome at the *glmS* locus; constitutive expression of *sfgfp* through the *S. oneidensis* MR-1 *motAB* promoter	This study
S2909	*glmS*::*motABp-mcherry*, insertion of pNPTS138-R6KT-*glmS-motABp-mcherry* into the wild-type chromosome at the *glmS* locus; constitutive expression of *mcherry* through the *S. oneidensis* MR-1 *motAB* promoter	This study
S2910	Δ*flaAB*$_1$ *glmS*::*motABp-sfgfp*, insertion of pNPTS138-R6KT-*glmS-motABp-sfgfp* into the Δ*flaAB*$_1$-mutant chromosome at the *glmS* locus; constitutive expression of *sfgfp* through the *S. oneidensis* MR-1 *motAB* promoter	This study
S2911	Δ*flaAB*$_1$ *glmS*::*motABp-mcherry*, insertion of pNPTS138-R6KT-*glmS-motABp-mcherry* into the Δ*flaAB*$_1$-mutant chromosome at the *glmS* locus; constitutive expression of *mcherry* through the *S. oneidensis* MR-1 *motAB* promoter	This study
S2912	Δ*flaAB*$_2$ *glmS*::*motABp-sfgfp*, insertion of pNPTS138-R6KT-*glmS-motABp-sfgfp* into the Δ*flaAB*$_2$-mutant chromosome at the *glmS* locus; constitutive expression of *sfgfp* through the *S. oneidensis* MR-1 *motAB* promoter	This study
S2913	Δ*flaAB*$_2$ *glmS*::*motABp-mcherry*, insertion of pNPTS138-R6KT-*glmS-motABp-mcherry* into the Δ*flaAB*$_2$-mutant chromosome at the *glmS* locus; constitutive expression of *mcherry* through the *S. oneidensis* MR-1 *motAB* promoter	This study

1. Miller VL, Mekalanos JJ (1988) A novel suicide vector and its use in construction of insertion mutations: Osmoregulation of outer membrane proteins and virulence determinants in *Vibrio cholerae* requires *toxR*. *J Bacteriol* 170(6):2575–2583.
2. Fredrickson JK, et al. (1998) Biogenic iron mineralization accompanying the dissimilatory reduction of hydrous ferric oxide by a groundwater bacterium. *Geochim Cosmochim Acta* 62:3239–3257.
3. Bubendorfer S, et al. (2012) Specificity of motor components in the dual flagellar system of *Shewanella putrefaciens* CN-32. *Mol Microbiol* 83(2):335–350.
4. Pédelacq JD, Cabantous S, Tran T, Terwilliger TC, Waldo GS (2006) Engineering and characterization of a superfolder green fluorescent protein. *Nat Biotechnol* 24(1):79–88.

Table S2. Plasmids that were used in this study

Name	Insert	Reference
pNPTS138-R6KT	*mob*RP4$^+$ *ori*-R6K *sacB*; beta-galactosidase fragment alpha; suicide plasmid for in-frame deletions or integrations; Km^r	(1)
pCR2.1 - mCherry - SO	monomeric *mCherry,* codon-optimized for *S. oneidensis* MR-1, Ap^r	GeneScript
pASK-IBA3plus	ori Col E1, Ap^r	IBA, Göttingen, Germany
pET21-sfGfp	*sfgfp; "super folder" gfp*, Ap^r	(2)
pNPTS138-R6KT-flag-cluster1-KO	insertion of *flaAB$_1$* deletion fragment in pNPTS138-R6KT	This study
pNPTS138-R6KT-flag-cluster2-KO	insertion of *flaAB$_2$* deletion fragment in pNPTS138-R6KT	This study
pNPTS138-R6KT-CheY1-KO	Sputcn32_2558 deletion fragment in pNPTS138-R6KT	This study
pNPTS138-R6KT-CheY-GOF	insertion of Sputcn32_2558 with substituted aspartic acid 12 to lysine and tyrosine 106 to tryptophan into pNPTS138-R6KT	This study
pNPTS138-R6KT-CheY-LOF	insertion of Sputcn32_2558 with substituted aspartic acid 56 to asparagine into pNPTS138-R6KT	This study
pNPTS138-R6KT-glmS-motP-sfgfp	insertion of *glmS*::*motABp-sfgfp* into pNPTS138-R6KT	This study
pNPTS138-R6KT-glmS-motP-mcherry	insertion of *glmS*::*motABp-mcherry* into pNPTS138-R6KT	This study
pASK-IBA3plus CN-32 CheY	CheY-strep overexpression plasmid, Ap^r	This study

Ap^r, ampicillin resistance; Km^r, kanamycin resistance.

1. Lassak J, Henche AL, Binnenkade L, Thormann KM (2010) ArcS, the cognate sensor kinase in an atypical Arc system of *Shewanella oneidensis* MR-1. *Appl Environ Microbiol* 76(10): 3263–3274.
2. Pédelacq JD, Cabantous S, Tran T, Terwilliger TC, Waldo GS (2006) Engineering and characterization of a superfolder green fluorescent protein. *Nat Biotechnol* 24(1):79–88.

Table S3. Oligonucleotides that were used in this study

Name	Sequence 5′-3′
markerless in-frame deletions in *S. putrefaciens* CN-32	
EcoRI-flagP-fwd	A GAA TTC GAA GTT AAA GTG TCT GGG AAA CCC
OL-flagP-rev	TCA CCT CTT AAC TGT AAT AGC CAT AGT ATT TTC CTC
OL-flagP-fwd	ATT ACA GTT AAG AGG TGA GAC AGT GAT AGG GA
PspOMI-flagP-rev	T CTA GGG CCC TAA GCC TCT GTT TTC ATC AAA AGC C
Check-flagP-fwd	AAT TTT GAT GCG ACT ACC CCC G
Check-flagP-rev	TAT CTA GAC CTG ACC CCA TGC C
BamHI-flagL-fwd	A GGA TCC TGA CAC TGT ATT TAT GGC GCA GG
OL-flagL-rev	CAG TAG ACC GTG AAC ACC TAA CAT ATT AAT TCT CCA G
OL-flagL-fwd	GGT GTT CAC GGT CTA CTG CGT TAA TCT AGC TC
PspOMI-flagL-rev	T GTC GGG CCC GTC GCC GTC GCA TTT TCG C
Check-flagL-fwd	GTA TTA GCT TCG ATC GGG ATT GG
Check-flagL-rev	GTT ACC CTT TGG CGC ATC GG
EcoRI-Sputcn32_2558-cheY1-fwd	A GAA TTC TCG TCG AGG TGA TTG GGT TCC
OL-Sputcn32_2558-cheY1-rev	CTA AGC GAG GTC CAA GGT TTC CTC CGG TG
OL-Sputcn32_2558-cheY1-fwd	ACC TTG GAC CTC GCT TAG GCA GGG ATG AG
PspOMI-Sputcn32_2558-cheY1-rev	TCC GGG CCC ATC TTG AAA ATC CTG CGC CAT C
Check-Sputcn32_2558-cheY1-fwd	GAA ACC TTC GCT GGC ATA CG
Check-Sputcn32_2558-cheY1-rev	TAA ATC GAT AAC ACG GCG GAT C
markerless in-frame substitutions in *S. putrefaciens* CN-32	
CheY-D12K-rev	TGT TGA AAA TTT GTC AAC AAT GAG AAT C
CheY-D12K-fwd	GTT GAC AAA TTT TCA ACA ATG AGA CG
CheY-Y105W-rev	TAC GAC CCA GCC GTT TAC CC
CheY-Y105W-fwd	GTA AAC GGC TGG GTC GTA AAA C
CheY-D56N-rev	GGG CAT ATT CCA ATT TGT AAC AAC G
CheY-D56N-fwd	GTT ACA AAT TGG AAT ATG CCC GG
constitutive expression of *sfgfp* or *mcherry*	
PstI-glmS-fwd	TCA CTG CAG GAA TTC CGT TAT CGC AAG TCG C
OL-glmS-MotP-rev	CAT TTT GAC CCG TCT ATT TAT TCT ACT GTT ACA GAT TTT GCC
OL-glmS-MotP-fwd	AGA ATA AAT AGA CGG GTC AAA ATG TTT CAG ATA TCC T
OL-MotP-sfGfp-rev	TCC TTT GCT CAT CTT AGA CTC TCA ATT AGT AAG CTG TAG
OL-MotP-sfGfp-fwd	TGA GAG TCT AAG ATG AGC AAA GGA GAA GAA CTT TTC AC
OL-MotP-mCherrySO-rev	TTT GGA AAC CAT CTT AGA CTC TCA ATT AGT AAG CTG TAG
OL-MotP-mCherrySO-fwd	TGA GAG TCT AAG ATG GTT TCC AAA GGG GAA GAG GA
PspOMI-sfGfp-rev	TGT GGG CCC TTA GTG GTG GTG GTG GTG GTG
PspOMI-mCherrySO-rev	TCA GGG CCC TTA TTT GTA TAA CTC ATC CAT ACC ACC A
heterologous expression of CheY-strep	
CheY_2_fw	TAC GAG CTC ACC TTG GAC AAG AAT ATG AAG ATT CTC
CheY_2_rv_pASK	ATA CTG CAG AGC GAG TCG TTC GAA TAT TTT ATC TAA

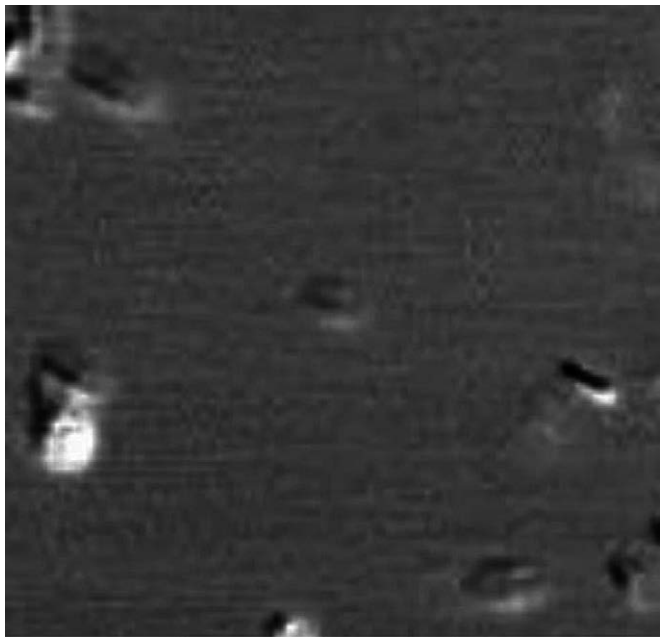

Movie S1. CCW rotation of the lateral filament. The movie shows a *ΔflaAB*$_1$ cell tethered to the surface by its lateral filament.

Movie S1

Chapter 3:

MinD-like ATPase FlhG effects location and number of bacterial flagella during C-ring assembly.

published in Proceedings of the National Academy of Sciences of the United States of America

MinD-like ATPase FlhG effects location and number of bacterial flagella during C-ring assembly

Jan S. Schuhmacher[a,b,1], Florian Rossmann[c,1], Felix Dempwolff[a,b], Carina Knauer[a,b], Florian Altegoer[a,b], Wieland Steinchen[a,b], Anja K. Dörrich[c], Andreas Klingl[a,b,d], Milena Stephan[a,b], Uwe Linne[a,b], Kai M. Thormann[c], and Gert Bange[a,b,2]

[a]LOEWE Center for Synthetic Microbiology (Synmikro) and [b]Department of Chemistry, Philipps University Marburg, 35043 Marburg, Germany; [c]Department of Microbiology and Molecular Biology, Justus-Liebig University, 35392 Giessen, Germany; and [d]Department of Biology I, Ludwig Maximilian University Munich, 82152 Planegg-Martinsried, Germany

Edited by Joe Lutkenhaus, University of Kansas Medical Center, Kansas City, KS, and approved February 10, 2015 (received for review October 8, 2014)

The number and location of flagella, bacterial organelles of locomotion, are species specific and appear in regular patterns that represent one of the earliest taxonomic criteria in microbiology. However, the mechanisms that reproducibly establish these patterns during each round of cell division are poorly understood. FlhG (previously YlxH) is a major determinant for a variety of flagellation patterns. Here, we show that FlhG is a structural homolog of the ATPase MinD, which serves in cell-division site determination. Like MinD, FlhG forms homodimers that are dependent on ATP and lipids. It interacts with a complex of the flagellar C-ring proteins FliM and FliY (also FliN) in the Gram-positive, peritrichous-flagellated *Bacillus subtilis* and the Gram-negative, polar-flagellated *Shewanella putrefaciens*. FlhG interacts with FliM/FliY in a nucleotide-independent manner and activates FliM/FliY to assemble with the C-ring protein FliG in vitro. FlhG-driven assembly of the FliM/FliY/FliG complex is strongly enhanced by ATP and lipids. The protein shows a highly dynamic subcellular distribution between cytoplasm and flagellar basal bodies, suggesting that FlhG effects flagellar location and number during assembly of the C-ring. We describe the molecular evolution of a MinD-like ATPase into a flagellation pattern effector and suggest that the underappreciated structural diversity of the C-ring proteins might contribute to the formation of different flagellation patterns.

flagellum | FlhG | C-ring | *Bacillus* | *Shewanella*

Most bacteria move by flagella. The flagellar architecture is conserved and can be divided into the cytoplasmic C-ring, the basal body, the rod, and the exterior hook and filament structures (1). Bacterial species differ in the number and arrangement of their flagella (flagellation pattern) (2). However, the mechanisms that allow bacteria to establish their specific flagellation patterns reproducibly during each cell division are poorly understood. The protein FlhG (also known as "YlxH," "MinD2," "FleN," or "MotR") is essential for the correct flagellation pattern of polar- (3–5), lophotrichous- (6), amphitrichous- (7), and peritrichous-flagellated bacteria (8, 9). Deletion of *flhG* in polar-flagellated bacteria leads to hyperflagellation and impaired motility (3–5). In the amphitrichous-flagellated *Campylobacter jejuni*, ∼40% of the cells of a Δ*flhG* strain exhibited more than one flagellum at one pole and were impaired in motility (7). The peritrichous-flagellated bacterium *Bacillus subtilis* exhibits ∼26 flagellar basal bodies arranged symmetrically around midcell in a gridlike pattern (8). Furthermore, flagella are discouraged at the cell pole. Deletion of *flhG* does not result in swimming or swarming defects, although multiple flagella appear in tufts from constrained loci on the cell, and flagellar basal bodies often are aggregated (8). FlhG acts in concert with the signal recognition particle (SRP)-GTPase FlhF (10–14) that recruits the flagellar protein FliF to the cell pole in the polar-flagellated *Vibrio cholerae* (15). FlhG is predicted to belong to the MinD/ParA ATPase family (6, 16) whose characterized members act in orchestrated spatiotemporal processes (e.g., cell-division site determination and plasmid/chromosome partitioning (summarized in ref. 17). Together with MinC, MinD constitutes the conserved center of the Min system which regulates bacterial cell division by restricting cytokinetic Z-ring assembly to midcell (reviewed in ref. 18). MinD forms ATP-dependent homodimers (19) that interact with the inner membrane through a C-terminal amphipathic helix (membrane-targeting sequence, MTS) (20, 21). By this mechanism, MinD recruits MinC to the membrane where MinC inhibits polymerization of FtsZ into the Z-ring (22). Interestingly, *Campylobacter jejuni* does not contain a Min system, and FlhG is involved in flagellation pattern control and regulation of cell division (7). In contrast to MinD, the molecular framework in which the putative MinD-like ATPase FlhG controls flagellation is unknown. Also, it is enigmatic how conserved homologs of FlhG can control different flagellation patterns in different species. Here, we investigated the mechanism and function of FlhG in the Gram-positive, peritrichous-flagellated *B. subtilis* (*Bs*) and the Gram-negative, polar-flagellated *Shewanella putrefaciens* (*Sp*).

Results

FlhG Is a MinD-Like ATPase. First, we determined the crystal structure of FlhG. We used FlhG from the moderate thermophile *Geobacillus thermodenitrificans* (*Gt*), because thermophilic proteins tend

Significance

Flagella are bacterial organelles of locomotion. The number and location of flagella (flagellation pattern) are species specific and represent one of the earliest taxonomic criteria in microbiology. During each round of cell division, bacteria reproduce their flagellation pattern. FlhG is essential to a variety of flagellation patterns (e.g., polar, lateral) by yet-unknown mechanisms. We show that FlhG is an MinD-like ATPase that interacts with the flagellar C-ring proteins FliM/FliY in a nucleotide-independent manner. FlhG activates FliM/FliY to assemble with the C-ring protein FliG. FlhG-driven assembly of the FliM/FliY/FliG complex is strongly enhanced by ATP and lipids. We identify an underappreciated structural diversity of flagellar building blocks that contribute to formation of different flagellation patterns.

Author contributions: J.S.S., F.R., M.S., U.L., K.M.T., and G.B. designed research; J.S.S., F.R., F.D., C.K., F.A., W.S., A.K.D., A.K., and G.B. performed research; J.S.S., F.R., F.D., A.K., U.L., K.M.T., and G.B. analyzed data; and J.S.S., K.M.T., and G.B. wrote the paper.

The authors declare no conflict of interest.

This article is a PNAS Direct Submission.

Data deposition: Crystallography, atomic coordinates, and structure factors have been deposited in the Protein Data Bank, www.pdb.org/ (PDB ID codes 4RZ2 and 4RZ3).

[1]J.S.S. and F.R. contributed equally to this work.

[2]To whom correspondence should be addressed. Email: gert.bange@synmikro.uni-marburg.de.

This article contains supporting information online at www.pnas.org/lookup/suppl/doi:10.1073/pnas.1419388112/-/DCSupplemental.

to crystallize better than their mesophilic counterparts (Fig. S1*A*). The crystal structure of *Gt*FlhG was determined at 2.8-Å resolution (Table S1) and lacked residues 1–20 and 265–274, likely because of flexibility. The structures of *Gt*FlhG and *Escherichia coli* (*Ec*) MinD [Protein Data Bank (PDB) ID code 3Q9L] superimpose with an rmsd of 2.3 Å^2 for 160 Cα atoms, revealing a conserved protein core with minor deviations in the helical periphery (Fig. 1*A* and Fig. S1*B*). Structural differences between *Gt*FlhG and *Ec*MinD are most pronounced in an extension of helix α7 and a loop that replaces a helical turn between α6 and β7 found in MinD. Our structural analysis shows conservation of the key active-site motifs required for ATP–Mg^{2+} binding and hydrolysis in FlhG and MinD (Fig. S1*C*). HPLC-based ATP hydrolysis assays proved that *Gt*FlhG is an ATPase with an activity of 51.2 ± 2.4 nmol (ATP)·h^{-1}·nmol(enzyme)$^{-1}$ under our in vitro assay conditions. A *Gt*FlhG D60A variant, which disrupts a catalytically relevant magnesium-binding site, lacks catalytic activity (Fig. 1*B*) (19, 23). Thus, we demonstrate that FlhG is a MinD-like ATPase.

Lipid Interaction of FlhG is ATP Dependent and Mediated by its C-Terminal MTS. The interaction of MinD with membrane lipids is mediated by its MTS (20, 21). Its amphipathic nature is conserved between FlhG and MinD proteins (Fig. S1*C*). The *Gt*FlhG structure resolves the putative MTS (helix α10) that packs into a hydrophobic groove formed by helices α4 and α5 of FlhG (Fig. 2*A*). To investigate whether α10 also serves as an MTS in FlhG, we fused α10 of *Gt*FlhG to the C terminus of GFP (GFP-α10) and investigated its subcellular localization. GFP-α10 localized predominantly at the plasma membrane (Fig. 2*B*, *Left*). Substitution of the conserved phenylalanines 276 and 277 in α10 by alanines (GFP-α10-F2A) abolished its membrane association (Fig. 2*B*, *Right*). Thus, helix α10 of FlhG constitutes an MTS. To validate these findings biochemically, we performed flotation assays of *Gt*FlhG with large unilamellar vesicles (LUVs) composed of 70% phosphatidylethanolamine (PE) and 30% phosphatidylglycerol (PG) as a model membrane (24). In short, the protein was incubated with LUVs and applied to gradient ultracentrifugation. Upon binding to LUVs, FlhG relocates to the top of the gradient, and unbound protein remains at the bottom of the gradient. In addition, we investigated the influence of ADP and ATP [mimicked by the nonhydrolysable ATP-analog 5′-adenylyl-imidodiphosphate (AMPPNP)] on the lipid binding of FlhG. Although *Gt*FlhG interacted with LUVs in the presence of AMPPNP, no interaction was observed with ADP (Fig. 2*C*). These results demonstrate that FlhG interacts with lipids and imply that ATP-binding to FlhG is required for its lipid interaction.

Crystal Structure of the FlhG Homodimer. By analogy to MinD (19), we reasoned that FlhG also might form ATP-dependent homodimers. To increase the success of crystallizing the FlhG homodimer, we used a catalytically inactive *Gt*FlhG variant (i.e., D60A; Fig. 1*B*) that was used previously to crystallize the MinD homodimer (19). The crystal structure of *Gt*FlhG-D60A was determined at 1.9-Å resolution (Fig. 2*D* and Table S1). The *Gt*FlhG and *Ec*MinD homodimers resemble an ellipselike shape with similar dimensions of 60 Å, 45 Å, and 40 Å and significant structural homology (rmsd of 2.8 Å^2 over 329 Cα atoms; Fig. 2*D* and Fig. S2 *A* and *B*). The subunits are arranged in the same face-to-face orientation, and no differences in the active sites exist (for a detailed structure comparison, see Fig. S2 *C–E*). Electron density corresponding to the MTS was clearly visible in the *Gt*FlhG monomer but was lacking for the MTS in the homodimer. To understand this phenomenon better, we compared the structures of the *Gt*FlhG monomer and homodimer (Fig. 2*E*). In particular, helix α4 and the preceding helical segment α4a undergo significant structural rearrangements of 10 Å and 12 Å, respectively. Also, α4a looses its helical propensity in the homodimer and appears as an elongated loop that contributes to the dimer interface. However, helix α4 (together with α5) also establishes the hydrophobic groove that harbors the MTS in the monomeric state. Our structural comparison shows that the conformational state of helix α4 in the homodimer closes the MTS-binding groove and therefore fosters solvent and lipid accessibility to the MTS. Conversely, binding of the MTS to the hydrophobic groove precludes the movement of α4 and α4a into a configuration suitable for homodimer formation. Thus, MTS-mediated lipid binding and ATP-dependent homodimerization of FlhG are highly dependent on each other. We conclude that FlhG can switch between two mutually exclusive states: (*i*) an ATP-bound homodimer that associates with the plasma membrane through its MTS and (*ii*) an ADP (or nucleotide-free) monomer that is unable to interact with the membrane (Fig. 2*F*).

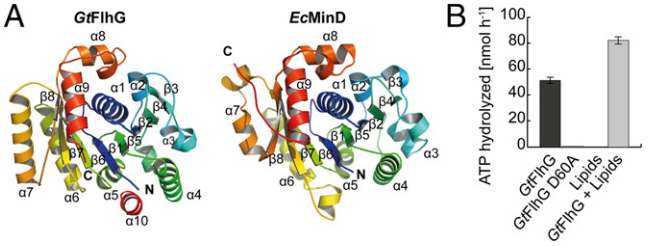

Fig. 1. Crystal structure of the MinD ATPase FlhG. (*A*) Cartoon representation of the crystal structures of *Gt*FlhG (this study, *Left*) and *Ec*MinD (PDB ID: 3Q9L, *Right*). Both structures are rainbow-colored from the N to the C terminus as indicated by "N" and "C," respectively. (*B*) ATPase activity of *Gt*FlhG and the *Gt*FlhG D60A variant (in nanomoles per hour) in the absence or presence of lipids. *Gt*FlhG (20 μM) was incubated with 2 mM ATP at 37 °C for 1 h.

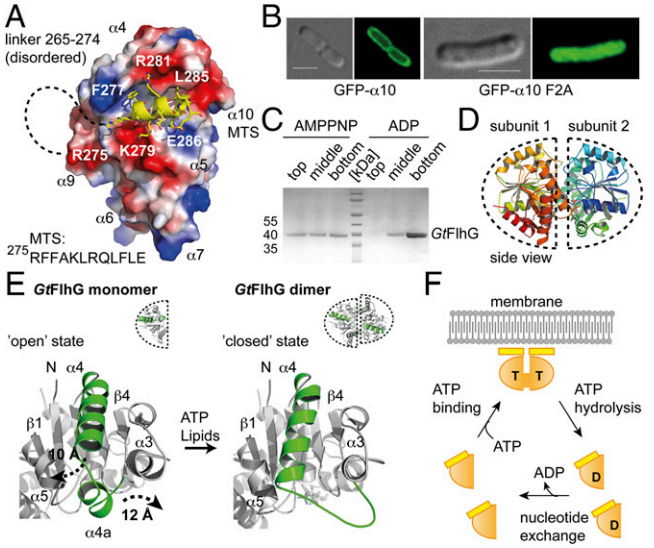

Fig. 2. Lipid- and ATP-dependent homodimerization of FlhG. (*A*) Electrostatic surface view of *Gt*FlhG with the MTS shown in yellow. Dashed lines indicate the disordered linker (residues 265–274) connecting ATPase and the MTS. (*B*) In vivo fluorescence micrographs of GFP-α10 and GFP-α10-F2A show that α10 of *Gt*FlhG is a functional MTS. (Scale bars, 2 μm.) (*C*) Coomassie-stained SDS/PAGE of the flotation assay of *Gt*FlhG with LUVs in the presence of ADP and AMPPNP (from top to bottom fractions). Note: *Gt*FlhG interacting with LUVs is found in the top fraction. (*D*) Cartoon representation of the *Gt*FlhG homodimer. Dashed lines indicate each monomer. Note: Although ATP was added before crystallization, the crystal structure of the *Gt*FlhG homodimer has only ADP bound in its active sites, likely because of residual ATPase activity during crystal growth (3–4 wk). (*E*) Structural differences between the monomeric and dimeric states of *Gt*FlhG. Major conformational changes are shown in green. (*F*) Model of the FlhG ATPase mechanism (orange) showing the ATP (T)-dependent homodimerization and expulsion of the MTS (yellow), membrane interaction of the homodimer through the MTS, and ATP hydrolysis-dependent dissociation of the homodimer.

MICROBIOLOGY

Nucleotide-Independent Interaction of FlhG with the C-Ring Proteins FliM and FliY. To understand the function of *Bs*FlhG, we performed pulldown assays in whole-cell lysates of *B. subtilis* using purified GST-tagged *Bs*FlhG. Mass spectrometry suggested the proteins FliM and FliY as binding partners of FlhG (Fig. S3*A*). FliM interacts directly with FliY (a homolog of FliN), and, together with FliG, all three constitute the flagellar C-ring (reviewed in ref. 1). To validate these findings, we performed in vitro pulldown assays using GST-FlhG and the FliM/FliY complex that were overexpressed in *E. coli* and purified by Ni-ion affinity and size-exclusion chromatography (SEC). The interaction of FlhG and FliM/FliY was validated in vitro for the proteins from *B. subtilis* and *G. thermodenitrificans* (Fig. 3*A* and Fig. S3 *B* and *C*). Finally, we reconstituted the *Gt*FlhG/FliM/FliY complex on SEC (Fig. S3*D*). Proteins from *G. thermodenitrificans* showed more stable biochemical behavior. To correlate biochemical behavior with the structural data, we decided to perform our in vitro experiments with *Gt*FlhG and *Gt*FliM/FliY. Nucleotides (i.e., ADP, ATP, or AMPPNP) did not affect the interaction of GST-*Gt*FlhG with *Gt*FliM/FliY (Fig. 3*A* and Fig. S3*E*). Furthermore, two *Gt*FlhG variants, which are defective in ATP and magnesium binding (i.e., K36Q and D60A, respectively), retained their ability to bind *Gt*FliM/FliY (Fig. S3*F*). Thus, we show that FlhG interacts with a complex of the flagellar C-ring proteins FliM and FliY in a nucleotide-independent manner. To specify which part of the FliM/FliY complex provides the binding site for FlhG, we used hydrogen-deuterium exchange (HDX) mass spectrometry. This method allows rapid determination of protein–protein interfaces (24). Specifically, *Gt*FliM/FliY was incubated with and without *Gt*FlhG and, after completion of the HX-labeling reaction, was digested with pepsin. Peptic peptides were analyzed by electrospray ionization-mass spectrometry. HDX mass spectrometry suggested that FlhG binds to the N terminus of FliY (i.e., amino acids 12–28 of *Gt*FliY) (Fig. 3*B* and Fig. S4). Indeed, a *Gt*FliM/FliY complex in which FliY lacked its N terminus (FliY-ΔNtr), was unable to interact with *Gt*FlhG (Fig. 3*C*). FliY-Ntr contains a highly conserved amino acid motif (i.e., the EIDAL motif), which also is present in the N-terminal region of FliM (FliM-Ntr) (25). However, the absence of the FliM-Ntr at the *Gt*FliM/FliY complex did not influence its ability to bind to *Gt*FlhG (Fig. 3*C*). Thus, FliY-Ntr primarily mediates the interaction of FlhG with the FliM/FliY complex.

Molecular Evolution of a MinD-Like ATPase into a Flagellar Biogenesis Factor. Next, we wanted to determine which part of FlhG interacts with FliM/FliY. HDX experiments identified two regions in *Gt*FlhG (Fig. 3*B* and Fig. S5) that are located at helices α6 and α7 (Fig. 3*E*). To verify this observation, we varied solvent-exposed amino acid residues at helices α6 and α7 in *Gt*FlhG and probed their binding to *Gt*FliM/FliY by pulldown assays (Fig. 3*D*). Three residues (Lys177, Arg207, and Phe215), which are located on helices α6 and α7 of FlhG, are essential for FliM/FliY binding (Fig. 3 *D* and *E*). As described above, this region represents the major difference between FlhG and MinD. In MinD, the corresponding region is essential for MinC binding (19). Accordingly, *Gt*FlhG is unable to interact with *Gt*MinC (Fig. S3*G*). Therefore, the described structural differences between MinD and FlhG are the basis for their different interactions during cell division (via MinC) and flagella assembly (via FliM/FliY), respectively (Fig. 3*E*). These differences also illustrate how evolution relies on the modification of existing structures for new functions.

Subcellular Behavior of FlhG in *B. subtilis*. To place our findings in a biological context, a *Bs*FlhG-YFP fusion protein was introduced into the native genomic locus in *B. subtilis*. *Bs*FlhG-YFP was monitored using high-resolution fluorescence microscopy in cells that were grown to the exponential or stationary phase. The majority of *Bs*FlhG-YFP localized at the membrane in distinct foci (Fig. 4*A*). These foci could be divided into two main subpopulations that either were stationary for more than 5 s or were dynamic in the millisecond range (n = 200) (Fig. 4*A* and Movie S1). Stationary foci did not show any change in location with an average resting time of 29.0 ± 22.6 s (n = 61). The ratio of stationary to dynamic foci was 23.4:76.6%, indicating that the majority of FlhG is highly mobile. To investigate the cellular function of FlhG further, we used a strain carrying *Bs*FlhG-YFP and the flagellar C-ring protein FliM C terminally fused to CFP (FliM-CFP). As described earlier (8), FliM-CFP is functional and is almost completely static at the membrane, indicating its incorporation into the flagellum. We observed colocalization of FliM and a subfraction of FlhG that occurred for ∼30 s (average colocalization: 33.0 ± 20.1 s; n = 31) (Fig. 4 *B* and *C* and Movies S2, S3, and S4). These data corroborate our biochemical analysis and indicate that the static fraction of FlhG might be involved in allocating flagellar C-ring proteins in *B. subtilis*.

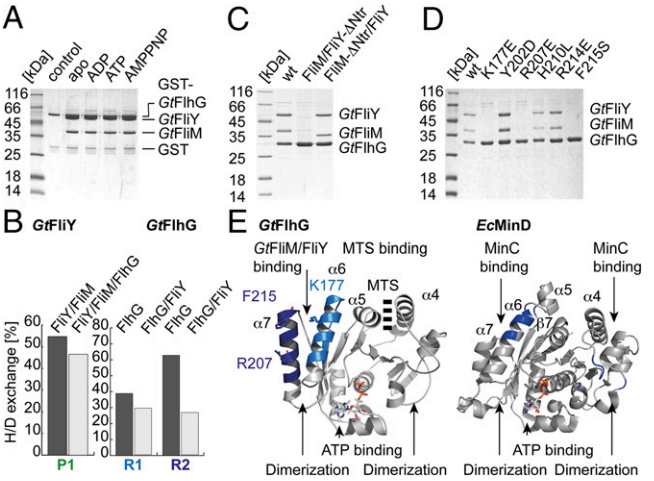

Fig. 3. FlhG interacts with the flagellar C-ring proteins FliM/FliY. (*A*) Coomassie-stained SDS/PAGE of an in vitro pulldown assay of GST-*Gt*FlhG and *Gt*FliM/FliY in the absence and presence of ADP, ATP, or AMPPNP. (*B*) Deuterium incorporation of depicted peptides of free protein and the dimeric *Gt*FlhG/FliY complex are given in percent H/D exchange. Decreased deuterium content upon complex formation indicates potential interfaces (peptides *Gt*FliY R1: DALLRGMDDSDHVPALH; *Gt*FlhG P1: TDAYAMMKYMHAAGSEAPFSV and P2: VFERLKHVTGRFLNKD). (*C*) Coomassie-stained SDS/PAGE of an in vitro pulldown assay using $(His)_6$-tagged *Gt*FlhG, *Gt*FliM/FliY, and *Gt*FliM/FliY variants lacking the FliY-Ntr and FliM-Ntr. (*D*) Coomassie-stained SDS/PAGE of an in vitro pulldown assay using different $(His)_6$-tagged *Gt*FlhG variants and the *Gt*FliM/*Gt*FliY complex. (*E*) Major differences that allow FlhG (*Left*) and MinD (*Right*) to bind FliM/FliY and MinC, respectively, are shown in blue.

The FlhG ATPase Enhances Formation of the FliM/FliY/FliG Complex. The FliM/FliY complex interacts with FliG within the C-ring of a mature flagellum. Therefore, we performed in vitro pulldown assays using GST-tagged *Gt*FliG (GST-*Gt*FliG), *Gt*FliM/FliY, and *Gt*FlhG that were produced in *E. coli* and purified by Ni-ion affinity and SEC. First, we analyzed the in vitro binding of purified *Gt*FliM/FliY to GST-*Gt*FliG in the absence or presence of *Gt*FlhG. In the absence of FlhG, FliM/FliY did not interact with GST-FliG. However, the presence of FlhG yielded an almost stoichiometric binding of FliM/FliY and FlhG to GST-FliG (Fig. 4*D*). These data show that FlhG mediates efficient formation of the FliM/FliY/FliG complex in vitro. Delivery of FliM/FliY to FliG would position FlhG in close proximity to the membrane, where FlhG could interact with membrane lipids through its MTS and dimerize in an ATP-dependent manner. Possible spatial restraints of FlhG by the membrane on the one hand and by FliM/FliY on the other suggested that FlhG also might contact FliG. Therefore, we investigated whether FlhG could interact with FliG and whether this interaction would be nucleotide and/or lipid dependent. GST-*Gt*FliG and *Gt*FlhG were incubated in the absence and presence of ADP, ATP, lipids, and their combinations. FliG/FlhG interaction was observed in the presence of ATP+lipids,

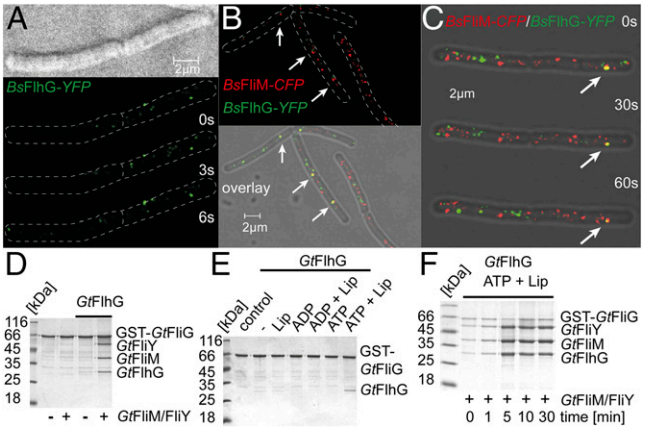

Fig. 4. Physiological role of FlhG. (*A*) Localization of a *Bs*FlhG-YFP fusion protein in *B. subtilis* displays distinct foci at the membrane. (*B* and *C*) Localization of FlhG and FliM was detected in *B. subtilis* carrying *Bs*FlhG-YFP (green) and *Bs*FliM-CFP (red). (*D*) Coomassie-stained SDS/PAGE of an in vitro pulldown assay of GST-*Gt*FliG with *Gt*FliM/FliY in the absence and presence of *Gt*FlhG. (*E*) Coomassie-stained SDS/PAGE investigating the ability of *Gt*FlhG to bind to GST-*Gt*FliG and its dependence on lipids, ADP, ADP+lipids, ATP, and ATP+lipids. (*F*) Coomassie-stained SDS/PAGE of a time-resolved pulldown assay (0, 1, 5, 10, and 30 min) investigating the binding of *Gt*FliM/FliY and *Gt*FlhG to GST-*Gt*FliG in presence of ATP and lipids.

but no interaction occurred with lipids alone, ADP, ADP+lipids, or ATP (Fig. 4*E*). Thus, we conclude that lipid-mediated and ATP-dependent homodimerization of FlhG is a prerequisite for its interaction with FliG. These findings also indicate that ATP and lipids might influence the FlhG-mediated assembly of FliM/FliY into FliG. Therefore, we analyzed the *Gt*FlhG-mediated binding of *Gt*FliM/FliY to GST-*Gt*FliG at different time points in the presence of ATP and lipids (Fig. 4*F* and Fig. S3*H*). We observed a gradual increase of FliM/FliY/FlhG binding to GST-FliG over time. After ∼5 min, we observed a stoichiometric ratio exceeding 1 of FliM/FliY/FlhG compared with GST-FliG, suggesting the oligomeric assembly of FliM/FliY structures at GST-FliG. These findings strongly indicate that FlhG coordinates the assembly of FliM/FliY to FliG in an ATP- and lipid-dependent manner.

FlhG Is Essential for the Polar Flagellation Pattern in *S. putrefaciens*. FlhG also is conserved among other bacteria with polar, lophotrichous, and amphitrichous flagellation (2, 11, 26). To understand whether the functional role and mechanistic principles of FlhG could be applied to other flagellated bacteria, we chose the Gram-negative γ-proteobacterium *S. putrefaciens* (*Sp*) CN-32. This species possesses gene clusters encoding two distinct flagellar systems (27, 28). Expression of the primary cluster, which also comprises *flhG*, leads to production of a single flagellar filament at the cell pole (Fig. 5*A*, *Upper*). Subpopulations expressing the secondary system develop a secondary flagellum at a lateral position (27). An in-frame deletion of *flhG* in *S. putrefaciens* resulted in cells that were hardly motile and were hyperflagellated (2–16 filaments) at the cell pole (Fig. 5*A*, *Lower* and Fig. S6 *A* and *B*). Western blot analysis confirmed successful gene deletion (Fig. S6*C*). This observation agrees with the hyperflagellation phenotypes of *flhG* deletions in other polar-flagellated γ-proteobacteria (12, 15, 26, 29). Using fluorescence labeling on $FlgE_{2\text{-}Cys}$ (the T242C mutant) as a marker for the secondary lateral flagellum (30, 31), we found that the size, number, and position of the secondary flagellum did not change significantly in Δ*flhG* mutants (14.1% wild-type; 15.2% Δ*flhG*) (Fig. S6 *D* and *E*). Thus, we conclude that *Sp*FlhG addresses the primary polar flagellum. *Sp*FlhG exhibited ATPase activity (Fig. 5*B*), and strains bearing a hydrolysis-deficient FlhG variant (i.e., K29A) displayed a hyperflagellation phenotype comparable to that of the Δ*flhG* strain (Fig. S6*A*). Therefore, ATPase activity of *Sp*FlhG is essential to restrict the number of polar flagella to one. Similarly, mutants within the C-terminal MTS of *Sp*FlhG (i.e., with phenylalanines 275/276 replaced by alanines) exhibited a hyperflagellated phenotype (Fig. S6*A*). The presence of these proteins was verified by Western blot analysis (Fig. S6*C*). Thus, we confirmed the hallmark features of *Bs*FlhG in *Shewanella*.

FlhG Interacts with the C-Ring Proteins $FliM_1/FliN_1$ of the Polar Flagellum in *S. putrefaciens*. We reasoned that *Sp*FlhG interacts with the C-ring proteins $FliM_1$ and $FliN_1$ (a homolog of FliY) of the polar flagellum but not with $FliM_2$ and $FliN_2$ of the lateral flagellum. In fact, our in vitro pulldown assays show that *Sp*FlhG interacts with the $FliM_1/FliN_1$ complex but does not interact with $FliM_2/FliN_2$ (Fig. 5*C*). In *S. putrefaciens*, only $FliM_1$, but not $FliM_2$, harbors the conserved EIDAL motif within its N-terminal region (28). A $FliM_1/FliN_1$ complex that lacked the $FliM_1$-Ntr did not interact with *Sp*FlhG in vitro (Fig. 5*D*). Complementary in vivo experiments demonstrated that deletion of *fliM*$_1$ in *S. putrefaciens* or removal of the $FliM_1$-Ntr from $FliM_1$ phenocopied an *flhG* deletion strain with respect to hyperflagellation and motility (Fig. S6 *A* and *F*). An *S. putrefaciens* strain carrying the red fluorescent reporter protein mCherry fused to the C terminus of $FliM_1$ was constructed to determine its cellular localization. Distinct foci were observed at one pole in 41% of the cells (Fig. 5*E*, *Left*). Deletion of the $FliM_1$-Ntr in the mCherry fusion protein reduces the proportion of cells exhibiting a correct localization to 22% (Fig. 5*E*, *Right*). Western blot analysis confirmed the expression of the fluorescently labeled proteins (Fig. S6*G*). Thus, we show that FlhG interacts with $FliM_1/FliN_1$ through a conserved motif at the N terminus of $FliM_1$.

Discussion

Similarities and Differences Between MinD and FlhG. FlhG preserved the hallmarks of MinD such as the overall fold, active site architecture, and ATPase activity. Both proteins form ATP-dependent homodimers that interact with membranes through a conserved MTS (this study and refs. 19–21). Therefore, like MinD, FlhG can cycle between two distinct states: a membrane-associated, ATP-bound homodimer and an ADP-bound (or nucleotide-free) monomer. In the *E. coli* Min system, MinE stimulates the activity of the MinD ATPase (32–34) and therefore releases MinD from the membrane. By analogy to MinD, we

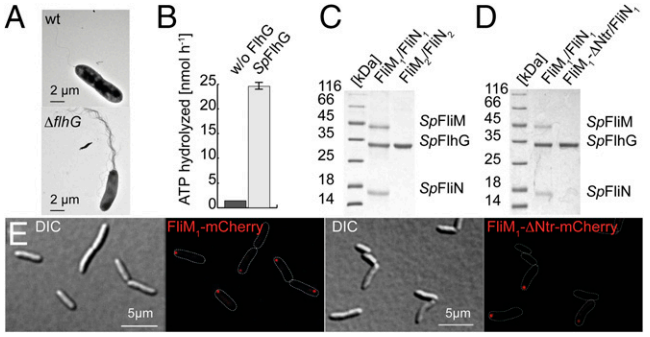

Fig. 5. Role of FlhG in the polar- and lateral-flagellated *S. putrefaciens*. (*A*) Electron micrographs of *S. putrefaciens* (*Upper*) and its Δ*flhG* mutant (*Lower*). (*B*) *Sp*FlhG ATPase activity (in nanomoles per hour). FlhG (100 μM) was incubated with 1 mM ATP at 37 °C for 30 min. (*C*) Coomassie-stained SDS/PAGE of an in vitro pulldown assay shows that $(His)_6$-tagged *Sp*FlhG interacts with *Sp*$FliM_1/FliN_1$ but not with *Sp*$FliM_2/FliN_2$. (*D*) Coomassie-stained SDS/PAGE of an in vitro pulldown assay shows that $(His)_6$-tagged *Sp*FlhG does not interact with an *Sp*$FliM_1/FliN_1$ variant lacking the N-terminal 27 amino acids of $FliM_1$ ($FliM_1$-ΔNtr). (*E*, *Left*) $FliM_1$-mCherry localizes in distinct foci at the cell pole of *S. putrefaciens* in 41% of the cells (n = 576). (*Right*) $FliM_1$-ΔNtr-mCherry displays decreased polar localization (22% of cells; n = 456).

MICROBIOLOGY

speculate that accessory factors influence the FlhG ATPase. FlhG deviates from MinD mainly at helices α6 and α7, which have been shown to mediate the interaction of MinD and MinC. The molecular differences at α6 and α7 create a new interface that enables FlhG to interact with the flagellar C-ring proteins but also prevent FlhG from binding MinC. Taken together, these observations provide the molecular basis for the evolution of a MinD-ATPase into a flagellar assembly factor.

Physiological Role of FlhG. In *B. subtilis*, FlhG shows a highly dynamic behavior, suggesting that FlhG cycles between the cytoplasm and basal bodies/membrane. FlhG interacts with the FliM/FliY complex in a nucleotide-independent manner. Therefore, we speculated that FlhG might capture FliM/FliY in the cytoplasm and deliver the complex to FliG at nascent flagellar structures. Indeed, binding of FlhG to FliM/FliY seems to be a prerequisite for their productive interaction with FliG under our in vitro assay conditions. This observation suggests that FlhG induces a conformational change in FliM/FliY enabling their interaction with FliG. Whether FlhG-mediated assembly of FliM/FliY/FliG takes place in the cytoplasm before their attachment to FliF or whether FliG already resides at the nascent flagellar structure cannot yet be resolved. Furthermore, our in vitro assays show an FlhG-dependent assembly of oligomeric FliM/FliY structures at FliG in the presence of lipids and ATP that also are required for FlhG homodimerization. This observation suggests the homodimer has a role in coordinating the FliM/FliY/FliG assembly. However, the precise mechanism requires further research. A puzzling observation is that FlhG is not released from C-rings in vitro. In contrast, in vivo FlhG resides at the nascent flagellar structure/plasma membrane only temporarily, suggesting accessory factors are needed to release FlhG from the C-ring. In the peritrichous-flagellated *B. subtilis*, basal bodies appear in a grid-like pattern as monitored by a fluorescently labeled FliM (8). Deletion of *flhG* leads to severe aggregation of basal bodies. Deletion of *flhG* in *S. putrefaciens*, which contains a polar and lateral flagellar system, leads to an increased number of polar flagella, but neither the position of the lateral flagellum nor its number is changed. This finding is in agreement with other polar-flagellated bacteria in which deletion of *flhG* also increases the number of polar flagella (3–5). In *S. putrefaciens*, FlhG interacts with $FliM_1/FliN_1$ of the polar flagellar system but not with $FliM_2/FliN_2$ of the lateral one. Moreover, deletion of the $FliM_1$-Ntr, which binds FlhG, results in an increased number of polar flagella in *S. putrefaciens* (as observed for Δ*flhG*). Also, in the amphitrichous-flagellated *C. jejuni*, a functional connection between FlhG and flagellar C-ring proteins was shown, although no direct protein–protein interaction data are available thus far (7). Taken together, these findings suggest that FlhG executes its role in the formation of the flagellation pattern during the assembly of the flagellar C-ring. However, at this point we cannot say whether FlhG delivers C-ring proteins to the nascent flagellum or if FlhG binding to these proteins blocks the assembly of a nascent flagellum. Both models are equally plausible, and further experiments are needed for clarification.

FlhG and the Diversity of Flagellar C-Ring Proteins. FlhG interacts with FlhF in polar-, amphitrichous-, and peritrichous-flagellated bacteria (11, 12, 14), and a conserved motif at the N terminus of FlhG stimulates the GTPase activity of FlhF in *B. subtilis* (11). Although the FlhF–FlhG interaction seems to be conserved, subtle differences might contribute to the regulation of different flagellation patterns. Moreover, FlhG also might be involved in the regulation of flagellar gene expression. In *Pseudomonas aeruginosa* and *V. cholerae*, FlhG interacts with FleQ (also FlrA), a master regulator of flagella gene expression (35–37), adding another layer of complexity to the role of FlhG. However, *C. jejuni* and *B. subtilis* lack FleQ, and whether FlhG contributes to transcriptional regulation in these bacteria is unknown. In *B. subtilis* and *S. putrefaciens* FlhG binds to a region at the N termini of FliY and $FliM_1$, respectively, that contains the

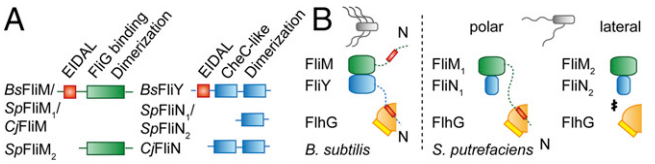

Fig. 6. FlhG and the diversity of flagellar C-ring proteins. (*A*) Diversity in the architecture of the C-ring proteins FliM (*Left*, green) and FliY/FliN (*Right*, blue) from *B. subtilis*, *S. putrefaciens*, and *C. jejuni*. The conserved EIDAL motif is shown in red. (*B*) Interaction of FlhG with flagellar C-ring complexes in *B. subtilis* (*Left*) and *S. putrefaciens* (*Right*). The EIDAL motifs are shown in red. "N" indicates N termini.

conserved EIDAL motif. In mature flagella, this motif binds phosphorylated CheY that switches the flagellar rotor in response to chemosensory signals (Fig. S7) (38–40). Thus, FlhG might shield the CheY-binding site to prevent futile communication of the chemosensory system with nascent flagella. Further differences in the C-ring protein architectures exist (Fig. 6*A*): In *S. putrefaciens*, $FliN_1$ and $FliN_2$ constitute a conserved dimerization domain. However, $FliM_1$ differs from $FliM_2$ in the N-terminal extension to which FlhG binds (Fig. 6*B*). Thus, FlhG affects the polar flagellum but not the lateral one. In *B. subtilis*, FliY is the functional equivalent of FliN, and both proteins share the dimerization domain. However, FliY contains a CheC-like domain (25) and an N-terminal extension to which FlhG binds (Fig. 6*B*). Based on these observations, we speculate that the diversity in flagellar C-ring proteins represents a determinant of flagellation pattern control. In *C. jejuni*, FliN differs from its counterparts in a yet undefined domain that resides N-terminally to its dimerization domain (Fig. 6*A*). *C. jejuni* lacks the MinCD system, and, in addition to their canonical role, FliM, FliN, and FlhG are important for inhibiting futile cell division at the cell poles (7). These observations suggest that the diversity of the C-ring components not only is important for flagellation pattern control but also may link other cellular processes to flagella assembly.

Materials and Methods

Experimental procedures are described in detail in *SI Materials and Methods* and a strain list is given in Table S2.

Protein Purification. Proteins from *B. subtilis*, *G. thermodenitrificans*, and *S. putrefaciens* were obtained as described in *SI Materials and Methods*. Briefly, all proteins were produced in *E. coli* BL21 (DE3) and were purified by Ni-ion affinity and SEC. The SEC buffer consisted of 20 mM Hepes-Na (pH 7.5), 200 mM NaCl, 20 mM KCl, and 20 mM $MgCl_2$. FliM and FliY were coproduced and purified via the same protocol with a $(His)_6$ tag at the C terminus of FliM.

Crystallization and Structure Determination. Crystallization was performed by the sitting-drop method at 20 °C as further detailed in *SI Materials and Methods*. Data were collected at the European Synchrotron Radiation Facility and were processed with iMosflm (41) and SCALA (42). Structures were determined by molecular replacement with PHASER (43), built in COOT (44), and refined with PHENIX (45). Search models were *Ec*MinD (PDB ID code: 3QL9) and *Gt*FlhG (PDB ID code: 4RZ2).

HDX. HDX is described in detail in *SI Materials and Methods*. Briefly, purified proteins and their complexes were incubated in deuterated buffer at 37 °C, and the $^1H/^2H$ exchange reaction was quenched after 30 s by ice-cold quenching buffer (pH 2.2). Peptic peptides were generated by an online pepsin column and separated by reversed-phase HPLC. Data were analyzed using the HDX workbench (46).

Flotation Assays. Floatation assays are described in detail in *SI Materials and Methods*. Briefly, LUVs (PE:PG ratio 70:30) were prepared by extrusion (100-nm pores). FlhG and LUVs were incubated for 10 min at 20 °C and were subjected to iodixanol gradient ultracentrifugation. Proteins were precipitated with trichloroacetic acid (TCA) and analyzed by Coomassie-stained SDS/PAGE.

GST-Binding Assays. GST assays are described in detail in *SI Materials and Methods*. All assays were performed in PBS at 4 °C. GST-protein (1 nmol) was immobilized to glutathione-Sepharose beads (GE Healthcare). Next, 2 nmol of a potential interaction partner was incubated for 10 min at 4 °C. Beads were washed with PBS, and GST-proteins or their complexes were eluted with 20 mM glutathione in 50 mM Tris·HCl (pH 7.5) and were analyzed by Coomassie-stained SDS/PAGE.

Hydrolysis Assays. ATPase activity was monitored by HPLC referenced to ADP and ATP standards (see also *SI Materials and Methods*). Nucleotides were separated on a C^{18} column (isocratic flow; 0.8 mL/min) with a phosphate buffer containing 10 mM tetrapentylammonium bromide (TPAB) and 15% (vol/vol) acetonitrile. Nucleotides were quantified (by peak area) using ChemStation (B.04.03).

Motility Assays. Spreading of *S. putrefaciens* CN-32 or its mutants was monitored by light microscopy or on soft-agar plates, using protocols that were established earlier (28) and are described in detail in *SI Materials and Methods*.

Fluorescence Microscopy. Fluorescence microscopy was performed with *B. subtilis* immobilized on agarose pads at a laser-scanning microscope using a 100× objective. For colocalization, YFP and CFP were recorded simultaneously to allow highest spatial accuracy over time. Microscopy on *S. putrefaciens* CN-32 was executed as described (28) with a DMI 6000B microscope (Leica) equipped with a 100× objective. Images were collected and processed with the VisiView Premier software (Visitron Systems) and ImageJ 1.47v software (47).

Transmission Electron Microscopy. Cells were applied to carbon-coated copper grids and negatively stained with 2% (wt/vol) uranyl acetate (27). Electron microscopy was performed on a JEOL JEM-2100 at 120 kV. Further details are given in *SI Materials and Methods*.

Atomic coordinates and structure factors have been deposited with the Protein Data Bank (PDB) under ID codes 4RZ2 and 4RZ3.

ACKNOWLEDGMENTS. We thank Irmi Sinning for continuous support; Peter Graumann and Uwe-G. Maier for support with fluorescence and electron microscopy, respectively; Daniel B. Kearns for providing *B. subtilis* strains; Nico Kümmerer for his contribution in the beginning of the project; and Ulrike Ruppert for technical assistance. We are grateful to Matthew McIntosh for commenting on the manuscript. We acknowledge the assistance of the European Synchrotron Radiation Facility (Grenoble). This project was supported by the LOEWE Program of the State of Hesse (G.B.), the Peter and Traudl Engelhorn Foundation (G.B.), Fonds der Chemischen Industrie (G.B. and J.S.S.), and the Deutsche Forschungsgemeinschaft through TH831/5-1 within the framework SPP1617 (to K.M.T.) and INST 160/621-1 FUGG (to G.B. and U.L.).

1. Chevance FF, Hughes KT (2008) Coordinating assembly of a bacterial macromolecular machine. *Nat Rev Microbiol* 6(6):455–465.
2. Altegoer F, Schuhmacher J, Pausch P, Bange G (2014) From molecular evolution to biobricks and synthetic modules: A lesson by the bacterial flagellum. *Biotechnol Genet Eng Rev* 30:49–64.
3. Kusumoto A, et al. (2006) Regulation of polar flagellar number by the *flhF* and *flhG* genes in *Vibrio alginolyticus*. *J Biochem* 139(1):113–121.
4. Campos-García J, Nájera R, Camarena L, Soberón-Chávez G (2000) The *pseudomonas aeruginosa motR* gene involved in regulation of bacterial motility. *FEMS Microbiol Lett* 184(1):57–62.
5. Dasgupta N, Arora SK, Ramphal R (2000) *fleN*, a gene that regulates flagellar number in *Pseudomonas aeruginosa*. *J Bacteriol* 182(2):357–364.
6. van Amsterdam K, van der Ende A (2004) *Helicobacter pylori* HP1034 (*ylxH*) is required for motility. *Helicobacter* 9(5):387–395.
7. Balaban M, Hendrixson DR (2011) Polar flagellar biosynthesis and a regulator of flagellar number influence spatial parameters of cell division in *Campylobacter jejuni*. *PLoS Pathog* 7(12):e1002420.
8. Guttenplan SB, Shaw S, Kearns DB (2013) The cell biology of peritrichous flagella in *Bacillus subtilis*. *Mol Microbiol* 87(1):211–229.
9. Mukherjee S, Kearns DB (2014) The structure and regulation of flagella in *Bacillus subtilis*. *Annu Rev Genet* 48:319–340.
10. Bange G, Petzold G, Wild K, Parlitz RO, Sinning I (2007) The crystal structure of the third signal-recognition particle GTPase FlhF reveals a homodimer with bound GTP. *Proc Natl Acad Sci USA* 104(34):13621–13625.
11. Bange G, et al. (2011) Structural basis for the molecular evolution of SRP-GTPase activation by protein. *Nat Struct Mol Biol* 18(12):1376–1380.
12. Kusumoto A, et al. (2008) Collaboration of FlhF and FlhG to regulate polar-flagella number and localization in *Vibrio alginolyticus*. *Microbiology* 154(Pt 5):1390–1399.
13. Schniederberend M, Abdurachim K, Murray TS, Kazmierczak BI (2013) The GTPase activity of FlhF is dispensable for flagellar localization, but not motility, in *Pseudomonas aeruginosa*. *J Bacteriol* 195(5):1051–1060.
14. Parrish JR, et al. (2007) A proteome-wide protein interaction map for *Campylobacter jejuni*. *Genome Biol* 8(7):R130.
15. Green JC, et al. (2009) Recruitment of the earliest component of the bacterial flagellum to the old cell division pole by a membrane-associated signal recognition particle family GTP-binding protein. *J Mol Biol* 391(4):679–690.
16. Leipe DD, Wolf YI, Koonin EV, Aravind L (2002) Classification and evolution of P-loop GTPases and related ATPases. *J Mol Biol* 317(1):41–72.
17. Lutkenhaus J (2012) The ParA/MinD family puts things in their place. *Trends Microbiol* 20(9):411–418.
18. Lutkenhaus J, Pichoff S, Du S (2012) Bacterial cytokinesis: From Z ring to divisome. *Cytoskeleton (Hoboken)* 69(10):778–790.
19. Wu W, Park KT, Holyoak T, Lutkenhaus J (2011) Determination of the structure of the MinD-ATP complex reveals the orientation of MinD on the membrane and the relative location of the binding sites for MinE and MinC. *Mol Microbiol* 79(6):1515–1528.
20. Szeto TH, Rowland SL, Habrukowich CL, King GF (2003) The MinD membrane targeting sequence is a transplantable lipid-binding helix. *J Biol Chem* 278(41):40050–40056.
21. Zhou H, Lutkenhaus J (2003) Membrane binding by MinD involves insertion of hydrophobic residues within the C-terminal amphipathic helix into the bilayer. *J Bacteriol* 185(15):4326–4335.
22. Dajkovic A, Lan G, Sun SX, Wirtz D, Lutkenhaus J (2008) MinC spatially controls bacterial cytokinesis by antagonizing the scaffolding function of FtsZ. *Curr Biol* 18(4):235–244.
23. Leonard TA, Butler PJ, Löwe J (2005) Bacterial chromosome segregation: Structure and DNA binding of the Soj dimer—a conserved biological switch. *EMBO J* 24(2): 270–282.
24. Stjepanovic G, et al. (2011) Lipids trigger a conformational switch that regulates signal recognition particle (SRP)-mediated protein targeting. *J Biol Chem* 286(26): 23489–23497.
25. Szurmant H, Bunn MW, Cannistraro VJ, Ordal GW (2003) *Bacillus subtilis* hydrolyzes CheY-P at the location of its action, the flagellar switch. *J Biol Chem* 278(49):48611–48616.
26. Kazmierczak BI, Hendrixson DR (2013) Spatial and numerical regulation of flagellar biosynthesis in polarly flagellated bacteria. *Mol Microbiol* 88(4):655–663.
27. Bubendorfer S, et al. (2012) Specificity of motor components in the dual flagellar system of *Shewanella putrefaciens* CN-32. *Mol Microbiol* 83(2):335–350.
28. Bubendorfer S, Koltai M, Rossmann F, Sourjik V, Thormann KM (2014) Secondary bacterial flagellar system improves bacterial spreading by increasing the directional persistence of swimming. *Proc Natl Acad Sci USA* 111(31):11485–11490.
29. Murray TS, Kazmierczak BI (2006) FlhF is required for swimming and swarming in *Pseudomonas aeruginosa*. *J Bacteriol* 188(19):6995–7004.
30. Blair KM, Turner L, Winkelman JT, Berg HC, Kearns DB (2008) A molecular clutch disables flagella in the *Bacillus subtilis* biofilm. *Science* 320(5883):1636–1638.
31. Courtney CR, Cozy LM, Kearns DB (2012) Molecular characterization of the flagellar hook in *Bacillus subtilis*. *J Bacteriol* 194(17):4619–4629.
32. Lackner LL, Raskin DM, de Boer PA (2003) ATP-dependent interactions between *Escherichia coli* Min proteins and the phospholipid membrane in vitro. *J Bacteriol* 185(3):735–749.
33. Park KT, et al. (2011) The Min oscillator uses MinD-dependent conformational changes in MinE to spatially regulate cytokinesis. *Cell* 146(3):396–407.
34. Park KT, Wu W, Lovell S, Lutkenhaus J (2012) Mechanism of the asymmetric activation of the MinD ATPase by MinE. *Mol Microbiol* 85(2):271–281.
35. Dasgupta N, Ramphal R (2001) Interaction of the antiactivator FleN with the transcriptional activator FleQ regulates flagellar number in *Pseudomonas aeruginosa*. *J Bacteriol* 183(22):6636–6644.
36. Correa NE, Peng F, Klose KE (2005) Roles of the regulatory proteins FlhF and FlhG in the *Vibrio cholerae* flagellar transcription hierarchy. *J Bacteriol* 187(18):6324–6332.
37. Jain R, Kazmierczak BI (2014) A conservative amino acid mutation in the master regulator FleQ renders *Pseudomonas aeruginosa* aflagellate. *PLoS ONE* 9(5):e97439.
38. Bren A, Eisenbach M (1998) The N terminus of the flagellar switch protein, FliM, is the binding domain for the chemotactic response regulator, CheY. *J Mol Biol* 278(3): 507–514.
39. Welch M, Oosawa K, Aizawa S, Eisenbach M (1993) Phosphorylation-dependent binding of a signal molecule to the flagellar switch of bacteria. *Proc Natl Acad Sci USA* 90(19):8787–8791.
40. Sourjik V, Armitage JP (2010) Spatial organization in bacterial chemotaxis. *EMBO J* 29(16):2724–2733.
41. Battye TGG, Kontogiannis L, Johnson O, Powell HR, Leslie AGW (2011) iMOSFLM: A new graphical interface for diffraction-image processing with MOSFLM. *Acta Crystallogr D Biol Crystallogr* 67(Pt 4):271–281.
42. Winn MD, et al. (2011) Overview of the CCP4 suite and current developments. *Acta Crystallogr D Biol Crystallogr* 67(Pt 4):235–242.
43. McCoy AJ, et al. (2007) Phaser crystallographic software. *J Appl Cryst* 40(Pt 4):658–674.
44. Emsley P, Cowtan K (2004) Coot: Model-building tools for molecular graphics. *Acta Crystallogr D Biol Crystallogr* 60(Pt 12 Pt 1):2126–2132.
45. Adams PD, et al. (2010) PHENIX: A comprehensive Python-based system for macromolecular structure solution. *Acta Crystallogr D Biol Crystallogr* 66(Pt 2):213–221.
46. Pascal BD, et al. (2012) HDX workbench: Software for the analysis of H/D exchange MS data. *J Am Soc Mass Spectrom* 23(9):1512–1521.
47. Schneider CA, Rasband WS, Eliceiri KW (2012) NIH Image to ImageJ: 25 years of image analysis. *Nat Methods* 9(7):671–675.

Supporting Information

Schuhmacher et al. 10.1073/pnas.1419388112

SI Materials and Methods

Plasmids. Genes encoding for the proteins used in this study were amplified from genomic DNAs of *B. subtilis* PY79, *G. thermodenitrificans* NG80-2, and *S. putrefaciens* CN-32 by PCR using Q5 High-Fidelity DNA polymerase (New England Biolabs) according to the manufacturer's manual. Primers were designed according to the following gene annotations: *B. subtilis* PY79: U712_08620 (*flhG*), U712_08570 (*fliM*), and U712_08575 (*fliY*); *G. thermodenitrificans* NG80-2: GTNG_1094 (*flhG*), GTNG_1083 (*fliM*), GTNG_1084 (*fliY*,; GTNG_1073 (*fliG*), and GTNG_2544 (*minC*); and *S. putrefaciens* CN-32: Sputcn32_2560 (*flhG*), Sputcn32_2569 ($fliM_1$), Sputcn32_2568 ($fliN_1$), Sputcn32_3479 ($fliM_2$), and Sputcn32_3480 ($fliN_2$). A protocol for isolating *S. putrefaciens* CN-32 genomic DNA was described previously (1). A $(His)_6$ tag was encoded in either the forward or reverse primer. The PCR fragment was cloned into pET24d(+) or pET16b vectors (Novagen) via commonly used restriction sites (i.e., *NcoI*/*PciI*/*BamHI*/*XhoI*). Enzymes used in this study were purchased from New England Biolabs, Biozym Scientific GmbH, and Fermentas. Mutations within FlhG were generated using QuikChange II site-directed mutagenesis (Agilent). The FlhG-YFP fusion was made by cloning the last 500 coding base pairs of *flhG* (*ylxH* gene) into the plasmid pSG1164 (2). Constructions of markerless in-frame deletion or integration mutants in *S. putrefaciens* CN-32 based on the suicide vector pNPTS138-R6KT were performed as described previously (3, 4). Amino acid substitutions in FlhG were introduced by appropriate codon modifications in *flhG* and reintegration into a Δ*flhG* mutant. Production and stability of the FlhG variants were confirmed by Western immunoblotting. To construct $FliM_1$-ΔNtr, the sequence corresponding to amino acid positions 2–28 was deleted in $fliM_1$ in the background strains. Western immunoblotting and fluorescence microscopy confirmed the stable production of the mCherry-labeled proteins. To enable fluorescence labeling of $FlgE_2$, an ACC-to-TGC codon substitution was introduced into $flgE_2$, yielding a Thr242Cys substitution ($FlgE_{2\text{-}Cys}$). The modified gene was reintroduced into the corresponding Δ$flgE_2$ mutant of *S. putrefaciens* CN-32. The substitution did not affect the motility of the resulting mutant as determined by soft-agar assays (Fig. S6*E*) and light microscopy.

Strains, Growth Conditions, and Media. All strains used and constructed in this study are summarized in Table S2. In *B. subtilis*, FlhG-YFP fusion protein is expressed from the original genetic locus, and a xylose-inducible promotor controls downstream genes. For colocalization studies, a strain expressing FliM-CFP from the ectopic *amyE* locus (a kind gift of Daniel B. Kearns, Indiana University, Bloomington, IN) was transformed with chromosomal DNA of the FlhG-YFP strain. Functionality of FliM-CFP fusion has been demonstrated in the literature (5). The functionality of FlhG was verified intrinsically by coexpression with FliM-CFP, because defective FlhG would have led immediately to aberrant FliM foci, which were not observed (5). *E. coli* strains DH5α λpir, BL-21, and WM3064, *B. subtilis* strain PY 79, and *S. putrefaciens* CN-32 were grown routinely in lysogeny broth (LB) medium at 37 °C and 30 °C, respectively. The medium for the 2,6-diaminopimelic acid (DAP)-auxotroph *E. coli* WM3064 was supplemented with DAP at a final concentration of 300 μM. To solidify media, LB agar was prepared using 1.5% (wt/vol) agar. When required, media were supplemented with 100 μg/mL ampicillin, 50 μg mL kanamycin, and/or 10% (wt/vol) sucrose. To prepare agarose pads for fluorescence microscopy, PBS (137 mM NaCl, 2.7 mM KCl, 10 mM Na_2HPO_4, 1.8 mM KH_2PO_4, pH 7.4) was solidified by adding 1% (wt/vol) agarose. *B. subtilis* strains were plated onto LB-agar plates containing 0.5% xylose and the respective antibiotics. The strains used in this study are listed in Table S2.

Protein Production and Purification. For gene expression, *E. coli* BL21 (DE3) were grown in LB medium under autoinduction conditions [D(+)-lactose-monohydrate, 1.75% (wt/vol)] supplemented with the respective antibiotics (50 μg/mL kanamycin or 100 μg/mL ampicillin) at 30 °C for ∼16 h under constant shaking (150 rpm). Cells were harvested by centrifugation (4,000 rpm/3,500 × *g* for 20 min at 4 °C), suspended in lysis buffer [20 mM Hepes-Na (pH 8.0), 250 mM NaCl, 40 mM imidazole, 20 mM $MgCl_2$, and 20 mM KCl] and subsequently lysed using the M-110L Microfluidizer (Microfluidics). After centrifugation (23,000 rpm/63,000 × *g* for 20 min at 4 °C), the clarified lysate was applied to a 1-mL HisTrap FF column (GE Healthcare) equilibrated with 10 column volumes of lysis buffer. After washing with 70 mL lysis buffer, proteins were eluted using 15 mL elution buffer (lysis buffer containing 500 mM imidazole). Elution fractions containing protein were concentrated using Amicon Ultracel-10K (Millipore) and subsequently applied to SEC (HiLoad 26/600 Superdex 200 pg, GE Healthcare) equilibrated in SEC buffer [20 mM of Hepes-Na (pH 7.5), 200 mM NaCl, 20 mM $MgCl_2$, and 20 mM KCl]. Fractions were analyzed using SDS/PAGE. Protein containing fractions were pooled and concentrated according to experimental requirements. Concentration was determined by a spectrophotometer (NanoDrop Lite; Thermo Scientific). FliM and FliY were coexpressed and copurified via a $(His)_6$ tag at the C terminus of FliM. A trimeric complex containing FliM, FliY, and FlhG was copurified using two His tags at the C terminus of FliM and the N terminus of FlhG.

Crystallization of *Gt*FlhG. All crystallization experiments were carried out by the sitting-drop method in SWISSCI MRC two-well crystallization plates at room temperature. The reservoir volume was 50 μL, and the drop volume was 1 μL, with a 1:1 mixture of protein and crystallization solution. Crystals of apo-*Gt*FlhG were obtained from a 20.0 mg/mL solution after ∼3 wk in 0.1 M Hepes (pH 7.5), 10% (wt/vol) PEG 8000, 0.1 urea. Crystals of the dimeric state of FlhG were obtained from a 20.0 mg/mL solution of the *Gt*FlhG D60A variant after ∼3 wk in a buffer containing 0.1 M Hepes (pH 7.0) and 20% (wt/vol) PEG 6000. Before crystallization, FlhG-D60A was incubated with 4.4 mM ATP for 1 h on ice.

Data Collection, Structure Determination, and Analysis. Before data collection, crystals were flash-frozen in liquid nitrogen after a short incubation in a cryo-protecting solution that consisted of mother liquor supplemented with 20% (vol/vol) glycerol. Data collection was performed at the European Synchrotron Radiation Facility in Grenoble, France under cryogenic conditions beamlines: ID 23-2 (apo-state of FlhG) and ID 23-1 (dimeric state of FlhG). Data were recorded with a DECTRIS PILATUS 6M detector. Data were processed using iMosflm (6) and the CCP4-implemented program SCALA (7). The structure of apo-FlhG was solved by molecular replacement with CCP4-integrated PHASER (8) using *Ec*MinD (PDB ID code: 3QL9) and monomeric FlhG (this study) as search models. Structures were built manually in COOT (9) and were refined using PHENIX refine (10). Figures were designed with PyMol (www.pymol.org).

HDX Mass Spectroscopy. HDX experiments were performed as described previously (11–13). Minor adjustments of the setup mainly concerned the HPLC pumps (isocratic: 1100 series; Agilent Technologies/Hewlett Packard; gradient: 1260 Infinity; Agilent Technologies) and the mass analyzer (Orbitrap Velos Pro; Thermo Scientific). Purified and concentrated *Gt*FlhG and *Gt*FliY, and the *Gt*FlhG-FliY complex (200 pmol, 50 μM) were diluted 10-fold into D_2O-containing SEC buffer [20 mM Hepes (pH 7.5), 200 mM NaCl, 20 mM KCl, and 20 mM $MgCl_2$] and were incubated at 37 °C to start H/D exchange. After 30 s the reaction was quenched by decreasing the temperature to 0 °C and adding one equivalent (50 μL) of Quench buffer [400 mM KH_2PO_4/H_3PO_4 (pH 2.2)]. The samples were injected immediately onto HPLC. Peptic peptides from the on-line digest were analyzed directly by mass spectrometry, and the deuterium content was calculated using HDX workbench (14). Relative deuteron incorporation was calculated based upon the centroids of the molecular ion isotope distribution extracted from the software. For adjustment, the 0% control was treated with H_2O buffer. Complete exchange was defined as 90% of the possible incorporation and applied to all samples, because of dilution and re-exchange during the HPLC run.

GST-Binding Assays. GST pulldown assays were performed in PBS buffer at 4 °C. Purified GST-protein (i.e., GST-FlhG, GST-FliG) (1 nmol) was applied to 15 μL glutathione Sepharose 4B (GE Healthcare) in small filter columns (MoBiTec) by incubation on a wheel for 15 min. Subsequently, 2 nmol of putative binding partners (i.e., FlhG, FliY, FliM) and 2.5 mM of appropriate nucleotides were added and incubated for 10 min at 4 °C on the wheel. After centrifugation [4,000 rpm (3,500 × *g*), for 1 min at 4 °C] the column was washed three times with PBS buffer. Proteins were eluted with 40 μL of GSH buffer [50 mM Tris·HCl, 20 mM GSH (pH 7.5)] and analyzed by Coomassie-stained SDS/PAGE. Conditions for time-resolved GST pulldown assays were adjusted toward physiological temperature (37 °C) and carried out using SEC-buffer.

Ni-NTA Affinity Binding Assays. FlhG variants were investigated for their ability to bind FliM/FliY by Ni-NTA affinity pulldown assays from expression cultures. Expression culture of $(His)_6$-tagged FlhG variants (100 mL) and untagged FliM/FliY coexpression were mixed, harvested, and lysed as stated (*Protein Production and Purification*). Ni-NTA agarose (300 μL) (Qiagen) was added to the clarified lysate and incubated for 15 min on ice. After centrifugation (4,000 rpm/3,500 × *g* for 15 min at 4 °C), the lysate was discarded, and the loaded Ni-NTA agarose was washed three times with 500 μL of lysis buffer and subsequently was centrifuged (4,000 rpm/3,500 × *g* for 5 min at 4 °C). Proteins were eluted with 300 μL of elution buffer and were analyzed by Coomassie-stained SDS/PAGE.

Fluorescence Microscopy. *B. subtilis* cells were cultivated in LB medium at 37 °C to exponential growth phase (OD_{600} 0.5) and were immobilized on coverslips by $S7_{50}$ medium containing agarose pads (1% wt/vol). Fluorescence microscopy was performed on a fully automated Leica SP 8 laser scanning microscope equipped with a 100× HCX PL APO STED objective (NA 1.4), an argon ion laser source, and Leica HyD detectors. Images were analyzed using the Huygens (Scientific Volume Imaging) and LAS AF (Leica) software. Foci that were immobile within the resolution limit (250 nm) for more than 5 s were defined as static.

Shewanella strains were cultured to midexponential phase before imaging. Appropriately diluted cultures (2–5 μL) were added on top of an agar pad to immobilize cells. A DMI6000 B fluorescence microscope (Leica) equipped with a HCX PL APO 100×/1.4 differential interference contrast (DIC) objective was used to visualize single cells. Image acquisition and processing were carried out using the VisiView Premier software (Visitron Systems GmbH) and ImageJ 1.47v software (National Institutes of Health) (15).

Hydrolysis Assays. The ATPase activity was investigated using an HPLC-based assay. FlhG, its D60A variant, and FliG were diluted to 20 μM (1 nmol) and supplemented with 2 mM ATP (100 nmol) and 25 μL of *E. coli* lipid vesicles. Hydrolysis assays were performed in SEC buffer at 37 °C with an incubation time of 1 h. Subsequent flash freezing in liquid nitrogen stopped the hydrolysis reaction. HPLC measurements were performed with an Agilent 1100 Series HPLC system (Agilent Technologies) and a C18 column (EC 250/4.6 Nucleodur HTec 3 μm; Macherey-Nagel). The samples were injected onto HPLC and run for 30 min with a buffer containing 50 mM KH_2PO_4, 50 mM K_2HPO_4, 10 mM TPAB, and 15% (vol/vol) acetonitrile at flow rate of 0.8 mL/min. ADP and ATP were detected by UV light at 260.8 nm and were quantified (by peak area) using ChemStation (B.04.03).

Flotation Assays. PE and PG were supplied by Avanti Polar Lipids. Lipids were mixed in ratio of 70% PE:30% PG, and the chloroform was evaporated under reduced pressure for 30 min. LUVs were prepared in assay buffer [100 mM phosphate, 750 mM NaCl, 10 mM $MgCl_2$, 1.2 M sucrose (pH 7.5)] by extrusion (16). After 10 freeze–thaw cycles, lipids were passed 21 times through a 100-nm pore polycarbonate filter (Nuclepore) in a two-syringe extruder (Avanti Polar Lipids), resulting in LUVs. Proteins were mixed with 50 μL of the LUV solution and were incubated for 20 min. Flotation gradient centrifugation was performed as described previously (17). Samples were mixed with 360 μL of assay buffer containing 50% iodixanol, overlaid with 1.16 mL of assay buffer with 30% iodixanol, and finally overlaid by 450 μL of assay buffer. After ultracentrifugation (Beckmann Coulter) for 3 h at 45,000 rpm (217,000 × *g*) in a swing-out rotor (MLS 50; Beckmann Coulter), the gradient was collected in three fractions (600 μL top, 800 μL middle, 600 μL bottom) and analyzed by SDS/PAGE after TCA precipitation. Briefly, the separated fractions were treated with 100 μL TCA and were incubated overnight at −20 °C. After centrifugation (Heraeus Fresco 17; Thermo Scientific) for 20 min at 13,000 rpm (16,200 × *g*) and 4 °C, the pellets were washed twice with 500 μL chilled acetone. Before SDS/PAGE analysis, the remaining acetone was evaporated (2 min at 95 °C).

Flagellar Staining. Staining of flagellar filaments was performed as described earlier (18). Ten microliters of an exponentially growing culture were spotted onto a microscopy slide and stained before visualization. Microscopy and image acquisition were carried out with a Leica DMI6000B microscope equipped with an HCX PL APO 100×/1.4 DIC objective.

Immunoblot Analysis. To determine production and stability of proteins, lysates from exponentially growing LB cultures were obtained for Western blot analyses. Subsequent to harvesting by centrifugation, cells corresponding to an OD_{600} of 10 were resuspended in sample buffer (19), heated at 99 °C for 5 min, and stored at −20 °C. Ten microliters of sample were resolved by SDS/PAGE using 11% polyacrylamide gels. Subsequently, proteins were transferred to PVDF Immobilon-P membrane (Millipore) through semidry transfer. To detect the fusion proteins, polyclonal antibodies raised against mCherry (Biovision Life Sciences), GFP (Roche GmbH) or purified *Sp*FlhG (in dilutions of 1:10,000, 1:5,000, and 1:1,000, respectively) were used. Secondary anti-rabbit IgG-HRP antibody was used at a dilution of 1:20,000 to detect mCherry and She-FlhG antibodies. For Roche GFP antibodies, a secondary anti-mouse IgG-alkaline phosphatase antibody was used at a dilution of 1:15,000. Signals were detected using the SuperSignal West Pico Chemiluminescent

Substrate (Thermo Scientific) or CDP-Star chemiluminescent substrate (Roche Diagnostics) and were documented using the CCD System Fusion SL4 (PEQLAB Biotechnologie).

Motility Assays. Spreading of *S. putrefaciens* CN-32 wild-type or mutant cell cultures was monitored by light microscopy or on soft-agar plates using previously established protocols (4, 20). Soft-agar plates had an agar concentration of 0.25% (wt/vol); 3 μL of an exponentially growing planktonic culture of the appropriate strain was spotted for a motility assay. The plates were incubated for an adequate amount of time at 30 °C, and the radial extension of the cultures was documented. To compare the radial extension of different mutant strains with that of wild-type *S. putrefaciens* CN-32, the appropriate cultures always were spotted onto the same soft-agar plate.

Fluorescence Staining of $FlgE_{2\text{-}Cys}$. Fluorescence coupling of $FlgE_{2\text{-}Cys}$, as a marker for intact secondary lateral flagella, was carried out essentially according to a previously published protocol (21, 22) with several modifications. One milliliter of a culture of the appropriate strain at 0.5 OD_{600} was pelleted and resuspended in 50 μL PBS buffer containing 5 μg/mL Alexa Fluor 488 C_5 maleimide (Molecular Probes), followed by incubation for 5 min at room temperature. Subsequently, cells were pelleted again and resuspended in 500 μL PBS. For fluorescence microscopy, 5 μL of the suspension was put on top of an agarose pad.

Transmission Electron Microscopy. To prepare samples for electron microscopy according to the methods described in ref. 4, cells were grown to midexponential phase. Glutaraldehyde was added to a final concentration of 1.25% (vol/vol) to fix cells for 15 min before washing once with lactate medium (LM) (10 mM Hepes, pH 7.5; 200 mM NaCl; 0.02% yeast extract; 0.01% peptone; 15 mM lactate). After washing, cells were concentrated via centrifugation at 13,000 rpm. The resulting pellet was suspended in 50 μL of medium, and 5 μL of the cell suspension was applied to glow-discharged and carbon-coated copper grids (400 square mesh; Plano). The samples were washed immediately twice with ddH_2O and were negatively stained with uranyl acetate (2%) for 20 s. Electron microscopy was performed on a JEOL 2100 TEM (JEOL Ltd.) equipped with a LaB_6 cathode and operated at 120 kV. To record images, a fast-scan 2 × 2k camera F214 combined with the EM-Menu 4 software (TVIPS) was used.

1. Pospiech A, Neumann B (1995) A versatile quick-prep of genomic DNA from gram-positive bacteria. *Trends Genet* 11(6):217–218.
2. Lewis PJ, Marston AL (1999) GFP vectors for controlled expression and dual labelling of protein fusions in *Bacillus subtilis*. *Gene* 227(1):101–110.
3. Lassak J, Henche AL, Binnenkade L, Thormann KM (2010) ArcS, the cognate sensor kinase in an atypical Arc system of *Shewanella oneidensis* MR-1. *Appl Environ Microbiol* 76(10):3263–3274.
4. Bubendorfer S, et al. (2012) Specificity of motor components in the dual flagellar system of *Shewanella putrefaciens* CN-32. *Mol Microbiol* 83(2):335–350.
5. Guttenplan SB, Shaw S, Kearns DB (2013) The cell biology of peritrichous flagella in *Bacillus subtilis*. *Mol Microbiol* 87(1):211–229.
6. Battye TGG, Kontogiannis L, Johnson O, Powell HR, Leslie AGW (2011) iMOSFLM: A new graphical interface for diffraction-image processing with MOSFLM. *Acta Crystallogr D Biol Crystallogr* 67(Pt 4):271–281.
7. Winn MD, et al. (2011) Overview of the CCP4 suite and current developments. *Acta Crystallogr D Biol Crystallogr* 67(Pt 4):235–242.
8. McCoy AJ, et al. (2007) Phaser crystallographic software. *J Appl Cryst* 40(Pt 4):658–674.
9. Emsley P, Cowtan K (2004) Coot: Model-building tools for molecular graphics. *Acta Crystallogr D Biol Crystallogr* 60(Pt 12 Pt 1):2126–2132.
10. Adams PD, et al. (2010) PHENIX: A comprehensive Python-based system for macromolecular structure solution. *Acta Crystallogr D Biol Crystallogr* 66(Pt 2): 213–221.
11. Rist W, Jørgensen TJ, Roepstorff P, Bukau B, Mayer MP (2003) Mapping temperature-induced conformational changes in the *Escherichia coli* heat shock transcription factor sigma 32 by amide hydrogen exchange. *J Biol Chem* 278(51):51415–51421.
12. Stjepanovic G, et al. (2011) Lipids trigger a conformational switch that regulates signal recognition particle (SRP)-mediated protein targeting. *J Biol Chem* 286(26):23489–23497.
13. Kressler D, et al. (2012) Synchronizing nuclear import of ribosomal proteins with ribosome assembly. *Science* 338(6107):666–671.
14. Pascal BD, et al. (2012) HDX workbench: Software for the analysis of H/D exchange MS data. *J Am Soc Mass Spectrom* 23(9):1512–1521.
15. Schneider CA, Rasband WS, Eliceiri KW (2012) NIH Image to ImageJ: 25 years of image analysis. *Nat Methods* 9(7):671–675.
16. Hope MJ, Bally MB, Webb G, Cullis PR (1985) Production of large unilamellar vesicles by a rapid extrusion procedure: Characterization of size distribution, trapped volume and ability to maintain a membrane potential. *Biochim Biophys Acta* 812(1):55–65.
17. Parlitz R, et al. (2007) *Escherichia coli* signal recognition particle receptor FtsY contains an essential and autonomous membrane-binding amphipathic helix. *J Biol Chem* 282(44):32176–32184.
18. Heimbrook ME, Wang WL, Campbell G (1989) Staining bacterial flagella easily. *J Clin Microbiol* 27(11):2612–2615.
19. Laemmli UK (1970) Cleavage of structural proteins during the assembly of the head of bacteriophage T4. *Nature* 227(5259):680–685.
20. Bubendorfer S, Koltai M, Rossmann F, Sourjik V, Thormann KM (2014) Secondary bacterial flagellar system improves bacterial spreading by increasing the directional persistence of swimming. *Proc Natl Acad Sci USA* 111(31):11485–11490.
21. Blair KM, Turner L, Winkelman JT, Berg HC, Kearns DB (2008) A molecular clutch disables flagella in the *Bacillus subtilis* biofilm. *Science* 320(5883):1636–1638.
22. Courtney CR, Cozy LM, Kearns DB (2012) Molecular characterization of the flagellar hook in *Bacillus subtilis*. *J Bacteriol* 194(17):4619–4629.

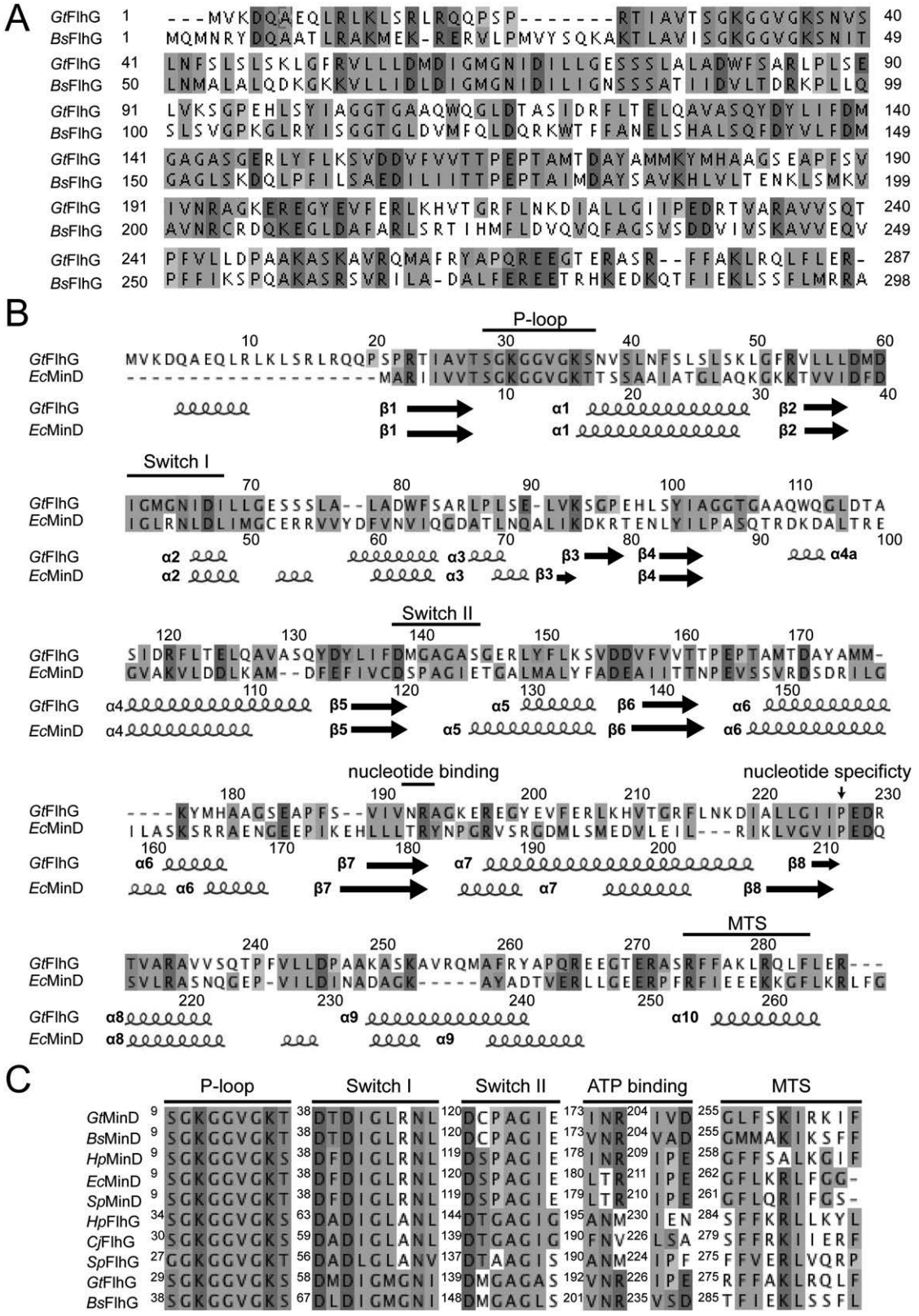

Fig. S1. Sequence and secondary structure alignments. (*A*) The color code indicates conservation and identity of amino acids between the FlhG homologs of *B. subtilis* and *G. thermodenitrificans*. (*B*) Alignment of *Gt*FlhG and *Ec*MinD shows the similarity of these ATPases. Secondary structure elements and important catalytic regions are indicated. *Ec*, *Escherichia coli*; *Gt*, *Geobacillus thermodenitrificans*. (*C*) FlhG and MinD share the catalytically important regions for ATP/magnesium binding and ATP hydrolysis: P-loop, Switch regions I and II, ATP-binding residues and a C-terminal, amphipathic helix. *Bs*, *Bacillus subtilis*; *Cj*, *Campylobacter jejuni*; *Ec*, *Escherichia coli*; *Gt*, *Geobacillus thermodenitrificans*; *Hp*, *Helicobacter pylori*; *Sp*, *Shewanella putrefaciens*.

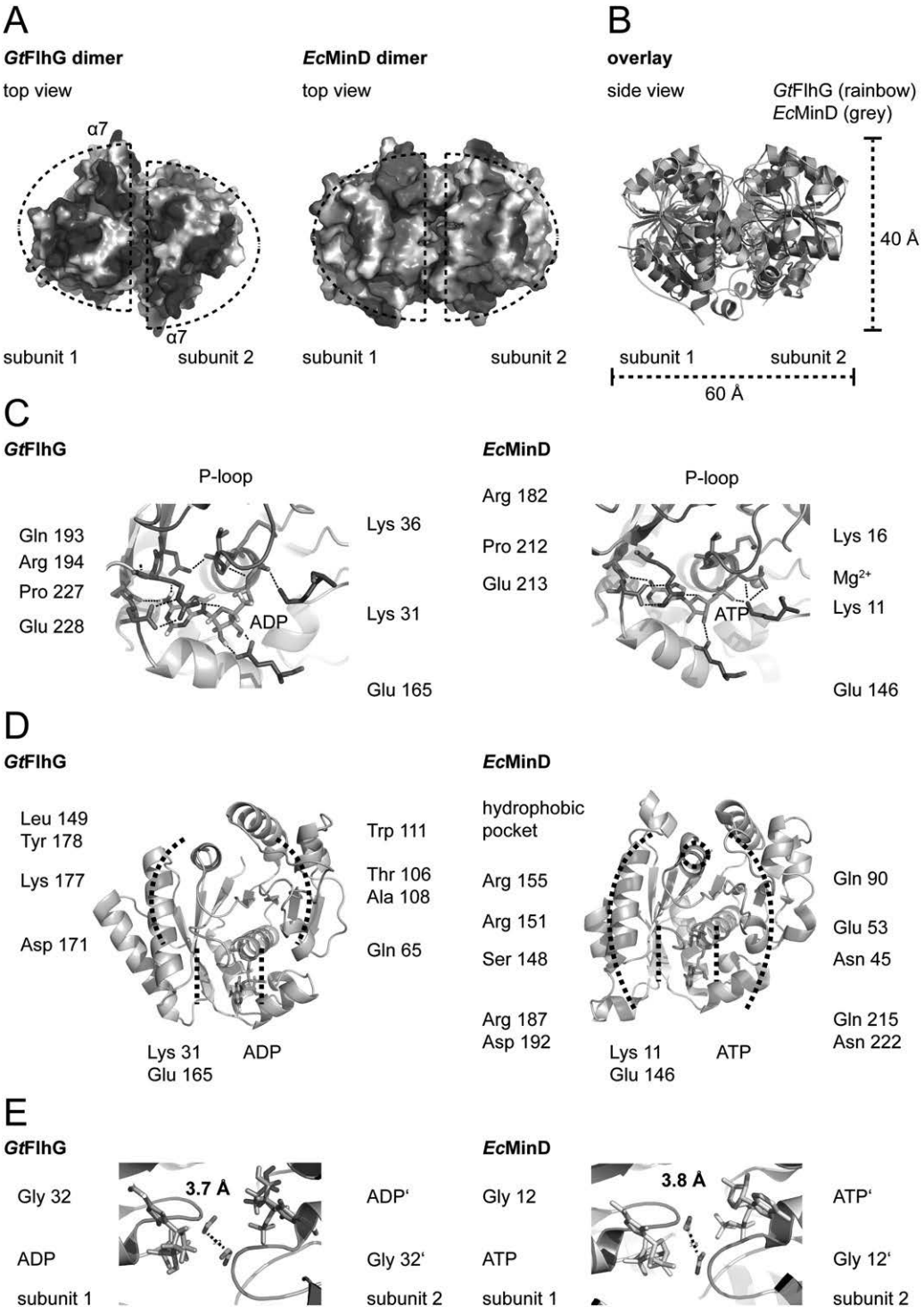

Fig. S2. Detailed structural analysis of the FlhG dimer. (*A*) Electrostatic surface views of the *Gt*FlhG (*Left*) and *Ec*MinD (*Right*) homodimers. The half-sites of each the homodimers are indicated by dashed lines. A protrusion caused by the extension of helix α7is visible in the FlhG homodimer. (*B*) Superimposition of the FlhG and MinD homodimers shown in rainbow color and gray, respectively. The dashed lines indicate approximate dimensions in angstroms. (*C*) A comparison of the active site of FlhG (*Left*) and MinD (*Right*) shows high structural resemblance and conservation of important residues. (*D*) The dimerization interface is larger in MinD than in FlhG (MinD: ~1,100 Å^2; FlhG: ~700 Å^2). Important elements are colored in green. Dashed lines represent the interaction interface. (*E*) The space between the subunits in FlhG (3.7 Å, *Left*) and MinD (3.8 Å, *Right*) is similar and was measured as the distance between conserved glycine residues (indicated as sticks) in the P-loop.

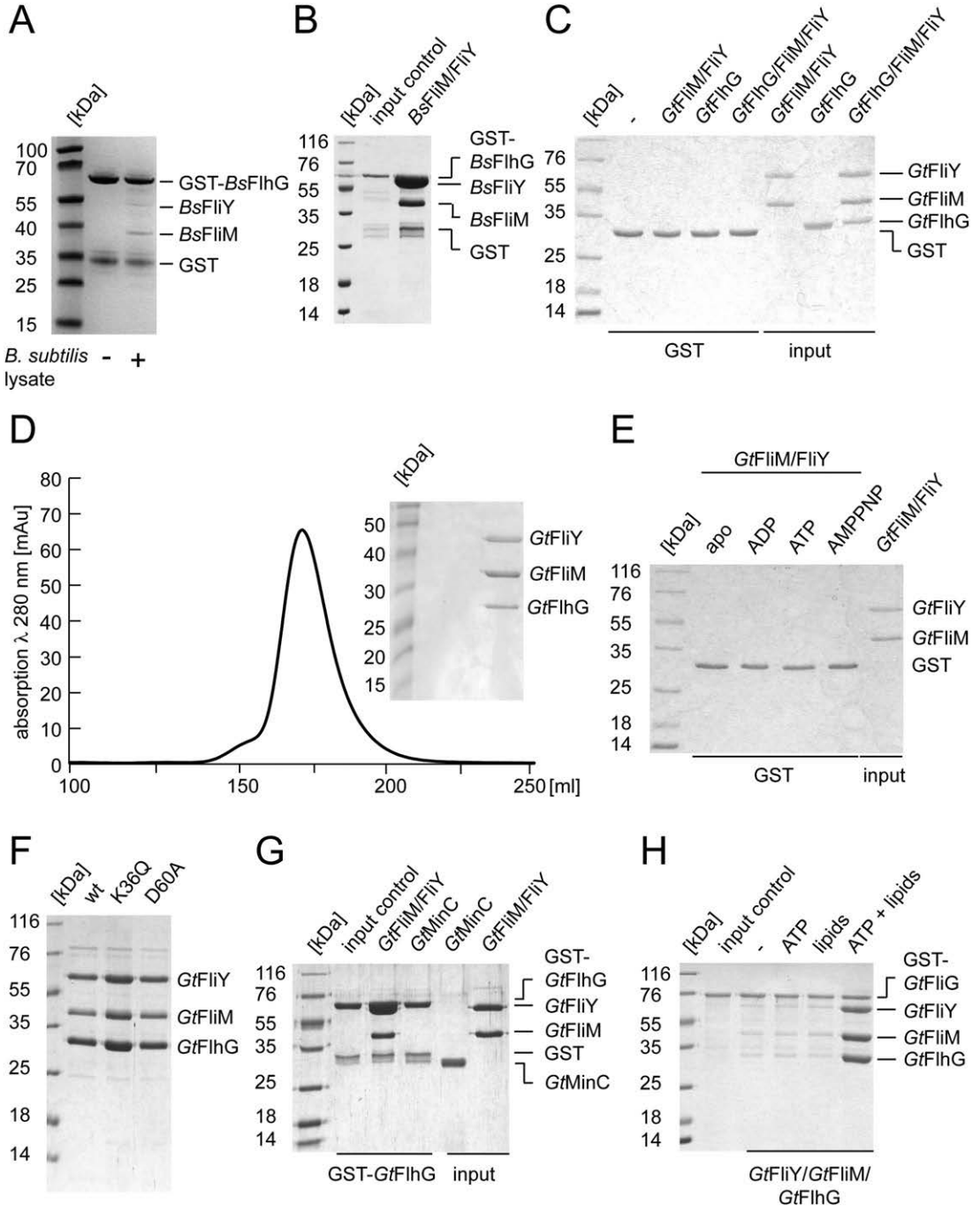

Fig. S3. FlhG binds FliM/FliY independent of nucleotides. (*A*) SDS/PAGE of an in vitro pulldown assay from whole-cell lysate of *B. subtilis* using GST-*Bs*FlhG. Mass spectrometry identified the potential interaction partners FliM and FliY. (*B*) Coomassie-stained SDS/PAGE of an in vitro pulldown assay demonstrates that GST-*Bs*FlhG (input control) interacts directly with *Bs*FliM/FliY. (*C*) In vitro pulldown assays using GST show that a *Gt*FliM/FliY complex, *Gt*FlhG, and a *Gt*FlhG/FliM/FliY complex do not interact with GST. Input controls are identified on the right. (*D*) Size-exclusion chromatogram of the *Gt*FliM/FliY/FlhG complex. (*Inset*) A Coomassie-stained SDS/PAGE of the peak fraction. (*E*) Coomassie-stained SDS/PAGE of the control pulldown assays reveals no unspecific interaction of a *Gt*FliM/FliY complex with GST in the presence of ADP, ATP, or AMPPNP. (*F*) In vitro pulldown assays show that two hydrolysis-deficient variants of *Gt*FlhG (K36Q and D60A) are as able to bind a *Gt*FliM/*Gt*FliY complex as the wild-type. (*G*) Coomassie-stained SDS/PAGE of an in vitro pulldown assay using GST-*Gt*FlhG. *Gt*MinC does not interact with GST-*Gt*FlhG, but the *Gt*FliM/FliY complex does. Input controls are shown in lanes 1 (GST-*Gt*FlhG), 4 (*Gt*MinC), and 5 (*Gt*FliM/FliY). (*H*) Coomassie-stained SDS/PAGE of an in vitro pulldown assay using GST-tagged *Gt*FliG incubated without (input control) and with *Gt*FliM/*Gt*FliY and *Gt*FlhG for 10 min. A stoichiometric ratio of FliM/FliY/FlhG exceeding 1 compared with GST-FliG was seen only in the presence of ATP and lipids.

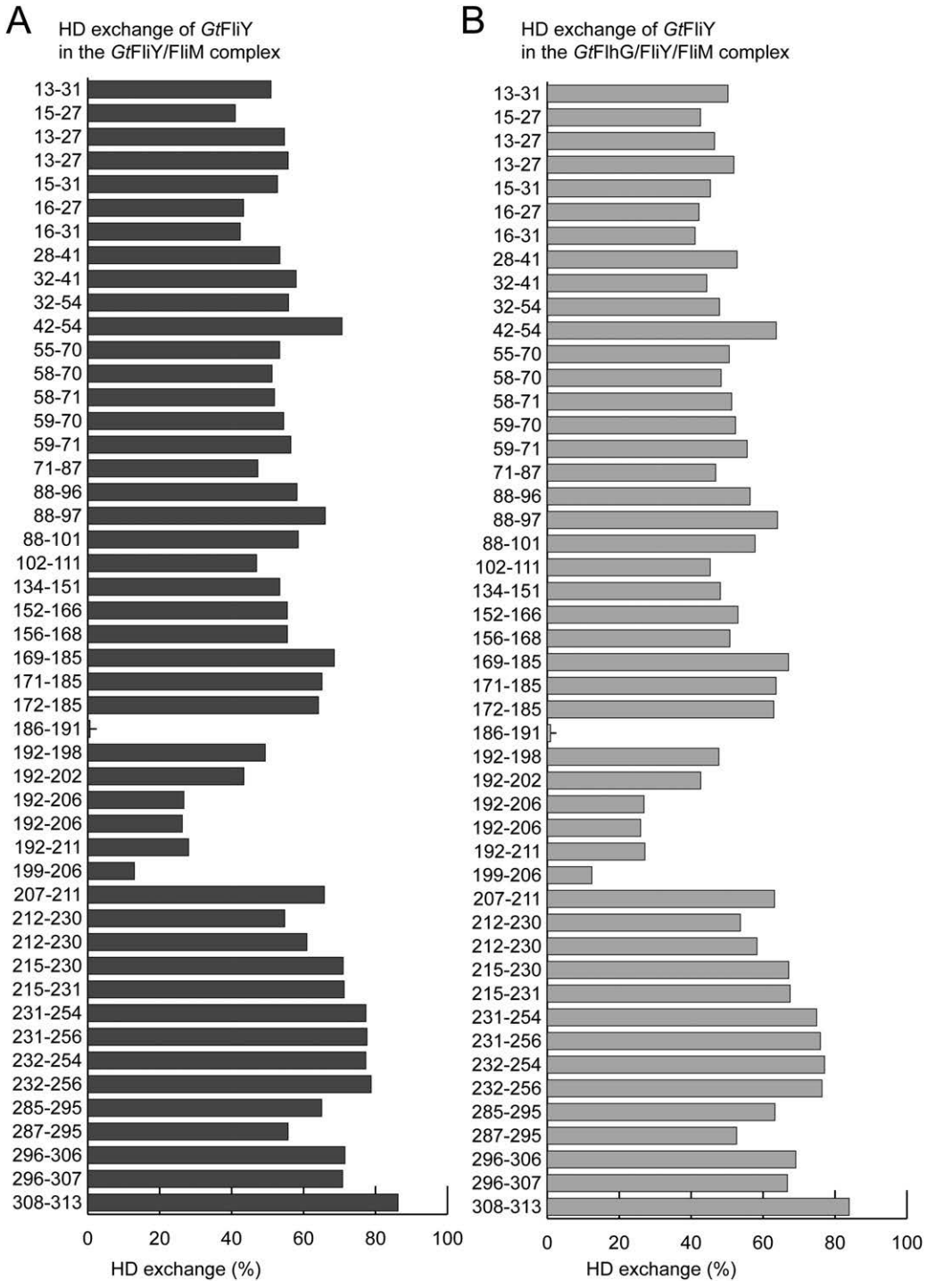

Fig. S4. Incorporation of deuterium into *Gt*FliY. (*A*) The percentage of deuterium incorporated into the peptic peptides of *Gt*FliY in a *Gt*FliM/FliY complex. (*B*) The deuterium content of the same peptic peptides from a *Gt*FlhG/FliY/FliM complex is displayed as percent (original mass spectrometric data are available on request to G.B.).

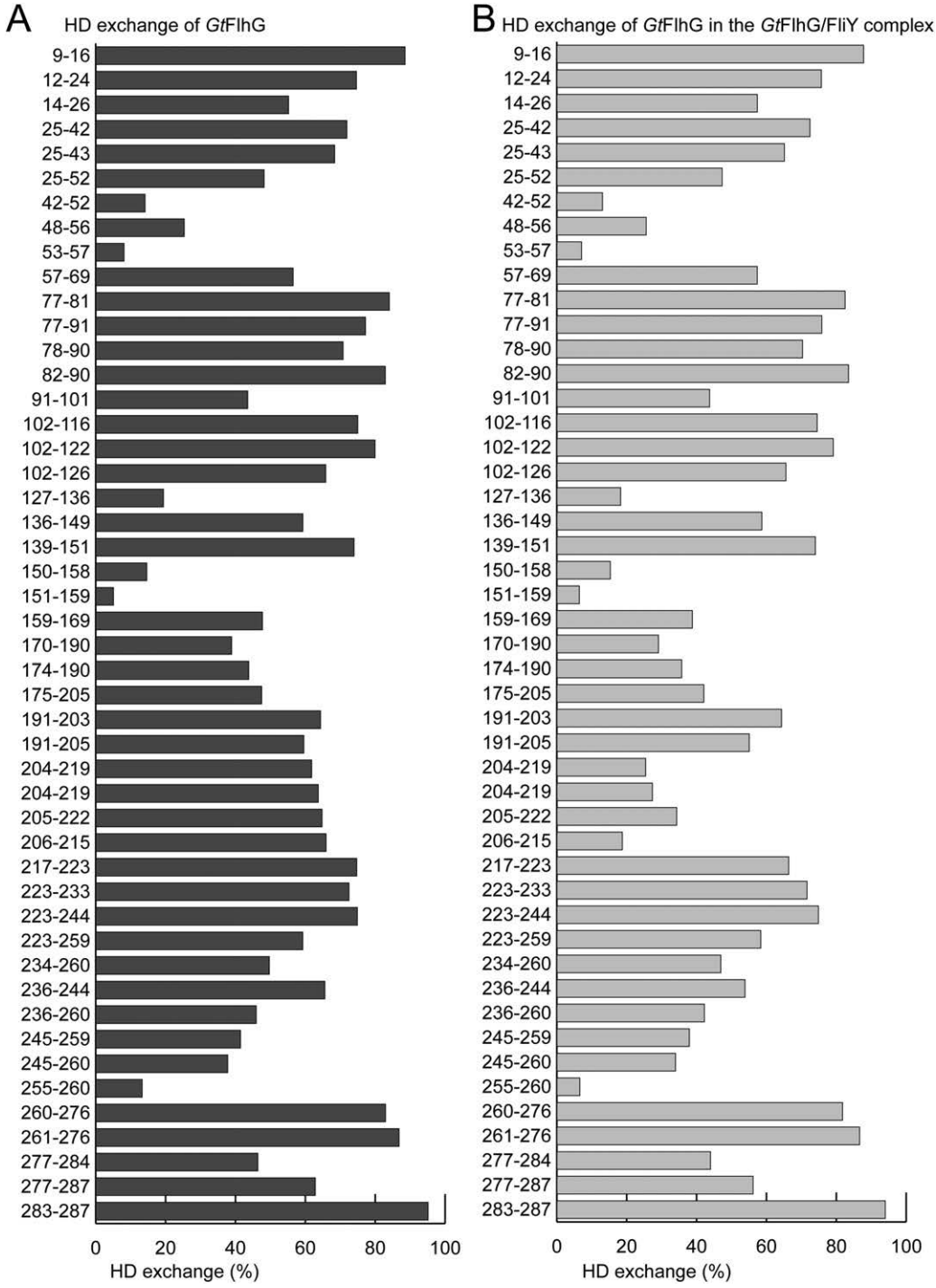

Fig. S5. Incorporation of deuterium into *Gt*FlhG. (*A*) The percentage of deuterium incorporated into *Gt*FlhG is shown for each peptide. (*B*) Incorporation of deuterium into peptic peptides obtained from a *Gt*FlhG/FliY complex is given as percent (original mass-spectrometric data are available on request to G.B.)

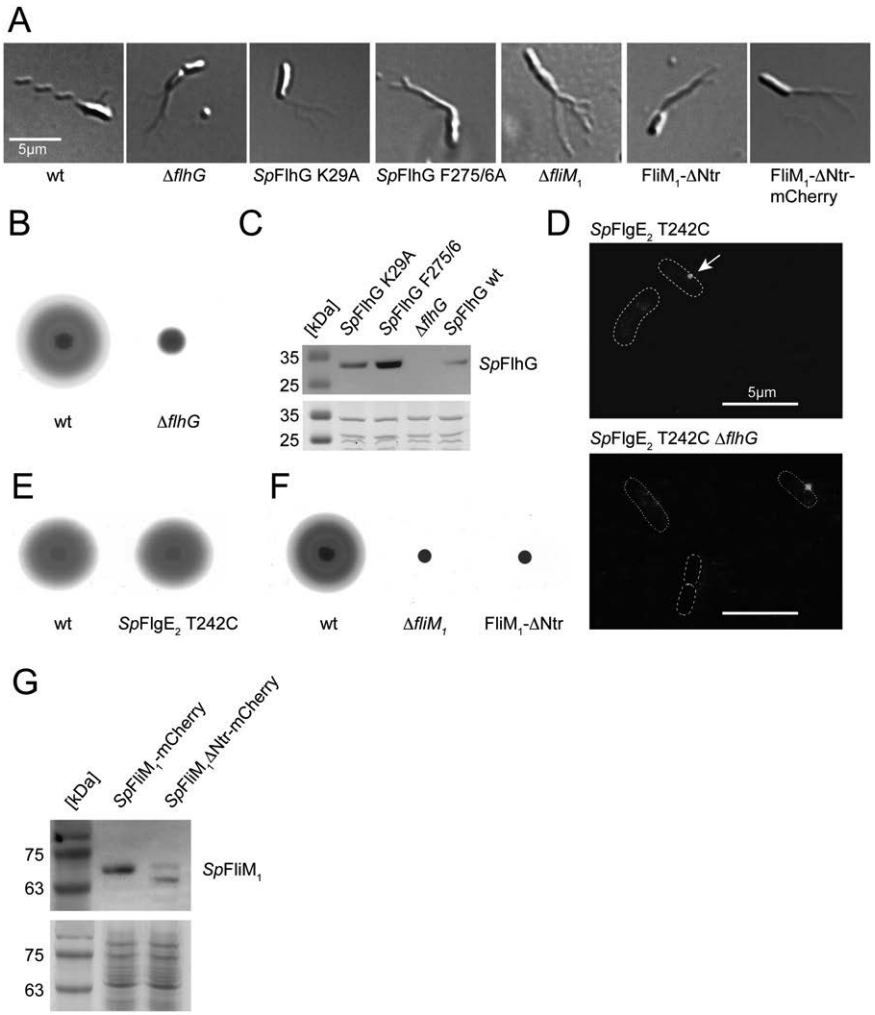

Fig. S6. Characteristics of FlhG from *S. putrefaciens*. (*A*) Flagella staining of various *flhG* and *fliM*$_1$ mutants in *S. putrefaciens* CN-32. Substitution mutants of *Sp*FlhG affecting membrane targeting (*Sp*FlhG F275/6A) and ATPase function (*Sp*FlhG K29A) display a hyperflagellation state similar to that of the *flhG* deletion mutant. *S. putrefaciens* mutant strains lacking the Ntr of FliM$_1$ (FliM$_1$-ΔNtr and FliM$_1$-ΔNtr-mCherry) show hyperflagellation similar to that of a *ΔfliM*$_1$ strain. (*B*) A soft-agar assay demonstrates that *Shewanella ΔflhG* mutants lack motility. (*C*) Western blot analysis shows the expression and stability of *Sp*FlhG and its variants K29A and F275/276A. In the Δ*flhG* strain of *S. putrefaciens,* no FlhG was observed. (*D*) Staining of the hook protein *Sp*FlgE$_2$ of the secondary lateral flagellum was performed as described, and the cells were used for fluorescence microscopy. Arrows point at clusters of FlgE$_2$, the hook protein of the lateral flagellar system, indicating the presence of a complete secondary flagellum. (*E*) A soft-agar assay demonstrates that the T242C substitution, which enables effective labeling, does not affect flagellar function. (*F*) Motility of *S. putrefaciens* (*Left*) and its *ΔfliM1* (*Center*) and *fliM1ΔNtr* (*Right*) mutant strains was monitored on swimming plates (0.25% agarose) at 30 °C. (*G*) Expression and protein integrity of *Sp*FliM$_1$-mCherry and its N-terminal deletion variant *Sp*FliM$_1$-ΔNtr-mCherry was verified by Western blot analysis.

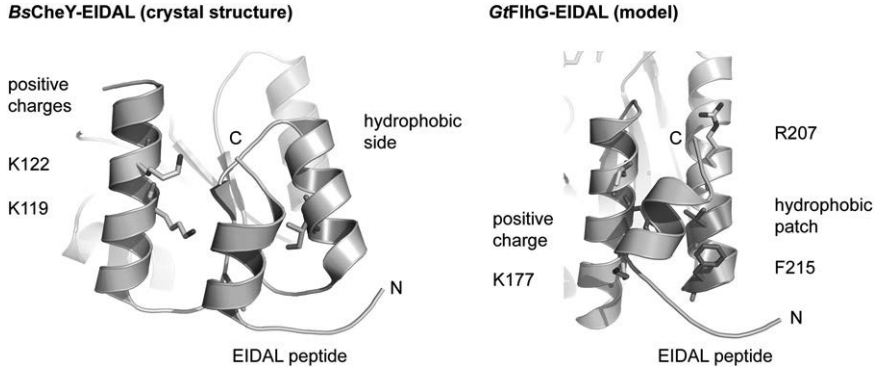

Fig. S7. Molecular mimicry. (*Left*) The interaction of *Bs*CheY with the EIDAL motif of *Bs*FliM from *B. subtilis* (PDB ID code: 2B1J). Important residues and characteristics of the interaction interface are depicted. (*Right*) The EIDAL motif in an arbitrary placement at the *Gt*FliY-binding site of *Gt*FlhG. Amino acid residues of FlhG, that are essential for binding of FliM/FliY as shown in this study, are highlighted. Note: The model of FlhG with the EIDAL peptide is intended to suggest size relationships rather than presenting a precise molecular model.

Table S1. Data collection and refinement

Data collection	*Gt*FlhG-monomer	*Gt*FlhG-dimer
Space group	P $2_12_12_1$	P 2_1
Cell dimensions		
a, *b*, *c*, Å	63.87	51.25
	89.36	72.56
	111.88	65.62
α, β, γ, °	90.00	90.00
	90.00	93.73
	90.00	90.00
Energy, keV	12.6616	
Resolution, Å	51.96–2.80	41.8–1.90
	(2.95–2.80)	(2.00–1.90)
R_{merge}	0.136 (0.47)*	0.058 (0.247)*
$I/\sigma I$	11.7 (5.2)	12.0 (5.8)
Completeness, %	100 (100)	99.2 (99.4)
Redundancy	5.1 (5.2)	3.9 (3.9)
Refinement		
Resolution, Å	47.4–2.80	29.84–1.90
No. reflections	15916	36165
R_{work}/R_{free}, %	17.7/22.8	22.1/26.0
No. atoms		
Protein	3,952	3,743
Ligand	0	38
Water	57	246
Rmsd		
Bond lengths, Å	0.008	0.008
Bond angles, °	1.228	1.229
Ramachandran, %		
Preferred	96.64	96.90
Allowed	3.12	2.69
Outliers	0.20	0.41

*Values in parentheses are for the highest-resolution shell.

Table S2. Description of bacterial strains

Bacterial strain	Relevant genotype or description	Source
Escherichia coli		
DH5α λpir	ϕ80dlacZ ΔM15 Δ(lacZYA-argF)U169 recA1 hsdR17 deoR thi-l supE44 gyrA96 relA1/λpir	(1)
WM3064	thrB1004 pro thi rpsL hsdS lacZ ΔM15 RP4 - 1360 Δ(araBAD) 567ΔdapA 1341::[erm pir(wt)]	W. Metcalf, University of Illinois at Urbana-Champaign, Urbana, IL
Shewanella putrefaciens		
CN-32	CN-32, wild-type	(2)
S 2576	Δ*flaAB*$_2$; markerless deletion of lateral flagellin genes *flaA*$_2$ and *flaB*$_2$ (Sputcn32_3455–Sputcn32_3456)	(3)
S 3133	Δ*flhG*, ΔSputcn32_2560; markerless deletion of the MinD-like ATPase FlhG	This study
S 3218	Δ*flaAB*$_2$ Δ*flhG*; markerless deletion of the *flhG* gene in the Δ*flaAB*$_2$ background	This study
S 3414	Δ*flgE*$_2$, ΔSputcn32_3465; markerless deletion of lateral flagellar hook protein	This study
S 3419	FlgE$_2$-T242C, markerless insertion of *flgE*$_2$ with substituted threonin 242 to cysteine into Δ*flgE*$_2$; used for fluorescence labeling of lateral flagellar hook proteins	This study
S 3470	Δ*flaAB*$_2$ Δ*flhG*; markerless deletion of *flhG* in the FlgE$_2$-T242C background	This study
S 3498	FliM$_1$-ΔNtr; markerless deletion of residues 2–28 of the polar motor protein FliM$_1$ (Sputcn32_2569)	This study
S 3523	FliM$_1$-ΔNtr-mCherry; markerless chromosomal fusion of FliM$_1$-ΔNtr to mCherry (C-terminal)	This study
S 3334	FlhG_F275AF276A, markerless insertion of *flhG* with substituted phenylalanine 275 to alanine and phenylalanine 276 to alanine into Δ*flhG*; disables the function of the membrane targeting sequence	This study
S 3335	FlhG_K29A, markerless insertion of *flhG* with substituted lysine 29 to alanine into Δ*flhG*; disables dimer formation and ATP hydrolysis	This study
S 3481	*flhG* KI; markerless insertion of *flhG* into Δ*flhG*; complements mutation	This study
S 3472	Δ*fliN*$_1$; markerless deletion of the polar C ring motor with protein FliN$_1$	This study
Bacillus subtilis		
PY79	PY79; wild-type	(4)
Jss01	PY79 *flhG-yfp* (Cm^R)	This study
Jss02	PY79 *flhG-yfp* (Cm^R) *amyE*::*fliM-cfp* (Spec^R)	This study

1. Miller VL, Mekalanos JJ (1988) A novel suicide vector and its use in construction of insertion mutations: Osmoregulation of outer membrane proteins and virulence determinants in *Vibrio cholerae* requires *toxR*. *J Bacteriol* 170(6):2575–2583.
2. Fredrickson JK, et al. (1998) Biogenic iron mineralization accompanying the dissimilatory reduction of hydrous ferric oxide by a groundwater bacterium. *Geochim Cosmochim Acta* 62(19–20):3239–3257.
3. Bubendorfer S, Koltai M, Rossmann F, Sourjik V, Thormann KM (2014) Secondary bacterial flagellar system improves bacterial spreading by increasing the directional persistence of swimming. *Proc Natl Acad Sci USA* 111(31):11485–11490.
4. Zeigler DR, et al. (2008) The origins of 168, W23, and other *Bacillus subtilis* legacy strains. *J Bacteriol* 190(21):6983–6995.

Movie S1. The dynamics of *Bs*FlhG-YFP in *B. subtilis* were followed over 30 s. Images were acquired every 3.24 s and are displayed with a frame rate of three frames/s.

Movie S1

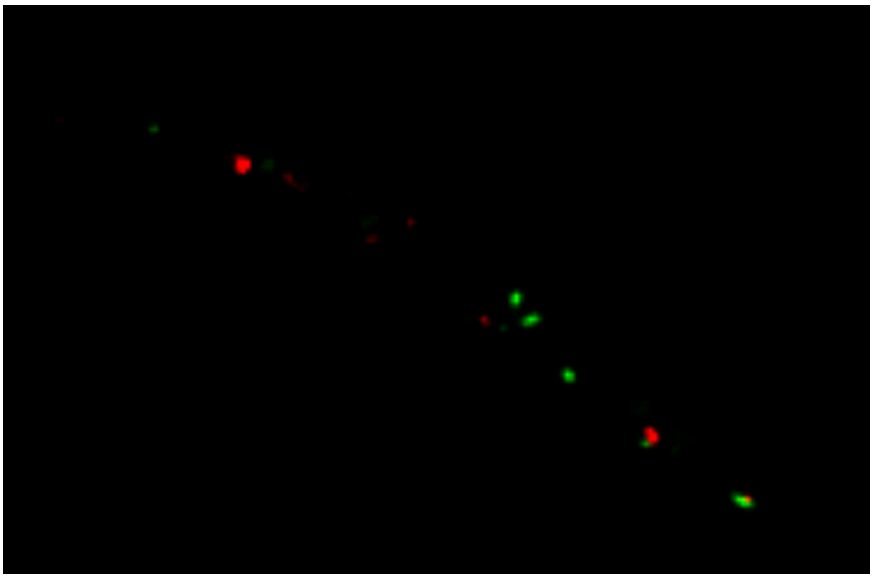

Movie S2. Time-resolved colocalization of *Bs*FliM-CFP and *Bs*FlhG-YFP in *B. subtilis* was monitored by time-lapse fluorescence microscopy over 5 min. We did not observe that stationary FlhG precedes FliM puncta. However, we hardly observed the occurrence of new FliM puncta and therefore can draw no conclusions from this experiment. Images were taken every 10.48 s and are displayed with a frame rate of three frames/s.

Movie S2

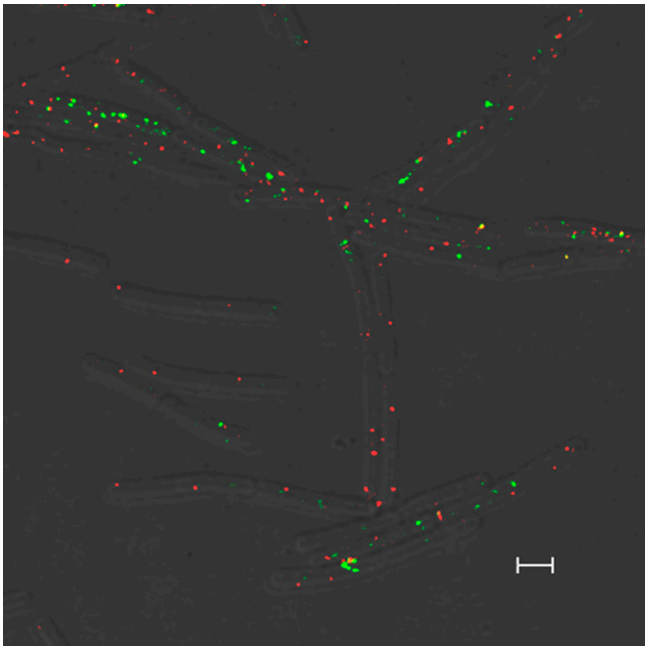

Movie S3. Time-resolved colocalization of *Bs*FliM-CFP and *Bs*FlhG-YFP in *B. subtilis* was monitored by time-lapse fluorescence microscopy over 6.5 min. Images were acquired every 20.33 s and are displayed with a frame rate of three frames/s.

Movie S3

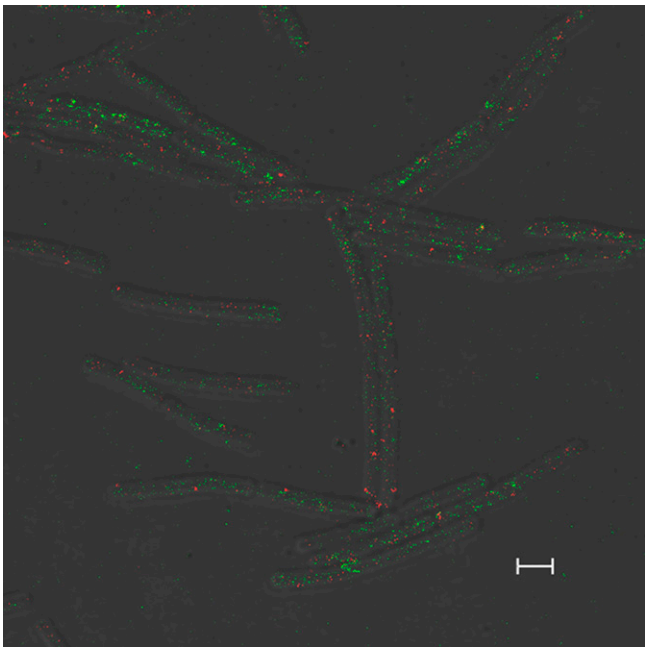

Movie S4. The original data of Movie S3 without deconvolution. Specifications are as stated for Movie S3.

Movie S4

Chapter 4:

The role of FlhF and HubP as polar landmark proteins in *Shewanella putrefaciens* CN-32.

published in Molecular Microbiology

Molecular Microbiology (2015) 98(4), 727–742 ■
doi:10.1111/mmi.13152
First published online 10 September 2015

The role of FlhF and HubP as polar landmark proteins in *Shewanella putrefaciens* CN-32

Florian Rossmann,[1,2†] Susanne Brenzinger,[1,2†] Carina Knauer,[3] Anja K. Dörrich,[1] Sebastian Bubendorfer,[1‡] Ulrike Ruppert,[1] Gert Bange[3] and Kai M. Thormann[1*]

[1]*Department of Microbiology and Molecular Biology, Justus-Liebig Universität, 35392 Giessen, Germany.*
[2]*Department of Ecophysiology, Max-Planck-Institut für terrestrische Mikrobiologie, 35043 Marburg, Germany.*
[3]*LOEWE Center for Synthetic Microbiology (Synmikro) & Department of Chemistry, Philipps University Marburg, 35043 Marburg, Germany.*

Summary

Spatiotemporal regulation of cell polarity plays a role in many fundamental processes in bacteria and often relies on 'landmark' proteins which recruit the corresponding clients to their designated position. Here, we explored the localization of two multi-protein complexes, the polar flagellar motor and the chemotaxis array, in *Shewanella putrefaciens* CN-32. We demonstrate that polar positioning of the flagellar system, but not of the chemotaxis system, depends on the GTPase FlhF. In contrast, the chemotaxis array is recruited by a transmembrane protein which we identified as the functional ortholog of *Vibrio cholerae* HubP. Mediated by its periplasmic N-terminal LysM domain, *Sp*HubP exhibits an FlhF-independent localization pattern during cell cycle similar to its *Vibrio* counterpart and also has a role in proper chromosome segregation. In addition, while not affecting flagellar positioning, *Sp*HubP is crucial for normal flagellar function and is involved in type IV pili-mediated twitching motility. We hypothesize that a group of HubP/FimV homologs, characterized by a rather conserved N-terminal periplasmic section required for polar targeting and a highly variable acidic cytoplasmic part, primarily mediating recruitment of client proteins, serves as polar markers in various bacterial species with respect to different cellular functions.

Accepted 30 July, 2015. *For correspondence. E-mail kai.thormann@mikro.bio.uni-giessen.de; Tel. +49 (0) 641 9935545; Fax +49 (0)641 9935549. †These authors contributed equally to this study. ‡Present address: Institute for Medical Microbiology and Hospital Epidemiology, Hannover Medical School, Hannover 30625, Germany.

Introduction

During the recent decades, numerous studies have provided evidence that in bacteria, a variety of fundamental cellular functions depend on the proper spatial and temporal organization of proteins and other macromolecules within the cell. A paradigmatic example for spatiotemporal organization in bacteria is cell division where correct positioning of the cell division proteins and distribution of replicated chromosomal DNA are critical for propagation (Thanbichler, 2010; Reyes-Lamothe *et al.*, 2012). Unlike the cell division machinery of most bacteria, numerous other complexes are specifically targeted to the cell pole for proper function. Several different systems involved in the regulation of cell polarity have been identified and studied; this topic has been the subject of recent reviews (Laloux and Jacobs-Wagner, 2014; Treuner-Lange and Søgaard-Andersen, 2014).

One major multiprotein complex that needs to be specifically positioned is the flagellar machinery of polarly flagellated bacterial species. The mechanisms by which this localization is achieved are still poorly understood for most bacteria (summarized in Schuhmacher *et al.*, 2015a). In those species that have been studied in detail, polar recruitment of the flagellar system appears to rely on landmark proteins to assign the desired position, and the absence of these polar markers commonly leads to misplacement of the flagella. In the alphaproteobacterium *Caulobacter crescentus*, TipN has been identified as such a landmark protein (Huitema *et al.*, 2006; Lam *et al.*, 2006). TipN localizes to the new pole of both daughter cells after cell division and recruits a second protein, TipF, a positive regulator of flagellar assembly. TipF in turn recruits PflI, a third protein required for proper flagellar placement (Obuchowski and Jacobs-Wagner, 2008; Davis *et al.*, 2013). The concerted action of these three proteins is required for formation of a single flagellum at the designated cell pole (Davis *et al.*, 2013).

However, homologs of the TipN/F proteins appear to be absent outside the group of alphaproteobacteria. In many other bacterial species, a set of two proteins, FlhF and FlhG, has been implicated in regulating diverse aspects of

flagellar localization, number, and activity (reviewed in Kazmierczak and Hendrixson, 2013; Altegoer *et al*., 2014). Potential orthologs of the two proteins are present in a wide range of bacterial species (Bange *et al*., 2011). FlhG (orthologs also named YlxH, MinD2, FleN or MotR) belongs to the MinD/ParA ATPase family, and the recently solved crystal structure revealed striking structural homologies to the ATPase MinD of *Escherichia coli* (Schuhmacher *et al*., 2015b). Loss of FlhG in polarly flagellated bacterial species commonly results in hyperflagellation and severe perturbation of flagella-mediated motility (Dasgupta *et al*., 2000; Correa *et al*., 2005; Kusumoto *et al*., 2006; 2008; Schuhmacher *et al*., 2015b). The exact mechanism by which FlhG exerts its role is still elusive; however, its mode of action involves binding to major components of the flagellar rotor, FliM and FliN/FliY, putatively to facilitate their incorporation into the nascent basal body structure (Schuhmacher *et al*., 2015b). The second protein of the system, FlhF, belongs to the signal recognition particle SRP-type GTPase subfamily of the SIMIBI class of nucleotide-binding proteins, and the crystal structure of FlhF from *Bacillus subtilis* has been solved (Bange *et al*., 2007; Bange and Sinning, 2013). Loss of the protein has a range of different consequences with respect to flagellar gene expression, assembly and function in various polarly flagellated species, but consistently results in displacement of the flagellum away from the cell pole (Pandza *et al*., 2000; Murray and Kazmierczak, 2006; Kusumoto *et al*., 2008; Balaban *et al*., 2009; Green *et al*., 2009). FlhF was demonstrated to co-localize with the flagellum to the old cell pole (Murray and Kazmierczak, 2006; Kusumoto *et al*., 2008; Ewing *et al*., 2009). Moreover, studies on *Vibrio cholerae* FlhF have provided evidence that the same spatial organization occurs in the absence of any other flagellar components (Green *et al*., 2009) or upon heterologous production of *Vibrio alginolyticus* FlhF in *E. coli* (Kusumoto *et al*., 2008), indicating that polar localization is an intrinsic feature of the protein. The presence of FlhF at the cell pole is required for correct placement of the early flagellar basal body protein FliF. Thus, it has been speculated that FlhF represents the polar landmark protein which recruits early components of the flagellar machinery to the appropriate subcellular location by a mechanism which is yet elusive. In addition, for *Pseudomonas aeruginosa*, it was reported that the chemotaxis protein CheA also localizes away from the cell pole in the absence of FlhF in a pattern resembling that of the flagellar basal body system (Kulasekara *et al*., 2013). This finding strongly indicates that FlhF might also mediate the recruitment of the chemotaxis machinery in *P. aeruginosa* or that the chemotaxis machinery is directly associated with the flagellar system.

Recent studies on *V. cholerae* have identified another major landmark protein which is involved in the polar accumulation of flagella but primarily directs the chemotaxis system and the chromosome segregation machinery to the cell pole. According to its proposed function as a polar hub, the protein was named HubP (Yamaichi *et al*., 2012). HubP is a transmembrane protein with an N-terminal periplasmic peptidoglycan-binding (LysM) domain and a large cytoplasmic section comprising 10 copies of an imperfect 46-amino-acid repeat. Fluorescence microscopy demonstrated that, mediated by the N-terminal LysM domain, HubP localizes to the cell pole and the cellular division plane. Deletion of *hubP* in *V. cholerae* results in delocalization of the chemotaxis machinery, leading to a defect in chemotactic swimming. In addition, the origin of the larger of the two *V. cholerae* chromosomes, *oriCI*, is not fully targeted to the cell pole and a small fraction of cells displays an increased number of flagella. Interaction of these large complexes with HubP is thought to be mediated through a set of different ParA-like ATPases, ParAI for *oriCI*, ParC for the chemotaxis machinery and FlhG for the flagellar machinery. Potential homologs of HubP have been identified in several other species among the gammaproteobacteria; however, it is not clear whether or not these proteins are functional orthologs and which role they might play in these species.

Shewanella putrefaciens CN-32 is a gammaproteobacterium which possesses two complete flagellar systems encoded by two distinct separate gene clusters (Bubendorfer *et al*., 2012). The primary gene cluster, which is present in all *Shewanella* species and encodes orthologs of FlhF and FlhG, leads to formation of a single polar Na^+-driven flagellum. The secondary flagellar system lacks *flhF* and *flhG* and is expressed in a subpopulation of cells when cultivated in complex media. These cells form one or more lateral flagella which are rotated at the expense of the proton gradient and enable a more effective motility of the corresponding subpopulation by increasing the directional persistence of swimming. However, our studies strongly indicated that the single chemotaxis system of *S. putrefaciens* CN-32 predominantly or even exclusively addresses the primary polar system but not the lateral flagellar motors (Bubendorfer *et al*., 2014). To further elucidate the spatial arrangement of the chemotaxis machinery with respect to the two flagellar systems of *S. putrefaciens* CN-32, we performed localization studies by fluorescence microscopy. We identified the functional ortholog of the *V. cholerae* polar landmark protein HubP in *S. putrefaciens* CN-32, and we demonstrate that FlhF and HubP independently localize the primary flagellar system and the chemotaxis and chromosome segregation machinery, respectively. We thus show that general features and mechanisms are conserved between HubP-like proteins of different species and suggest that HubP-dependent polar localization might be more widespread among bacteria.

Results

The chemotaxis machinery of S. putrefaciens *CN-32 localizes to the flagellated cell pole*

To first explore the subcellular position of the chemotaxis system in *S. putrefaciens* CN-32, we performed fluorescence microscopy on cells producing fluorescently labeled components of the chemotaxis machinery. *S. putrefaciens* CN-32 possesses a single chemotaxis system with 37 predicted putative methyl-accepting sensor proteins (MCPs). To determine the localization of the chemotaxis machinery within CN-32 cells, we generated C-terminal fluorescent protein fusions to 16 of the 37 MCPs. Because all fusions yielded very similar results, we will, within this manuscript, only refer to MCP0796-eGFP. MCP0796 is an MCP with a periplasmic helical bimodular (HBM) sensor domain followed by the typical cytoplasmic HAMP and methyl-accepting chemotaxis-like (MA) domain. The function of this MCP is not yet characterized; however, the fluorescent fusion reliably allowed localization of the protein which was therefore chosen as representative. We further generated a C-terminal fluorescent fusion to CheA (CheA-mCherry) as well as N-terminal fluorescent protein fusions to CheY (sfGFP-CheY) and CheZ (Venus-CheZ). The genes encoding these fusions were separately introduced into the CN-32 chromosome where they replaced the corresponding native genes. Immunoblotting and swimming assays demonstrated that the fluorescently labeled proteins were mostly stably produced (Fig. S1) and fully (Venus-CheZ and CheA-mCherry) or partially (sfGFP-CheY) supported movement through soft agar (Fig. S2). To enable localization of the chemotaxis machinery with respect to the position of the primary polar flagellar system, all fusions were introduced into a CN-32 strain in which $FliM_1$ was functionally labeled with sfGFP or mCherry (Bubendorfer *et al.*, 2012) as a marker for the primary basal body complex.

Subsequent fluorescence microscopy revealed that MCP0769-eGFP as well as sfGFP-CheY, CheA-mCherry and Venus-CheZ distinctly localized to the cell pole marked by $FliM_1$ in 73% (CheY and CheA) and 89% (CheZ) respectively (Fig. 1). In addition, some cells displayed a bipolar localization pattern of labeled chemotaxis components (CheY, 19%; CheA, 29%; CheZ, 21%). In cells with a $FliM_1$ focus, the signal intensity of co-localizing foci formed by the labeled chemotaxis components was always stronger than that of foci at the opposite cell pole: For sfGFP-CheY, the signal at the opposite cell poles only reached 38% intensity compared to that of the flagellated pole, CheA-mCherry reached 27% and Venus-CheZ 24%. In contrast, co-localization of any of the labeled chemotaxis components with $FliM_2$-mCherry as a marker for the position of the secondary lateral flagellum was not observed, unless $FliM_2$-mCherry was located close to the cell pole (data not shown). Based on these results, we concluded that in *S. putrefaciens* CN-32, the chemotaxis machinery is localized at, or in close proximity to, the cell pole decorated with the primary flagellar complex and is assembled at the old cell pole during cell division.

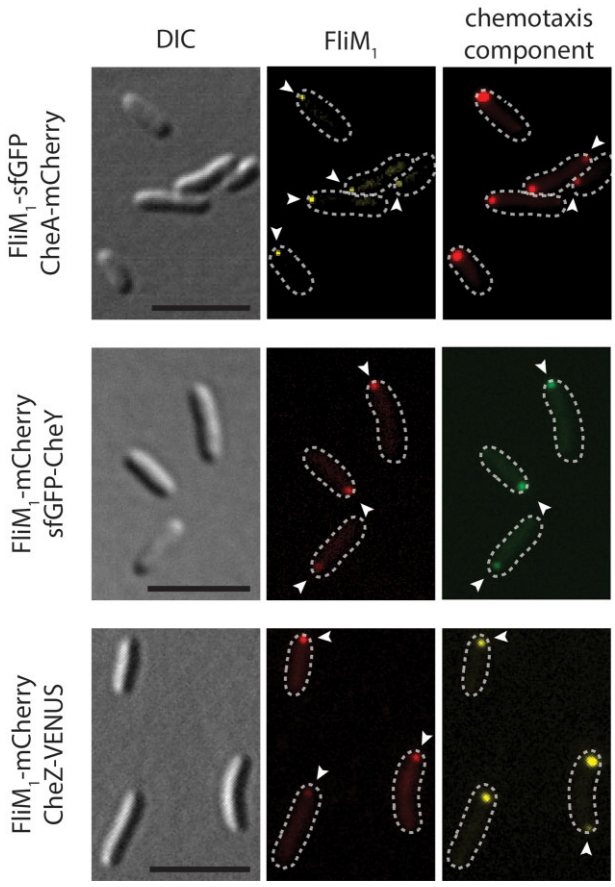

Fig. 1. Localization of the chemotaxis cluster in *S. putrefaciens* CN-32. Displayed are DIC (left panel) and fluorescent micrographs in which $FliM_1$ (middle panels) and CheA, CheY and CheZ (right panel) are fluorescently labeled as indicated. The arrows point out fluorescent foci. The scale bar equals 5 μm.

The SRP-like GTPase FlhF is required for polar localization of the primary flagellar system, but not of the chemotaxis cluster, in CN-32

The SRP-like GTPase FlhF has been demonstrated to be the major determinant for flagellar placement and number in various polarly flagellated gammaproteobacteria. We therefore determined whether this protein has a similar role in *S. putrefaciens* CN-32 and whether *Sp*FlhF also dictates the localization of the chemotaxis system, as has previously been suggested for *P. aeruginosa* (Kulasekara *et al.*, 2013). FlhF acts in concert with its antagonist, the MinD-like ATPase FlhG (Kusumoto *et al.*, 2008; Ono *et al.*, 2015), and in *B. subtilis* it has been shown that the conserved N-terminal region of FlhG stimulates the

GTPase activity of FlhF by approximately three to fivefold (Bange *et al*., 2011). To assess whether FlhF from *S. putrefaciens* CN-32 is an active GTPase whose activity is affected by FlhG, both proteins were purified and the impact of *Sp*FlhG on the GTPase activity of *Sp*FlhF was assessed by high-pressure liquid chromatography (HPLC). While SpFlhF alone showed only minor GTPase activity, an approximately three to fivefold stimulation of SpFlhF was observed in the presence of either full-length FlhG or its N-terminal region. As expected, this stimulation was almost abolished in a GTP hydrolysis-deficient FlhF variant (FlhF-R285A; Fig. 2A). This agrees with observations made for FlhF and FlhG from *B. subtilis*. Correspondingly, an *flhG-ΔN20* mutant in CN-32 displayed a hyperflagellated phenotype (Fig. S3B) which was drastically impaired in flagella-mediated motility similar to a cell completely lacking *flhG* (Fig. S3A). This indicates that FlhG may also stimulate the FlhF GTPase in polarly flagellated gammaproteobacteria such as *S. putrefaciens* CN-32 and that this interaction likely is required for proper flagellation.

To localize *Sp*FlhF within the cells, we created a hybrid gene encoding a C-terminal fusion of FlhF to mCherry (*flhF-mCherry*) which we integrated into the chromosome to replace native *flhF*. FlhF-mCherry was partially stable (Fig. S1) and predominantly localized to the flagellated cell pole in 85% of the population (Fig. 2B). A bipolar localization frequently occurred in cells that evidently were within the process of cell division. To further determine whether FlhF has a function in regulating flagellar placement and number, we studied the localization of $FliM_1$ and the flagellar filament in the absence of *flhF*. To this end, we introduced in-frame deletions of *flhF* into CN-32 wild-type cells and into cells bearing a $FliM_1$-sfGFP fusion. To specifically enable visualization of the primary flagellum, cysteine residues were introduced in both flagellins forming the primary flagellar filament to enable fluorescent labeling ($FlaAB_1$-Cys) in the wild-type and *ΔflhF* background. In mutants lacking FlhF (*ΔflhF*), we observed a significantly lower amount of cells exhibiting $FliM_1$-mCherry foci (wild type, 72%; *ΔflhF*, 27%), and these foci were commonly displaced from the cell pole to lateral positions (Fig. 2D). Fluorescence labeling of the flagellins confirmed that, in the relatively few flagellated *ΔflhF* cells, the filament frequently originated from lateral positions. Significantly fewer cells were observed to be motile, and cells exhibited irregular swimming patterns when observed by light microscopy and decreased lateral extension when moving through soft-agar plates (Fig. 2C). When FlhF or FlhF-mCherry was ectopically overproduced from an inducible promoter in wild-type cells, we observed increased accumulation at the cell pole accompanied by hyperflagellation of the cells which solely occurred at the same cell pole (Fig. S4B). In contrast, deletion of *flhF* had no significant effect on the production or placement of the secondary filaments (Fig. S4C). We then determined the localization of MCP0796, CheY, CheA or CheZ in the absence of FlhF to explore potential effects on the localization of any of the fluorescently labeled components. In contrast to the primary flagellar system, all chemotaxis components retained a polar localization pattern indistinguishable from that observed in the wild-type background (Fig. 2D; Fig. S5).

We thus confirmed that, in *S. putrefaciens* CN-32, FlhF is an active GTPase that shares the common features and properties which have been described for other species of the gammaproteobacteria and serves as a polar landmark protein and regulator for polar flagellar assembly. Furthermore, we showed that FlhF does not direct the chemotaxis system to the flagellated cell pole, which prompted us to screen for other potential landmark proteins that might be required for cell polarity in *Shewanella*.

Shewanella *sp. possess a HubP ortholog*

In *V. cholerae*, polar localization of the chemotaxis machinery was recently demonstrated to be dependent on the transmembrane landmark protein HubP. Genome analysis revealed that HubP showed significant similarities to Sputcn32_2442, a gene of 3294 bp, predicted to encode a protein of 1097 aa. Sputcn32_2442 was preliminary annotated as pilus assembly protein FimV based on its similarity to *P. aeruginosa* FimV, a protein regulating cell polarity during type IV pili-mediated twitching motility (Semmler *et al*., 2000; Wehbi *et al*., 2011). However, at the amino-acid level, significant identity or similarity between Sputcn32_2442, *Vibrio* HubP or *P. aeruginosa* FimV was only observed for the N- and very C-terminal segments of the deduced protein sequence (Fig. S6). Despite the rather low overall similarity and a lower molecular mass (estimated 117 kDa compared with ~ 178 kDa of HubP), the predicted protein exhibited striking similarities to *Vibrio* HubP with respect to domain architecture and some other features (Fig. S7). Both Sputcn32_2442 and *Vibrio* HubP are highly acidic proteins (pI 3.87 and 3.22 respectively). Similar to HubP, Sputcn32_2442 is predicted to possess an N-terminal signal sequence (likely to be cleaved between aa 24 and 25) followed by a putative LysM peptidoglycan-binding domain and a transmembrane domain. Sputcn32_2442 is annotated to directly begin with the signal sequence, while *Vc*HubP features a short cytoplasmic stretch of amino acids prior to the rather hydrophobic residues. Both proteins harbor within their cytoplasmic C-terminal segment a number of copies of an imperfect repeat that is highly enriched in acidic amino acids (10 in *Vc*HubP; 9 in Sputcn32_2442). With a length of 37 aa, these repeats are shorter in Sputcn32_2442 than in *Vc*HubP (46 aa) and are also less well conserved.

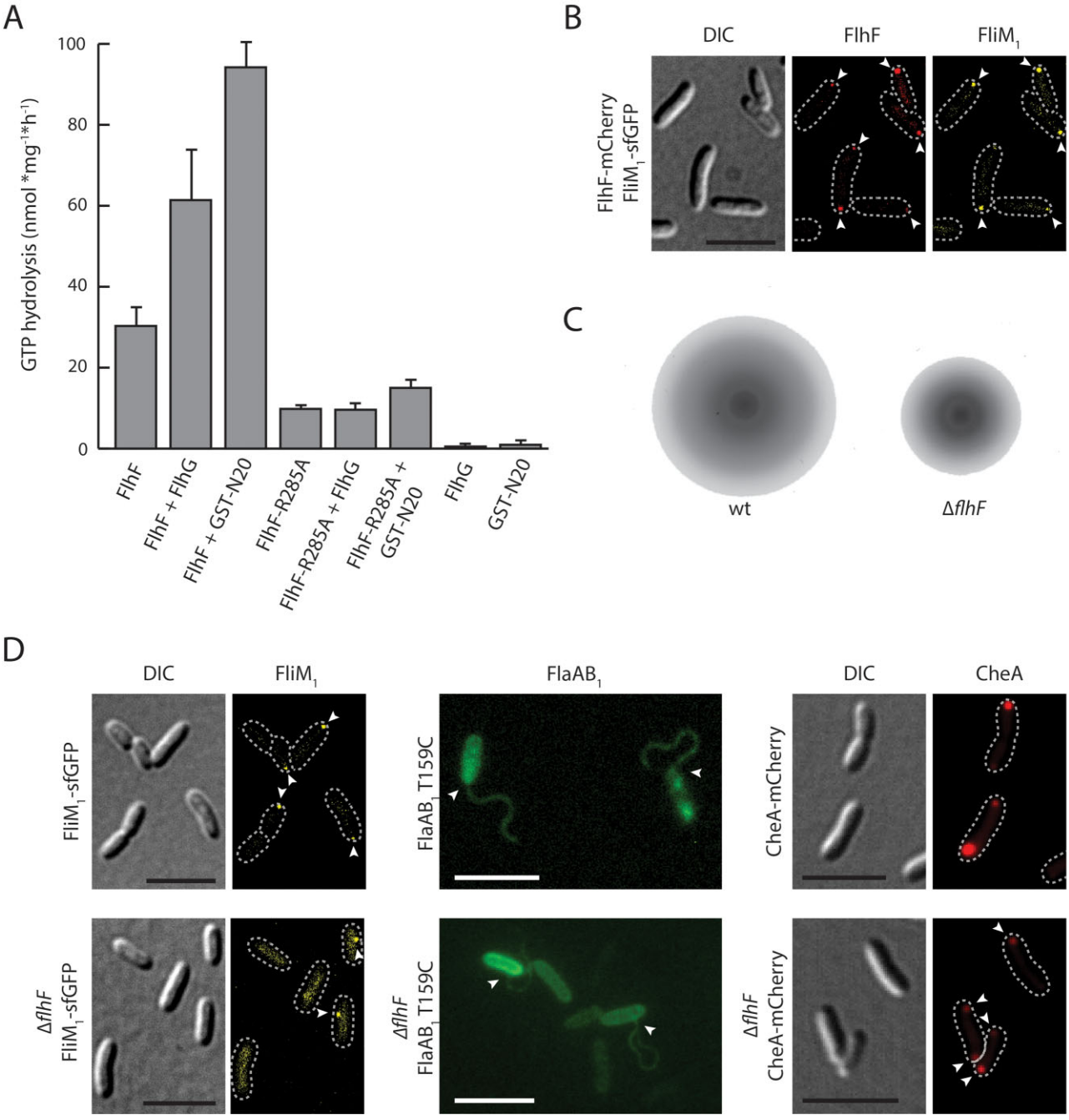

Fig. 2. Activity and role of FlhF in flagellar placement.
A. The GTPase activity of FlhF is stimulated by the N-terminus of FlhG. GTP hydrolysis in nmol per mg FlhF per hour is given as mean value ± standard deviation of three independent measurements.
B. FlhF localizes to the flagellated cell pole. Shown are DIC (left) and corresponding fluorescence micrographs of cells harboring fluorescent fusions to both FlhF and $FliM_1$ as indicated (right).
C. Loss of FlhF results in decreased swimming abilities in soft agar. 3 µl of exponentially growing cultures of the indicated strain were placed on 0.25% soft agar plates and incubated at 30°C for 16 h. Please note that the complete soft agar plate is displayed in Fig. S2.
D. FlhF has a role in localization of flagellar but not of chemotaxis components. In wild-type cells (upper panel), $FliM_1$, the flagellar filaments and CheA occur at the cell pole. In the absence of FlhF (lower panel), both $FliM_1$ and flagellar filaments are shifted to lateral positions. In contrast, chemotaxis components, here CheA, still occur at the cell poles. Displayed are DIC and fluorescent images in which the FlhF, $FliM_1$, CheA or the flagellins are fluorescently labeled (FlhF-mCherry; $FliM_1$-sfGFP, CheA-mCherry, Alexa-Fluor 488). Arrows mark fluorescent clusters and the positions of the flagellar filaments' origins respectively. The scale bar equals 5 µm.

With respect to the genetic context, both *hubP* and Sputcn32_2442 are flanked downstream by *truA*, a gene predicted to encode tRNA pseudouridine synthase A. Potential orthologs to Sputcn32_2442 can be readily identified in many other sequenced *Shewanella* species, but these exhibit variations in protein length and similarity particularly within the repeat domain of the protein (Fig. S7). Based on the similarities, and despite the low overall conservation at protein level, we hypothesized that Sputcn32_2442, henceforth *Sp*HubP, represents the functional ortholog of *Vc*HubP.

Sp*HubP localizes the chemotaxis, but not the flagellar system, to the cell pole*

In *V. cholerae*, HubP has been demonstrated to mediate polar localization of the chemotaxis cluster and to be involved in restricting the number of polar flagella to a single filament. To determine whether this similarly applies to *Sp*HubP, corresponding fluorescent protein fusions to $FliM_1$, MCP0976 (Sputcn32_0796-eGFP), CheY (sfGFP-CheY), CheA (CheY-mCherry) and CheZ (Venus-CheZ) were introduced into the CN-32 *ΔhubP* background and their localization was analyzed by fluorescence microscopy (Fig. 3A; Fig. S8A). We observed that, in the absence of *Sp*HubP, $FliM_1$-sfGFP exclusively remained at the pole in all cells. In addition, fluorescence labeling of the flagellar filament in *ΔhubP*-mutants revealed that the cells still displayed a single polar filament undistinguishable from the wild type. However, the number of cells with polar $FliM_1$-sfGFP clusters dropped significantly in the absence of *Sp*HubP (wild type, 72%; *ΔhubP*, 42%), and, accordingly, the number of flagellated cells was correspondingly lower. In contrast to the flagellar system, components of the chemotaxis machinery were no longer restricted to the cell pole but also localized to lateral positions within the cell envelope (Fig. 3A; Fig. S8A).

We also analyzed the major determinants for polar flagellar localization and number, FlhF and FlhG, in the CN-32 *ΔhubP* background (Fig. 3B; Fig. S8B). Polar positioning of FlhF occurred independently of *Sp*HubP as FlhF-mCherry exclusively localized in distinct clusters to the cell poles in both wild-type and the *ΔhubP*-mutant cells. However, as already observed with $FliM_1$-sfGFP, the frequency of cells displaying polar FlhF-mCherry foci dropped significantly in a population of cells lacking *Sp*HubP (wild type, 73%; *ΔhubP*, 46%). As previously observed in *Vibrio* species (Kusumoto *et al*., 2008; Yamaichi *et al*., 2012; Ono *et al*., 2015), stable and fully functional FlhG-sfGFP displayed a cytoplasmic localization but also accumulated at the flagellated pole in a number of cells (51%). These discrete polar foci were virtually absent in a *ΔhubP* mutant (0.25%), strongly suggesting that polar localization of FlhG depends on *Sp*HubP as has previously been observed in *V. cholerae* (Yamaichi *et al*., 2012). Taken together, the results strongly indicate that localization of the chemotaxis cluster is exclusively conferred by *Sp*HubP. Positioning of the polar flagellar system is primarily dictated by FlhF/FlhG; however, *Sp*HubP directly or indirectly affects the amount of polar accumulation of FlhF and FlhG and the size of the cellular subpopulation forming a flagellum.

The absence of Sp*HubP negatively affects motility*

To further determine whether *Sp*HubP might have a direct or indirect effect on the flagellar function, we analyzed the swimming behavior of cells by soft-agar assays and light microscopy (Fig. 4A and B). When placed on soft agar, the *ΔhubP* mutant displayed a significantly lower lateral extension than wild-type cells, indicating a decreased chemotactic drift and/or slower swimming. Analysis of cellular swimming by light microscopy revealed that *ΔhubP* mutant cells, in fact, exhibit a significant decrease in average swimming speed (wild type: 52.7 μm s^{-1}; *ΔhubP*: 29.5 μm s^{-1}). Such a phenotype has not been described for *Vc*HubP before and indicates that *Sp*HubP has further functions in motor performance in addition to ensuring close proximity between the chemotaxis and flagellar motor system.

Because the potential homolog of *Vc*- and *Sp*HubP in *P. aeruginosa*, FimV, is required for normal twitching motility (Semmler *et al*., 2000; Wehbi *et al*., 2011), we also determined type IV pili-mediated twitching motility of *S. putrefaciens* CN-32 wild-type and *ΔhubP* mutant cells. Although this type of movement was not very pronounced under the conditions tested, cells lacking *Sp*HubP showed a significant reduction in the area covered by twitching by a factor of about 4 (Fig. 4C).

Taken together, the results provide evidence that *Sp*HubP has different functions with respect to various aspects of motility in *S. putrefaciens* CN-32.

Sp*HubP has a complex localization pattern in* S. putrefaciens *CN-32*

To determine the localization of *Sp*HubP in *S. putrefaciens* CN-32 cells, we constructed a hybrid gene encoding a C-terminal fusion to sfGFP or mCherry, which we integrated into the chromosome to replace the native *hubP*. Immunoblotting analysis confirmed that *Sp*HubP-sfGFP and *Sp*HubP–mCherry were stably produced, and swimming analysis indicated that the labeled proteins were fully functional (Figs S1 and S2). Fluorescence microscopy revealed that *Sp*HubP-sfGFP mainly co-localizes with $FliM_1$-mCherry to the flagellated cell pole (Fig. 5A). The majority of cells (95%) also displayed minor fluorescence foci at the opposite pole with about half the intensity (47%) of that of the main cluster. In addition, in cells which were in the process of dividing, *Sp*HubP-mCherry was

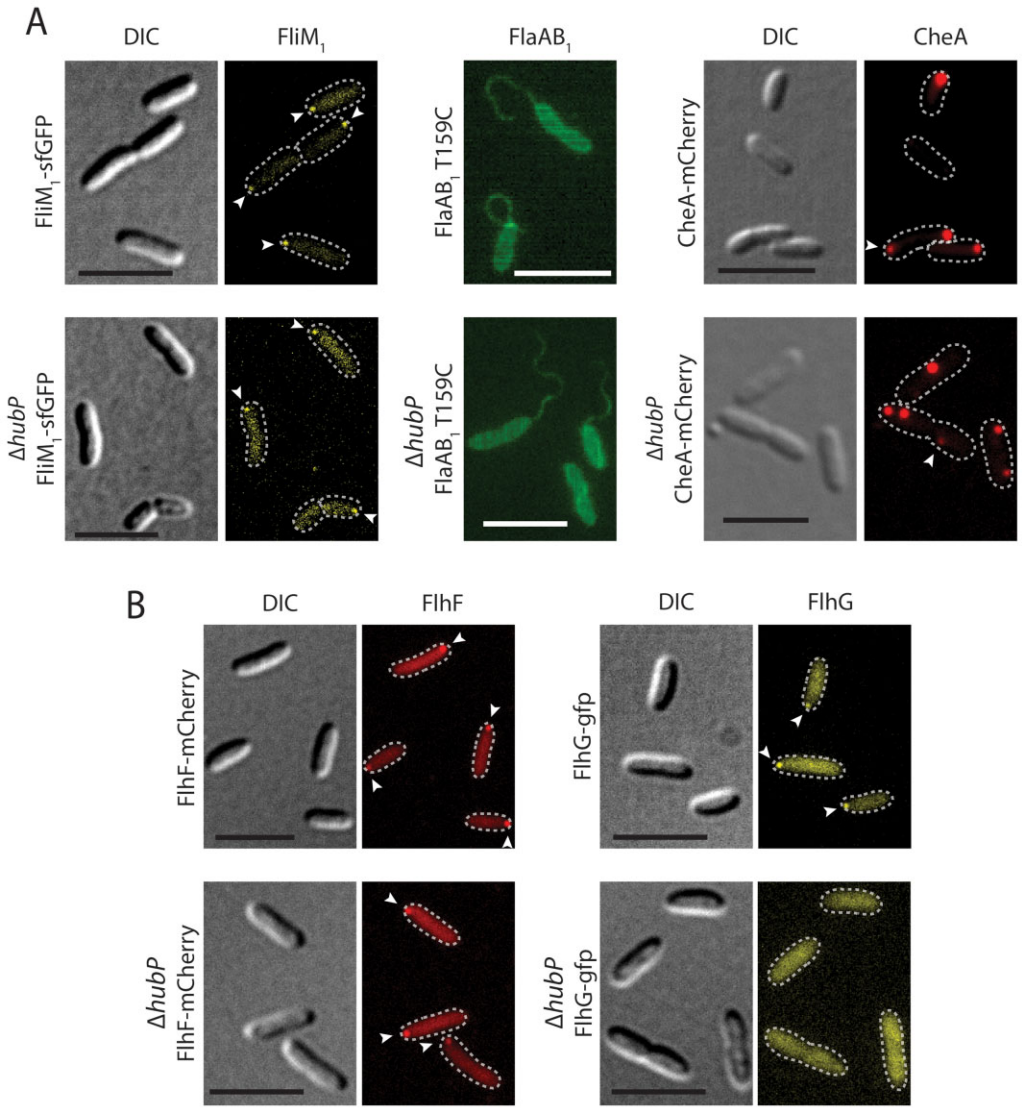

Fig. 3. Localization of flagellar and chemotaxis components in dependence of *Sp*HubP.
A. In the absence of *Sp*HubP, $FliM_1$ and flagellar filaments remain at the cell pole, while chemotaxis components, such as CheA, are delocalized to subpolar positions.
B. In the presence of *Sp*HubP, both FlhF and FlhG occur at the cell pole (upper panels, the corresponding line scan analysis can be found in Fig. S8). In *ΔhubP*-mutant cells (lower panel), FlhF remains at the cell pole while FlhG loses its polar accumulation pattern. Displayed are DIC and fluorescent micrographs in which $FliM_1$, CheA and the flagellar filament are appropriately labeled ($FliM_1$-sfGFP, CheA-mCherry, Alexa-Fluor 488). Arrows mark fluorescent clusters. The scale bar equals 5 μm.

observed to accumulate at the division plane where it co-localized with the fluorescently labeled cell division protein ZapA-sfGFP (Fig. 5B). Time-lapse microscopy and quantification of the fluorescent foci's fluorescence intensity (Fig. 6A and B) strongly suggested that targeting of *Sp*HubP to the cell division plane resulted in formation of the minor *Sp*HubP cluster that is observed at the new, nonflagellated cell poles after completion of cell division and fission. The fluorescent signal at the new cell pole rapidly gained intensity (almost reaching fluorescent intensity observed in the division plane within 10 min; Fig. 6B), strongly indicating an immediate recruitment of further copies of *Sp*HubP to the new cell pole. The signal further increased significantly during cell growth over 40 min (corresponding to one generation time) until reaching the intensity observed at the opposite pole. Both major and minor *Sp*HubP clusters displayed fluorescence recovery after complete bleaching with a half-time of about 3.2 min (major cluster) and 3.7 min (minor cluster). Thus, at least a fraction of *Sp*HubP proteins within the clusters is constantly exchanged, or further copies of the protein are constantly recruited to both clusters (Fig. 5D).

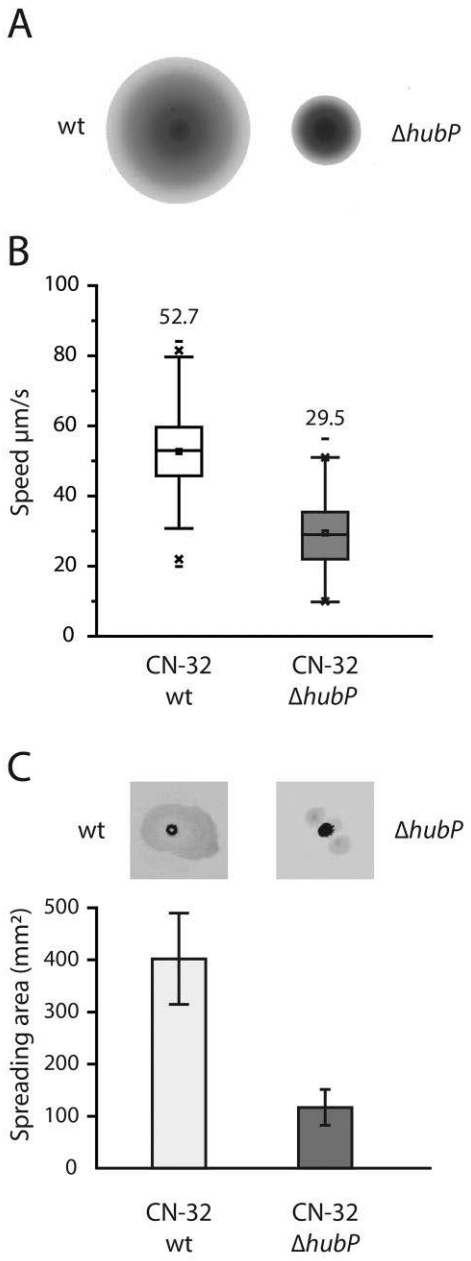

Fig. 4. *Sp*HubP is required for normal motility in *S. putrefaciens* CN-32.
A. Contribution of *Sp*HubP to spreading in soft agar. There was 3 µl of exponentially growing cultures of the corresponding strains placed on an agar plate solidified with 0.25 % agar and incubated for 16 h.
B. Contribution of *Sp*HubP to flagellar performance. Displayed is the swimming speed of wild-type and *ΔhubP* strains. The box represents the interquartile range of the data. The average and the median are shown as '□' and '—', and the whiskers denote the data range of the 5th and 95th percentile. Minimum and maximum are represented by 'x'. Swimming speed was determined for 200 cells each. Performance of the wild-type flagellar motor is significantly different from that of *ΔhubP*-mutant cells (ANOVA, *P* value 0.05).
C. Contribution of *Sp*HubP to twitching motility. The micrographs show images of the radial extension formed by twitching cells, the quantification of which is displayed below. The error bars show the standard deviation of five independent experiments.

The same localization pattern for *Sp*HubP occurred in *S. putrefaciens* cells in which the full gene locus encoding the primary polar flagellar system including *flhF* was deleted (ΔclusterI) (Fig. S9B), confirming that neither FlhF nor any other component of the polar flagellum is directly or indirectly required to target *Sp*HubP to the cell pole or division plane. When expressing a truncated version of *hubP* which only encodes the N-terminal part including the signal sequence and the predicted peptidoglycan-binding LysM domain (aa 1–134), we observed a localization pattern reminiscent to that of full-length *Sp*HubP-sfGFP (Fig. 5C). We thus concluded that the N-terminal LysM-containing domain of *Sp*HubP is sufficient for specific cellular targeting of the protein. When full-length *Sp*HubP-sfGFP or LysM-mCherry was heterologously produced in *E. coli*, both proteins similarly localized to the cell pole regions, the cell envelope, and the division plane (Figs S5 and S9C). Thus, the LysM-targeted localization of *Sp*HubP is not specific for *Shewanella*. Notably, ectopic overproduction of *Sp*HubP-sfGFP in *S. putrefaciens* CN-32 did not result in polar enrichment of the protein, but the excessive amounts were rather targeted to and accumulated at the cell envelope and division plane. These cells exhibited a distinct phenotype during growth in planktonic cultures, i.e. the occurrence of numerous smaller and elongated cells as well as chains of cells that had not separated after completion of cell division. This finding is indicating that an excess of *Sp*HubP interferes with normal cell division (Fig. S9B and D). Because a similar phenotype was observed upon overproduction of LysM-sfGFP, the effect is likely conferred by the N-terminal periplasmic domain of *Sp*HubP.

Sp*HubP, but not FlhF, targets the* oriC *to the cell pole during cell division*

*Vc*HubP has been shown to orchestrate polar localization of the *oriCI* of the larger of the two *V. cholerae* chromosomes. To determine whether or not *Sp*HubP fulfills a similar function in *S. putrefaciens* CN-32, we fused the ParB (Sputcn32_3965) C-terminus to mCherry. The hybrid gene was chromosomally integrated to replace the native *parB*. ParB is an origin-associated centromere-binding protein and thus marks the localization of the chromosomal origin. We observed no phenotype with respect to cell morphology or growth rate in the resulting strain (*mCherry-parB*), indicating that the fusion protein is fully functional.

The mCherry-ParB fusion enabled us to follow chromosome segregation in CN-32 over the cell cycle by fluorescence microscopy (Fig. 6A). Under the growth conditions

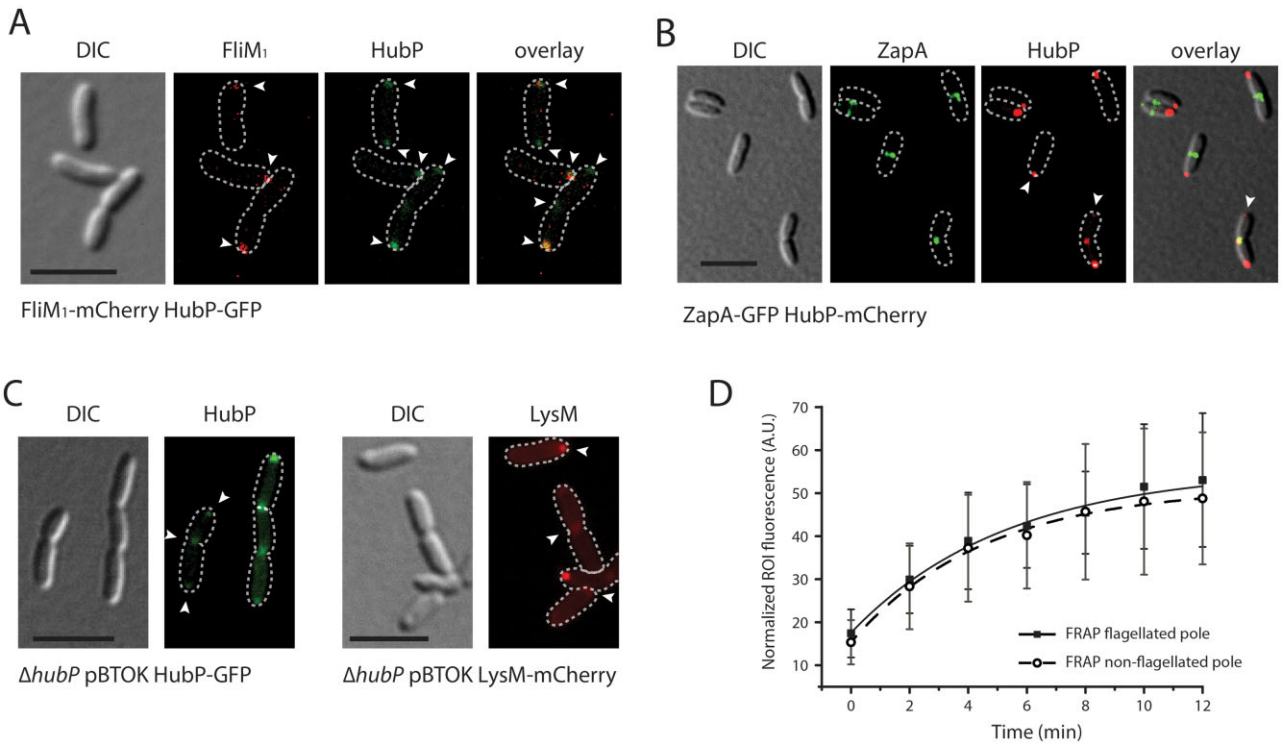

Fig. 5. Localization patterns of *Sp*HubP. Displayed are DIC and fluorescent micrographs of cells harboring fluorescently labeled components as indicated below the corresponding panels. Arrows indicate the position of fluorescent clusters. The scale bar equals 5 μm.
A. *Sp*HubP-sfGFP co-localizes with FliM$_1$ at the corresponding poles but also forms a minor cluster at the opposite cell pole.
B. *Sp*HubP-mCherry also accumulates at the division plane where it co-localizes with ZapA-sfGFP.
C. Localization pattern of *Sp*HubP-sfGFP (left panels) and its periplasmic domain (LysM-mCherry; right panels) upon ectopic production.
D. Rate of *Sp*HubP exchange as determined by FRAP. Displayed is the normalized averaged fluorescence intensity as a function of time for *Sp*HubP-sfGFP at the flagellated (black squares) and the non-flagellated (white circles) pole. Error bars display the standard error. The poles were defined prior to bleaching by co-localization with FliM$_1$-mCherry.

applied, a new replication was already initiated before cell separation, resulting in cells with four mCherry-ParB foci (33% of the population). In wild-type cells, mCherry-ParB fluorescent foci moved towards the opposite cell pole until they co-localized with fluorescently tagged *Sp*HubP directly at the cell pole. In contrast, when *Sp*HubP was absent, the mCherry-ParB foci remained at 1/4 or 3/4 position of the cell and did not resume full localization to the cell pole (Fig. 6C and D, Fig. S10A and B). Based on these observations, we concluded that *Sp*HubP has a function in chromosome segregation and is required for recruitment of *oriC* to the cell pole. Notably, the difference in chromosome segregation between wild-type and *ΔhubP* cells did not result in a significant phenotype with respect to growth or cell morphology. However, we noticed a slight difference in the timing of cell division: Under our experimental conditions, wild-type cells consistently exhibited a visible constriction when cells reached a length of 4.5 μm. In contrast, in *ΔhubP*-mutant cells, formation of the constriction occurred at less-defined cell lengths in a range of 3.6–4.4 μm. In contrast, polar localization of mCherry-ParB-marked *oriC* was unaffected by the presence or absence of FlhF (Fig. S10B).

Taken together, we have shown here that *S. putrefaciens* CN-32 possesses two distinct polar landmark systems, FlhF and *Sp*HubP. Both proteins display distinct localization patterns, and while FlhF regulates the number and polarity of the primary flagellar system, *Sp*HubP is required to target the chromosomal origin region and the chemotaxis system to the designated cell pole and likely performs some additional functions with respect to cellular motility (Fig. S11).

Discussion

For the vast majority of bacterial species, proper spatiotemporal regulation of cell polarity is crucial for a number of important or even essential cellular processes, such as chromosome segregation and cell division, differentiation, and cell motility (Treuner-Lange and Søgaard-Andersen, 2014). The latter is particularly evident for polarly flagellated bacterial species. These bacteria need to synthesize one or more new flagellar machineries at the designated cell pole, and this process often has to be strictly coordinated with the cell cycle to ensure that the daughter cell is immediately motile after separation from the mother cell

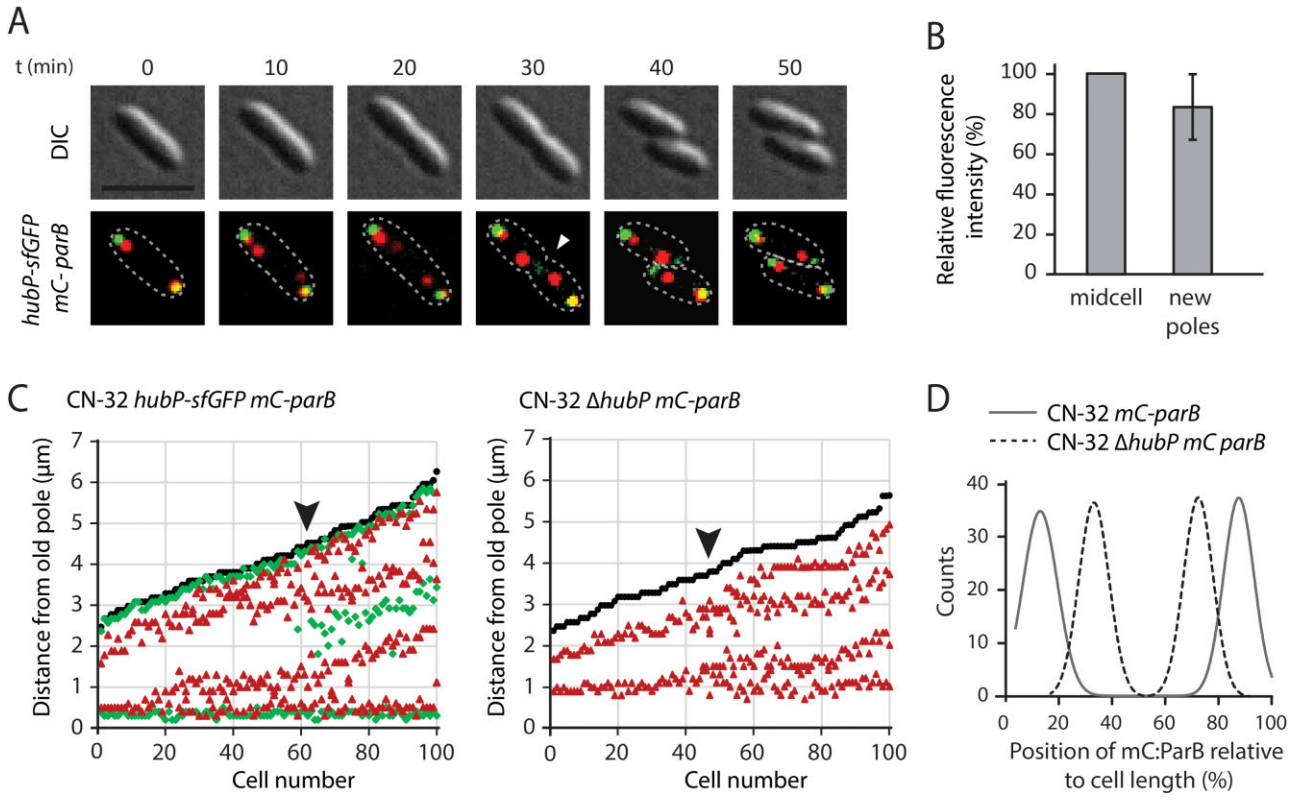

Fig. 6. Localization of *oriC* in dependence of *Sp*HubP.
A. Localization patterns of *Sp*HubP-sfGFP and ParB-mCherry during a full cell cycle. Shown are DIC (upper panel) and corresponding fluorescent micrographs (lower panel) of cells in which ParB as a marker for *oriC* was labeled with mCherry and *Sp*HubP was labeled with sfGFP. Yellow spots mark areas in which ParB and *Sp*HubP co-localize. The scale bar represents 5 µm.
B. HubP-sfGFP fluorescence intensity at midcell prior to cell fission and at each new cell pole 5–10 min after cell fission.
C. Left panel: Positioning of *Sp*HubP-sfGFP (green) and mCherry-ParB (*mC-parB*; red) relative to the cell length (black line). Right panel: Positioning of mCherry-ParB (*mC-parB*; red) relative to the cell length (black line) in the absence of *Sp*HubP. A corresponding image also displaying fluorescence intensity can be found in Fig. S10A.
D. Line scan analysis of the average mCherry-ParB (*mC-parB*) fluorescence intensity relative to the cell length. In wild-type cells (solid line) the *oriC* is localized close to the cell poles while it remains at a 1/3 position in *ΔhubP* cells (dashed line).

(Chilcott and Hughes, 2000; Ryan and Shapiro, 2003). In most bacterial species, motor functions can be modulated by one or more associated chemotaxis systems which allow biased movement towards a source of attractant or away from a repellent (Porter *et al.*, 2011; Sourjik and Wingreen, 2012). Components of bacterial chemotaxis systems are commonly arranged in large macromolecular clusters whose size has allowed their visualization and structural characterization by means of electron cryo tomography (Zhang *et al.*, 2007; Briegel *et al.*, 2009; 2012; Liu *et al.*, 2012). In a number of bipolarly or unisemipolarly flagellated bacterial species, such as *Caulobacter crescentus*, *P. aeruginosa* and *V. cholerae*, specific chemotaxis arrays localize in discrete foci at or close to the flagellated cell pole (Alley *et al.*, 1992; Wadhams *et al.*, 2003; Bardy and Maddock, 2005; Ringgaard *et al.*, 2011). This proximity of the chemotaxis system and the receiving flagellar motors has been suggested to facilitate rapid signal exchange via CheY and, hence, chemotactic efficiency (Sourjik and Berg, 2002; Lipkow *et al.*, 2005; Ringgaard *et al.*, 2014), and to ensure the inheritance of a functional chemotaxis array upon division (Jones and Armitage, 2015). *S. putrefaciens* CN-32 belongs to the bacterial species which are equipped with two complete distinct flagellar systems, a primary polar and a secondary lateral system. Under appropriate conditions, both systems are synchronously assembled (Bubendorfer *et al.*, 2012). Our study demonstrates that also in *Shewanella*, the chemotaxis cluster is localized to the flagellated cell pole. We have previously shown that the polar flagellar system primarily mediates cellular propulsion and is directly addressed by CheY. In contrast, the secondary system constantly rotates in a counterclockwise direction and does not respond to the chemotaxis system. This is likely due to the absence of the conserved N-terminal CheY-binding motif in the $FliM_2$ motor protein of the secondary system (Bubendorfer *et al.*, 2014). Thus, in *S. putrefaciens* CN-32, the primary flagellar motor and its

corresponding chemotaxis system are localized in close proximity, which likely enables rapid signal exchange via phosphorylated CheY. In contrast, the lateral filaments operate independently to curb the cellular turning angles during chemotaxis to increase spreading efficiency of the population (Bubendorfer *et al*., 2014).

The close proximity of chemotaxis and flagellar systems in various bacterial species might lead to the speculation that polar localization of both molecular machines is mediated by the same polar landmark system. Correspondingly, previous studies on *P. aeruginosa* strongly indicated that both the polar flagellar system as well as at least one of the chemotaxis arrays depend on the polar targeting system FlhF/FlhG (Kulasekara *et al*., 2013). In contrast, in *V. cholerae*, polar localization of the chemotaxis cluster is independent of FlhF (Ringgaard *et al*., 2011) but instead requires the multidomain protein HubP (Yamaichi *et al*., 2012). Our studies demonstrate that in *S. putrefaciens* CN-32, the GTPase FlhF specifically serves as the landmark protein for polar localization of the flagellar system and exhibits the corresponding localization to the old cell pole. In *S. putrefaciens* CN-32, deletion of *flhF* negatively affects production of flagella and results in displacement of the flagellum from the cell pole to more lateral positions. These data are fully consistent with those obtained for other polarly flagellated gammaproteobacteria (summarized in Kazmierczak and Hendrixson, 2013). In contrast to the primary flagellar system, normal polar localization of the chemotaxis system in *S. putrefaciens* CN-32 occurs independently of FlhF and requires the presence of another polar multidomain landmark protein, which we identified as the functional ortholog of *Vc*HubP.

Along most of their length, *Vc*HubP and *Sp*HubP exhibit little similarity at the amino acid level with the exception of the N-terminal and far C-terminal sections (Figs S6, S7, S11). The conserved N-terminal section harbors the periplasmic part of HubP including the LysM domain and the downstream transmembrane domain. In both species, this LysM-containing part of the protein appears to be required for targeting HubP to the designated cellular compartment. The localization pattern of *Sp*HubP is complex: In most cells, the protein forms a distinct cluster at the flagellated cell pole and a smaller cluster at the opposite pole. As indicated by FRAP experiments, *Sp*HubP molecules in both major and minor clusters are constantly exchanged at a similar rate. During cell division, the minor *Sp*HubP cluster appears to increase in size while the chromosomal origin is moved towards that pole. Overproduction of both full-length *Sp*HubP-sfGFP and LysM-sfGFP did not lead to infinite growth of the polar clusters, indicating that only a certain amount of *Sp*HubP may join these clusters. Excess *Sp*HubP occurring in the cell envelope may then be targeted to the cellular division plane. After completion of division, the new poles of both mother and daughter cells bear the minor *Sp*HubP cluster while the major cluster remains at the old pole which is decorated with the primary flagellar and the corresponding chemotaxis system. Thus, similar to what has been shown for TipN in *C. crescentus*, this minor *Sp*HubP cluster might serve as a marker for future polar assembly sites in the progeny cells (Huitema *et al*., 2006; Lam *et al*., 2006). Overproduction of TipN in *C. crescentus* results in the formation of lateral cell poles and leads to cellular branching. In contrast, in *S. putrefaciens* CN-32, *Sp*HubP-sfGFP and LysM-sfGFP do not form subpolar clusters upon overproduction but diffusively accumulate in the cell envelope and at the cell division plane. We thus hypothesize that the observed phenotype with respect to cell size and cell separation in *S. putrefaciens* CN-32 at excessive levels of *Sp*HubP (or its periplasmic part) might rather be due to interference between cell division proteins and the periplasmic domain of *Sp*HubP. The homologous periplasmic region of *P. aeruginosa* FimV has previously been shown to bind peptidoglycan (Wehbi *et al*., 2011) and, upon overproduction, may lead to cell elongation, vaguely reminiscent of the phenotype observed in CN-32 (Semmler *et al*., 2000). It remains to be shown how *Vc*HubP, *Sp*HubP or FimV are targeted to the cell pole and/or the division site. It might be speculated that this targeting is due to specific regions within the peptidoglycan, such as the nascent cell wall formed during cell fission, and that the resulting minor cluster of HubP is then required to recruit further HubP copies to the new cell pole after cell separation. When *Sp*HubP-sfGFP or LysM-sfGFP are ectopically produced in *E. coli*, the protein localizes to the cell poles and cell division plane as observed in *Shewanella*, suggesting that similar structures are recognized by the periplasmic region of *Sp*HubP in both species. However, it should be noted that *Vc*HubP is directed to the cell envelope in *E. coli*, but does not exhibit its normal localization pattern in this species.

In contrast to the periplasmic region, the cytoplasmic parts of *Sp*HubP and *Vc*HubP are far less conserved and, in addition, this section is considerably shorter in *Sp*HubP (Figs S6 and S7). However, both proteins harbor within this domain 9 or 10 copies of an imperfect repeat of an amino acid motif that is highly enriched in aspartate and glutamate residues and thus imparts a highly acidic character on the protein. Studies on *Vc*HubP have provided evidence that the protein exerts its function as a polar hub by directing ParA-like ATPases, which are commonly implicated in spatiotemporal organization processes in bacteria (Lutkenhaus, 2012), to the designated cell pole (Yamaichi *et al*., 2012). ParA1, required for segregation of the larger of the two *V. cholerae* chromosomes, has been shown to directly interact with the repeat region of *Vc*HubP and this might be similarly true for *Sp*ParA and *Sp*HubP, because a deletion in *hubP* results in a very similar phenotype with respect to chromosome segregation in both *V. cholerae*

and *S. putrefaciens*. Direct interaction of *Vc*ParC, which is implicated in positioning of the chemotaxis machinery (Ringgaard *et al*., 2011), and *Vc*HubP could not be demonstrated, strongly indicating that not all *Vc*HubP client proteins have been identified yet (Yamaichi *et al*., 2012). Accordingly, deletion of the obvious *Vc*ParC ortholog in *S. putrefaciens* CN-32 (Sputcn32_2553) did not exhibit a major phenotype with respect to chemotactic swimming (data not shown). The findings strongly suggest that other, yet unidentified, factors are required to mediate polar recruitment of the chemotaxis complex by HubP.

In *S. putrefaciens*, polar targeting of FlhF and *Sp*HubP and localization of flagellar and chemotaxis systems appear to occur independently. However, when *Sp*HubP is absent, FlhF and, accordingly, $FliM_1$ was observed at the cell pole in a significantly smaller cell population, indicating that *Sp*HubP might be involved in regulating the ability of FlhF to accumulate at the cell pole and to recruit basal body proteins. A previous study has provided evidence that a high amount of FlhG negatively affects polar localization of FlhF in *V. alginolyticus* (Kusumoto *et al*., 2008). Recent work on the same species provided further conclusive evidence that polar localization of FlhG strongly depends on the ATPase activity of the protein and has a strong effect on the polar accumulation of FlhF and, hence, the formation of flagella at the cell pole (Ono *et al*., 2015). Notably, HubP was shown to directly interact with FlhF and FlhG in *V. cholerae* (Yamaichi *et al*., 2012), and we have shown here that also in *S. putrefaciens* CN-32, FlhG localizes to the flagellated cell pole in a *Sp*HubP-dependent fashion. This may suggest that while *Sp*HubP might not directly localize FlhF, it might mediate proper FlhF-FlhG interactions at the cell pole to restrict the formation of the number of polar flagella to one in the appropriate number of cells. In addition, we could provide evidence that *Sp*FlhF and *Sp*FlhG interact *in vitro* and that the N-terminal section of *Sp*FlhG stimulates the GTPase activity of *Sp*FlhF. Thus, *Sp*HubP-mediated interaction between FlhF and FlhG and control of the GTPase activity might affect FlhF-related functions such as polar accumulation and recruitment of flagellar components, but also flagellar performance, as has recently been suggested for *P. aeruginosa* (Schniederberend *et al*., 2013). Accordingly, a deletion of *hubP* in both *V. cholerae* and *S. putrefaciens* CN-32 resulted in a significantly decreased ability to navigate through soft agar. In *V. cholerae*, this phenotype has been mainly attributed to a decrease in the chemotactic drift of the population due to the, on average, increased distance between the chemotaxis machinery and the flagellar motor, resulting in a limited ability to induce directional switches appropriately (Ringgaard *et al*., 2011; Yamaichi *et al*., 2012). However, we additionally found that in *S. putrefaciens* CN-32 *ΔhubP* mutants, the average swimming speed in planktonic cultures was significantly reduced which cannot be solely attributed to the loss of chemotaxis (Bubendorfer *et al*., 2014). While this observed decrease in swimming speed might be due to *Sp*HubP-FlhF/FlhG interaction as elaborated above, it might similarly be speculated that *Sp*HubP directly or indirectly recruits other proteins that affect flagellar functions (Boehm *et al*., 2010; Fang and Gomelsky, 2010; Paul *et al*., 2010; Kulasekara *et al*., 2013). We have shown that also type IV pili-mediated twitching motility, which requires polar assembly and disassembly of pili fibers (Burrows, 2012), is affected in *S. putrefaciens ΔhubP*. We thus expect that further interaction partners, or 'client' proteins, of *Sp*HubP remain to be identified which do not belong to the group of ParA-like proteins.

Potential HubP or FimV orthologs can be identified in a number of different bacterial genera (Semmler *et al*., 2000; Yamaichi *et al*., 2012). All of these proteins share an N-terminal periplasmic domain comprising the, putatively peptidoglycan-binding, LysM-domain. This N-terminal domain might also be involved in mediating protein–protein interactions within the periplasm or membrane (Wehbi *et al*., 2011). In addition, all these proteins are characterized by a highly acidic cytoplasmic part which appears to function as the docking region for other appropriate interaction partners. This cytoplasmic region is little conserved at the amino acid level but also with respect to protein length and the presence and organization of repeat units, and even within a group of closely related species, such as in various *Shewanella* sp., the cytoplasmic part of HubP/FimV exhibits a high degree of variation. It might thus be speculated that polar targeting within the cell by the LysM domain is conserved throughout the species. In contrast, the cytoplasmic and also the periplasmic parts may have adapted to the specific requirement of the host species for polar localization of client proteins or protein complexes. These differences might be the reason why the chemotaxis system is localized by HubP in *V. cholerae* and *S. putrefaciens* CN-32, but directly or indirectly depends on FlhF in *P. aeruginosa*. Thus, HubP/FimV proteins might have numerous different functions, including various aspects of motility and chromosome segregation as shown for *P. aeruginosa*, *V. cholerae* and *S. putrefaciens* CN-32 (Semmler *et al*., 2000; Wehbi *et al*., 2011; Yamaichi *et al*., 2012; Fig. S11). We expect that future studies on different species will identify further processes which are spatiotemporally organized by HubP/FimV proteins.

Experimental procedures

Strains, growth conditions and media

All strains used in this study are listed in Table S1. *E. coli* strains were routinely cultured in LB medium at 37°C if not indicated otherwise. *S. putrefaciens* CN-32 strains were cultivated in LB or LM (10 mM HEPES, pH 7.5; 200 mM NaCl;

0.02% yeast extract; 0.01% peptone; 15 mM lactate) media at 30°C. When required, media were supplemented with 50 μg ml^{-1} kanamycin or 10% (w/v) sucrose. Cultures of the *E. coli* conjugation strain were supplemented with 2,6-diamino-pimelic acid (DAP) to a final concentration of 300 μM. Solid media were made by an addition of 1.5% (w/v) agar. Soft agar plates for swimming assays were prepared with LB medium solidified with 0.25% (w/v) agar.

Strain constructions

General DNA manipulations were carried out according to standard protocols (Sambrook *et al*., 1989) using appropriate kits (VWR International GmbH, Darmstadt, Germany) and enzymes (Fermentas, St Leon-Rot, Germany). All vectors/plasmids used in this study are summarized in Table S2. Plasmids were delivered to *S. putrefaciens* CN-32 by conjugation from *E. coli* WM3064. Markerless in-frame deletions were generated by sequential homologous crossover using vector pNTPS-138-R6K essentially as described previously (Lassak *et al*., 2010). Vectors were constructed either by common restriction/ligation approaches using appropriate restriction enzymes, or by enzymatic assembly as previously reported (Gibson *et al*., 2009). The corresponding oligonucleotides used for cloning are listed in Table S3. To complement in-frame deletion mutants, the mutated locus was exchanged with the wild-type gene using the same sequential crossover approach. To generate fluorescent fusions, target proteins were either C- or N-terminally tagged with sfGFP, mCherry, Venus or eCFP using a flexible linker of either 6xGly, 2x(Gly-Gly-Ser), 3x(Gly-Gly-Ser) or (Gly-Ser) (for ectopic overproduction of FlhF-sfGFP and C-terminal tagging of FlhG). The nature of each fluorescent fusion is specified in detail in Table S1. All genetic fusions except those for the MCPs and for ectopic (over-)production were introduced into the chromosome to replace the native copy of the gene essentially as previously described (Bubendorfer *et al*., 2012) by markerless sequential crossover using pNTPS-138-R6K as delivery vector. The fusion to MCP0796 was established by cloning an appropriate PCR-derived DNA fragment of about 500 bp encoding the C-terminal region of the proteins into vector pJP5603-gfp (Koerdt *et al*., 2009) followed by conjugation and single homologous integration, yielding a chromosomal fusion expressed under its native promoter. Correct insertions or deletions were verified by polymerase chain reaction (PCR). Production levels and stability of fusion proteins were checked by immunofluorescence approaches and appropriate phenotypic analysis (Fig. S1). To enable coupling of maleimide-ligated Alexa dyes to the flagellar filaments, a threonine-to-cysteine (T159C) were introduced in both $FlaA_1$ and $FlaB_1$ flagellins by exchange of the appropriate codons within the corresponding genes on the chromosome, resulting in strain $FlaAB_1$-Cys. Accordingly, variants of $FlaA_2$ (T159C; T160C) and $FlaB_2$ (T156C; T159C) were constructed for specific labeling of secondary flagella. For overproduction of FlhF and FlhG and derivatives, the corresponding genes (Sputcn32_2561, *flhF*; Sputcn32_2560, *flhG*) were amplified from *S. putrefaciens* CN-32 genomic DNA by PCR using appropriate primer pairs (Table S3). The forward primer encoded a hexa-histidine tag in frame with the DNA sequence of *flhF* or *flhG*. The resultant PCR fragments were cloned into pET24d(+) (Novagen) or pGAT3 (Peränen *et al*., 1996) vectors via the introduced restriction sites. Due to enhanced purification properties of the produced protein, a truncated version of *flhF* lacking the first 10 codons of the 5′-end was overexpressed.

Overproduction of Sp*HubP-sfGFP and LysM-mCherry*

The vector pBTOK was derived by assembly of the anhydrotetracycline-inducible promoter region of pASK-IBA3plus (IBA GmbH, Göttingen, Germany) followed by the *E. coli rrnB1* T_1 and lambda phage T_0 terminator set into pBBR1-MCS5 (Kovach *et al*., 1995). The vector backbone fragment was amplified with primer pair SH501/SH502 using pBBR1-MCS5 as a template; the promoter region including the MCS of pAS-IBA3plus was derived using SH503/SH504; and the terminator region was produced using SH505/SH506 and pUC18-mini-Tn*7*T-Gm-lux (Choi *et al*., 2005) as a template. Fragment assembly was carried as previously described (Gibson *et al*., 2009). Sequence and vector map are available upon request. The sequence of *hubP-sfgfp*, the LysM domain [*Sp*HubP_AA1-134 (Sputcn32_2442_nt1-402)] and mCherry were amplified with the corresponding primer pairs. The LysM-encoding gene region and *mCherry* were joined by an overlap PCR. The resulting inserts were processed with XbaI and PspOMI and ligated into the vector. The resulting plasmid was transferred into CN-32 *ΔhubP* via conjugation. Prior to overproduction, CN-32 pBTOK-HubP-sfGFP and CN-32 pBTOK-LysM-mCherry were cultured in LB media to an OD_{600} of ~ 0.3 followed by induction with 20 ng·ml^{-1} anhydrotetracycline for 45 min.

Flagellar and hook staining

Fluorescent staining of flagellar filaments (CN-32 $FlaAB_1$-Cys) or hook structures ($FlgE_2$-Cys; Schuhmacher *et al*., 2015b) was essentially carried out on exponentially growing cells as previously described (Guttenplan *et al*., 2013) using Alexa Fluor 488 maleimide (Molecular Probes, Life Technologies) prior to microscopy.

Fluorescence microscopy

Prior to microscopy, strains were cultivated overnight in LM media and subcultured in LM until reaching exponential growth phase (OD_{600} of ~ 0.2). There was 3 μl of culture spotted on an agarose pad (LM media solidified by 1% (w/v) agarose). Fluorescence images were recorded by a Leica DMI 6000 B inverse microscope (Leica, Wetzlar, Germany) equipped with an sCMOS camera and a HCX PL APO 100×/1.4 objective using the VisiView software (Visitron Systems, Puchheim, Germany). Images were further processed using ImageJ and Adobe Illustrator CS6.

Fluorescence recovery after photobleaching (FRAP)

FRAP analyses were carried out with a Axio Imager.M1 microscope (Zeiss), a Zeiss Plan Apochromat 100×/1.40 Oil DIC (Differential Interference Contrast) objective and a

Cascade:1K CCD camera (Photometrics) equipped with a 488 nm-solid state laser and a 2D-VisiFRAP Galvo System multi-point FRAP module (Visitron Systems, Germany). Cells were cultured and immobilized on agarose pads as described above. After acquisition of a pre-bleach image, a single laser pulse of 30 ms was used to bleach individual *Sp*HubP-sfGFP clusters. Fluorescence recovery was subsequently monitored at 2-min intervals for 12 min. The integrated fluorescence intensities of the whole cell, the bleached region and an equally sized unbleached region were measured for each time point using ImageJ. After background correction, the fluorescence intensities of the bleached and unbleached regions were divided by the whole cell intensity to correct for general photobleaching during the imaging process. Average values of 10–13 cells were plotted using OriginPro 9.1. Recovery rates were determined by fitting the data obtained for the bleached region to the single exponential function F(t) = F0*exp(-x/t1) + A, where F(t) is the fluorescence at time t, A the maximum intensity, x the time in min, 1/t1 the rate constant in min^{-1} and F0 the relative fluorescence intensity at t = 0 min. In all cases, fits with $R2 \geq 0.99$ were obtained. Recovery half-times were calculated according to the equation $t_{1/2} = \ln(2)*t1$.

Determination of swimming speed

Cells of *S. putrefaciens* CN-32 and *S. putrefaciens* CN-32 Δ*hubP* from overnight cultures were used to inoculate LM medium to an OD_{600} of 0.02 and cultivated for 3–4 h to an OD_{600} of ~ 0.2. An aliquot of each culture was placed under a coverslip fixed by four droplets of silicone to create a space of 1–2 mm width. Movies of 12 s (157 frames) were taken with an inverse microscope (for specification, see above). Speeds of 200 cells per strain were determined using the MTrackJ plugin of ImageJ. The resulting data were tested for significance by using ANOVA ($P = 0.05$) in R version 3.0.1. Motility was further assessed by placing 3 µl of a planktonic culture of the corresponding strains on soft agar plates containing LB medium with an agar concentration of 0.25% (w/v). Plates were incubated for 12h at 30°C or overnight at room temperature. Strains to be directly compared were always placed on the same plate.

Analysis of twitching motility

Type IV pili-mediated twitching motility was assayed as described previously (Semmler *et al*., 1999) using 1.0 % LB-agar plates at 30°C for up to 48 h.

Protein production and purification

E. coli BL21(DE3) (New England BioLabs, Frankfurt, Germany) cells carrying the appropriate expression plasmid were grown in LB medium supplemented with kanamycin (100 µg ml^{-1}) and D(+)-lactose-monohydrate (12.5 g l^{-1}) for 16 h at 30°C under rigorous shaking (150 r.p.m.). Cells were harvested (3500×*g*, 20 min, 4°C) and resuspended in lysis buffer (20 mM HEPES, pH 8.0; 250 mM NaCl; 40 mM imidazole; 20 mM $MgCl_2$ and 20 mM KCl). Cells were lysed with the M-110L Microfluidizer (Microfluidics). After centrifugation (47 850×*g*, 20 min, 4°C), the clear supernatant was loaded on a 1 ml HisTrap column (GE Healthcare) equilibrated with 10 column volumes (CV) of lysis buffer. After washing with 10 CV lysis buffer, the protein was eluted with 15 ml elution buffer (lysis buffer containing 500 mM imidazole). The protein was concentrated to ≈ 15 mg ml^{-1} using an Amicon Ultracel-10K (Millipore). The concentrated sample was applied to size-exclusion chromatography (HiLoad 26/600 Superdex 200 pg, GE Healthcare) equilibrated with SEC-buffer (20 mM HEPES, pH 7.5, 200 mM NaCl 20 mM MgCl2 and 20 mM KCl). Protein concentration was determined by a spectrophotometer (NanoDrop Lite, Thermo Scientific).

GTPase activity of FlhF

GTPase activity of FlhF was monitored by HPLC. There was 100 µM of each protein (FlhF, FlhG and/or corresponding derivatives as indicated) incubated together with 1 mM GTP in SEC-buffer for 30 min at 37°C. Reactions were stopped by flash-freezing with liquid nitrogen and stored at −20°C until measurement. HPLC measurements were performed with an Agilent 1100 Series HPLC system (Agilent Technologies, Santa Clara) and a C18 column (EC 250/4.6 Nucleodur HTec 3 µm; Macherey-Nagel, Düren, Germany). GDP and GTP were eluted with a buffer containing 50 mM KH_2PO_4, 50 mM K_2HPO_4, 10 mM tetrapentylammonium bromide and 15% (v/v) acetonitrile at 0.8 ml min^{-1} flow rate and detected at a wavelength of 253 nm in agreement with standards. GDP originating from non-enzymatic hydrolysis of GTP was determined by triplicate measurement of 1 mM GTP treated similar as the enzymatic reactions and subtracted from the quantified GDP.

Immunoblot (Western blot) analysis

Production and stability of the fusions were determined by immunoblot analyses. Protein lysates were prepared from exponentially growing cultures. Cell suspensions were uniformly adjusted to an OD_{600} of 10. Protein separation and immunoblot detection were essentially carried out as described earlier (Bubendorfer *et al*., 2012; Binnenkade *et al*., 2014) using polyclonal antibodies raised against mCherry, GFP (Eurogentec Deutschland GmbH, Köln, Germany) or FlhG (Schuhmacher *et al*., 2015b). Signals were detected using the SuperSignal® West Pico Chemiluminescent Substrate (Thermo Scientific, Schwerte, Germany) and documented using a FUSION-SL chemiluminescence imager (Peqlab, Erlangen, Germany).

Acknowledgements

This project was supported by grants from the Deutsche Forschungsgemeinschaft (DFG) to KMT (TH831/5-1) in the framework of the priority program SPP1617. FR and SB were supported by the International Max Planck Research School. The project was further supported by the LOEWE excellence initiative of the state of Hesse (to GB).

We are grateful to Oliver Leicht and Martin Thanbichler at the Philipps-Universität Marburg for help with the FRAP analysis and to Wieland Steinchen of the Bange lab for his assistance during HPLC measurements. We would also like

to thank Martin Thanbichler and Anke Treuner-Lange for critically reading and commenting on the manuscript.

Conflict of interest

The authors declare no conflict of interest.

References

Alley, M.R., Maddock, J.R., and Shapiro, L. (1992) Polar localization of a bacterial chemoreceptor. *Genes Dev* **6:** 825–836.

Altegoer, F., Schuhmacher, J., Pausch, P., and Bange, G. (2014) From molecular evolution to biobricks and synthetic modules: a lesson by the bacterial flagellum. *Biotechnol Genet Eng Rev* **30:** 49–64.

Balaban, M., Joslin, S.N., and Hendrixson, D.R. (2009) FlhF and its GTPase activity are required for distinct processes in flagellar gene regulation and biosynthesis in *Campylobacter jejuni*. *J Bacteriol* **191:** 6602–6611.

Bange, G., and Sinning, I. (2013) SIMIBI twins in protein targeting and localization. *Nat Struct Mol Biol* **20:** 776–780.

Bange, G., Petzold, G., Wild, K., Parlitz, R.O., and Sinning, I. (2007) The crystal structure of the third signal-recognition particle GTPase FlhF reveals a homodimer with bound GTP. *Proc Natl Acad Sci USA* **104:** 13621–13625.

Bange, G., Kümmerer, N., Grudnik, P., Lindner, R., Petzold, G., Kressler, D., *et al*. (2011) Structural basis for the molecular evolution of SRP-GTPase activation by protein. *Nat Struct Mol Biol* **18:** 1376–1380.

Bardy, S.L., and Maddock, J.R. (2005) Polar localization of a soluble methyl-accepting protein of *Pseudomonas aeruginosa*. *J Bacteriol* **187:** 7840–7844.

Binnenkade, L., Teichmann, L., and Thormann, K.M. (2014) Iron triggers lambdaSo prophage induction and release of extracellular DNA in *Shewanella oneidensis* MR-1 biofilms. *Appl Environ Microbiol* **80:** 5304–5316.

Boehm, A., Kaiser, M., Li, H., Spangler, C., Kasper, C.A., Ackermann, M., *et al*. (2010) Second messenger-mediated adjustment of bacterial swimming velocity. *Cell* **141:** 107–116.

Briegel, A., Ortega, D.R., Tocheva, E.I., Wuichet, K., Li, Z., Chen, S., *et al*. (2009) Universal architecture of bacterial chemoreceptor arrays. *Proc Natl Acad Sci USA* **106:** 17181–17186.

Briegel, A., Li, X., Bilwes, A.M., Hughes, K.T., Jensen, G.J., and Crane, B.R. (2012) Bacterial chemoreceptor arrays are hexagonally packed trimers of receptor dimers networked by rings of kinase and coupling proteins. *Proc Natl Acad Sci USA* **109:** 3766–3771.

Bubendorfer, S., Held, S., Windel, N., Paulick, A., Klingl, A., and Thormann, K.M. (2012) Specificity of motor components in the dual flagellar system of *Shewanella putrefaciens* CN-32. *Mol Microbiol* **83:** 335–350.

Bubendorfer, S., Koltai, M., Rossmann, F., Sourjik, V., and Thormann, K.M. (2014) Secondary bacterial flagellar system improves bacterial spreading by increasing the directional persistence of swimming. *Proc Natl Acad Sci USA* **111:** 11485–11490.

Burrows, L.L. (2012) *Pseudomonas aeruginosa* twitching motility: type IV pili in action. *Annu Rev Microbiol* **66:** 493–520.

Chilcott, G.S., and Hughes, K.T. (2000) Coupling of flagellar gene expression to flagellar assembly in *Salmonella enterica* serovar *typhimurium* and *Escherichia coli*. *Microbiol Mol Biol Rev* **64:** 694–708.

Choi, K.H., Gaynor, J.B., White, K.G., Lopez, C., Bosio, C.M., Karkhoff-Schweizer, R.R., and Schweizer, H.P. (2005) A Tn*7*-based broad-range bacterial cloning and expression system. *Nat Methods* **2:** 443–448.

Correa, N.E., Peng, F., and Klose, K.E. (2005) Roles of the regulatory proteins FlhF and FlhG in the *Vibrio cholerae* flagellar transcription hierarchy. *J Bacteriol* **187:** 6324–6332.

Dasgupta, N., Arora, S.K., and Ramphal, R. (2000) fleN, a gene that regulates flagellar number in *Pseudomonas aeruginosa*. *J Bacteriol* **182:** 357–364.

Davis, N.J., Cohen, Y., Sanselicio, S., Fumeaux, C., Ozaki, S., Luciano, J., *et al*. (2013) De- and repolarization mechanism of flagellar morphogenesis during a bacterial cell cycle. *Genes Dev* **27:** 2049–2062.

Ewing, C.P., Andreishcheva, E., and Guerry, P. (2009) Functional characterization of flagellin glycosylation in *Campylobacter jejuni* 81–176. *J Bacteriol* **191:** 7086–7093.

Fang, X., and Gomelsky, M. (2010) A post-translational, c-di-GMP-dependent mechanism regulating flagellar motility. *Mol Microbiol* **76:** 1295–1305.

Gibson, D.G., Young, L., Chuang, R.Y., Venter, J.C., Hutchison, C.A., 3rd, and Smith, H.O. (2009) Enzymatic assembly of DNA molecules up to several hundred kilobases. *Nat Methods* **6:** 343–345.

Green, J.C., Kahramanoglou, C., Rahman, A., Pender, A.M., Charbonnel, N., and Fraser, G.M. (2009) Recruitment of the earliest component of the bacterial flagellum to the old cell division pole by a membrane-associated signal recognition particle family GTP-binding protein. *J Mol Biol* **391:** 679–690.

Guttenplan, S.B., Shaw, S., and Kearns, D.B. (2013) The cell biology of peritrichous flagella in *Bacillus subtilis*. *Mol Microbiol* **87:** 211–229.

Huitema, E., Pritchard, S., Matteson, D., Radhakrishnan, S.K., and Viollier, P.H. (2006) Bacterial birth scar proteins mark future flagellum assembly site. *Cell* **124:** 1025–1037.

Jones, C.W., and Armitage, J.P. (2015) Positioning of bacterial chemoreceptors. *Trends Microbiol* **23:** 247–256.

Kazmierczak, B.I., and Hendrixson, D.R. (2013) Spatial and numerical regulation of flagellar biosynthesis in polarly flagellated bacteria. *Mol Microbiol* **88:** 655–663.

Koerdt, A., Paulick, A., Mock, M., Jost, K., and Thormann, K.M. (2009) MotX and MotY are required for flagellar rotation in *Shewanella oneidensis* MR-1. *J Bacteriol* **191:** 5085–5093.

Kovach, M.E., Elzer, P.H., Hill, D.S., Robertson, G.T., Farris, M.A., Roop, R.M., 2nd, and Peterson, K.M. (1995) Four new derivatives of the broad-host-range cloning vector pBBR1MCS, carrying different antibiotic-resistance cassettes. *Gene* **166:** 175–176.

Kulasekara, B.R., Kamischke, C., Kulasekara, H.D., Christen, M., Wiggins, P.A., and Miller, S.I. (2013) c-di-GMP heterogeneity is generated by the chemotaxis machinery to regulate flagellar motility. *Elife* **2:** e01402.

Kusumoto, A., Kamisaka, K., Yakushi, T., Terashima, H., Shinohara, A., and Homma, M. (2006) Regulation of polar

flagellar number by the *flhF* and *flhG* genes in *Vibrio alginolyticus*. *J Biochem* **139:** 113–121.
Kusumoto, A., Shinohara, A., Terashima, H., Kojima, S., Yakushi, T., and Homma, M. (2008) Collaboration of FlhF and FlhG to regulate polar-flagella number and localization in *Vibrio alginolyticus*. *Microbiology* **154:** 1390–1399.
Laloux, G., and Jacobs-Wagner, C. (2014) How do bacteria localize proteins to the cell pole? *J Cell Sci* **127:** 11–19.
Lam, H., Schofield, W.B., and Jacobs-Wagner, C. (2006) A landmark protein essential for establishing and perpetuating the polarity of a bacterial cell. *Cell* **124:** 1011–1023.
Lassak, J., Henche, A.L., Binnenkade, L., and Thormann, K.M. (2010) ArcS, the cognate sensor kinase in an atypical Arc system of *Shewanella oneidensis* MR-1. *Appl Environ Microbiol* **76:** 3263–3274.
Lipkow, K., Andrews, S.S., and Bray, D. (2005) Simulated diffusion of phosphorylated CheY through the cytoplasm of *Escherichia coli*. *J Bacteriol* **187:** 45–53.
Liu, J., Hu, B., Morado, D.R., Jani, S., Manson, M.D., and Margolin, W. (2012) Molecular architecture of chemoreceptor arrays revealed by cryoelectron tomography of *Escherichia coli* minicells. *Proc Natl Acad Sci USA* **109:** E1481–E1488.
Lutkenhaus, J. (2012) The ParA/MinD family puts things in their place. *Trends Microbiol* **20:** 411–418.
Murray, T.S., and Kazmierczak, B.I. (2006) FlhF is required for swimming and swarming in *Pseudomonas aeruginosa*. *J Bacteriol* **188:** 6995–7004.
Obuchowski, P.L., and Jacobs-Wagner, C. (2008) PfIl, a protein involved in flagellar positioning in *Caulobacter crescentus*. *J Bacteriol* **190:** 1718–1729.
Ono, H., Takashima, A., Hirata, H., Homma, M., and Kojima, S. (2015) The MinD homolog FlhG regulates the synthesis of the single polar flagellum of *Vibrio alginolyticus*. *Mol Microbiol* **98:** 130–141. doi: 10.1111/mmi.13109
Pandza, S., Baetens, M., Park, C.H., Au, T., Keyhan, M., and Matin, A. (2000) The G-protein FlhF has a role in polar flagellar placement and general stress response induction in *Pseudomonas putida*. *Mol Microbiol* **36:** 414–423.
Paul, K., Nieto, V., Carlquist, W.C., Blair, D.F., and Harshey, R.M. (2010) The c-di-GMP binding protein YcgR controls flagellar motor direction and speed to affect chemotaxis by a 'backstop brake' mechanism. *Mol Cell* **38:** 128–139.
Peränen, J., Rikkonen, M., Hyvonen, M., and Kaariainen, L. (1996) T*7* vectors with modified T*7lac* promoter for expression of proteins in *Escherichia coli*. *Anal Biochem* **236:** 371–373.
Porter, S.L., Wadhams, G.H., and Armitage, J.P. (2011) Signal processing in complex chemotaxis pathways. *Nat Rev Microbiol* **9:** 153–165.
Reyes-Lamothe, R., Nicolas, E., and Sherratt, D.J. (2012) Chromosome replication and segregation in bacteria. *Annu Rev Genet* **46:** 121–143.
Ringgaard, S., Schirner, K., Davis, B.M., and Waldor, M.K. (2011) A family of ParA-like ATPases promotes cell pole maturation by facilitating polar localization of chemotaxis proteins. *Genes Dev* **25:** 1544–1555.
Ringgaard, S., Zepeda-Rivera, M., Wu, X., Schirner, K., Davis, B.M., and Waldor, M.K. (2014) ParP prevents dissociation of CheA from chemotactic signaling arrays and tethers them to a polar anchor. *Proc Natl Acad Sci USA* **111:** E255–E264.
Ryan, K.R., and Shapiro, L. (2003) Temporal and spatial regulation in prokaryotic cell cycle progression and development. *Annu Rev Biochem* **72:** 367–394.
Sambrook, K., Fritsch, E.F., and Maniatis, T. (1989) *Molecular Cloning: A Laboratory Manual*. Cold Spring Harbor, NY: Cold Spring Harbor Press.
Schniederberend, M., Abdurachim, K., Murray, T.S., and Kazmierczak, B.I. (2013) The GTPase activity of FlhF is dispensable for flagellar localization, but not motility, in *Pseudomonas aeruginosa*. *J Bacteriol* **195:** 1051–1060.
Schuhmacher, J.S., Thormann, K.M., and Bange, G. (2015a) How bacteria maintain location and function of flagella? *FEMS Microbiol Rev* (in press). pii: fuv034.
Schuhmacher, J.S., Rossmann, F., Dempwolff, F., Knauer, C., Altegoer, F., Steinchen, W., *et al*. (2015b) MinD-like ATPase FlhG effects location and number of bacterial flagella during C-ring assembly. *Proc Natl Acad Sci USA* **112:** 3092–3097.
Semmler, A.B., Whitchurch, C.B., and Mattick, J.S. (1999) A re-examination of twitching motility in *Pseudomonas aeruginosa*. *Microbiology* **145** (Part 10): 2863–2873.
Semmler, A.B., Whitchurch, C.B., Leech, A.J., and Mattick, J.S. (2000) Identification of a novel gene, *fimV*, involved in twitching motility in *Pseudomonas aeruginosa*. *Microbiology* **146:** 1321–1332.
Sourjik, V., and Berg, H.C. (2002) Binding of the *Escherichia coli* response regulator CheY to its target measured in vivo by fluorescence resonance energy transfer. *Proc Natl Acad Sci USA* **99:** 12669–12674.
Sourjik, V., and Wingreen, N.S. (2012) Responding to chemical gradients: bacterial chemotaxis. *Curr Opin Cell Biol* **24:** 262–268.
Thanbichler, M. (2010) Synchronization of chromosome dynamics and cell division in bacteria. *Cold Spring Harb Perspect Biol* **2:** a000331.
Treuner-Lange, A., and Søgaard-Andersen, L. (2014) Regulation of cell polarity in bacteria. *J Cell Biol* **206:** 7–17.
Wadhams, G.H., Warren, A.V., Martin, A.C., and Armitage, J.P. (2003) Targeting of two signal transduction pathways to different regions of the bacterial cell. *Mol Microbiol* **50:** 763–770.
Wehbi, H., Portillo, E., Harvey, H., Shimkoff, A.E., Scheurwater, E.M., Howell, P.L., and Burrows, L.L. (2011) The peptidoglycan-binding protein FimV promotes assembly of the *Pseudomonas aeruginosa* type IV pilus secretin. *J Bacteriol* **193:** 540–550.
Yamaichi, Y., Bruckner, R., Ringgaard, S., Möll, A., Cameron, D.E., Briegel, A., *et al*. (2012) A multidomain hub anchors the chromosome segregation and chemotactic machinery to the bacterial pole. *Genes Dev* **26:** 2348–2360.
Zhang, P., Khursigara, C.M., Hartnell, L.M., and Subramaniam, S. (2007) Direct visualization of *Escherichia coli* chemotaxis receptor arrays using cryo-electron microscopy. *Proc Natl Acad Sci USA* **104:** 3777–3781.

Supporting information

Additional supporting information may be found in the online version of this article at the publisher's web-site.

The role of FlhF and HubP as polar landmark proteins in *Shewanella putrefaciens* CN-32

Florian Rossmann[#,1,2], Susanne Brenzinger[#,1,2], Carina Knauer[3], Anja K. Dörrich[1], Sebastian Bubendorfer[1,4], Ulrike Ruppert[1], Gert Bange[3], Kai M. Thormann[1*]

[1] Justus-Liebig Universität, Department of Microbiology and Molecular Biology, 35392 Giessen, Germany
[2] Max-Planck-Institut für terrestrische Mikrobiologie, Department of Ecophysiology, 35043 Marburg, Germany
[3] LOEWE Center for Synthetic Microbiology (Synmikro) & Department of Chemistry, Philipps University Marburg, 35043 Marburg, Germany
[4]current address: Institute for Medical Microbiology and Hospital Epidemiology, Hannover Medical School, 30625 Hannover, Germany

[#] equal contribution

[*] corresponding author

- supplemental material -

Supplemental Tables

Supplemental Figures

Table S1: Bacterial strains that were used in this study

Strain	Genotype	Reference
Escherichia coli		
DH5α λpir	φ80d*lacZ* ΔM15 Δ*(lacZYA-argF)*U169 *recA1 hsdR17 deoR thi-l supE44 gyrA96 relA1*/λpir	Miller VL, Mekalanos JJ (1988)
WM3064	*thrB1004 pro thi rpsL hsdS lacZ* ΔM15 RP4-1360 Δ(*araBAD*) 567Δ*dapA* 1341::[*erm pir*(wt)]	W. Metcalf, University of IIlinois, Urbana-Champaign
BL21(DE3)	*fhuA2 [lon] ompT gal (λ DE3) [dcm] ΔhsdS λ DE3 = λ sBamHIo ΔEcoRI-B int::(lacI::PlacUV5::T7 gene1) i21 Δnin5*	
E3743	DH5α λpir pBTOK *hubP-sfgfp*, ΔSputcn32_2442 pBTOK- Sputcn32_2442-3xGly-Gly-Ser- sfGFP (N-terminal)	This study
E3744	DH5α λpir pBTOK *lysM-mcherry*, ΔSputcn32_2442 pBTOK-mCherry-2xPro- Sputcn32_2442-AA1-134 tagged with mCherry (N-terminal)	This study
Shewanella putrefaciens		
S271	CN-32, wild type	Fredrickson JK, et al. (1998)
S1995	*Δ$fliF_1$ Δ$fliF_2$*, ΔSputcn32_2576 ΔSputcn32_3476, markerless deletion of *Δ$fliF_1$* and *Δ$fliF_2$*	Bubendorfer et al., (2012)
S2025	*Δcluster I*, ΔSputcn32_2549–ΔSputcn32_2605, markerless deletion of polar flagellar gene cluster	Bubendorfer et al., (2012)
S2240	*$fliM_1$-sfgfp*, Sputcn32_2569-6xGly-sfGFP-His6; markerless chromosomal fusion of *$fliM_1$* to *sfgfp* (C-terminal)	Bubendorfer et al., (2012)
S2241	*$fliM_1$*-mcherry, Sputcn32_2569-6xGly-mcherry-His6; markerless chromosomal fusion of *$fliM_1$* to *mcherry* (C-terminal)	Bubendorfer et al., (2012)
S2866	*sfgfp-cheY*, sfGFP-His6-3xGly-Gly-Ser-Sputcn32_2558; markerless chromosomal fusion of *sfgfp* to *cheY* (N-terminal)	This study
S2875	*sfgfp-cheY $fliM_1$-mcherry*, *sfGFP*-His6-3xGly-Gly-Ser-Sputcn32_2558 Sputcn32_2569-6xGly-mcherry-His6; markerless chromosomal fusion of *sfgfp* to *cheY* (N-terminal) and *$fliM_1$* to *mcherry* (C-terminal)	This study
S3132	*ΔflhF,* ΔSputcn32_2561, markerless deletion of *flhF*	This study
S3133	*ΔflhG*, ΔSputcn32_2560; markerless deletion of *flhG*	Schuhmacher et al., (2015)
S3145	*ΔhubP*, ΔSputcn32_2442, markerless deletion of *hubP*	This study
S3163	*$fliM_1$-mcherry mcp0796-sfgfp*, Sputcn32_2569-6xGly-mCherry Sputcn32_0794-3xGly-Gly-Ser-sfGFP, markerless chromosomal fusion of *mcherry* to *$fliM_1$* (N-terminal) and insertion of pJP5603_Sputcn32_0796-sfGFP chromosomal locus of Sputcn32_0796	This study

S3165	*fliM$_1$-mcherry ΔhubP*, Sputcn32_2569-6xGly-mCherry ΔSputcn32_2442; markerless chromosomal fusion of *mcherry* to *fliM$_1$* (N-terminal) and markerless deletion of *hubP*	This study
S3213	*Δflhf fliM$_1$-sfgfp*, ΔSputcn32_2561 Sputcn32_2569-6xGly-sfGFP-His6, markerless deletion of *flhF* and chromosomal fusion of *fliM$_1$* to *sfgfp* (C-terminal)	This study
S3299	*flaA2-Cys*, Sputcn32_3455_T156CT169C Sputcn32_3456_T159CT160C; markerless exchange of Thr156Cys and Thr159Cys in Sputcn32_3455 and Thr159Cys and Thr160Cys in Sputcn32_3456	This study
S3300	*flaAB1 Cys*, Sputcn32_2585-T159C Sputcn32_2586-T159C, markerless substitution of Threonine 159 with Cysteine in *flaA$_1$* and Threonine 159 with Cysteine in *flaB$_1$*	This study
S3344	*Δflhf fliM2-sfgfps*, ΔSputcn32_2561 Sputcn32_3479-6xGly-sfGFP-His6, markerless deletion of *flhF* and chromosomal fusion of fliM2 to sfgfp (C-terminal)	This study
S3419	*FlgE$_2$-T242C*, Sputcn32_3465_T242C; markerless exchange of Thr242Cys in Sputcn32_3465	Schuhmacher et al., (2015)
S3469	*ΔflhF FlgE$_2$-T242C*, ΔSputcn32_2560 Sputcn32_3465_T242C; markerless deletion of *flhF* and exchange of Thr242Cys in Sputcn32_3465	This study
S3475	*flhF KI*; markerless insertion of *flhF* into *ΔflhF*; complements mutation	This study
S3481	*flhG KI*; markerless insertion of *flhG* into *ΔflhG*; complements mutation	Schuhmacher et al., (2015)
S3555	*mcherry-parB flaAB1 Cys*, mCherry-2xGly-Gly-Ser-Sputcn32_3964 Sputcn32_2586_T159C Sputcn32_2585_S159C, markerless chromosomal fusion of *mcherry* to *parB* (N-terminal) and substitution of Threonine 159 with Cysteine in *flaA$_1$* and Threonine 159 with Cysteine in *flaB$_1$*	This study
S3568	*ΔhubP mcherry-parB flaAB$_1$ Cys*, ΔSputcn32_2442 mCherry-2xGly-Gly-Ser-Sputcn32_3964 Sputcn32_2586_T159C Sputcn32_2585_T159C, markerless deletion of Sputcn32_2442 and chromosomal fusion of mcherry to *parB* (N-terminal) combined with the exchange of Thr159Cys in Sputcn32_2586 and Sputcn32_2585	This study
S3636	*hubP-sfgfp*, Sputcn32_2442-3xGly-Gly-Ser-sfGFP; markerless chromosomal fusion of *hubP* to *sfgfp* (C-terminal)	This study
S3637	*fliM$_1$-mcherry hubP-sfgfp*, Sputcn32_2569-6xGly-mCherry Sputcn32_2442-3xGly-Gly-Ser-sfGFP; markerless chromosomal fusion of *fliM$_1$* to *mcherry* and *hubP* to *sfgfp* (C-terminal)	This study
S3685	*hubP-sfgfp mcherry-parB*, Sputcn32_2442-3xGly-Gly-Ser-sfGFP mCherry-2xGly-Gly-Ser-Sputcn32_3964, markerless chromosomal fusion of *mcherry* to *parB* (N-terminal) and of *hubP* to *sfgfp* (C-terminal)	This study
S3710	*mcherry-parB*, mCherry-2xGly-Gly-Ser-Sputcn32_3964, markerless chromosomal fusion of *mcherry* to *parB* (N-terminal)	This study
S3715	*ΔflhF mcp0796-sfgfp*, ΔSputcn32_2561 Sputcn32 _0794-3xGly-Gly-Ser-sfGFP, markerless deletion of *flhF* and insertion of pJP5603_Sputcn32_0796-sfGFP chromosomal locus of Sputcn32_0796	This study
S3716	*ΔhubP mcp0796-sfgfp*, ΔSputcn32_2442 Sputcn32_0794-3xGly-Gly-Ser-sfGFP, markerless deletion of *hubP* and insertion of pJP5603_Sputcn32_0796-sfGFP chromosomal locus of Sputcn32_0796	This study
S3721	*ΔflhF mcherry-parB*, ΔSputcn32_2561 mCherry-2xGly-Gly-Ser-Sputcn32_3964, markerless deletion of *flhF* and chromosomal fusion of *mcherry* to *parB* (N-terminal)	This study

S3722	*Δcluster I hubP-sfgfp*, ΔSputcn32_2549–ΔSputcn32_2605 Sputcn32_2442-3xGly-Gly-Ser-sfGFP, markerless deletion of polar flagellar cluster and chromosomal fusion of *hubP* to *sfgfp*	This study
S3724	*ΔhubP sfgfp-cheY*, ΔSputcn32_2442 sfGFP-His6-3xGly-Gly-Ser-Sputcn32_2558; markerless deletion of *hubP* and chromosomal fusion of *sfgfp* to *cheY* (N-terminal)	This study
S3725	*ΔflhF sfgfp-cheY*, ΔSputcn32_2561 sfGFP-His6-3xGly-Gly-Ser-Sputcn32_2558; markerless deletion of *flhF* and chromosomal fusion of *sfgfp* to *cheY* (N-terminal)	This study
S3733	*ΔflhG mcp0796-sfgfp*, ΔSputcn32_2560 Sputcn32_0794-3xGly-Gly-Ser-sfGFP, markerless deletion of *flhG* and insertion of pJP5603_Sputcn32_0796-sfGFP chromosomal locus of Sputcn32_0796	This study
S3747	*ΔflhF venus-cheZ*, ΔSputcn32_2561 VENUS-6xGly-Sputcn32_2557, markerless deletion of *flhF* and chromosomal fusion of *venus* to *cheZ* (C-terminal)	This study
S3748	*ΔhubP venus-cheZ*, ΔSputcn32_2442 VENUS-6xGly-Sputcn32_2557, markerless deletion of *hubP* and chromosomal fusion of *venus* to *cheZ* (C-terminal)	This study
S3749	*ΔflhF cheA-mcherry*, ΔSputcn32_2561 Sputcn32_2556-2xGly-Gly-Ser-mCherry, markerless deletion of *flhF* and chromosomal fusion of *mcherry* to *cheA* (C-terminal)	This study
S3750	*cheA-mcherry fliM$_1$-sfgfp*, Sputcn32_2556-2xGly-Gly-Ser-mCherry Sputcn32_2569-6xGly-sfGFP, markerless chromosomal fusion of *mcherry* to *cheA* and *sfgfp* to *fliM$_1$* (N-terminal)	This study
S3751	*ΔhubP cheA-mcherry*, ΔSputcn32_2442 Sputcn32_2556-2xGly-Gly-Ser-mCherry, markerless deletion of *hubP* and chromosomal fusion of *mcherry* to *cheA* (C-terminal)	This study
S3752	*venus-cheZ fliM$_1$-mcherry*, VENUS-6xGly-Sputcn32_2557 Sputcn32_2569-6xGly-mCherry, markerless chromosomal fusion of *venus* to *cheZ* (C-terminal) and *mcherry* to *fliM$_1$* (N-terminal)	This study
S3753	*hubP KI*; markerless insertion of *hubP* into *ΔhubP*; complements mutation	This study
S3754	*ΔflhF flaAB$_1$ Cys*, ΔSputcn32_2561 Sputcn32_2585-T159C Sputcn32_2586-S159C, markerless deletion of *flhF* and substitution of Threonine 159 with Cysteine in *flaA$_1$* and Threonine 159 with Cysteine in *flaB$_1$*	This study
S3755	*ΔhubP flaAB$_1$ Cys*, ΔSputcn32_2442 Sputcn32_2585-T159C Sputcn32_2586-S159C, markerless deletion of *hubP* and substitution of Threonine 159 with Cysteine in *flaA$_1$* and Threonine 159 with Cysteine in *flaB$_1$*	This study
S3761	*ΔhubP* pBTOK hubP-sfgfp, ΔSputcn32_2442 pBTOK- Sputcn32_2442-3xGly-Gly-Ser-sfGFP; markerless deletion of *hubP* and stable integration of overproduction vector pBTOK producing SpHubP tagged with sfGFP (N-terminal)	This study
S3762	Δ*hubP* pBTOK *lysM-mcherry*, ΔSputcn32_2442 pBTOK-mCherry-2xPro- Sputcn32_2442-AA1-134; markerless deletion of *hubP* and stable integration of overproduction vector pBTOK producing the first 134 amino acids of SpHubP tagged with mCherry (N-terminal)	This study
S3771	*flhF-mcherry*, Sputcn32_2561-3xGly-Gly-Ser-mCherry, markerless chromosomal fusion of *mcherry* to *flhF* (C-terminal)	This study
S3772	Δ*hubP flhF-mcherry*, ΔSputcn32_2442 Sputcn32_2561-3xGly-Gly-Ser-mCherry, markerless deletion of *hubP* and chromosomal fusion of *mcherry* to *flhF* (C-terminal)	This study
S3778	*hubP-mcherry*, Sputcn32_2442-3xGly-Gly-Ser-mCherry; markerless chromosomal fusion of *hubP* to *mcherry* (C-terminal)	This study

S3779	*hubP-mcherry zapA-sfgfp*, Sputcn32_2442-3xGly-Gly-Ser-mCherry Sputcn32_3215-2xGly-Gly-Ser-sfGFP; markerless chromosomal fusion of *hubP* to *mcherry* (C-terminal) and of *zapA* to *sfgfp* (C-terminal)	This study
S3783	pBTOK, stable integration of overproduction vector pBTOK as empty vector control	This study
S3859	pBTOK *flhF*, pBTOK-Sputcn32_2561; stable integration of overproduction vector pBTOK producing the full length protein SpFlhF	This study
S4028	*flhG-sfgfp*, Sputcn32_2560-1xGly-Ser-sfGFP, markerless chromosomal fusion of sfgfp to *flhG* (C-terminal)	This study
S4029	Δ*hubP flhG-sfgfp*, ΔSputcn32_2442 Sputcn32_2560-1xGly-Ser-sfGFP, markerless chromosomal fusion of sfgfp to *flhG* (C-terminal)	This study
S4033	*flaAB$_1$ Cys* pBTOK *flhF-mcherry*, Sputcn32_2586_T159C Sputcn32_2585_T159C pBTOK-Sputcn32_2561-1xGly-Ser-mCherry; markerless exchange of Thr159Cys in Sputcn32_2586 and Sputcn32_2585 and stable integration of overproduction vector pBTOK producing SpFlhF tagged with mCherry (C-terminal)	This study
S4034	*fliM$_1$ -sfgfp* pBTOK *flhF*, Sputcn32_2569-6xGly-sfGFP-His6 pBTOK-Sputcn32_2561; markerless chromosomal fusion of *fliM$_1$* to *sfgfp* (C-terminal) combined with stable integration of overproduction vector pBTOK producing the full length protein SpFlhF	This study
S4035	*flaAB$_1$ Cys* pBTOK, Sputcn32_2586_T159C Sputcn32_2585_T159C pBTOK; markerless exchange of Thr159Cys in Sputcn32_2586 and Sputcn32_2585 and stable integration of overproduction vector pBTOK as empty vector control	This study
S4036	*ΔflhF flaA$_2$-Cys flaB$_2$-Cys*, ΔSputcn32_2560 Sputcn32_3455_T156CT159C Sputcn32_3456_T159CT160C; markerless deletion of *flhF* and exchange of Thr156Cys and Thr159Cys in Sputcn32_3455 and Thr159Cys and Thr160Cys in Sputcn32_3456	This study
S4037	*fliM$_1$* -sfgfp pBTOK, Sputcn32_2569-6xGly-sfGFP-His6 pBTOK; markerless chromosomal fusion of *fliM$_1$* to sfgfp (C-terminal) combined with stable integration of overproduction vector pBTOK as empty vector control	This study
S4040	*flhG* ΔN20, Sputcn32_2560 ΔN20; markerless deletion of the first 20 amino acid residues (1-20) in *flhG*	This study
S4041	*flhG* ΔN20 *flaAB$_1$ Cys*, Sputcn32_2560 ΔN20 Sputcn32_2586_T159C Sputcn32_2585_T159C, markerless deletion of the first 20 amino acid residues (1-20) in *flhG* combined with the exchange of Thr159Cys in Sputcn32_2586 and Sputcn32_2585	This study

Table S2: Plasmids that were used in this study

Plasmid	Relevant genotype or phenotype	Source or reference
pNPTS138-R6KT	*mob*RP4$^+$ *ori*-R6K *sacB*, suicide plasmid for in frame deletions, Km^r	Lassak *et al*., 2010
pBTOK	pBBR1-MCS2 backbone (pBBR origin, Km^r); TetR, Promoter and multiple cloning site of pASK-IBA3plus and *E.coli* rrnB1 T1 and lambda phage T0 terminator	this study
pET24d(+)	T7 promoter, his-tag fusion site, T7 terminator, *lacI*, pBR322 ori, f1 ori, Km^r	Novagen
pGAT3	Bla, lacI, T7-lacO promoter, SP6 promoter, T7 terminator, Ap^r	Peränen et al., 1996
In-frame deletion vectors (in pNPTS138-R6KT)		
pNPTS138-R6KT-HubP-KO	*hubP* (Sputcn32_2442), in-frame deletion fragment	this study
pNPTS138-R6KT-FlhF-KO	*flhF* (Sputcn32_2561), in-frame deletion fragment	this study
pNPTS138-R6KT-FlhG ΔN20	*flhG* ΔN20 (deletion of first 20 amino acids in Sputcn32_2560), in-frame deletion fragment	this study
In-frame complementation vectors (in pNPTS138-R6KT)		
pNPTS138-R6KT-HubP-KI	*hubP* (Sputcn32_2442), in-frame insertion fragment for complementation of Δ*hubP*	this study
pNPTS138-R6KT-FlhF-KI	*flhF* (Sputcn32_2561), in-frame insertion fragment for complementation of Δ*flhF*	this study
Fluorescent fusion vectors (in pNPTS138-R6KT)		
pNPTS138-R6KT-FlaAB$_2$-Cys	*flaAB$_2$*-Cys (Sputcn32_3455_T156CT159C, Sputcn32_3456_T159CT160C), in-frame substitution fragment	
pNPTS138-R6KT-FliM$_1$-GL-sfGFP-His6	*fliM$_1$*-6xGly-sfGFP-His6 in pNPTS138-R6KT in-frame insertion fragment	Bubendorfer *et al*., 2012
pNPTS138-R6KT-FliM$_1$-GL-mCherrySO-His6	*fliM$_1$*-6xGly-mCherrySO-His6 in pNPTS138-R6KT in-frame insertion fragment	Bubendorfer *et al*., 2012
pNPTS138-R6KT-mCherry-ParB	mCherry-2xGly-Gly-Ser-*parB* (Sputcn32_3964), in-frame insertion fragment	this study
pNPTS138-R6KT-FlaAB$_1$-Cys	*flaAB$_1$*-Cys (Sputcn32_2586_T159C, Sputcn32_2585_T159C), in-frame substitution fragment	this study
pNPTS138-R6KT-sfGfp-3GGS-CheY	sfGFP-His6-3xGly-Gly-Ser-*cheY* (Sputcn32_2558), in-frame insertion fragment	this study
pNPTS138-R6KT-VENUS-GL-CheZ	VENUS-6xGly-*cheZ* (Sputcn32_2557), in-frame insertion fragment	this study
pNPTS138-R6KT-CheA-mCherry	*cheA*-2xGly-Gly-Ser-mCherry (Sputcn32_2556), in-frame deletion fragment	this study
pNPTS138-R6KT-HubP-sfGFP	*hubP*-3xGly-Gly-Ser-sfGFP (Sputcn32_2442), in-frame insertion fragment	this study
pNPTS138-R6KT-HubP-mCherry	*hubP*-3xGly-Gly-Ser-mCherry (Sputcn32_2442), in-frame insertion fragment	this study
pNPTS138-R6KT-FlhF-mCherry	*flhF*-3xGly-Gly-Ser-mCherry (Sputcn32_2561), in-frame insertion fragment	this study
pNPTS138-R6KT-ZapA-sfGFP	*zapA*-2xGly-Gly-Ser-sfGFP (Sputcn32_3215), in-frame insertion fragment	this study
pJP5603_Sputcn32_0796-sfGFP	*MCP_0796*-sfGFP (Sputcn32_0796), for single homologous insertion	this study
pNPTS138-R6KT-FlhG-sfGFP	*flhG*-1xGly-Ser-sfGFP (Sputcn32_2560), in-frame insertion fragment	This study

Overproduction vectors		
pBTOK-HubP-sfGFP	*hubP*-3xGly-Gly-Ser-*sfGFP* (Sputcn32_2442) in pBTOK	this study
pBTOK-LysM-mCherry	*hubP*_AA1-134-2xPro-*mCherry* (Sputcn32_2442_nt1-402) in pBTOK	this study
pBTOK-FlhF-mCherry	*flhF*-1xGly-Ser-*mCherry* (Sputcn32_2561) in pBTOK	This study
pFlhF	*flhF* (Δ-10) in pET24d	this study
pFlhG	*flhG* in pET24d	this study
pN-FlhG	N-terminus of *flhG* (aa 1-20) in pGAT3	this study

References Table S1 and Table S2

Bubendorfer, S., Held, S., Windel, N., Paulick, A., Klingl, A., and Thormann, K.M. (2012) Specificity of motor components in the dual flagellar system of *Shewanella putrefaciens* CN-32. *Mol Microbiol* 83: 335-350.

Fredrickson, J.K., Zachara, J.M., Kennedy, D.V., Dong, H., Onstott, T.C., Hinman, N.W., and Li, S. (1998) Biogenic iron mineralization accompanying the dissimilatory reduction of hydrous ferric oxide by a groundwater bacterium. *Geochim Cosmochim Acta* **62**: 3239-3257.

Lassak, J., Henche, A.L., Binnenkade, L., and Thormann, K.M. (2010) ArcS, the cognate sensor kinase in an atypical Arc system of *Shewanella oneidensis* MR-1. *Appl Environ Microbiol* **76**: 3263-3274.

Miller, V.L., and Mekalanos, J.J. (1988) A novel suicide vector and its use in construction of insertion mutations: osmoregulation of outer membrane proteins and virulence determinants in *Vibrio cholerae* requires *toxR*. *J Bacteriol* **170**: 2575-2583.

Peränen, J., Rikkonen, M., Hyvonen, M., and Kaariainen, L. (1996) T7 vectors with modified T7*lac* promoter for expression of proteins in *Escherichia coli*. *Anal Biochem* **236**: 371-373.

Schuhmacher, J.S., Rossmann, F., Dempwolff, F., Knauer, C., Altegoer, F., Steinchen, W.*, et al.* (2015) MinD-like ATPase FlhG effects location and number of bacterial flagella during C-ring assembly. *Proc Natl Acad Sci U S A* **112**: 3092-3097.

Table S3: Oligonucleotides that were used in this study

Identifier of oligonucleotides	Sequence 5'-3'	Purpose
AD39 ZapA-Cterm-fw	GCGAATTCGTGGATCCAGATGTAACGAAGGAGGGGTAGC	fusion of sfGFP to ZapA
AD40 ZapA-Cterm-3xGGS-OL-RV	GCTGCCGCCGCTGCCGCCGCTGCCGCCTTTAGTTGAACGCTCAACT AAG	
AD41 3xGGS-sfGFP-OL-FW	GGCGGCAGCGGCGGCAGCGGCGGCAGCATGAGCAAAGGAGAAG AACTTTTCAC	
AD42 sfGFP-Strep-OL-RV	TTATTTTTCGAACTGCGGGTGGCTCCAGGATCCTTTGTAGAGCTCA TCC	
AD43 ZapA-DS-Strep-OL-FW	TGGAGCCACCCGCAGTTCGAAAAATAAATTTAAACTGTGCAACTT GGTTATTTAG	
AD44 ZapA-DS-RV	CCAAGCTTCTCTGCAGGATTTCGCCATCGTGAGTTAAATAC	
B232 EcoRI-pJP-cn32_0796-gfp-fwd	A GAA TTC ACG ATA ATG CGC AGA GTG GTC	fusion of MCP_0796 to sfGFP
B233 BamHI-pJP-cn32_0796-gfp-rev	C GGA TCC GAT TTT AAA ATT GCT TAC TGC GCG	
B286 EcoRI-up-cheY1-fwd	A GAA TTC CGA GGT GAT TGG GTT CCA CG	fusion of sfGFP to CheY
B289 OL-GL-VENUS-rev	GCC GCC GCC GCC GCC CTT GTA CAG CTC GTC CAT GC	fusion of VENUS to CheZ
B300 EcoRI-up-cheZ1-fwd	A GAA TTC CGA ATC GCG AGT TAG CCA GAT	
B301 OL-up-cheZ1-rev	CTT GCT CAC CAT AGC TCA TCC CTG CCT AAG CG	
B302 OL-CheZ1-up-VENUS-fwd	CAG GGA TGA GCT ATG GTG AGC AAG GGC GAG G	
B303 OL-GL-cheZ1-Nterm-fwd	GGC GGC GGC GGC GGC ATG AAG TCA CAT ACA TCA GGG CT	
B304 PspOMI-cheZ1-Nterm-rev	CTC GGG CCC TGA GAT CTT GAA AAT CCT GCG C	
B361 3x-GGS-OL-CheY-fwd	GGC GGC AGC GGC GGC AGC GGC GGC AGC TTG GAC AAG AAT ATG AAG ATT CTC ATT	fusion of sfGFP to CheY
B413 OL-up-cheY1-sfGfp-rev	TCC TTT GCT CAT GGT TTC CTC CGG TGA GCT GA	
B415 OL-CheY1-up-sfGfp-fwd	CCG GAG GAA ACC ATG AGC AAA GGA GAA GAA CTT TTC AC	
B417 3x-GGS-OL-sfGFP-rev	GCT GCC GCC GCT GCC GCC GCT GCC GCC GTG GTG GTG GTG GTG GTG	
B31 BamHI-flagL-fwd	A GGA TCC TGA CAC TGT ATT TAT GGC GCA GG	substitution of T156C and T159C in $FlaA_2$ and T159C T160C in $FlaB_2$
B34 PspOMI-flagL-rev	T GTC GGG CCC GTC GCC GTC GCA TTT TCG C	
B480 flaA2-Cys-rev	TCA TCG ATA GCT GTA CAG CAA ACG GCC AAT G	
B481 flaA2-Cys-fwd	ATT GGC CGT TTG CTG TAC AGC TAT CGA TGA CG	
B482 flaB2-Cys-rev	TCA CAT CCA GAC ATT CTG CGC ATC CAG CTC CA	
B483 flaB2-Cys-fwd	GAG CTG GAT GCG CAG AAT GTC TGG ATG TGA AG	
B45 EcoRI-flagP-fwd	A GAA TTC GAA GTT AAA GTG TCT GGG AAA CCC	substitution of T159C in $FlaA_1$ and T159C in $FlaB_1$
B48 PspOMI-flagP-rev	T CTA GGG CCC TAA GCC TCT GTT TTC ATC AAA AGC C	
B476 flaA1-T159CS161C-rev	TAC CAA CGC AAA TAC AGA TAT CTT CAC C	
B477 flaA1-T159CS161C-fwd	TGA AGA TAT CTG TAT TTG CGT TGG TAC C	
B478 flaB1-T159CS161C-rev	TTT TTG ACA CAC AAA TGC AAA TAT CTT CAC C	
B479 flaB1-T159CS161C-fwd	TGA AGA TAT TTG CAT TTG TGT GTC AAA AAC C	
FR48 NheI_Sputcn32_2442_KO_fw	GTA GCT AGC AGT GAA TGC GAC AGC TGT ACG	in-frame deletion of HubP
FR49 OL_Sputcn32_2442_rv	A ACT AAT CTC CAT CAA TCC TTC CCT TTG AAG C	
FR50 OL_Sputcn32_2442_fw	A GGA TTG ATG GAG ATT AGT TAA TCT CGA TTA ACC GA	
FR51 PspOMI_Sputcn32_2442_KO_rv	TCC GGG CCC ATT ACC GTG ATA ATG GCT TAC ACC	
FR99 PspOMI_flhG_rv	TCC GGG CCC GAG CAA TTA GCG ACC TAT GGC	fusion of sfGFP to HubP
FR158 OL_3xGGS_sfGFP_rv	GGC GGC AGC GGC GGC AGC GGC GGC AGC ATG AGC AAA GGA GAA GAA CTT TTC AC	
FR100 NheI_flhF_fw	GTA GCT AGC GTA GGC TCG TCA CAT ACA ACG	
FR101 OL_flhF_KO_rv	GAT TAA ACG ATG TGC ATT TGA GTA GAG TTA TGA CC	in-frame deletion of FlhF
FR102 OL_flhF_KO_fw	CAA ATG CAC ATC GTT TAA TCT TCA CTT ATG CGT CC	

FR103 PspOMI_flhF_rv	TCC GGG CCC TTC CTG ATG TGA TGC CAC TGG	
FR156 OL_strep_flhF_rv	TGG AGC CAC CCG CAG TTC GAA AAA TAG AGT TAT GAC CCT GGA TCA AG	fusion of FlhF to mCherry
FR159 OL_flhF_3xGGS_fw	GCT GCC GCC GCT GCC GCC GCT GCC GCC CTC AAA TGC ACA GGC CAT ATT ATC	
FR262 EcoRI_HubP-Cterm_fw	GTA GAA TTC GAT GAT GAT CTC GAT TTA AGC ACA G	fusion of sfGFP to HubP
FR263 OL_hubP_3xGGS_rv	GCT GCC GCC GCT GCC GCC GCT GCC GCC ACT AAT CTC TTT TAG TAA ACG TCC GG	
FR264 OL_sfGFP_HubP-down_rv	TAG ATT GAA ACT CGG TTA ATC GAG ATT AGG ATC CTT TGT AGA GCT CAT CCA T	fusion of sfGFP to HubP
FR265 OL_HubP-down_fw	TAA TCT CGA TTA ACC GAG TTT CAA TCT A	
FR266 PstI_HubP-Cterm_rv	GTA CTG CAG GCC GCT TGG TGC ATT TTG TCG	
FR279 OL_mCherry_fw	ATG GTT TCC AAA GGG GAA GAG G	overexpression of FlhF-mCherry
FR330 XbaI_FlhF_OE_fw	CGC TCT AGA AGG AGG GCA AAT ATG AAG ATT AAA CGA TTT TTT GCC AAA GAC ATG	
FR332 EcoRV_HubP_komplement_fw	CAA GCT TCT CTG CAG GAT AGT GAA TGC GAC AGC TGT ACG	reconstitution of HubP
FR333 EcoRV_HubP_komplement_rv	GAA TTC GTG GAT CCA GAT ATT ACC GTG ATA ATG GCT TAC ACC	
FR385 OL_FlhF_GS_mCherry_rv	CCT CTT CCC CTT TGG AAA CCA TGC TGC CCT CAA ATG CAC AGG CCA TAT T	overexpression of FlhF-mCherry
FR386 PspOMI_mCherry_rv	TCC GGG CCC TTA TTT GTA TAA CTC ATC CAT ACC ACC A	
FR392 OL_FlhG_-m_gfp_rv	GAA AAG TTC TTC TCC TTT GCT GCT GCC TTC ACT CGT TTT TTC TTC TTG AAA ATC	fusion of FlhG to sfGFP
FR393 OL_-m_gfp_fw	AGC AAA GGA GAA GAA CTT TTC	
FR398 EcoRV_FlhG_fw	CAA GCT TCT CTG CAG GAT ATC CGT GCT TTC AGT GAG ATG C	
FR399 OL_gfp_RBS-fliA_rv	GCT TTA TTC ACT CGT TTT TTC CTC TTT TAG GAT CCT TTG TAG AGC TCA TCC	
FR400 OL_RBS-fliA_fw	AAG AGG AAA AAA CGA GTG AAT AAA GC	
FR401 EcoRV_FlhG_rv	GAA TTC GTG GAT CCA GAT TCT CAG CGA GAG CTT CAA ACG A	
FR402 EcoRV_FlhG_N20_fw	CAA GCT TCT CTG CAG GAT TGA GCA ATT AGC GAC CTA TGG C	deletion of the first 20 amino acids in FlhG
FR403 OL_FlhG_N20_rv	TTA CTT TCA CCA TAA CTC TAC TCA AAT GCA CAG G	
FR404 OL_FlhG_N20_fw	TAG AGT TAT GGT GAA AGT AAT CGC TGT CAC AGG	
FR405 EcoRV_FlhG_N20_rv	GAA TTC GTG GAT CCA GAT CGT AAA CTA CGC ACC ATA TTG GC	
SH501 pBTOK pBBR fw	TTG CGG TAC CAG CTC CAA TTC GCC CTA TAG TG	assembly of pBTOK
SH502 pBTOK pBBR rev	cATT AAT TCC TTC AGA AGA ACT CGT CAA GAA GGC G	
SH503 pBTOK pASK fw	GTT CTT CTG AAG GAA TTA ATG ATG TCT CGT TTA GAT A	
SH504 pBTOK pASK rev	TAA TGG GCC CAA GCT TAT TAT TTT TCG AAC TGC GG	
SH505 pBTOK pBBMt fw	TAA TAA GCT TGG GCC CAT TAG CTG AGC TTG	
SH506 pBTOK pBBMt rev	AAT TGG AGC TGG TAC CGC AAG CTC CTA GC	
SH534 CheA mC up fw	GCG AAT TCG TGG ATC CAG ATT GCC AGC CAA GAA GGT GAC C	fusion of CheA to mCherry
SH535 CheA mC up rev	CCA CCA GAG CCA CCA GTG CCA CTT TTA TTC TTT GCA TAA TGC TTT AAT AG	
SH536 CheA mC fw	AAG TGG CAC TGG TGG CTC TGG TGG CAG CAT GGT TTC CAA AGG GGA AGA GG	
SH537 CheA mC rev	CTT AGC TTG GAA ACT ATT TGT ATA ACT CAT CCA TAC CAC C	
SH538 CheA mC dwn fw	CAA ATA GTT TCC AAG CTA AGG AAT GGA ATG G	
SH539 CheA mC dwn rev	GCC AAG CTT CTC TGC AGG ATT ACA TAA CCC ATT TAG ACG ATT CGC	
SH558 HubP LysM OE fw	GGT CTA GAA GGA GGA CTG ACA TGA AAT TTC GCA CTT CGT ATC TTG	overproduction of LysM domain of HubP tagged with mCherry
SH559 HubP LysM OE OL rev	CCA TAG GAG GTA ACT TAT CAT CAC GTT CAG CAC G	
SH560 HubP LysM mC OE OL fw	GAT GAT AAG TTA CCT CCT ATG GTT TCC AAA GGG GAA GAG G	

SH561 HubP LysM mC OE rev	gcg GGG CCC TTA TTT GTA TAA CTC ATC CAT ACC ACC	
SH562 HubP sfGFP OE rev	gcg GGG CCC TTA GGA TCC TTT GTA GAG CTC ATC C	overproduction of HubP tagged with sfGFP
SH566 FlhF tag up fw	AAT ACG ACT CAC TAG TGG GGC CCG AGC AAT TAG CGA CCT ATG GC	fusion of FlhF to mCherry
SH572 FlhF tag GGS mC rev	CGA ACT GCG GGT GGC TCC ATT TGT ATA ACT CAT CCA TAC CAC CAG	
SH573 FlhF tag 3xGGS mC rev	GGC GGC AGC GGC GGC AGC GGC GGC AGC ATG GTT TCC AAA GGG GAA GAG G	
SpFlhF-BamHI-R	TTAAGGATCCTTACTCAAATGCACAG	overproduction FlhF
SpFlhFdN10-PciI-R	TTAAACATGTTGCACCATCACCATCACCATATGCGTGCCGCTCTGG CC	
SpFlhF-R285A-F	GATCATTATGCCATTGGCGCC	overproduction FlhF R285A
SpFlhF-R285A-R	GGCGCCAATGGCATAATGATC	
SpFlhG N20-XhoI-R	TTAACTCGAGTTACACTTTTTCGTTATA	overproduction FlhG N20
SpFlhG-NcoI-6H-F	TTAACCATGGGCCACCATCACCATCACCATACCCTGGATCAAGCAA G	overproduction FlhG
SpFlhG-XhoI-R	TTAACTCGAGTTATTCACTCGTTTTTTCCTCTT	

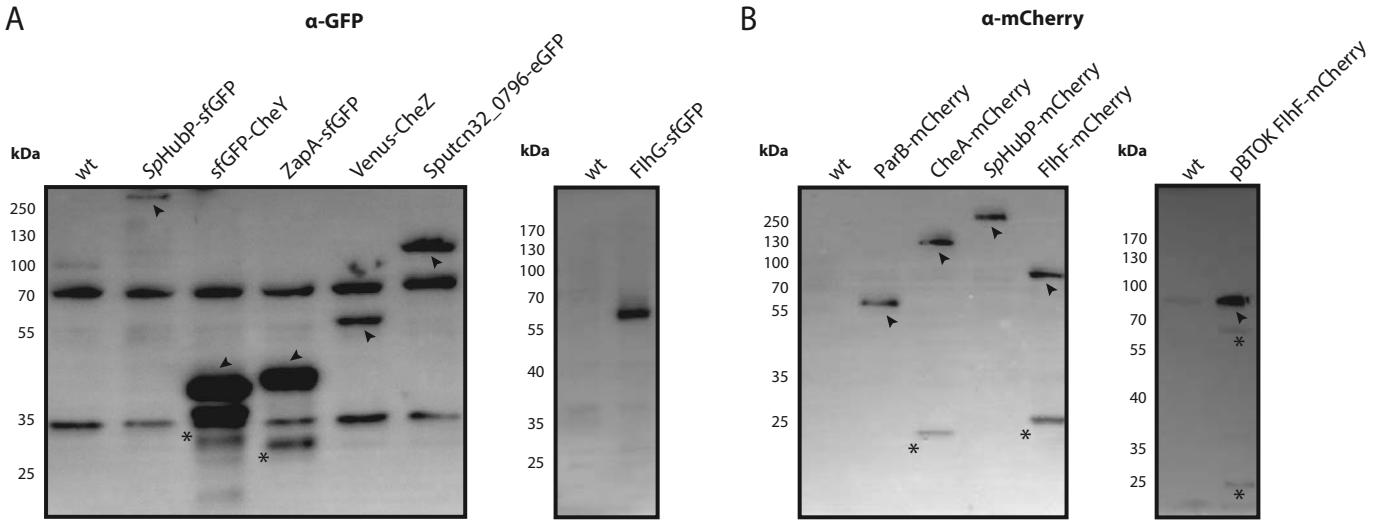

Figure S1: Protein stability assays for fluorescence tagging.
Depicted is the detection of proteins by immunoblotting using an antibody raised against GFP (A) or mCherry (B). The strains producing the corresponding proteins are indicated in each lane. Wild-type protein samples were used as negative control and revealed that the GFP antibody used leads to formation of two distinct signals due to unspecific binding, however, these were not interfering with the positions of the proteins to be detected. All proteins were produced yielding signals at position corresponding to the estimated molecular mass (sfGFP-CheY, 41.1 kDa; ZapA-sfGFP, 38.1 kDa; Venus-CheZ, 54.7 kDa; MCP0796-eGFP, 95.4 kDa; FlhG-sfGFP 59.6 kDa, ParB-mCherry, 59.3 kDa; CheA-mCherry, 105.9 kDa; FlhF-mCherry, 76.7 kDa). *Sp*HubP-sfGFP and –mCherry (145.4 kDa) exhibited mobility smaller than estimated, likely caused by its low overall pI. Arrows mark the positions of the fluorescently tagged proteins, asterisks mark signals likely caused by protein degradation.

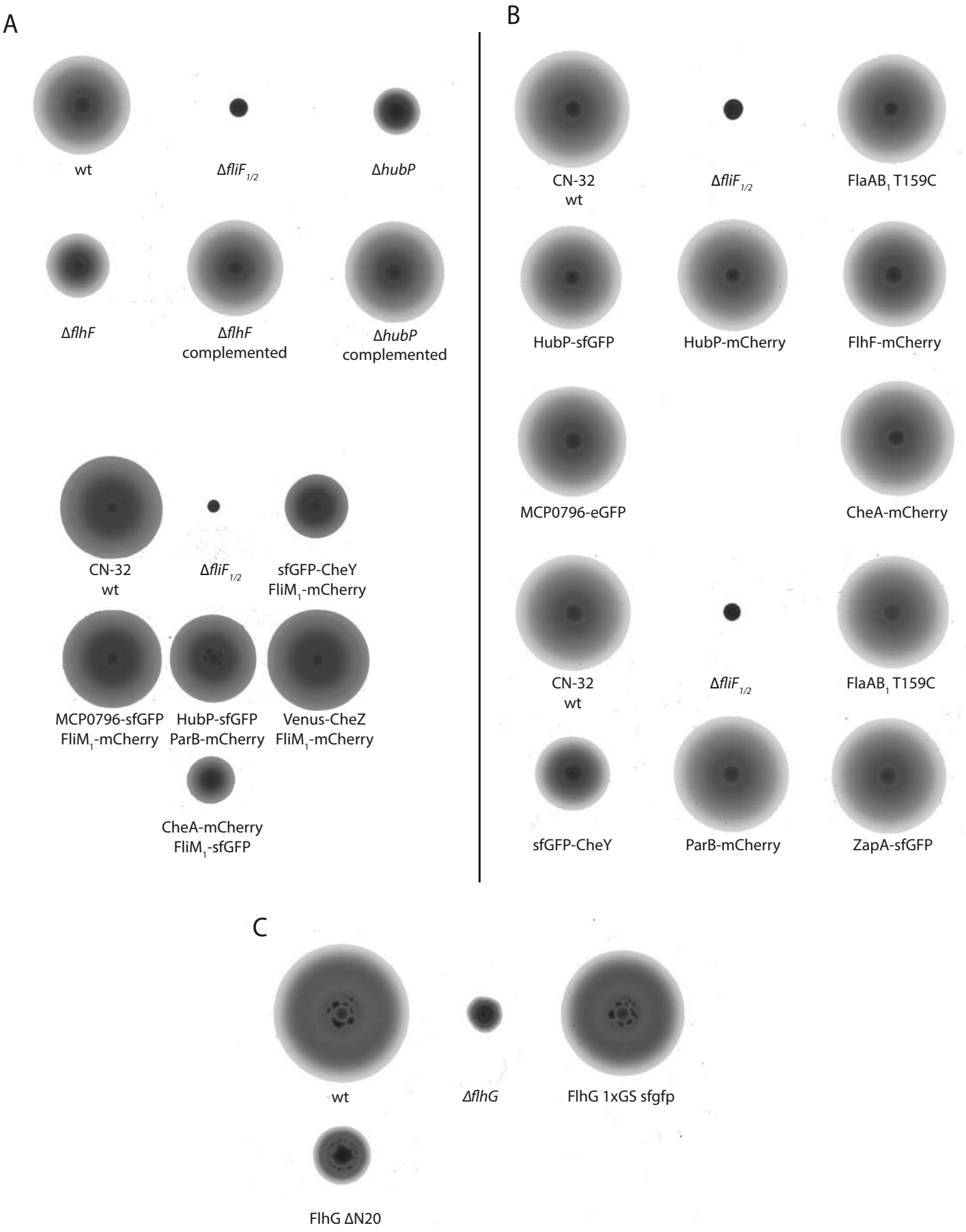

Figure S2: Complementation and motility assays for mutants and fluorescence tagging.
Soft agar assays of wild-type and mutant strains with the corresponding genotype as indicated below. 3 µl of exponentially growing cultures were spotted on 0.25% soft-agar plates and were incubated at 30 °C for 16 h prior documentation of the lateral extension zones. Please note that each experiment (**A**, **B**, **C**) is depicted at an individual scale. Therefore, every experiment has its own wild-type control.

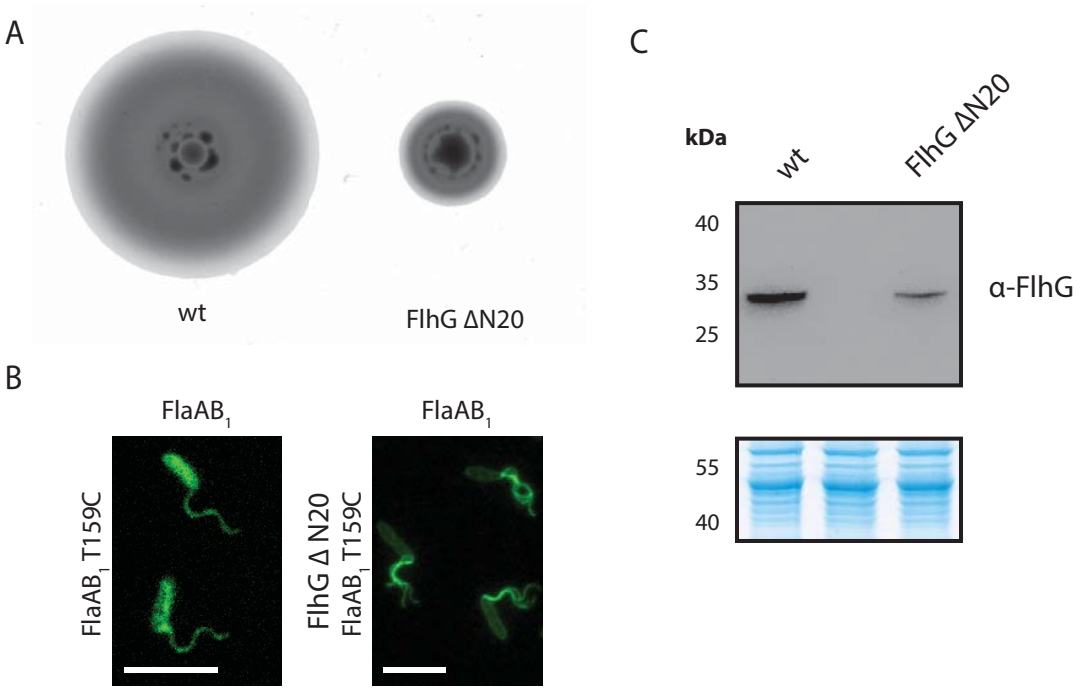

Figure S3: Phenotype of a FlhG variant lacking the N-terminal domain (FlhG ΔN20).
A) Soft-agar assays of wild-type and mutant strain with the corresponding genotype indicated below. 3 µl of exponentially growing cultures were spotted on 0.25% soft-agar plates and were incubated at 30 °C for 16 h prior documentation of the lateral extension zones. **B)** Flagellation phenotype of wild-type and FlhG ΔN20-mutant cells. Shown are micrographs of cells after flagellar staining using maleimide. The scale bar equals 5 µm. **C)** Immunoblot analysis of FlhG ΔN20 production. The corresponding Coomassie-stained gel is depicted below.

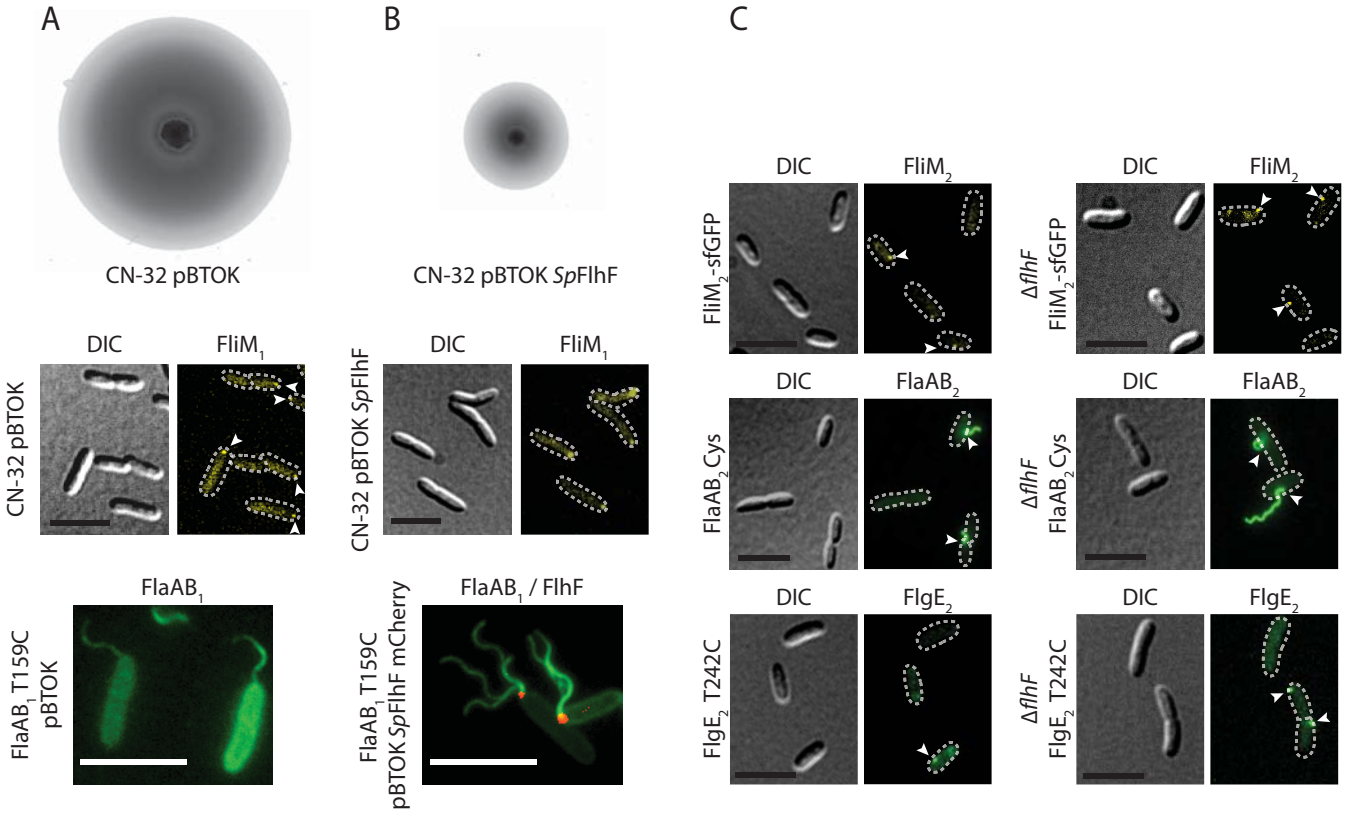

Figure S4: Effect of *flhF* deletion or overexpression on the flagellation of CN-32.
A/B) Effect of *flhF* overexpression on motility (upper panels), localization of $FliM_1$ ($FliM_1$-sfGFP; middle panels), and flagellation state (lower panels). The upper panels display soft-agar swimming assays of the empty-vector control **(A)** and overexpression strain **(B)** with the corresponding genotype indicated below. The middle panels show micrographs of $FliM_1$ localization (using $FliM_1$-sfGFP) in the wild-type control **(A)** and upon FlhF overproduction **(B)**. The lower panel shows the flagellation state in the empty-vector control **(A)** and upon FlhF-mCherry overproduction **(B)** along with localization of FlhF-mCherry. The flagellar filaments were fluorescently labeled by maleimide prior to imaging. **C)** Effect of *flhF* deletion on the production and position of the secondary flagellar system in CN32. Displayes are DIC and corresponding fluorescent micrographs of wild-type and *ΔflhF*-mutant cells bearing a *$fliM_2$-sfgfp* fusion (upper panel), or after maleimide labeling of the secondary flagellar filament (middle panels) or secondary hook structures (lower panels). No significant difference was noticed. In all micrographs, the scale bar equals 5 µm and the arrow mark fluorescent foci or flagellar filaments, respectively.

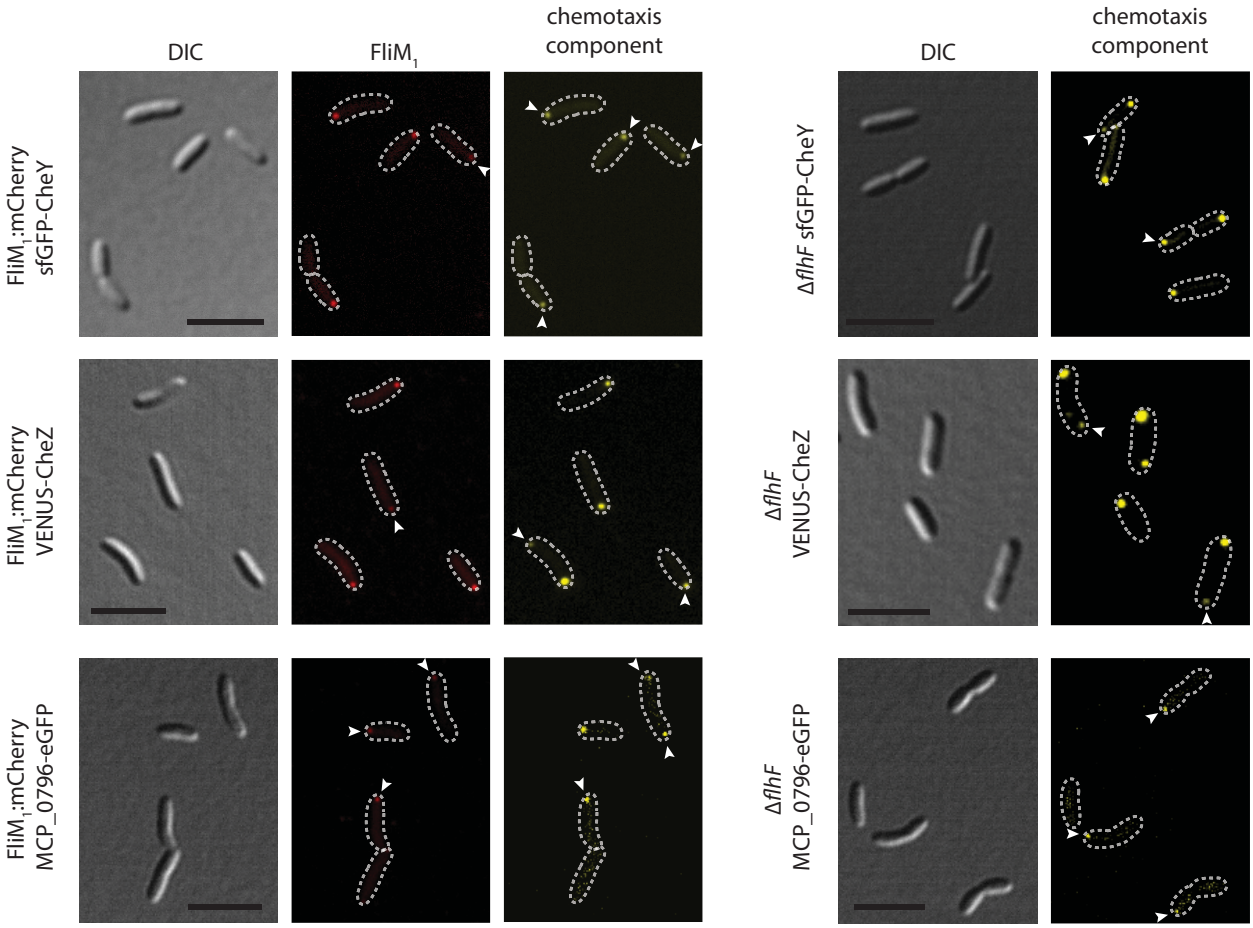

Figure S5: Effects of *flhF deletion* on the positioning of chemotaxis components. Shown are DIC and corresponding fluorescence micrographs of sfGFP-CheY, Venus-CheZ, and MCP_0796-eGFP in relation to the position of $FliM_1$-mCherry in the wild-type (left) and the *ΔflhF* background (right). In the absence of *flhF*, all chemotaxis components tested remained at a polar position. Arrows mark the position of minor fluorescence clusters. The scale bar equals 5 µm.

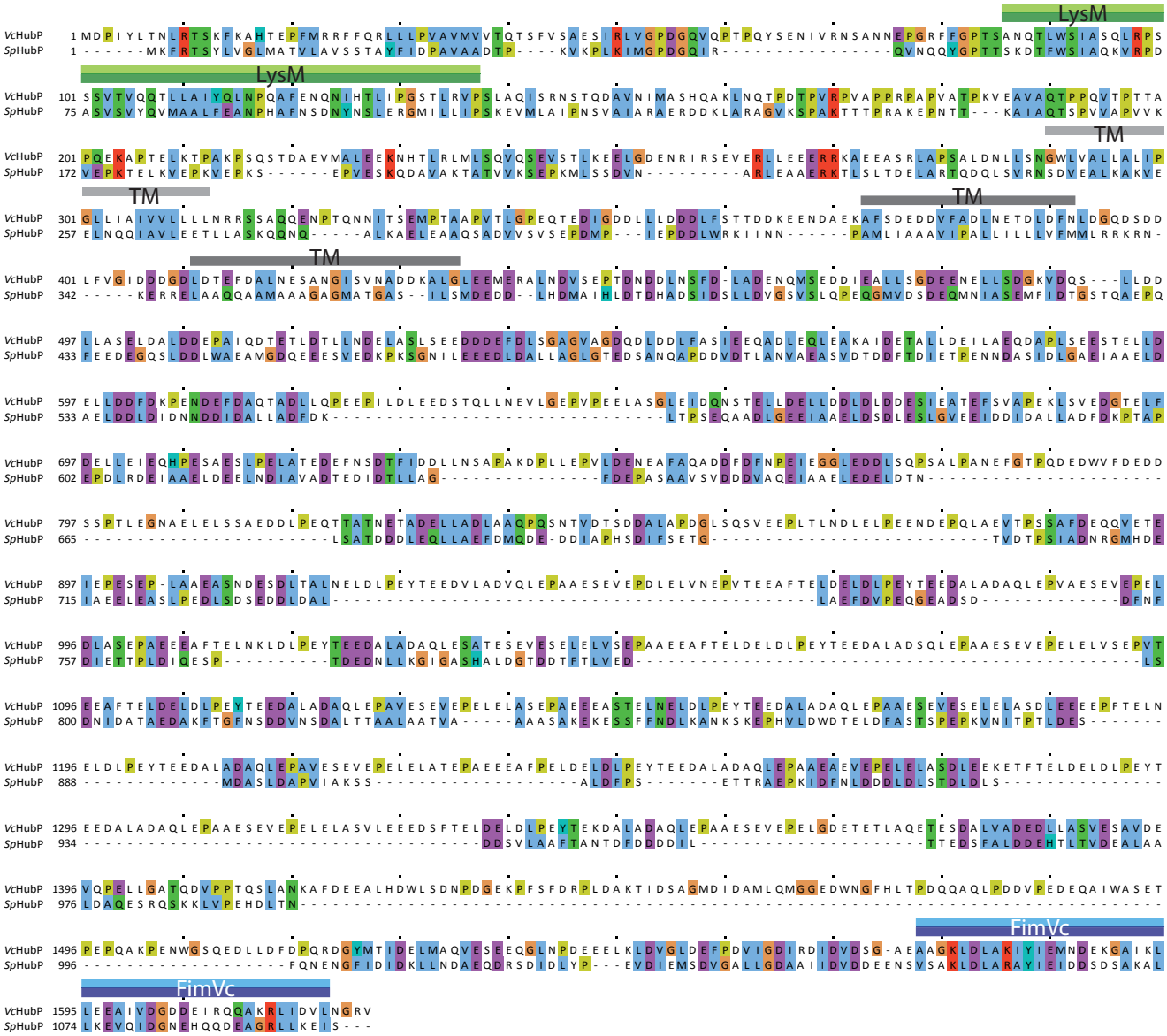

Figure S6: Amino acid sequence alignment of HubP of *Vibrio cholerae* (*Vc*HubP) and *S. putrefaciens* CN-32 (*Sp*HubP). The positions of the predicted LysM and C-terminal FimVc domains are highlighted in green and blue, respectively; the predicted transmembrane regions are marked in grey. Color code of the amino acid residues: A, I, L, M, F, W, V, blue; N, Q, S, T, green; E, D, magenta; G, orange, H, Y, cyan; P, yellow.

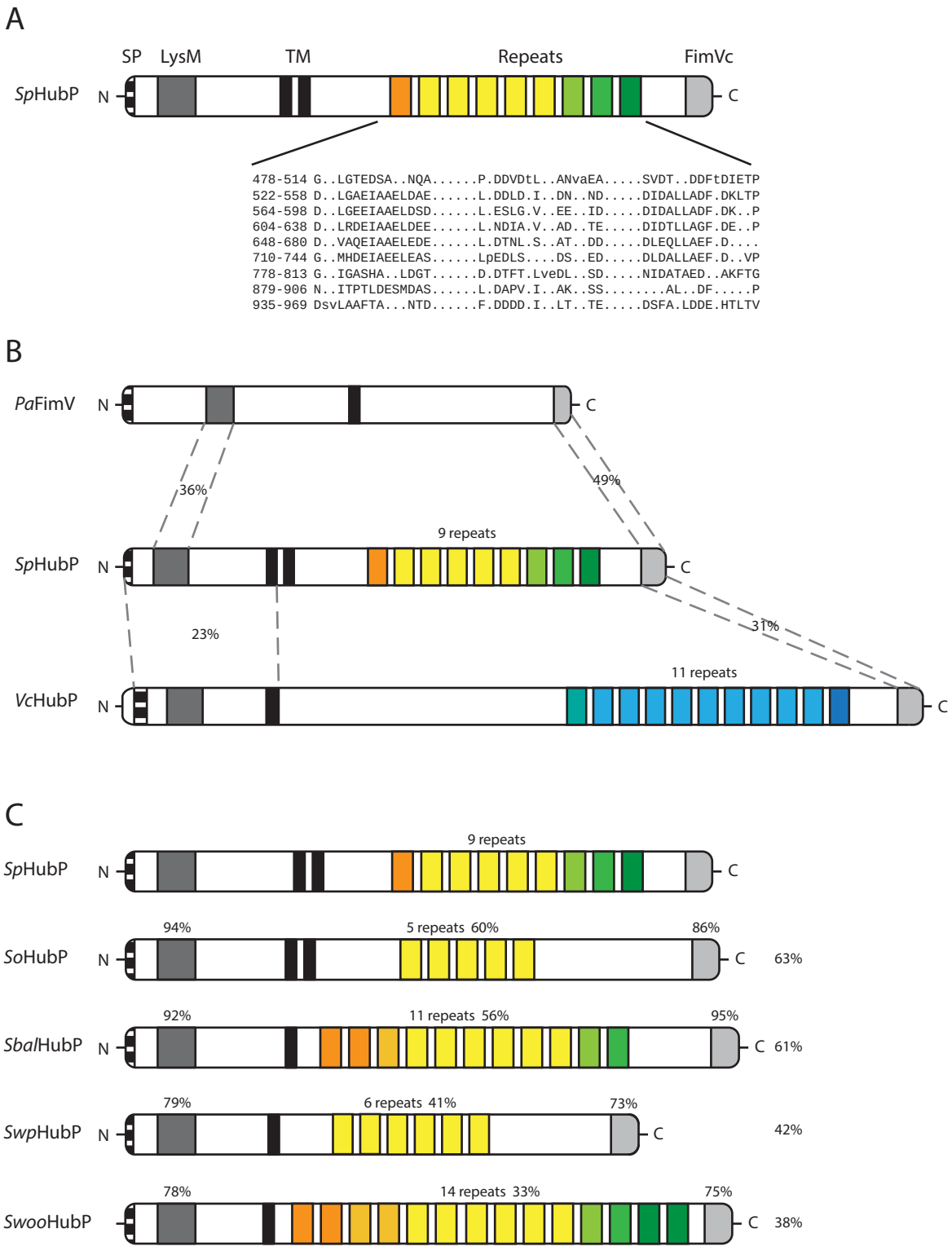

Figure S7: HubP/FimV domain organization. A) Domains of *S. putrefaciens* CN-32 HubP (*Sp*HubP). Indicated are the N-terminal signal domain (SP), the LysM domain, the transmembrane domain (TM), the C-terminal FimV domain (FimVc) and the number and position of repeated amino acid sequences. The sequence of these repeats is specified below. **B) Domain organization comparison of *P. aeruginosa* FimV (*Pa*FimV), *Sp*HubP and *V. cholerae* HubP (*Vc*HubP) drawn to scale.** The domains are indicated similarly as in A). The regions showing the indicated highest identity levels to SpHubP at the sequence level are marked by bracketed lines. It should be noted that, although the repeat structure in *Pa*FimV is little pronounced, the corresponding region is similarly enriched in acidic amino acids. **C) Comparison of putative HubP orthologs in various *Shewanella* sp.** The proteins show high conservation in the N- and C-terminal regions but little conservation with respect to the cytoplasmic repeat region as correspondingly indicated as percentage of identity at the amino acid level for each major region (LysM domain, repeat region, FimV C-terminal domain, overall). *So*HubP, *S. oneidensis* MR-1 SO_3069; *Sb*HubP, *S. baltica* Sbal_2743; *Swp*HubP, *S. piezotolerans* Swp_3117; *Swoo*HubP, *S. woodyi* Swoo_2985. Please note that these are only a few representatives of likely HubP orthologs in *Shewanella* to illustrate the difference in HubP domain organization in closely related species.

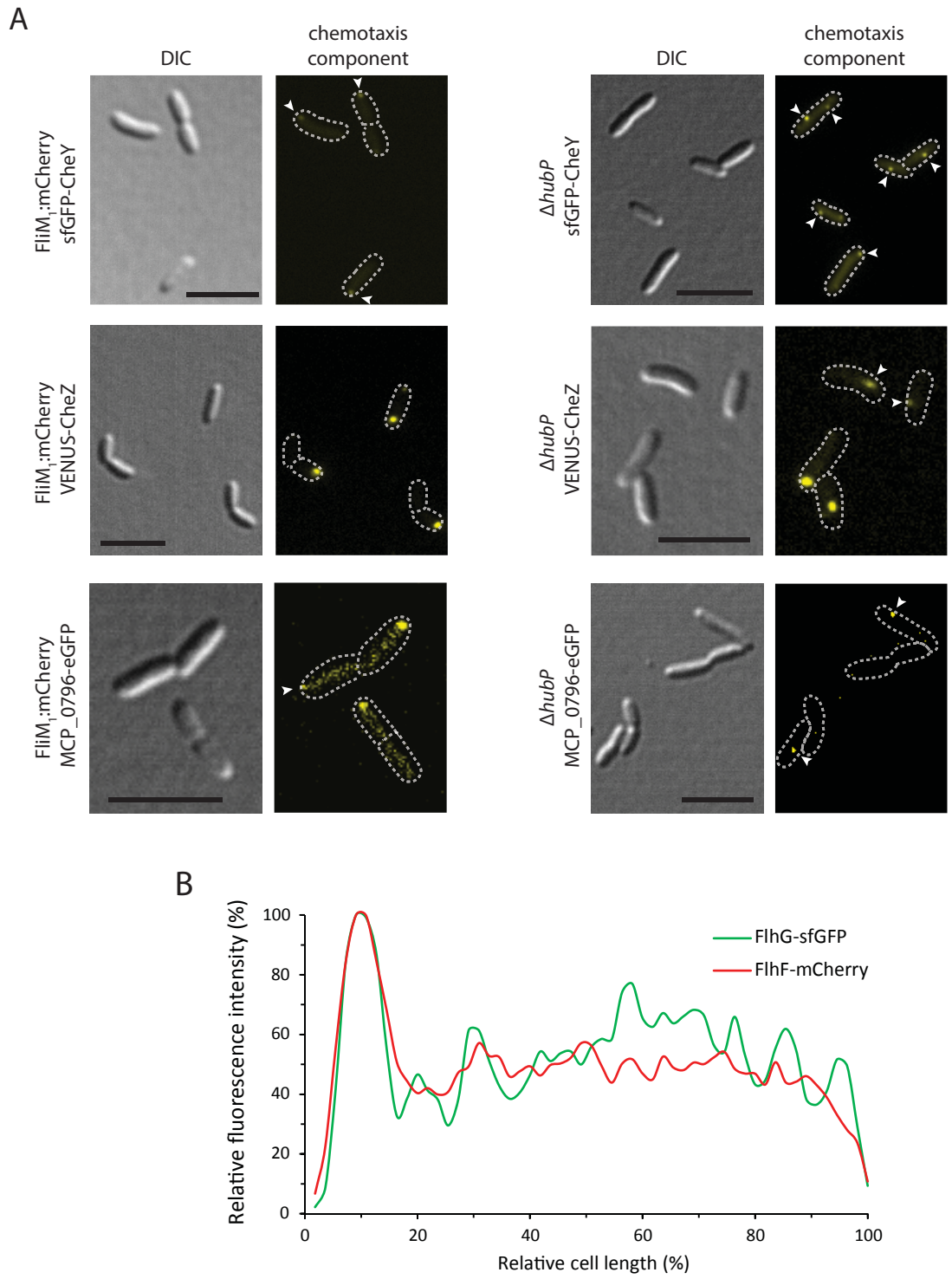

Figure S8: *Sp*HubP is required for proper localization of the chemotaxis components . A) Localization of components of the chemotaxis signaling array in the presence (left) and absence (right) of *Sp*HubP. Displayed are DIC and corresponding fluorescence micrographs of cells bearing sfGFP-CheY, Venus-CheZ, or MCP_0967-eGFP fusions. Loss of *hubP* results in displacement from the cell pole to more lateral position. Arrows indicate the position of fluorescence clusters, and the scale bar equals 5 µm. **B) Both FlhF and FlhG localize to the cell pole.** Displayed are line scans of the relative fluorescence intensity of cells producing FlhG-sfGFP (green line) or FlhF-mCherry (red line). Corresponding fluorescence micrographs are displayed in Fig. 3.

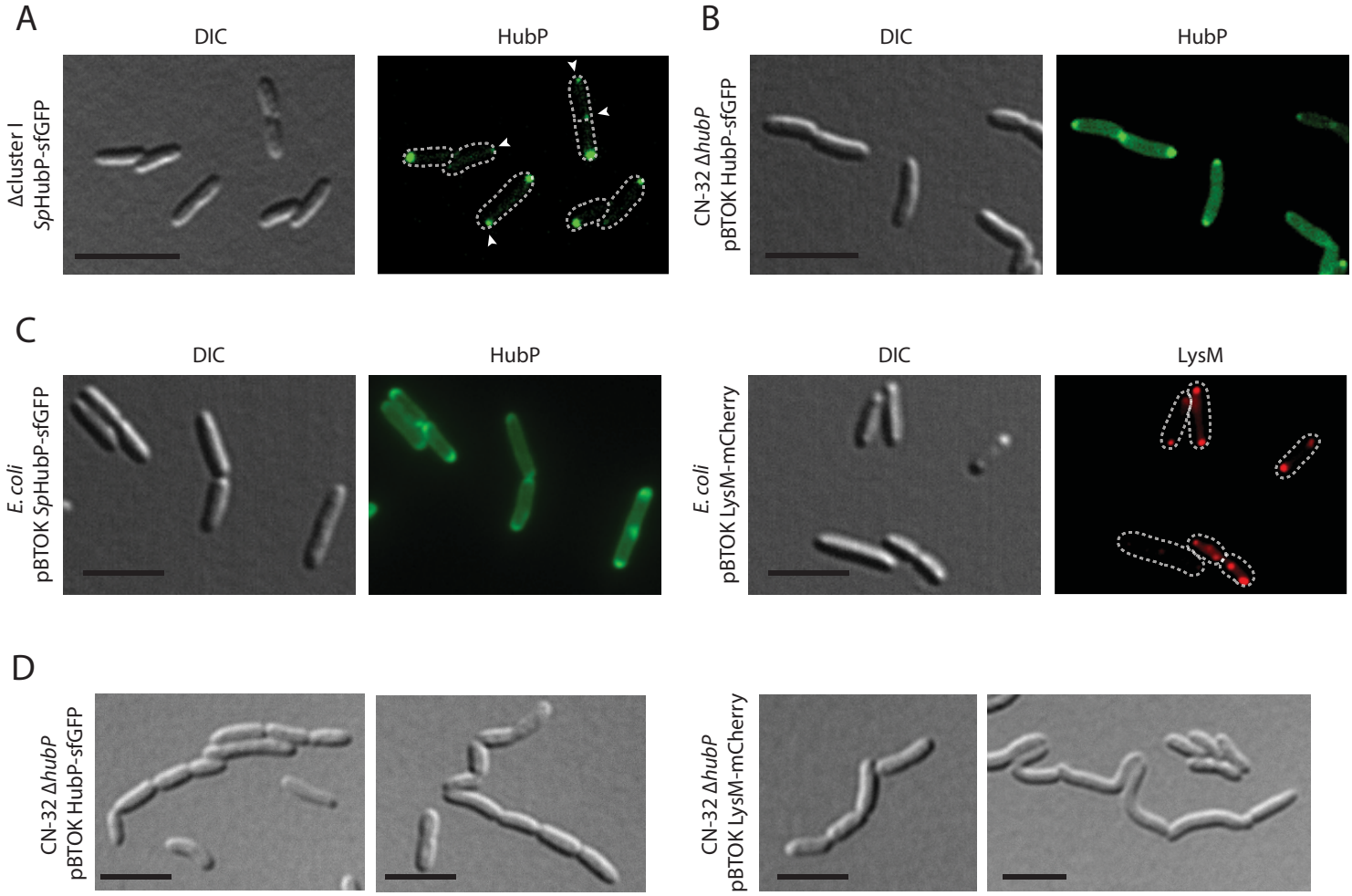

Figure S9: Localization and phenotypic analysis of *Sp*HubP-sfGFP and LysM-sfGFP production. A) *Sp*HubP localizes independently of flagellar components including FlhF. Displayed are a DIC and corresponding fluorescence micrograph of cells in which the complete primary flagellar cluster was deleted and which produce a HubP-sfGFP fusion. **B) Low amounts of *Sp*HubP-sfGFP show normal localization patterns.** Displayed are DIC and corresponding fluorescence micrographs of ΔhubP-mutants cells harboring pBTOK-HubP-sfGFP without induction. The arrow marks the localization of HubP-sfGFP at a newborn cell pole. **C) *Sp*SpHubP-sfGFP and LysM-sfGFP heterologously produced in *E. coli* localizes in similar patterns as in** *S. putrefaciens*. Displayed are DIC and corresponding fluorescence micrographs of *E. coli* cells harboring pBTOK-HubP-sfGFP (left) or pBTOK-LysM-sfGFP (right) at low induction. **D) Overproduction of full-length *Sp*HubP-sfGFP or LysM-sfGFP results in aberrant cell morphologies in *S. putrefaciens* CN-32.** Displayed are DIC micrographs of cells after gene induction for 45 min from pTBOK-HubP-sfGFP or pTBOK-LysM-sfGFP. The cells tend to form chains or elongated cell shapes. For all images: The scale bar equals 5 µm, arrows mark fluorescent foci.

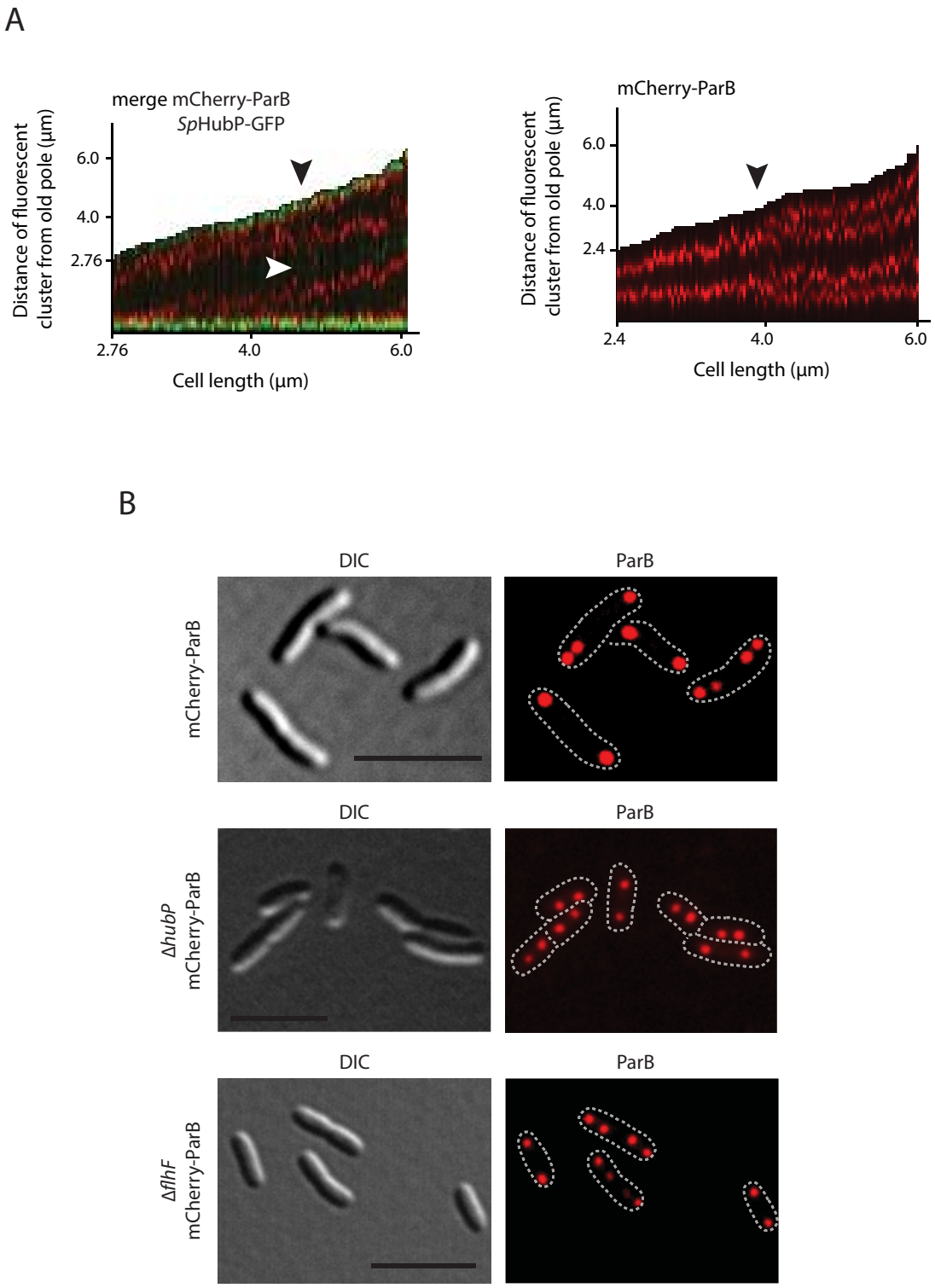

Figure S10: Localization of *oriC* in dependence of *Sp*HubP and FlhF. A) Position and fluorescent intensity of mCherry-ParB (red) and *Sp*HubP-sfGFP (green) as the distance from the old cell pole relative to the cell length over the cell cycle. The cell length is marked by the black area. The black arrows marks the earliest time point of visible cell constriction. The white arrow marks the appearance of *Sp*HubP-sfGFP at the division plane and at the newborn cell poles. In *ΔhubP* cells, the *oriC* marked by mCherry-ParB is never observed at the cell poles but remains at a certain distance to the pole. Also see the corresponding figure displaying the position without fluorescent intensities (Fig. 6). **B) FlhF does not localize the *oriC* to the cell pole.** Shown are DIC and corresponding fluorescence micrographs of wild-type (upper two panels) and *ΔflhF*-mutant (lower two panels) cells in which ParB was fluorescently tagged to mark the position of *oriC* within the cells. In the absence of FlhF, the fluorescent foci still move towards and localize at the cell pole as opposed to cells in which *hubP* was deleted (middle panels). The scale bar equals 5 µm.

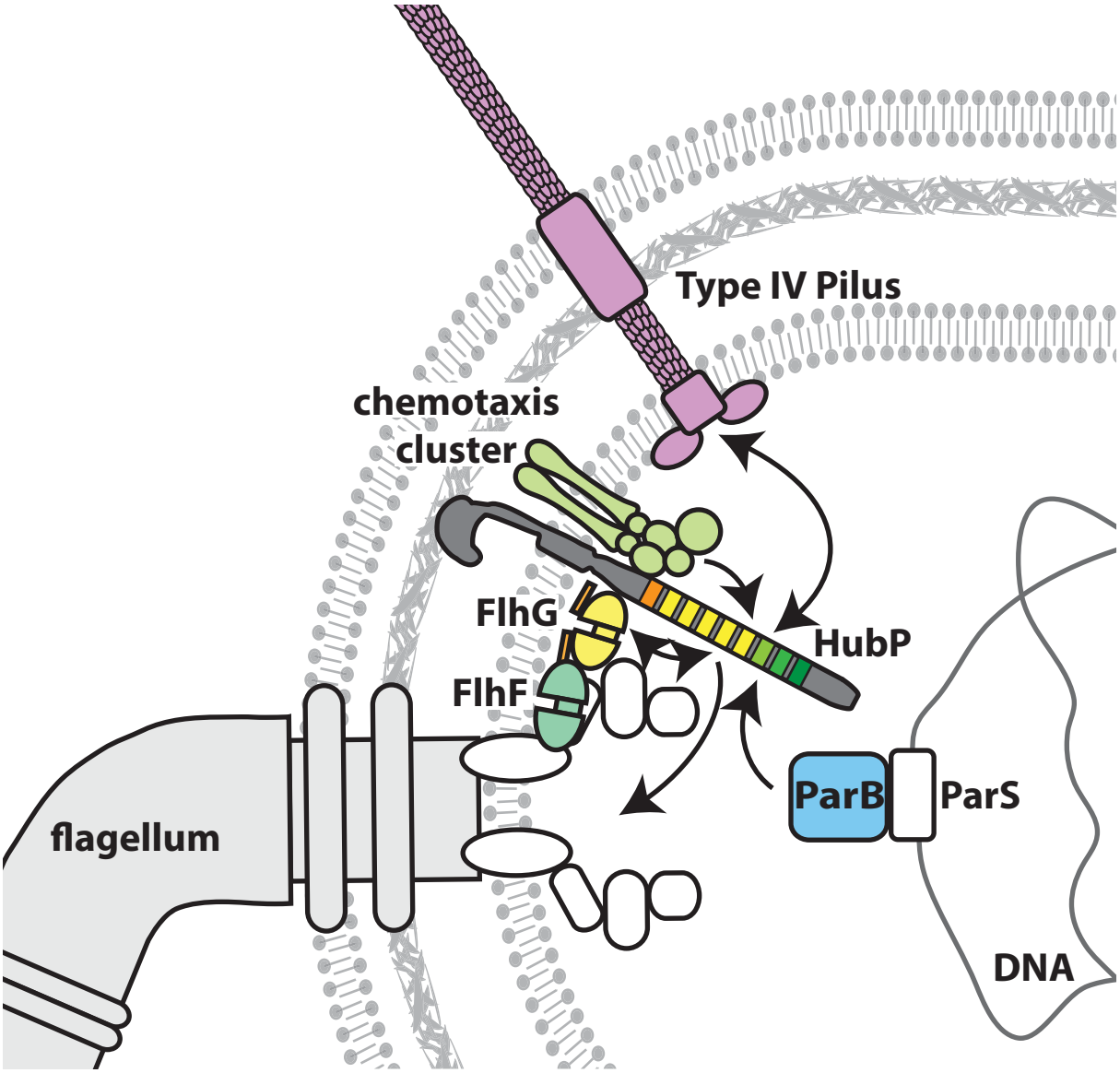

Figure S11: A model summarizing observed and potential functions of HubP/FimV-like proteins. HubP serves as a polar marker protein for recruitment of *oriC* and the chemotaxis array to the flagellated cell pole. In addition, HubP might directly or indirectly affect flagellar biosynthesis (maybe through interaction with the FlhF/G system which targets the flagellum to the cell pole) and affect flagellar performance and/or type IV pili-mediated twitching motility.

Chapter 5:

Discussion

5.1 What is the contribution of the polar and the additional lateral filament of *Shewanella putrefaciens* to motility under planktonic conditions?

5.1.1 Secondary flagella contribute to bacterial swimming

Although the formation of secondary flagella improves bacterial motility in changing environments by adjusting the cells capability to adhere to surfaces, swarm or swim in liquids with increased viscosity, little is known about the function of such additional flagella under planktonic conditions. The dual flagellar system of *S. putrefaciens* CN-32, closely related to the well-studied systems of *A. hydrophila*, *V. alginolyticus* and *V. parahaemolyticus*, is beneficial for spreading through a dense net of soft agar (1). It was shown that cells isolated from the outer rim of the lateral extension zone of a soft-agar plate exhibited a high amount of lateral-flagellated cells. These cells also displayed significantly more lateral flagella per cell compared to cells isolated from the center of the halo. In addition, wildtype cells (wt), expressing both polar and lateral flagella, and cells lacking the genes responsible for lateral flagellin production, *flaAB*$_2$, were shown to spread farther upon spotting in a 1:1 mixture on a soft-agar plate. To discriminate the two strains, wt and mutant cells constitutively expressed different fluorescent proteins. The number of wt cells compared to mutant cells also increased at the outlets of a chamber connected to a reservoir containing the same 1:1 wt/mutant mixture (Chapter 2). These results show that the lateral filament enables polarly flagellated cells to outperform cells with only a single polar flagellum, although the average swimming speed was lower in cells harboring a lateral filament (Bubendorfer et al. 2012; Chapter 2). Interestingly, this enhanced swimming performance was observed not only on soft-agar plates, where the branched, dense net of agarose might favor the lateral flagellation pattern, but also in liquid medium.

5.1.2 Lateral flagella affect turn events and chemotaxis

In addition to the speed of individual swimming cells, the turning event is essential for enabling chemotaxis. One hypothesis of how lateral filaments affect swimming efficiency is by altering the direction of motion. Studies determined a mean turn angle of 90° for polarly flagellated bacteria, generated by a previously described run-reverse-flick mechanism (2). Quantification of turn events in *S. putrefaciens* revealed similar turn angles in the absence of lateral flagella. Although most wt cells with both polar and lateral flagella also showed a similar distribution, a strong tendency for turn angles less than 90° was observed. In addition, the mean forward run period between two turn events increased from 10 s in the mutant to 20 s in wt cells. These results indicate that additional lateral flagella influence directional persistance, the ability of swimming cells to migrate toward a specific direction over time (Chapter 2).

Since chemotaxis triggers the frequency of rotational switching of the flagellar filament and thus directional changes of the swimming cell, the influence of the lateral system on chemotaxis was examined. In most other dual flagellated organisms, such as *V. parahaemolyticus* and (3) *V. alginolyticus* (4) the chemotaxis system acts on both flagellar systems. In contrast, *S. putrefaciens* mutant strains, where *cheY* was either deleted, constitutively active (gain-of-function) or inactive (loss-of-function), showed no effect on radial extension on swim plates if the polar filament was missing. However, if only the polar filament was present, chemotaxis and spreading on soft agar plates was strongly impaired (Chapter 2). The lateral flagellum was shown to rotate exclusively in a CCW direction at a significantly slower speed than the polar motor (1). Since the N-terminal CheY-binding motif is only present in the motor switch protein of the polar flagellum, $FliM_1$, and not in $FliM_2$ (Fig. 1A), phosphorylated CheY acts exclusively on the polar motor. In *S. putrefaciens*, the polar flagellum seems to be sufficient to enable chemotaxis-induced directional changes similar to the reported "run-reverse-flick" mechanism (Xie et al. 2011, Chapter 2, Fig. 1B). As the lateral FliMs of both *V. parahaemolyticus* and *V. alginolyticus* also lack this N-terminal putative CheY-docking site and the unidirectionally rotating motor seems to be solely slowed down by CheY, a different mechanism of CheY binding in these organisms can be assumed (4). A first hint comes from the group of Michael Eisenbach's lab, who observed alternative CheY binding sites in *E. coli* FliM when the N-terminal domain of FliM was missing (5). Although there is no evidence that cells use chemotaxis during swarming (6), the CheY-responsiveness of lateral flagella might be involved in improved swarming (4). The inability of lateral FliM to respond to CheY due to mutated binding sites might be one explanation why *S. putrefaciens* shows a low swarming ability. Future studies could identify these putative alternative CheY binding sites which might allow us to improve swarming in *S. putrefaciens*.

While the polar system is responsible for turning, the lateral flagellum reduces the turn angle. Computational modeling of the swimming movement in a two-dimensional random walk revealed that reduction of the turn angle leads to higher directional persistence, resulting in more efficient spreading behavior of the wt compared to a mutant lacking the lateral filament. The reduction in turn angle allows the cell to swim longer in the same direction (Chapter 2, Fig. 1C). This phenomenon was also previously described for moving insects as a strategy to increase spreading efficiency (7). Longer runs may result from invisible directional changes due to drastically decreased turn angles. In computer simulations altering the parameter describing the turn angle of the cell led to more efficient spreading even in steady shallow attractant gradients, such as those commonly encountered in *S. putrefaciens* marine or freshwater environments (Chapter 2). To fulfill its function, the lateral flagellum must function and rotate (1),

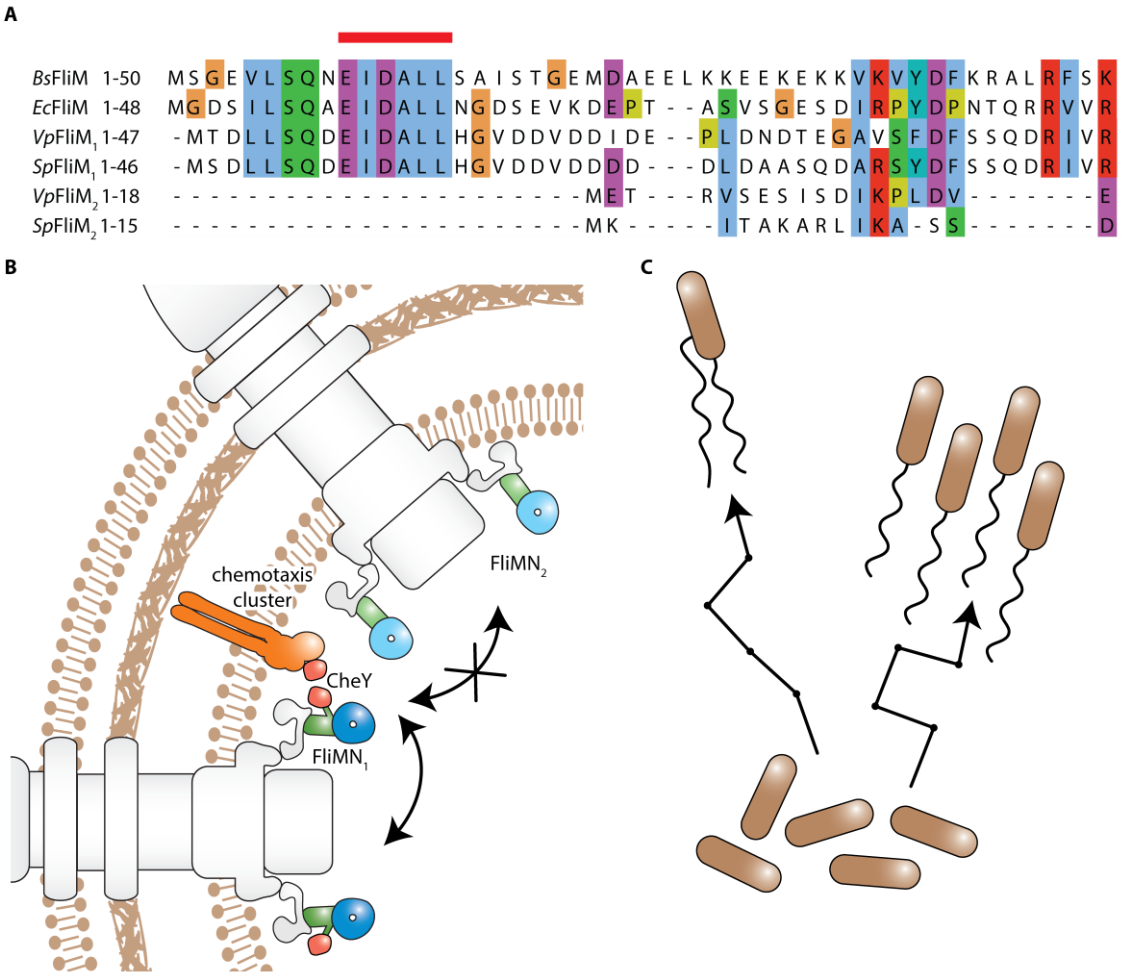

Fig: 1: The polar flagellum is responsible for main propulsion and chemotaxis while a subpopulation possesses a lateral flagellum which improves bacterial spreading by increasing directional persistence. (A) Alignment of the N-terminal part of the motor switch protein FliM with the highlighted CheY binding EIDAL-motif from different bacterial organisms (*Bs* = *B. subtilis*; *Ec* = *E. coli*; *Vp* = *V. parahaemolyticus*; *Sp* = *S. putrefaciens*). Alignment generated using Clustal Omega and edited using Jalview software. (B) The chemotaxis response regulator CheY (red) exclusively binds to the polar motor switch proteins $FliMN_1$ (dark green / dark blue), enabling only the polar flagellum to respond to chemotaxic signals. The required binding motif is missing in lateral $FliM_2$ (light green) allowing the lateral flagellum to rotate unidirectionally. (C) Impact on bacterial spreading by heterogeneous flagellation. Dual flagellated bacteria can spread farther than polar flagellated bacteria due to increased directional persistence. Arrows indicate the movement path of a representative cell with directional switches marked by black circles.

indicating an active role of the lateral flagellum in the cellular reorientation process.

The observations described above reveal a novel mechanism of lateral flagella in liquid environments. The lateral flagellum seems to constantly rotate without a positive contribution to the overall swimming speed. Together with preliminary high-resolution microscopy analysis these results indicate that the lateral flagella operate independently from the polar flagellum and do not form bundles like peritrichously

flagellated *E. coli* (8) or lophotrichously flagellated *Helicobacter pylori* (9). This mechanism could be a common theme in bacteria with two flagella systems expressed under planktonic conditions. This is supported by similar observations in the dually flagellated soil bacteria *Bradyrhizobium japonicum* (10) and *B. diazoefficiens* (11). In these bacteria, a single polar flagellum was shown to be sufficient to reach full swimming speed. In contrast, deletion of the polar flagellum causes an irregular swimming pattern in liquid medium. In addition, involvement of the lateral flagella in swimming under planktonic conditions without influencing the swimming speed was observed. *B. diazoefficiens* showed a tendency to shorter trajectories and decreased radial extension on soft agar in strains lacking the lateral filament (11). *V. alginolyticus* showed similarly decreased spreading on soft agar plates if lateral filaments were absent (12). Even in *E. coli* additional flagella, although they form bundles, do not substantially increase the speed of the cell, but contribute to the reorientation process during tumbling (13). These examples indicate that this mechanism of using additional lateral flagella to modify flagellar turning is a common strategy of bacteria and allows improved spreading in marine and soil environments.

5.2 How are the position and number of the polar and lateral flagella determined?

5.2.1 FlhF exclusively regulates positioning of the polar flagellum

Although the exact physical mechanisms by which the lateral flagellum lowers the turn angle remain elusive, the lateral position of the secondary flagella seems to be important, as only a lateral position can create the momentum necessary to modify the turn angle. In contrast to polar flagella, lateral flagella are thought to localize in a pattern across the cell surface, similar to the peritrichous flagellation patterns of *E. coli*. However, while the distribution of *E. coli* is thought to be stochastic, the regulators FlhF and FlhG are involved in spatial and numerical regulation of the lateral flagella in the also peritrichously flagellated *B. subtilis* (14). In *S. putrefaciens*, only the polar flagellar system encodes the regulators FlhF and FlhG, while the lateral flagellar gene cluster lacks *flhF* or *flhG*.

In the course of this thesis, the role of FlhF in the placement of the polar, lateral or both flagella in *S. putrefaciens* was examined. The domain structure of the well-characterized FlhF from *B. subtilis* (*Bs*FlhF) and *S. putrefaciens* FlhF (*Sp*FlhF) consist of a conserved C-terminal NG-domain, while the N-terminal B-domain of *S. putrefaciens* differs considerably from *Bs*FlhF. As in other polarly flagellated organisms (15–17), *Sp*FlhF was shown to be involved in polar flagella placement. Deletion of *flhF* resulted in significant reduced radial extension on soft agar plates compared to the wt. In addition, significantly fewer cells had flagella, ultimately resulting in fewer motile cells. In those, the primary flagella were frequently shifted to

lateral positions. Correspondingly, fluorescently labeled foci of the polar motor switch protein $FliM_1$, frequently appeared at positions along the lateral axis of the cell. Fluorescently labelled FlhF also localized to the flagellated cell pole, although bipolar localization was frequently observed. Weaker foci commonly appeared at the new, unflagellated pole indicating polar recruitment of FlhF at an early stage during the cell cycle. These results suggest that *Sp*FlhF regulates localization of polar flagella as previously described for other polar flagellated bacteria.

Although the specific flagellar components recruited by FlhF are unknown, polar accumulation of flagellar structures can be observed if FlhF is overrepresented at the cell pole (17–19). In *S. putrefaciens*, overproduction of FlhF also lead to polar accumulation of FlhF and, subsequently, $FliM_1$. Flagella staining of these cells revealed hyperflagellation with a complete loss of swimming ability on soft agar plates, likely resulting from an inhibition of flagellar motor function. These findings indicate an identical role of FlhF in recruiting early polar flagellar components in this dual flagellated organism, similar to other polarly flagellated organisms (Chapter 4).

Effects of *Sp*FlhF on lateral flagellation were, however, not observed. Fluorescently-labelled FlhF was never shown to co-localize with lateral $FliM_2$ foci. Furthermore, deletion of *flhF* had no effect on the amount of $FliM_2$ foci within a single cell or the whole population. Likewise, formation of lateral filaments were unaffected when *flhF* was missing. Thus, FlhF is not involved in the placement of lateral flagella. Lateral flagella might therefore localize independently of FlhF in a similar fashion as the peritrichous flagella of *E. coli* or *S. enterica* (Chapter 4, Fig. 2A).

It is unknown why only polar flagellar components are specifically targeted to the cell pole. One unverified hypothesis is that *Sp*FlhF recruits the membrane-embedded polar MS-ring protein $FliF_1$ (19). Alignment of $FliF_1$ and $FliF_2$ from the lateral system showed low protein sequence homology, with an identity of 31% and 52% similarity, respectively. A main component of the fT3SS, FlhA, has also a large cytoplasmic part (20) and is another candidate for an early recruitment (21) which might depend on FlhF in polarly flagellated bacteria. Lateral $FlhA_2$ and polar $FlhA_1$ have much higher sequence homology than $FliF_{1/2}$, with an identity of 51% and 72% similarity, respectively. Nevertheless, all of these proteins have variations in their cytoplasmic regions. Such variations might be responsible for specific binding of *Sp*FlhF, leading to polar recruitment of only $FliF_1$ and $FlhA_1$. It is, however, unknown if FlhF directly recruits such a component to the cell pole or if it is recruited itself by early flagellar components. Early flagella proteins could therefore also be required for polar localization of FlhF. Although the determinant for polar localization of FlhF has not yet been discovered, initial experiments in *Vibrio sp.* revealed that FlhF independently localizes to the cell pole upon the absence of the master transcriptional regulator FlrA (19) or the flagella-specific sigma

factor 54 RpoN (22). However, preliminary localization studies of overexpressed, fluorescently labelled FlhF in *S .putrefaciens* cells lacking the whole gene cluster encoding chemotaxis proteins and flagellar components of the polar systems did not reveal any specific foci. In contrast, lateral foci occasionally appeared if the same construct was expressed in a peritrichously flagellated *E. coli* cell. This indicates that the presence of flagellar components not regulated by RpoN and $FlrA_1$ accessible from the cytoplasm might be involved in polar localization of FlhF.

While the NG-domain of FlhF is highly conserved and homologous to the proteins of the SRP-system, FtsY and Ffh, the B-domain is highly unstructured and poorly conserved (23). It is possible that these variations are at least partly responsible for the different flagellation pattern in different species. Also unknown is weather FlhF plays a role in the SRP-system and in the process of protein translocation. FlhF could, for example, be involved in secretion of flagellar transmembrane proteins, like FliF or FlhA, during the early stages of flagellar assembly.

Future *in vitro* and *in vivo* interaction studies might lead to the identification of new binding partners of FlhF, allowing a better understanding of polar localization and client protein recruitment of this flagellar landmark protein.

5.2.2 FlhG limits polar localization of FlhF

The iinvolvement of FlhG in polar localization of FlhF also remains elusive. Until now, the major function of FlhG was thought to reside in the cytoplasma and to control polar localization of FlhF by directly binding FlhF (22). While polar localization of FlhF was previously shown to be independent of GTP binding or hydrolysis (24, 25), it is probably essential for recruitment of polar components. The GTPase activity of FlhF, which induces the dissociation of the homodimer, has been verified in several bacterial species (24–27).

So far, stimulation of the GTPase activity of FlhF by FlhG has been demonstrated only in the peritrichously flagellated, gram-positive bacterium *B. subtilis* (27). As demonstrated in Chapter 4, the presence of full-length FlhG or the N-terminal region of FlhG from *S. putrefaciens* was sufficient to stimulate the GTPase activity of FlhF *in vitro* (Fig. 2A). FlhG-activated hydrolysis induces dissociation of the homodimer and likely release from bound effector molecules. Although FlhF localizes independently of GTP binding, GTP hydrolysis ultimately leads to dissociation of FlhF from the cell pole in an unknown manner (28).

As an effect, deletion of *flhG* in *S. putrefaciens* resulted in increased polar amounts of FlhF and, consequently, basal body components like $FliM_1$ at the cell pole and the formation of multiple flagella in a manner similar to a FlhF overexpression. This was also observed, when an N-terminal amphipathic helix forming a membrane targeting sequence (MTS) or the residues responsible for ATP hydrolysis in FlhG were mutated, indicating that both membrane localization and ATPase activity are required for stimulating FlhF GTPase activity. The MTS of FlhG was demonstrated to mediate membrane attachment by fluorescent labeling of the first 20 amino acids. (Chapter 3). Hyperflagellation is therefore caused by polar accumulation of FlhF upon the absence of functional FlhG, which can be observed in other polar flagellated organisms (15, 25, 29).

However, since FlhG was also shown to localize to the cell pole in *V. alginolyticus* (28) and only membrane-bound FlhG induces FlhF dissociation, this might favor the hypothesis that interaction takes place at the cell pole. Indeed, FlhG was also shown to localize to the cell pole in *S. putrefaciens* in preliminary experiments. Membrane binding of FlhG was enhanced upon binding of a non-hydrolysable ATP variant. ATP binding mediated homodimerization and membrane binding of FlhG (Chapter 3). Similar to these findings, FlhG variants defective in ATP binding cannot localize to the cell pole in *V. alginolyticus*, indicating that polar localization was also dependent on ATP binding (28). Mutations in FlhG disrupting membrane targeting and ATPase function display a similar hyperflagellation phenotype as that observed for the *flhG* deletion strain. These observations strongly indicate that FlhG ATPase function and membrane targeting are crucial for polar targeting and interaction with FlhF (Chapter 3).

Our studies favour the hypothesis that interaction between FlhF and FlhG might not occur in the cytoplasm but rather at the cell pole. FlhG localizes to the cell pole and enhances the GTPase activity of FlhF, resulting in dissociation of FlhF from the cell pole and preventing polar accumulation of FlhF and hyperflagellation comparable to the situation in *Vibrio* (28). This model partly explains how polar flagellation can be restricted to a single flagellum by FlhF and FlhG.

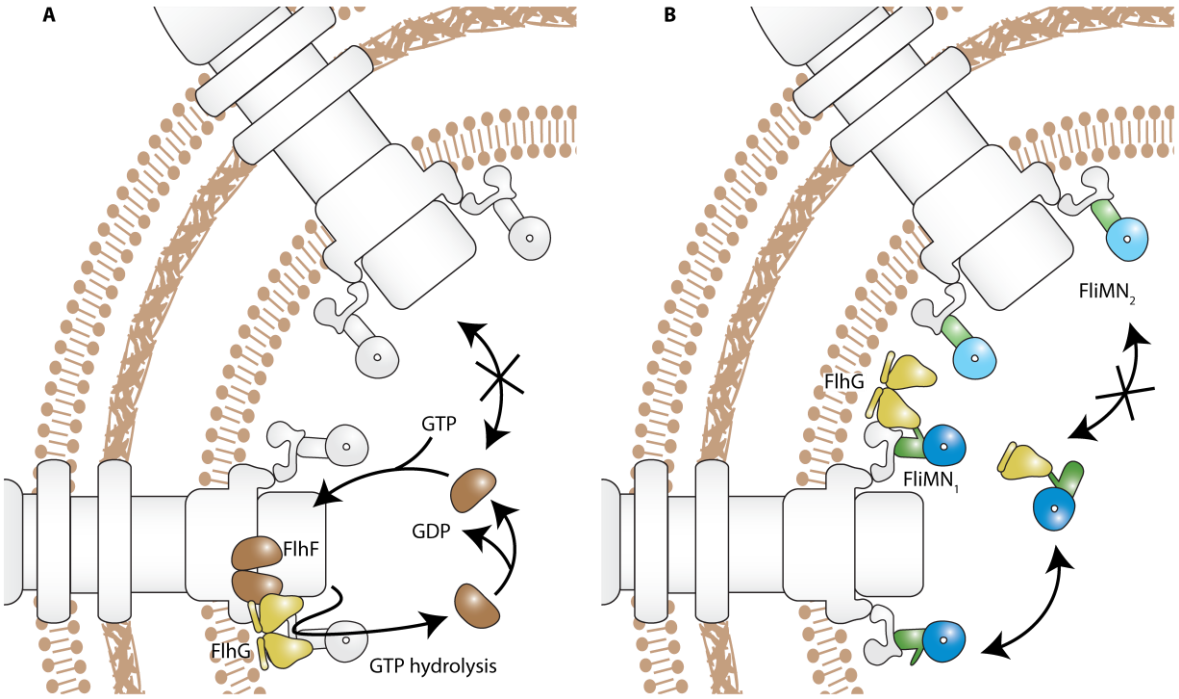

Fig: 2: The flagellar landmark proteins FlhF and FlhG regulate the position and number of the polar flagellum. (A) GTP-bound FlhF (brown) forms a homodimer and localizes to the cell pole by unknown cues where it is involved in recruitment of early components of the polar flagellar motor. Membrane-bound, dimeric FlhG (yellow) stimulates the GTPase activity of FlhF causing its monomerization and dissociation from the cell pole. The secondary flagellar system localizes to lateral positions independently of FlhF. (B) FlhG (yellow) is also involved in C-ring assembly by binding to the polar motor switch protein $FliM_1$ (dark green). Since the lateral motor switch protein $FliM_2$ (light green) lacks the binding motif, lateral C-ring assembly occurs independent from FlhG.

5.2.3 FlhG is exclusively involved in polar C-ring assembly

A similar hyperflagellation phenotype as that described for the FlhG deletion strain was observed in a strain lacking the polar motor switch protein $FliM_1$ (Chapter 3). Direct interaction between FlhG and $FliMN_1$ was detected both in *S. putrefaciens* and *B. subtilis* independent of nucleotid binding to FlhG. This indicates that FlhG might be able to bind $FliM_1$ both in its monomeric cytoplasmic or its dimeric membrane bound form. Since polar localization and membrane association depends on ATP binding to FlhG, FlhG might be involved in transporting $FliM_1$ to the cell pole. Interestingly, interaction of these two proteins was diminished if an N-terminal EIDAL motif in $FliM_1$ of *S. putrefaciens* was absent. This is the same binding domain required for CheY binding to the polar flagellum. It is unknown how FlhG binding interferes with CheY binding to the same interaction site. FlhG could prevent CheY binding during C-ring assembly process, though the mechanism of FlhG release from the C-ring is still unknown. Subsequent localization studies in *S. putrefaciens* provided further evidence that the interaction between $FliM_1$ and FlhG is also important

for polar localization and, likely, implementation of $FliM_1$ into the polar C-ring. Cells in which this N-terminal binding motif in $FliM_1$ was deleted had reduced polar localization of fluorescently labeled $FliM_1$ and a hyperflagellation pattern similar to the *flhG* and *fliM$_1$* deletion mutants. Interestingly, this reveals clear differences to the flagellar motor of *E. coli*, which was unable to secrete flagellins and form a filament if FliM was deleted. This impaired secretion is likely caused by an involvement of the C-ring in the fT3SS-mediated secretion process (30) which might underlie different mechanisms in *S. putrefaciens*. In polarly flagellated species of *Pseudomonas* and *Vibrio sp.* and the well-studied flagellar apparatus of *E. coli* and *S. enterica*, the EIDAL motif is present only in FliM (Sircar et al. 2013; Schuhmacher et al. 2015a Chapter 3; Fig. 1A). In the gram-positive bacteria *Geobacillus thermodenitrificans* and *B. subtilis*, an analogous interaction between FlhG and FliY, a FliN homolog, was determined. FliY or FliN are also components of the C-ring and contain an N-terminal EIDAL motif in these organisms. As FliM and FliY/FliN are likely incorporated into the C-ring as preassembled building blocks, these observations indicate an important role of FlhG in the C-ring assembly process (Chapter 3; Fig.2B).

Similar to FlhF, it is unknown how FlhG is localized to the cell pole. In *V. alginolyticus*, polar localization of both FlhF and FlhG was shown to be present if the gene encoding the flagellar sigma factor RpoN was missing (22). Preliminary experiments indicate that FlhF, FlhG and $FliM_1$ may not necessarily be transcribed together with other flagellar components. Binding of FlhG to $FliM_1$ suggests that $FliM_1$ is also responsible for polar localization of FlhG. This is supported by preliminary experiments which show that polar localization of an overexpressed, gfp-tagged version of FlhG is absent if $FliM_1$ or the EIDAL motif of $FliM_1$ is missing. The $FliM_1$-dependent polar localization of FlhG would also explain the hyperflagellation phenotype of the *fliM$_1$* knock-out strain, since FlhG then cannot induce FlhF dissociation from the cell pole. Thus, future studies must investigate the exact effects of the cooperative interaction of FlhG and $FliM_1$.

Although these findings remarkably improve our knowledge of the mechanisms behind polar flagella formation, the assembly process of lateral flagella remains unknown. The lack of exact flagellar interaction partners of FlhF in the polar system makes it difficult to determine why early motor components are specific to the polar or the lateral flagellar system. However, the interaction of FlhG with $FliM_1$ is known and appears to be conserved in other bacteria. Neither $FliM_2$ nor $FliN_2$, the C-ring proteins of the lateral flagellar apparatus, harbor the N-terminal EIDAL binding motif (Fig. 1A). Thus, $FliM_2$ was not targeted by FlhG in *in vitro* experiments. Deletion of FlhG did not impact the formation of fluorescently labeled $FliM_2$ foci compared to the wt, indicating that there is no direct influence of FlhG on lateral flagella formation and assembly (Chapter 3). It is likely that C-ring assembly of lateral flagella proceeds in a different fashion from polar flagella and similar to the peritrichous flagellation patterns of *E. coli* and *S. enterica*.

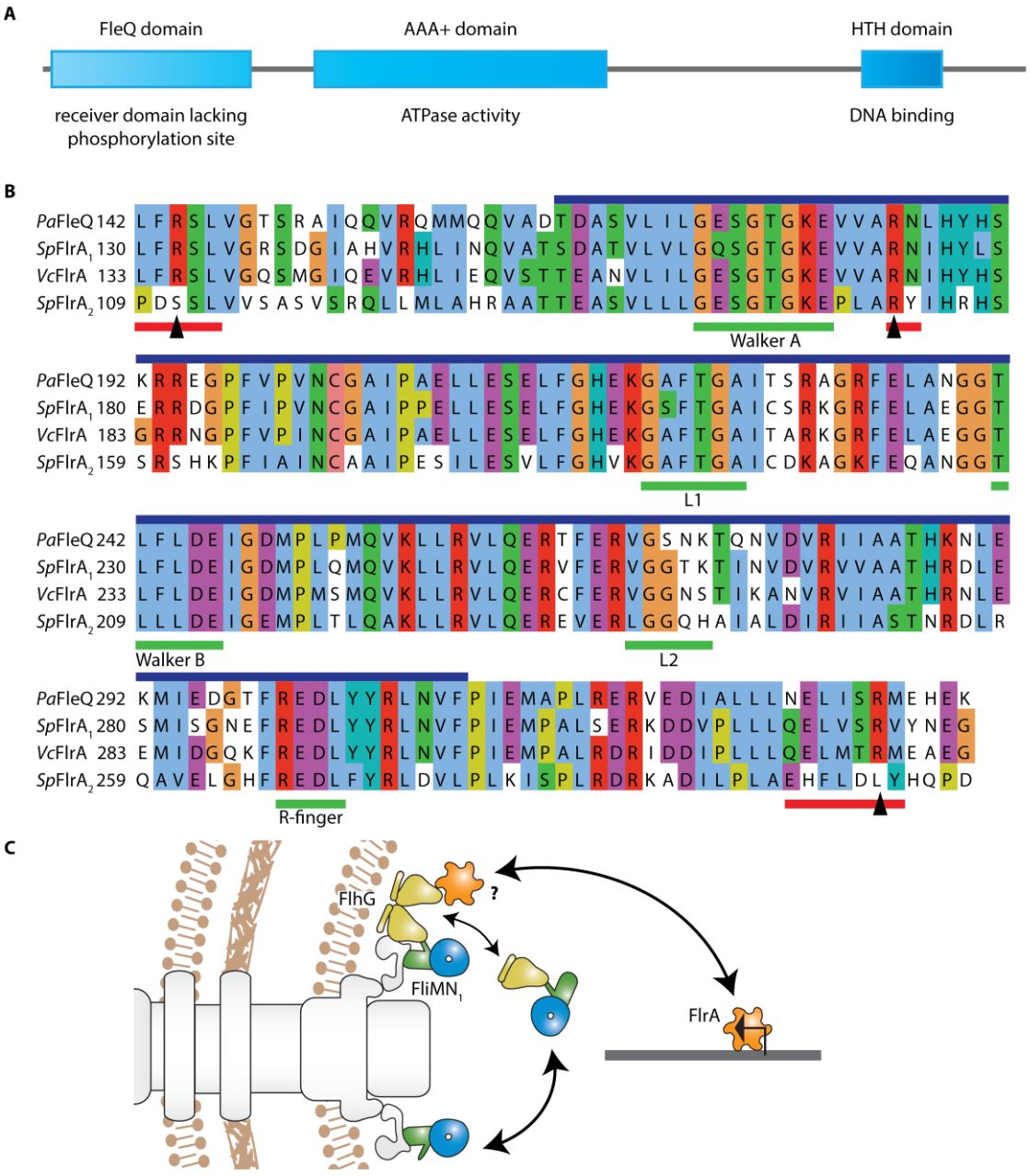

Fig: 3: The flagellar transcriptional master regulators $FlrA_1$ and $FlrA_2$. (A) Domain organization of $FlrA_1$ from *S. putrefaciens* and function of the domains. HTH = helic-turn-helix motif. (B) Alignment of the central part of representatives of the transcriptional master regulator FlrA/FleQ from different bacterial organisms (*Pa* = *P. aeruginosa*; *Vc* = *V. cholerae*; *Sp* = *S. putrefaciens*). The ATPase AAA+ domain (blue), the motifs involved in ATP binding (Walker A, Walker B), ATP hydrolysis (R finger), σ54 interaction (L1, L2) loops (all green) and the cdG-binding motifs (red) with conserved argines (black arrows) are highlighted. Alignment generated using Clustal Omega and edited using Jalview software. (C) Putative involvement of $FlrA_1$ in the assembly process of polar flagella. It is unknown how polarly localized, putatively $FliM_1$ (dark green) bound FlhG (yellow) affects the interaction of FlhG with the transcriptional master regulator of the polar flagellar system, $FlrA_1$ (orange). The presence of these two states of FlhG indicates a link between assembly and transcription of the polar flagellar system.

5.2.4 Spatiotemporal regulation of the dual flagellation pattern

The formation of multiple polar flagella in the *flhG* deletion strain is also caused by upregulation of flagella gene expression. This might be caused by the interaction between FlhG (or FleN in *P. aeruginosa*) and the flagellar transcriptional master regulator FlrA (or FleQ in *P. aeruginosa*) (33). Preliminary experiments indicate that the master regulators $FlrA_1$ from the polar flagellar system and $FlrA_2$ from the lateral system fulfill a similar role in transcriptional control in *S. putrefaciens*. While $FlrA_1$ seems to be involved in activation of both polar and lateral flagellar gene expression, $FlrA_2$ exclusively controls the expression of the lateral flagellar system. The domain structure of $FlrA_1$ from *S. putrefaciens* is illustrated in figure 3A.

In addition to flagellar gene expression, FleQ from *P. aeruginosa* also represses the expression of an operon involved in exopolysaccharide (EPS) biosynthesis and thereby inhibits biofilm formation. FleN binding negatively affects the activation of flagellar gene expression by FleQ and to a to a lesser extent the repression of EPS production by FleQ (34). Both FleN and the second messenger cdG, which was also shown to bind to FlrA in *Vibrio* (35) and FleQ in *Pseudomonas* (34) jointly reduce FleQ action in transcriptional control of EPS synthesis (36).

However, much less is known about how cdG, FlhG/FleN and FleQ/FlrA together affect flagellar biosynthesis. While in *P. aeruginosa* ATPase activity of FleQ is dispensible for EPS production (36), ATP binding and hydrolysis is inhibited by bound cdG leading to a reduced remodelling of the σ^{54}-RNA polymerase (37) and consequently to a downregulation of transcription of the downstream flagellar genes. The prescence of FleN enhances the reduction of FleQ ATPase activity by cdG binding, indicating a cooperative inhibition of flagellar gene expression (38). As most residues required for ATP binding, ATP hydrolysis, interaction with RpoN and cdG binding are conserved in $FlrA_1$ from *S. putrefaciens* (Fig. 3B), a similar mechanism might regulate flagellar gene expression in *S. putrefaciens*.

How are these interactions affected by the complex localization pattern of FlhF and FlhG? $FliM_1$ dependent polar localization of FlhG may spatially and sterically hinder interaction with $FlrA_1$. This could be part of a complex feedback loop, where the FlrA-FlhG complex can only be formed if FlhG no longer localizes at the cell pole. Polar localization of FlhG might prevent the deactivation of FlrA by reducing c-di-GMP binding and ensures a continuous supply of structural components of the basal body as long as C-ring assembly is still in progress and FlhG is bound to $FliM_1$. During this period of time, the other tiers of the flagellar gene expression hierarchy can be launched, including synthesis of flagellin components via the alternative sigma factor FliA. Upon completion of C-ring assembly, FlhG dissociates by a yet unidentified mechanism and binds to $FlrA_1$, repressing flagellar gene expression (32)(Fig.3C). The putative interaction between $FlrA_1$ and FlhG could be a trigger to release FlhG from the cell pole. FlhG was shown to be a MinD-like ATPase

with high structural homology to the cell cycle regulator MinD from *E. coli*, as determined by comparing the crystal structures of FlhG and MinD (Chapter 3). This oscillatory mechanism of FlhG between the flagellum at the cell pole and $FlrA_1$ in the cytoplasm might be very similar to the one described for the MinCDE system.

The lack of yet identified interaction partners of the lateral flagellar master regulator $FlrA_2$ makes it unlikely that a similar mechanism is also be observed in lateral flagellar systems. This is supported by the unaffected lateral flagellation in an *flhG* mutant strain. While most of the key motifs required for ATPase function and interaction with the sigma factor RpoN/σ54 are present, the cdG binding sites are often mutated (Fig. 3B), indicating that cdG cannot use the same mechanism to regulate $FlrA_2$. The lateral systems of *V. parahaemolyticus* (39) and *Aeromonas sp.* (40) were also shown to be negatively regulated by cdG, likely by the action of a regulative riboswitch upstream of *lafK*, which encodes a transcriptional activator homologous to $FlrA_2$. These putative riboswitches have also been predicted for various species of the genus *Shewanella* (41). Unknown cdG turnover enzymes with sensor domains could, therefore, modulate the cdG concentration in response to nutrient concentrations and the presence of surfaces, and in turn regulate lateral flagellation.

5.3 How is the position of the chemotaxis system in dual-flagellated systems determined?

5.3.1 The chemotaxis system localizes to the cell pole in *S. putrefaciens*

Chemotaxis receptors are commonly found at the cell pole. While it is conceivable that this close proximity of the chemotaxis system and the flagellum favors the diffusion of phosphorylated CheY in polar flagellated bacteria, its concentration seems to be constant throughout the cell (42) and the described mechanism of polar cluster formation might primarily ensure stable distribution of chemotaxis clusters to daughter cells (43, 44). If secondary flagellar systems do not respond to chemotaxis signals, close proximity to lateral flagellar motors are unnecessary. Studies in *P. aeruginosa* indicated interactions between the flagellum and the chemotaxis system. In this organism deletion of FlhF shifted the location of the chemotaxis protein CheA to a lateral position (45).

To determine the location of various chemotaxis components in *S. putrefaciens* and whether FlhF is also involved in the placement of the chemotaxis system, fluorescence microscopy analysis of various fluorescently labeled chemotaxis components was performed in the presence and the absence of *flhF*. The chemotaxis proteins CheA, CheY and various MCPs revealed polar localization of the chemotaxis system in the dual flagellated *S. putrefaciens*, even if *flhF* was deleted, resulting in a delocalized flagellar basal body

(Chapter 4). Polar localization of the chemotaxis cluster therefore occurs independently of the spatial regulation of the flagellar systems.

In *Vibrio* sp., the large polar transmembrane protein HubP plays an integral role in cell polarity by recruiting key players of various cellular processes to the cell pole. It localizes to the cell pole by binding to the peptidoglycan layer via an N-terminal LysM binding motif. HubP was demonstrated to control polar localization of the chemotaxis system, particularly CheA, independent of the flagellar system. It was also shown to be involved in flagella formation, likely by interacting with FlhF and FlhG (46, 47). As a third effect, HubP seems to be involved in chromosome segregation by recruiting the ATPase ParA1 (47). In *V. cholera*, ParA1 is responsible for polar targeting of the origin region of *V. cholera*'s larger chromosome via the DNA binding protein ParB1 (47, 48). As *S. putrefaciens* is closely related to *Vibrio* species, a similar protein might also regulate cell polarity in this organism.

5.3.2 HubP is involved in polar localization of the chemotaxis system in *S. putrefaciens*

In *S. putrefaciens* CN-32, the protein Sputcn32_2442 was identified as the functional ortholog of *V. cholerae* HubP and shown to be involved in flagellar-mediated motility in an unknown manner. Compared to wt cells the *hubP* deletion mutant exhibited a strongly reduced lateral extension on soft agar plates. *Sp*HubP possesses an N-terminal periplasmic peptidoglycan-binding domain and a large, acidic cytoplasmic domain with ten imperfect 46-amino-acid repeats and a C-terminal motif highly homologous to the Type IV-pili assembly protein FimV from *P. aeruginosa*. Analysis of fluorescently labeled HubP revealed a complex localization pattern, forming a distinct cluster at the flagellated cell pole and a minor cluster at the division plane that increased in size at the new cell pole. The LysM-domain alone was shown to be sufficient for polar localization. In *E. coli*, overexpressed GFP-tagged HubP also localized to the pole (Chapter 4).

Components of the chemotaxis machinery, namely CheA, CheZ, CheY and selected MCPs, showed *Sp*HubP-dependent recruitment to the cell pole. These findings demonstrate that the chemotaxis gene cluster of *S. putrefaciens* localization depends on HubP and not FlhF or any other flagellar component.

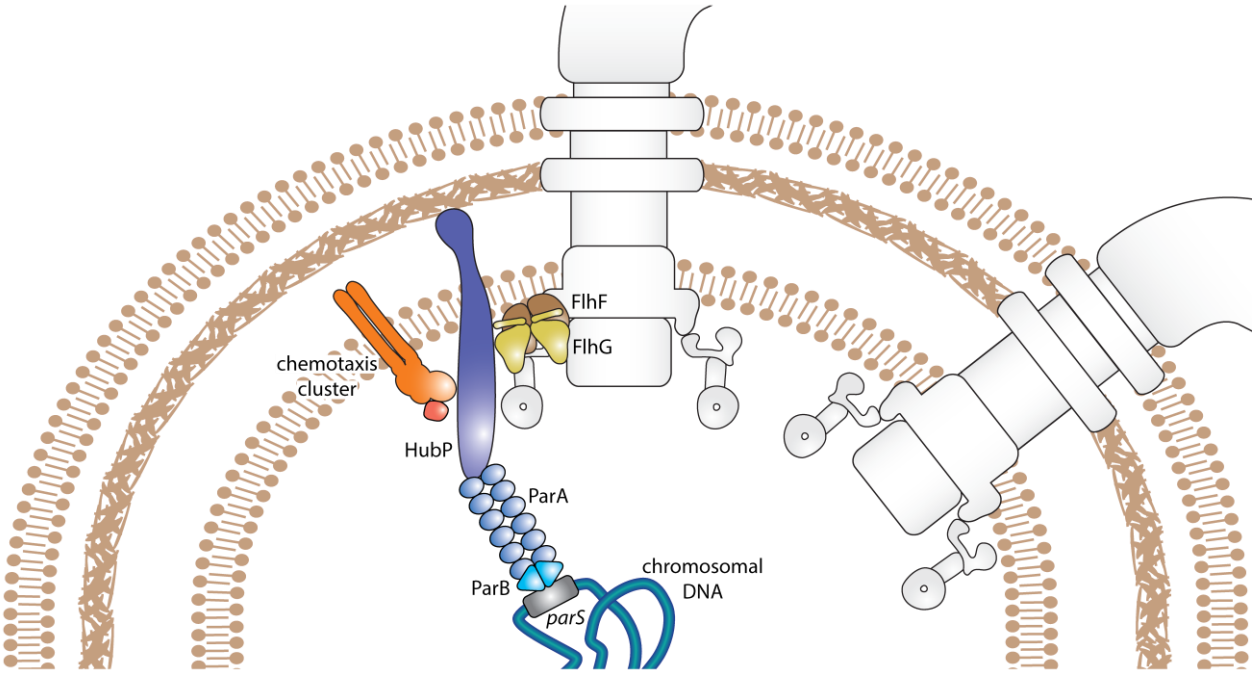

Fig: 4: Involvement of HubP in polar flagellar assembly and chemotaxis. FlhG (yellow) and FlhF (brown) directly interact with HubP (violet). Furthermore HubP is involved in polar accumulation of the chemotaxis cluster (orange) and chromosome segregation via the ParAB*parS* (dark blue / light blue / grey) system.

However, the exact interactions of the chemotaxis system with HubP are unknown. In *Vibrio*, both the ParA-like protein s and the CheW paralog ParP were shown to be responsible for polar localization of the chemotaxis system by directly interacting with CheA. While ParC controls recruitment of CheA, ParP primarily stabilizes complex formation (49). Direct interactions between HubP and ParC were not observed in bacterial-two-hybrid assays (47). ParP or another, yet unidentified, factor could act as an adapter for this interaction. As both *parP* and *parC* orthologs can be found in the genome of *S. putrefaciens*, further studies should focus on the potential interaction between HubP, ParP, and ParC.

5.3.3 Other effects of HubP on flagellar motility

Although HubP was shown to be important for localization of the chemotaxis system, the strong motility defect of a *hubP* deletion mutant on soft agar plates is likely not only based on this mechanism as cells lacking *hubP* also swam slower in liquid media. Since this motility defect was primarily caused by a reduction in swimming speed of the mutant cells by almost half of the wt, maintenance of the close proximity of the chemotaxis system to the cell pole and the flagellar motor cannot be the only function of HubP in flagella-mediated motility. *Vc*HubP was shown to interact with FlhF and FlhG (47) and might influence flagellar motility through these interactions. In *S. putrefaciens*, significantly fewer cells possessed

polar foci of fluorescently labeled FlhF, $FliM_1$ or polar flagella upon *hubP* deletion. Localization of chromosomally expressed FlhG with an in-frame fluorescent fusion was completely abolished in this mutant. However, as reported above, overexpressed FlhG still localized to the cell pole by binding to the EIDAL motif of $FliM_1$. Similar observations were found both in *V. cholerae* (47) and in initial experiments in *S. putrefaciens* where bacterial-two-hybrid analyses indicated an interaction between FlhF, FlhG, and HubP. This suggests an involvement of HubP in FlhF and FlhG localization. Although not essential for polar localization, HubP might act as a polar sponge or a sink to ensure that only the right stoichiometry of FlhF and FlhG are present at the flagellar assembly site. This would explain why in *Vibrio* sp. *hubP* deletion also causes an increased number of polar flagella without changing the amount of polarly localized FlhF (46). The motility phenotype of the *hubP* mutant might also derive from an impairment of the FlhG-mediated C-ring assembly process by misguiding FlhG at the cell pole. Overall, HubP seems to be an important determining factor for the localization of various components involved in bacterial motility.

5.3.4 HubP is a polar landmark protein involved in various cellular processes

The third important cellular function of HubP is its involvement in proper chromosome segregation, as suggested by studies in *V. cholerae*. This is performed by direct interaction with ParA1, which binds to the *parS1* site via ParB1 located next to the *oriC* of one of the chromosomes of *V. cholerae* (47). HubP seems to play a similar role in *S. putrefaciens*, as deletion of *hubP* inhibited the complete migration of fluorescently labeled ParB to the cell pole. In contrast, the accumulation of mCherry-ParB foci at the ¼ or ¾ positions of mutant cells indicated an impairment in bacterial chromosome segregation. This did not, however, lead to a significantly decreased in cell growth (Chapter 4).

This involvement of HubP in chromosome segregation might also affect flagella formation. Although HubP influences only the location of the *ori* of the chromosome, the topology of the chromosome as a whole might also be further affected. This might also lead to better accessibility of certain genomic areas, such as the flagella gene cluster. In *S. putrefaciens*, 1.7% of the annotated proteins are flagellar proteins and at least 1.1% are from the polar flagellar system. Many of the proteins are integral membrane proteins or secreted into the periplasm, partly by the fT3SS. Since HubP was shown to interact with SRP-like FlhF, HubP may also support spatiotemporally efficient transcription, translation, and translocation of this vast amount of proteins. This could also partly explain the slightly reduced amount of polarly flagellated cells in *hubP* mutants.

The C-terminus of HubP (FimVc) shows a high sequence homology to the type IV pilus assembly protein FimV from *P. aeruginosa* with a protein identity of 49%. In addition, both are transmembrane proteins harbouring an N-terminal peptidoglycan-binding LysM-domain (Chapter 4). FimV was shown to be involved in the assembly of type-IV-pili which enables twitching motility in *P. aeruginosa* (50, 51). Furthermore, deletion of *fimV* affected the function of the type II secretion system and was associated with components regulating quorum sensing and virulence in *P. aeruginosa* (52, 53). A reduced ability to perform twitching motility was also observed in *S. putrefaciens* (Chapter 4). As the FimVc-domain contains a conserved tetratricopeptide motif which mediates protein-protein interaction, this domain has a central role in recruiting other client proteins in various species (53). Indeed, interactions of HubP with ParA, FlhF and FlhG were reduced in *V. cholerae* if this this domain was missing (47). However, if this domain also interacts with these proteins in *P. aeruginosa* remains to be tested. The rest of the protein including the poorly conserved cytoplasmic repeat region is then probably responsible for direct or indirect polar recruitment of the chemotaxis proteins in *V. cholerae* and *S. putrefaciens*, which would explain why the recruitment mechanism of the chemotaxis system is different in *P. aeruginosa*, where it seems to localize FlhF dependent (45).

These findings indicate an involvement of HubP in polar localization of many important cellular processes (Fig. 4). However, much less is known about the initial recruitment of HubP to the cell pole. In *S. putrefaciens*, HubP appeared already in the cell division plane indicating an early recruitment to the cell pole. Foci of fluorescently labelled HubP frequently appeared at both cell poles with a major cluster at the old cell pole and a minor cluster at the new cell pole. This minor cluster became more intense during cell division (Chapter 4). The periplasmic region harboring the LysM domain in both *V. cholerae* and *S. putrefaciens* HubP was sufficient for localization at the cell pole. Polar localization was also observed when fluorescently labeled *Sp*HubP or its LysM domain alone were overproduced in *E. coli*, indicating the presence of a conserved recruitment mechanism for HubP in various representatives of the gammaproteobacteria (Chapter 4)(47). It is unknown whether this requires the presence of another landmark protein or a defined lipid composition at the cell pole. One hypothesis could be that the LysM-domain of HubP recognizes a “birth scar” in the peptidoglycan layer which could be formed in the nascent cell wall during cell fission in a similar fashion as previously hypothesized for TipN in *C. crescentus* (54). The growing minor cluster of HubP can then further recruit HubP molecules to the cell pole (Chapter 4).

In *P. aeruginosa*, where localization of the chemotaxis system was shown to be FlhF-dependent rather than HubP-dependent, the phosphodiesterase Pch, which is involved in cdG signaling, binds to CheA. The resulting polar localization of these proteins results in different intracellular cdG concentrations after cell

division and a population with heterogeneous motility behavior (45). Similar cdG-turnover proteins are also present in *S. putrefaciens*. Since HubP regulates CheA localization in *S. putrefaciens*, cdG proteins might be indirectly or directly localized to the cell pole, putatively affecting both polar and lateral flagellar motility on multiple levels. Such an interaction could be a cause for the heterogeneous dual flagellation in *S. putrefaciens*.

Together with other functions in flagellar motility, FlhFG interaction, chromosome organization, and localization of the chemotaxis system, HubP may be involved in making various processes at the cell pole more efficient by maintaining close proximity of all factors.

5.4 Localization of flagellar landmark proteins

While SIMIBI proteins require nucleoside triphosphate binding to function, HubP seems to function independently of these processes. Interestingly, several of the proteins that likely bind to HubP belong to the class of MinD/ParA-like ATPases or SRP-like GTPases, namely FlhF, FlhG and ParC. However, it is unknown what function HubP plays in the complex, cyclic targeting process of these proteins (55). HubP could be the missing recruitment partner for FlhF or FlhG (32), although this would presumably lead to a more severe flagellation phenotype similar to an *flhFG* deletion mutant, characterized by a very small fraction of peritrichously flagellated cells in *V. alginolyticus* (22). Instead, HubP could act as a storage platform, ensuring close proximity of FlhFG to the cell pole. Notably, HubP seems to be directly involved in FlhG localization, whereas FlhF binding might occur only transiently, indicated by the unaffected localization pattern in the *hubP* mutant. In concert with $FliM_1$, interaction with HubP could support polar localization of FlhG and perhaps its interaction with FlhF.

In addition to the ambiguous recruitment pattern, the release mechanism of these proteins is unknown. ATP-bound dimers are commonly bound to an effector, which is unknown for FlhF but likely $FliM_1$ for FlhG and HubP or ParP for ParC. ATP hydrolysis leads to dissociation to a monomeric state. While activation of FlhF GTP-hydrolysis was found to be FlhG-dependent (Chapter 4), the factor stimulating ATP-hydrolysis of FlhG has not been identified, yet. As mentioned previously, this function could be carried out by $FlrA_1$. As FlhG binding to $FlrA_1$ might inhibit flagellar gene expression, this cycle would also be an efficient mechanism linking C-ring assembly and transcriptional regulation of flagellar components. FlhG might thereby turn off flagellar gene expression after dissociation from $FliM_1$. ParC is also released by an unknown factor from HubP (or its adaptor protein ParP) at the old cell pole. It then relocalizes to the new

cell pole in a cell cycle-dependent fashion (56). Together, these proteins jointly determine the polar localization of CheA in *Vibrio* (49).

In contrast, proteins of the lateral flagellar system do not require landmark proteins like HubP, since assembly likely occurs in a stochastic manner and independent of FlhF and FlhG. The dual flagellar system of *S. putrefaciens* shows how spatially separated localized processes can be established. Landmark proteins play an important role in this process. In my PhD. project, I improved our understanding of the role of these landmark proteins in the regulation of flagellar-mediated motility. Only this complex spatiotemporal regulation cascade can enable the formation of such a complex dual flagellation pattern.

References:

1. **Bubendorfer S**, **Held S**, **Windel N**, **Paulick A**, **Klingl A**, **Thormann KM**. 2012. Specificity of motor components in the dual flagellar system of *Shewanella putrefaciens* CN-32. Mol Microbiol **83**:335–350.
2. **Xie L**, **Altindal T**, **Chattopadhyay S**, **Wu XL**. 2011. Bacterial flagellum as a propeller and as a rudder for efficient chemotaxis. Proc Natl Acad Sci U S A **108**:2246–2251.
3. **Sar N**, **McCarter L**, **Simon M**, **Silverman M**. 1990. Chemotactic control of the two flagellar systems of *Vibrio parahaemolyticus*. J Bacteriol **172**:334–341.
4. **Kojima M**, **Kubo R**, **Yakushi T**, **Homma M**, **Kawagishi I**. 2007. The bidirectional polar and unidirectional lateral flagellar motors of *Vibrio alginolyticus* are controlled by a single CheY species. Mol Microbiol **64**:57–67.
5. **Prüβ BM**, **Liu J**, **Higgs PI**, **Thompson LK**. 2015. Lessons in Fundamental Mechanisms and Diverse Adaptations from the 2015 Bacterial Locomotion and Signal Transduction Meeting. J Bacteriol **197**:3028–40.
6. **Mariconda S**, **Wang Q**, **Harshey RM**. 2006. A mechanical role for the chemotaxis system in swarming motility. Mol Microbiol **60**:1590–1602.
7. **Kareiva PM**, **Shigesada N**. 1983. Analyzing insect movement as a correlated random walk. Oecologia **56**:234–238.
8. **Turner L**, **Ryu WS**, **Berg HC**. 2000. Real-time imaging of fluorescent flagellar filaments. J Bacteriol **182**:2793–801.
9. **Suerbaum S**. 1995. The complex flagella of gastric Helicobacter species. Trends Microbiol **3**:168-170-171.
10. **Kanbe M**, **Yagasaki J**, **Zehner S**, **Gottfert M**, **Aizawa S-I**. 2007. Characterization of Two Sets of Subpolar Flagella in *Bradyrhizobium japonicum*. J Bacteriol **189**:1083–1089.
11. **Quelas JI**, **Althabegoiti MJ**, **Jimenez-Sanchez C**, **Melgarejo AA**, **Marconi VI**, **Mongiardini EJ**, **Trejo SA**, **Mengucci F**, **Ortega-Calvo J-J**, **Lodeiro AR**. 2016. Swimming performance of *Bradyrhizobium diazoefficiens* is an emergent property of its two flagellar systems. Sci Rep **6**:23841.

12. **Kawagishi I**, **Maekawa Y**, **Atsumi T**, **Homma M**, **Imae Y**. 1995. Isolation of the polar and lateral flagellum-defective mutants in *Vibrio alginolyticus* and identification of their flagellar driving energy sources. J Bacteriol **177**:5158–5160.

13. **Darnton NC**, **Turner L**, **Rojevsky S**, **Berg HC**. 2007. On torque and tumbling in swimming *Escherichia coli*. J Bacteriol **189**:1756–1764.

14. **Guttenplan SB**, **Shaw S**, **Kearns DB**. 2013. The cell biology of peritrichous flagella in *Bacillus subtilis*. Mol Microbiol **87**:211–229.

15. **Correa NE**, **Peng F**, **Klose KE**. 2005. Roles of the regulatory proteins FlhF and FlhG in the *Vibrio cholerae* flagellar transcription hierarchy. J Bacteriol **187**:6324–6332.

16. **Murray TS**, **Kazmierczak BI**. 2006. FlhF is required for swimming and swarming in *Pseudomonas aeruginosa*. J Bacteriol **188**:6995–7004.

17. **Kusumoto A**, **Kamisaka K**, **Yakushi T**, **Terashima H**, **Shinohara A**, **Homma M**. 2006. Regulation of polar flagellar number by the flhF and flhG genes in *Vibrio alginolyticus*. J Biochem **139**:113–121.

18. **Balaban M**, **Hendrixson DR**. 2011. Polar flagellar biosynthesis and a regulator of flagellar number influence spatial parameters of cell division in *Campylobacter jejuni*. PLoS Pathog **7**:e1002420.

19. **Green JC**, **Kahramanoglou C**, **Rahman A**, **Pender AM**, **Charbonnel N**, **Fraser GM**. 2009. Recruitment of the earliest component of the bacterial flagellum to the old cell division pole by a membrane-associated signal recognition particle family GTP-binding protein. J Mol Biol **391**:679–690.

20. **Bange G**, **Kummerer N**, **Engel C**, **Bozkurt G**, **Wild K**, **Sinning I**. 2010. FlhA provides the adaptor for coordinated delivery of late flagella building blocks to the type III secretion system. Proc Natl Acad Sci **107**:11295–11300.

21. **Li H**, **Sourjik V**. 2011. Assembly and stability of flagellar motor in *Escherichia coli*. Mol Microbiol **80**:886–899.

22. **Kusumoto A**, **Shinohara A**, **Terashima H**, **Kojima S**, **Yakushi T**, **Homma M**. 2008. Collaboration of FlhF and FlhG to regulate polar-flagella number and localization in *Vibrio alginolyticus*. Microbiology **154**:1390–1399.

23. **Bange G**, **Petzold G**, **Wild K**, **Parlitz RO**, **Sinning I**. 2007. The crystal structure of the third signal-recognition particle GTPase FlhF reveals a homodimer with bound GTP. Proc Natl Acad Sci U S A **104**:13621–13625.

24. **Schniederberend M**, **Abdurachim K**, **Murray TS**, **Kazmierczak BI**. 2013. The GTPase activity of FlhF is dispensable for flagellar localization, but not motility, in *Pseudomonas aeruginosa*. J Bacteriol **195**:1051–60.

25. **Gao T**, **Shi M**, **Ju L**, **Gao H**. 2015. Investigation into FlhFG reveals distinct features of FlhF in regulating flagellum polarity in *S hewanella oneidensis*. Mol Microbiol **98**:571–585.

26. **Balaban M**, **Joslin SN**, **Hendrixson DR**. 2009. FlhF and its GTPase activity are required for distinct processes in flagellar gene regulation and biosynthesis in *Campylobacter jejuni*. J Bacteriol **191**:6602–6611.

27. **Bange G**, **Kummerer N**, **Grudnik P**, **Lindner R**, **Petzold G**, **Kressler D**, **Hurt E**, **Wild K**, **Sinning I**. 2011. Structural basis for the molecular evolution of SRP-GTPase activation by protein. Nat Struct Mol Biol **18**:1376–1380.

28. **Ono H**, **Takashima A**, **Hirata H**, **Homma M**, **Kojima S**. 2015. The MinD homolog FlhG regulates the synthesis of the single polar flagellum of *Vibrio alginolyticus*. Mol Microbiol **98**:130–41.

29. **Dasgupta N**, **Arora SK**, **Ramphal R**. 2000. fleN, a gene that regulates flagellar number in *Pseudomonas aeruginosa*. J Bacteriol **182**:357–364.

30. **Erhardt M**, **Hughes KT**. 2010. C-ring requirement in flagellar type III secretion is bypassed by FlhDC upregulation. Mol Microbiol **75**:376–393.

31. **Sircar R**, **Greenswag AR**, **Bilwes AM**, **Gonzalez-Bonet G**, **Crane BR**. 2013. Structure and Activity of the Flagellar Rotor Protein FliY: A Member of the CheC Phosphatase Family. J Biol Chem **288**:13493–13502.

32. **Schuhmacher JS, Thormann KM, Bange G. 2015.** How bacteria maintain location and number of flagella? FEMS Microbiol Rev **39**:812-22

33. **Dasgupta N**, **Ramphal R**. 2001. Interaction of the antiactivator FleN with the transcriptional activator FleQ regulates flagellar number in *Pseudomonas aeruginosa*. J Bacteriol **183**:6636–6644.

34. **Hickman JW**, **Harwood CS**. 2008. Identification of FleQ from *Pseudomonas aeruginosa* as a c-di-GMP-responsive transcription factor. Mol Microbiol **69**:376–389.

35. **Srivastava D**, **Hsieh ML**, **Khataokar A**, **Neiditch MB**, **Waters CM**. 2013. Cyclic di-GMP inhibits *Vibrio cholerae* motility by repressing induction of transcription and inducing extracellular polysaccharide production. Mol Microbiol **90**:1262–1276.

36. **Matsuyama BY**, **Krasteva P V**, **Baraquet C**, **Harwood CS**, **Sondermann H**, **Navarro MVAS**. 2015. Mechanistic insights into c-di-GMP-dependent control of the biofilm regulator FleQ from *Pseudomonas aeruginosa*. Proc Natl Acad Sci U S A **113**:E209-18.

37. **Bush M**, **Dixon R**. 2012. The role of bacterial enhancer binding proteins as specialized activators of sigma54-dependent transcription. Microbiol Mol Biol Rev **76**:497–529.

38. **Baraquet C**, **Harwood CS**. 2013. Cyclic diguanosine monophosphate represses bacterial flagella synthesis by interacting with the Walker A motif of the enhancer-binding protein FleQ. Proc Natl Acad Sci U S A **110**:18478–83.

39. **Ferreira RBR**, **Chodur DM**, **Antunes LCM**, **Trimble MJ**, **McCarter LL**. 2012. Output targets and transcriptional regulation by a cyclic dimeric GMP-responsive circuit in the *Vibrio parahaemolyticus* scr network. J Bacteriol **194**:914–924.

40. **Anderson JK**, **Smith TG**, **Hoover TR**. 2010. Sense and sensibility: flagellum-mediated gene regulation. Trends Microbiol.

41. **Sudarsan N**, **Lee ER**, **Weinberg Z**, **Moy RH**, **Kim JN**, **Link KH**, **Breaker RR**. 2008. Riboswitches in eubacteria sense the second messenger cyclic di-GMP. Science **321**:411–413.

42. **Lipkow K**, **Andrews SS**, **Bray D**. 2005. Simulated diffusion of phosphorylated CheY through the cytoplasm of *Escherichia coli*. J Bacteriol **187**:45–53.

43. **Sourjik V**, **Armitage JP**. 2010. Spatial organization in bacterial chemotaxis. EMBO J **29**:2724–2733.

44. **Strahl H**, **Ronneau S**, **González BS**, **Klutsch D**, **Schaffner-Barbero C**, **Hamoen LW**. 2015. Transmembrane protein sorting driven by membrane curvature. Nat Commun **6**:8728.

45. **Kulasekara BR**, **Kamischke C**, **Kulasekara HD**, **Christen M**, **Wiggins PA**, **Miller SI**. 2013. c-di-GMP

heterogeneity is generated by the chemotaxis machinery to regulate flagellar motility. Elife **2**.

46. **Takekawa N**, **Kwon S**, **Nishioka N**, **Kojima S**, **Homma M**. 2016. HubP, a polar landmark protein, regulates flagellar number by assisting in the proper polar localization of FlhG in *Vibrio alginolyticus*. J Bacteriol 00462-16.

47. **Yamaichi Y**, **Bruckner R**, **Ringgaard S**, **Moll A**, **Cameron DE**, **Briegel A**, **Jensen GJ**, **Davis BM**, **Waldor MK**. 2012. A multidomain hub anchors the chromosome segregation and chemotactic machinery to the bacterial pole. Genes Dev **26**:2348–2360.

48. **Fogel MA**, **Waldor MK**. 2006. A dynamic, mitotic-like mechanism for bacterial chromosome segregation. Genes Dev **20**:3269–82.

49. **Ringgaard S**, **Zepeda-Rivera M**, **Wu X**, **Schirner K**, **Davis BM**, **Waldor MK**. 2014. ParP prevents dissociation of CheA from chemotactic signaling arrays and tethers them to a polar anchor. Proc Natl Acad Sci U S A **111**:E255-64.

50. **Wehbi H**, **Portillo E**, **Harvey H**, **Shimkoff AE**, **Scheurwater EM**, **Howell PL**, **Burrows LL**. 2011. The Peptidoglycan-Binding Protein FimV Promotes Assembly of the *Pseudomonas aeruginosa* Type IV Pilus Secretin. J Bacteriol **193**:540–550.

51. **Whitchurch CB**, **Leech AJ**, **Mattick JS**, **Semmler ABT**. 2000. Identification of a novel gene, fimV, involved in twitching motility in *Pseudomonas aeruginosa*. Microbiology **146**:1321–1332.

52. **Michel GPF**, **Aguzzi A**, **Ball G**, **Soscia C**, **Bleves S**, **Voulhoux R**. 2011. Role of fimV in type II secretion system-dependent protein secretion of *Pseudomonas aeruginosa* on solid medium. Microbiology **157**:1945–1954.

53. **Buensuceso RNC**, **Nguyen Y**, **Zhang K**, **Daniel-Ivad M**, **Sugiman-Marangos SN**, **Fleetwood AD**, **Zhulin IB**, **Junop MS**, **Howell PL**, **Burrows LL**. 2016. The Conserved Tetratricopeptide Repeat-Containing C-Terminal Domain of *Pseudomonas aeruginosa* FimV Is Required for Its Cyclic AMP-Dependent and -Independent Functions. J Bacteriol **198**:2263–74.

54. **Huitema E**, **Pritchard S**, **Matteson D**, **Radhakrishnan SK**, **Viollier PH**. 2006. Bacterial birth scar proteins mark future flagellum assembly site. Cell **124**:1025–37.

55. **Bange G**, **Sinning I**. 2013. SIMIBI twins in protein targeting and localization. Nat Struct Mol Biol **20**:776–80.

56. **Ringgaard S**, **Schirner K**, **Davis BM**, **Waldor MK**. 2011. A family of ParA-like ATPases promotes cell pole maturation by facilitating polar localization of chemotaxis proteins. Genes Dev **25**:1544–1555.

Abbreviations

ADP = adenosine diphosphate

ATP = adenosine triphosphate

bp = base pairs

Bs = *Bacillus subtilis*

CCW = counter-clockwise

cdg = cyclic diguanosine monophosphate

CW = clockwise

Ec = *Escherichia coli*

FRAP = fluorescence recovery after photobleaching

ft3SS = flagellar type III secretion system

GDP = guanosine diphosphate

GTP = guanosine triphosphate

HTH = helix-turn-helix motif

IM = inner membrane

MCP = methyl-accepting proteins

MTS = membrane targeting sequence

nm = nanometer

OM = outer membrane

ori = origin of replication

Pa = *Pseudomonas aeruginosa*

PG = peptidoglycan

RNA = ribonucleic acid

s = seconds

SIMIBI = SRP, MinD, and BioD type

Sp = *Shewanella putrefaciens*

SRP = signal recognition particle

Vc = *Vibrio alginolyticus*

Vc = *Vibrio cholerae*

Vc = *Vibrio parahaemolyticus*

wt = wild-type / wildtype

Acknowledgements - Danksagung

Als aller erstes möchte ich mich bei meinem Doktorvater Prof. Kai Thormann für die Bereitstellung meines unglaublich spannenden Themas und die intensive Betreuung bedanken. Seine Tür war sprichwörtlich immer offen für Fragen und Probleme, aus persönlichen Gesprächen mit ihm kam man immer motiviert und mit einem positiven Gefühl. Und wenn er mir nicht helfen konnte kannte er immer jemand, an den man sich wenden konnte.

Einer dieser Leute waren die besten Proteinkristallographen der Welt: Dr. Gert Bange und Carina, Jan, Devid, Wieland und alle anderen. Nicht nur durch seine Tätigkeit als Prüfer und Mitglied in meinem Thesis Advisory Comitee, sondern auch in unzähligen Meetings und auch Telefonisch war Gert Bange jederzeit bereit seine Ideen einfließen zu lassen.

Bedanken möchte ich mich auch bei Herrn Prof. Dr. Martin Thanbichler für die Übernahme des Zweitgutachtens und bei restlichen Mitgliedern meiner Prüfungskommission.

Desweiteren möchte ich mich auch bei den anderen Mitgliedern des IMPRS Thesis Advisory Comitees, Frau Prof. Anke Becker und Frau Prof. Lotte Soogard-Andersen für ihre Anmerkungen und kritische Fragen bedanken.

Auch bei den IMPRS Koordinatoren, Dr. Chris van der Does, Prof. Penelope Higgs, Simone Hain, Dr. Wiebke Wlotzla und allen Mitgliedern der IMPRS möchte ich mich für die schöne Zeit in der Research School bedanken.

Natürlich möchte ich mich bei meiner Arbeitsgruppe, die womöglich lustigste der Welt, bedanken. Dafür, dass sie jederzeit geholfen haben, ob durch Ideen oder Experimente. Und dafür, dass man trotzdem immer einen blöden Spruch bekommen hat. Das Beste an dieser Arbeitsgruppe ist, dass sie immer so war wie sie ist und hoffentlich auch immer so bleibt. Ihr seid super.

Danke an Ulrike, sowohl für Tipps als auch für die Herstellung unzähliger Stämme und dafür dass sie den ganzen Laden am Laufen hält. Durch ihre fürsorgliche Art und ihre Kompetenz konnten wir das Labor in Gießen schnell aufbauen.

Danke an Suse für ihre Tätigkeit als mein zweiter Chef, für die Mitarbeit in unserem gemeinsamen Projekt, viele wissenschaftliche, politische und gesellschaftliche Diskussionen, für ihre Kuchen und Gummibärchen und dafür dass sie mich auch in weniger angenehmen Momenten ausgehalten hat.

Danke an Max für seine Bildbearbeitungs-Kenntnisse, seine Hilfe bei diversen Recherche-Arbeiten und die interessanten Diskussionen über Ubootstahl, Betontrampolins und Laubbläser. Der Fußweg zur Mensa wird mir fehlen…

Bei diesen Diskussionen war auch oft Marco mit seiner „leidenschaftlichen“ Art dabei. Bei ihm muss ich mich weiterhin dafür bedanken, dass er oft der einzige war der mir bei Proteinarbeiten helfen konnte, mir dann erklärt hat, dass es immer auf das Protein ankommt und dann unzählige Male seine Masterarbeit (mit dem kleinen Uni Marburg-Wappen) ausgedruckt hat.

Danke an Anna, dafür dass sie einige Projekte weiterführt und dass auch mal einer aus meiner Arbeitsgruppe in Gießen wohnt und somit auch abends immer dabei ist.

Danke auch an Anja Paulick, Anja Dörrich, Basti und Lucas die alle dafür gesorgt haben, dass diese beste Arbeitsgruppe immer schon so war wie sie ist. Besonders Basti habe ich viel zu verdanken, da er es war der mir, auf die netteste Art und Weise, alles beigebracht hat was ich im Labor wissen musste um diese Doktorarbeit erfolgreich abzuschließen.

Natürlich hätte ich alles nie ohne all die Hiwis und Praktikanten hinbekommen. Tim, Kerstin und Arne, ihr wart super. Vor allem Tim hat sich wie wild in Proteinaufreinigungen und Pulldowns eingearbeitet und mich nebenher zum klettern und bouldern animiert.

Desweiteren muss ich mich bei allen anderen Mitarbeitern der AG Klug und AG Hackenberg für die nette Aufnahme in Gießen bedanken. Ohne sie wüsste ich nicht was Hfq macht, wie ein Northern Blot funktioniert, was nicht kodierende RNAs alles können und ich hätte nicht alle Kneipen in Gießen kennengelernt.

Danke an Lennart für die spätabendlichen, kontroversen Diskussionen, dafür dass er nie jemanden ausschließt und die Organisation der Aktivitäten außerhalb und innerhalb des Instituts. Aber auch danke dafür dass er bei manchen wissenschaftlichen Fragen oft der beste Ansprechpartner war.

Danke an Bernhard für die besonnene, ausgeglichene Art, wissenschaftliche Hilfe, als Kletterpartner und die verrückten Dinge in Eschwege, Stuttgart, Dresden…

Danke an Andrea und Susann für die Hilfe mit der ÄKTA und Tipps für Proteinarbeiten.

Danke an Julia und Carina für ihr freundliches Lachen.

Danke an Tom. Er war, während er noch da war, der erste Ansprechpartner für mich in der AG Klug.

Weiterer Dank gilt Frau Prof. Gabriele Klug und Prof. Elena Evguenieva-Hackenberg für die Unterstützung meiner Arbeit im Institut für Mikrobiologie und Molekularbiologie.

Ein besonderer Dank gilt meinen Eltern, meinen beiden Schwestern, meinen Neffen, meinen beiden Schwagern und meiner Oma. Es tut mir leid, dass ich so selten zuhause war. Trotzdem waren sie immer da für mich, ob persönlich oder via Telefon.

At the end, I would like to thank a really special person:

Janet, you made my life so much better. Sorry that we had to be separated for a long time. Thank you so much for your help, both scientific and editing… I love you and I'm really looking forward to our common future!!!

CURRICULLUM VITAE

Florian Roßmann

Gießen, October, 31th 2016

Florian Roßmann